UNIVERSITÄTSKLINIKUM HAMBURG-EPPENDORF

Entwicklungsneurophysiologie

Leiterin: Prof. Dr. Ileana L. Hanganu-Opatz

Optogenetic interrogation of prefrontal-hippocampal coupling in the neonatal mouse

Dissertation

zur Erlangung des Doktorgrades Dr. rer. biol. hum. / PhD
an der Medizinischen Fakultät der Universität Hamburg.

vorgelegt von:

Joachim Ahlbeck
aus Aalborg, Dänemark

Hamburg 2017

(wird von der Medizinischen Fakultät ausgefüllt)

Angenommen von der
Medizinischen Fakultät der Universität Hamburg am: 18.01.2018

Veröffentlicht mit Genehmigung der
Medizinischen Fakultät der Universität Hamburg.

Prüfungsausschuss, der/die Vorsitzende: Prof. Dr. Ileana Hanganu-Opatz

Prüfungsausschuss, zweite/r Gutachter/in: Prof. Dr. Christoph Mulert

~~**Prüfungsausschuss, dritte/r Gutachter/in:**~~

1 Table of Contents

2 Introduction

Our brain exerts a centralized control over our body. By processing the multitude of sensory inputs it enables rapid and coordinated responses to changes in our environment. To perform these tasks the neurons of the brain has to organize into complex anatomical and functional networks. They enable the processing of information and for communication between different regions of our brain (Engel et al., 2001; Fries, 2015). The coordinated and synchronous activity of multiple groups of neurons gives rise to oscillatory activity (Buzsaki and Draguhn, 2004; Wang, 2010; Buzsaki et al., 2012). Directed oscillatory coupling within prefrontal-hippocampal networks underlies cognitive processing and have been extensively investigated in the adult brain. This communication emerges early in life, long before the maturation of mnemonic abilities, with discontinuous hippocampal theta bursts driving the initial oscillatory entrainment of local prefrontal networks via direct axonal projections (Brockmann et al., 2011; Bitzenhofer and Hanganu-Opatz, 2014; Hartung et al., 2016a).

2.1 The adult prefrontal-hippocampal network

The medial prefrontal cortex (PFC) is a cortical brain region that is involved in numerous cognitive functions such as attention (Adhikari et al., 2010), working memory (Spellman et al., 2015) and decision making (Vertes, 2006). It can be subdivided into three different regions along its dorsal-ventral axis. These regions are from dorsal to ventral: anterior cingulate cortex (Cg), the prelimbic cortex (PL), and infralimbic cortex (IL) (Heidbreder and Groenewegen, 2003). The cellular structure of the PFC consists primarily of glutamatergic excitatory pyramidal neurons (80 - 90%) and inhibitory γ-aminobutyric acid (GABA)ergic interneurons (10 - 20%) (Riga et al., 2014; Harris and Shepherd, 2015). Several subtypes of interneurons have been classified such as the perisomatic targeting parvalbumin (PV) interneurons or dendritic targeting somatostatin (SOM) interneurons. Both these types exert strong control of the local activity by synchronizing the activity of pyramidal neurons. PV neurons primarily control the output of pyramidal neurons whereas SOM modulates the input that pyramidal neurons receive (Kvitsiani et al., 2013). Similar to other cortical areas PFC has a laminar structure, consisting of layer I, layer II/III, and layer V/VI, missing the typical input layer IV seen in other cortical regions (Uylings et al., 2003). The cortical neurons do not function independently but form local and long-

range circuits. In sensory cortices, thalamic inputs to layer IV is propagated to layer II/II which is further propagated to layer V/VI and then propagated to other brain regions (Harris and Shepherd, 2015). Despite the missing layer IV, PFC has a similar circuit, with inputs coming into both layer II/III and V/VI from subcortical regions such as amygdala, thalamus and hippocampus (HP) (Tierney et al., 2004; Riga et al., 2014).

HP is part of the limbic system and is associated with spatial learning and the consolidation of short-term memory to long-term memory (Sigurdsson and Duvarci, 2015; Eichenbaum, 2017). It can be subdivided into various subregions; four different subfields of cornu ammonis (CA)1 to CA4; dentate gurus (DG); and subiculum (Amaral and Witter, 1989). Within the hippocampal formation a unidirectional circuit is present. Inputs coming from granule cells of entorhinal cortex are projecting to DG. This is then transmitted from DG via mossy cell fibers to pyramidal neurons in CA3, which is further transmitted to pyramidal neurons in CA1 via Schaffer collateral fibers. Here, the signal is relayed to other brain regions such as back to the entorhinal cortex or to the PFC (Amaral and Witter, 1989; Buzsaki, 2015). In the work presented here the focus will be on the role of the output region CA1 of the hippocampal formation to PFC. The CA1 can be further subdivided on its dorsal-ventral axis into dorsal HP (dHP), and intermediate-ventral HP (i/vHP). These two regions are involved in different types of information processing in regard to PFC. Whereas dHP are involved spatial coding and object-location, i/vHP are primarily involved in context representations (Sigurdsson and Duvarci, 2015; Eichenbaum, 2017).

Different anatomical pathways connects the HP and PFC. The first consist of a unidirectional monosynaptic glutamatergic pathway originating primarily from subiculum and CA1 area of i/vHP, terminating in both superficial and deep layers of the PFC (Swanson, 1981; Jay et al., 1989; Thierry et al., 2000; Tierney et al., 2004). Two other pathways involve a single intermediary region between HP and PFC. One of these is through nucleus reunions of thalamus with bidirectional connections between HP and reunions, as well as bidirectional connections between PFC and reunions (Dolleman-van Der Weel and Witter, 1996; Vertes et al., 2007; Xu and Sudhof, 2013; Ito et al., 2015). The other pathway is through cortical regions such as the entorhinal or perirhinal cortex with similar connections as for reunion, with

bidirectional connections from PFC and HP to entorhinal or perirhinal cortex (Burwell and Amaral, 1998; Agster and Burwell, 2009).

These anatomical neuronal circuits give rise to our brains ability of sensory perception and cognitive processing through oscillatory activity (Schnitzler and Gross, 2005).

2.2 Oscillatory coupling within the adult prefrontal-hippocampal network

Neural oscillations consist of rhythmic electrical activity generated by the neuronal tissue. The timing of oscillatory rhythms is controlled through inhibitory interneurons that play an important role in producing neural synchrony by generating narrow windows for excitation and modulation of the firing rate of excitatory neurons (Womelsdorf et al., 2014). Brain oscillations have been found to enable communication between regions of the brain and is correlated with different behavioral and cognitive states (Engel et al., 2001; Buzsaki and Draguhn, 2004; Fries, 2015). In the adult prefrontal-hippocampal network two types of oscillatory activity are of special interest: Theta rhythms (4 - 12 Hz) and sharp wave (SPW)-ripple complexes (Buzsáki et al., 1983; Colgin, 2016). Each of these types of activity is involved in coordinating interactions between HP and other brain regions such as PFC (Colgin, 2011; Preston and Eichenbaum, 2013).

2.2.1 Theta rhythms in the adult prefrontal-hippocampal network

Theta rhythms represent slow oscillatory activity that occur during exploration and sleep and is capable of coordinating neuronal activity over long distances (Buzsaki, 2002; Colgin, 2016). The medial septum is known to be a generator of the hippocampal theta rhythm as GABAergic neurons subsiding in the medial septum project to inhibitory neurons in DG, CA3 and CA1 and consequently disinhibits pyramidal neurons rhythmically at the theta frequency (Freund and Antal, 1988; Robinson et al., 2016). However, theta rhythms can also be generated intrinsically in the absence of medial septum inputs in *in vitro* experiments indicating that different types of theta rhythms to be present in HP (Goutagny et al., 2009). Multiple studies have reported coherent theta rhythms while simultaneously recording the PFC and either i/vHP (Jones and Wilson, 2005; Young and McNaughton, 2009; Adhikari et al., 2010; Benchenane et al., 2010; Padilla-Coreano et al., 2016) or dHP (Adhikari et al.,

2010; O'Neill et al., 2013; Tamura et al., 2016). The monosynaptic delay between i/vHP and PFC have been reported to be ≈15 ms (Jay et al., 1992) which is short enough to fit within a single theta cycle (80 - 250 ms long). As dHP is primarily connected to PFC through an intermediary region, the interactions must come through polysynaptic projections. Due to the length of the theta cycle, polysynaptic interactions can still occur within a single cycle allowing for coordinated communication (Colgin, 2011). Thus, theta is capable of coordinating direct interactions between the two regions.

Inactivating i/vHP disrupts the theta coherence between dHP and PFC whereas inactivating dHP did not disrupt the theta coherence between i/vHP and PFC (O'Neill et al., 2013) illustrating i/vHP as critical for the communication with PFC. The role of hippocampal theta in entraining PFC can be further illustrated through phase-locking of single unit activity (SUA) in PFC to the theta rhythm in HP. Multiple studies have reported between 5 - 40 % of all neurons detected in PFC to be significantly locked to theta rhythms in i/vHP (Hyman et al., 2005; Siapas et al., 2005; Hartwich et al., 2009; Adhikari et al., 2010; Benchenane et al., 2010). During a memory learning task significantly more PFC neurons were locked after learning the paradigm illustrating a possible role in learning behavior (Benchenane et al., 2010). Simultaneous recordings of PFC, i/vHP and dHP have reported a stronger locking between SUA in PFC and theta rhythms in i/vHP than theta rhythms in dHP (Adhikari et al., 2010; O'Neill et al., 2013; Tamura et al., 2016).

2.2.2 Sharp waves and ripple events in the adult prefrontal-hippocampal network

Hippocampal SPWs are short large amplitude events (40 - 100 ms duration) that reverse across the CA1 stratum pyramidale during immobility or sleep. Brief high frequency ripple events (100 - 250 Hz) co-occur during the SPW. SPWs are generated by activation of CA3 pyramidal neurons that causes a depolarization of the dendritic layer of CA1 via the Schaffer collaterals. About 50.000 to 100.000 neurons discharge synchronously, thereby giving rise to the sharp amplitude that make up the SPW (Buzsaki and Silva, 2012). Simultaneous local activation of CA1 pyramidal neurons and interneurons give rise to local high frequency oscillations underlying the ripple event (Ylinen et al., 1995; Csicsvari et al., 1999; Buzsaki, 2015). Sleep spindle

activity and increased SUA in the PFC has been found to occur shortly following a SPW (Siapas and Wilson, 1998; Molle et al., 2006). This mechanism is believed to be central for facilitating the transfer of locally stored hippocampal short-term memory to cortically stored long-term memory during periods when the brains is disconnected from external stimuli (Takehara et al., 2003; Maviel et al., 2004; Wierzynski et al., 2009; Maingret et al., 2016).

2.3 The development of the brain

The development of the brain is a process that starts at conception and continues through to late adolescence and possible throughout the whole life-span (Stiles and Jernigan, 2010). This developmental process involves the cooperation of a multitude of genetic and environmental factors that has to be activated in a specific and timed manner (O'Leary and Nakagawa, 2002; Stiles and Jernigan, 2010). During the early embryonic period symmetrical division of neural progenitor cells occur to provide the maintenance for the generation of the billions of neurons that make up the brain (Bystron et al., 2008; Stiles and Jernigan, 2010). These progenitor cells reside at the neural plate which later will give rise to the ventricular zone (VZ) (Bystron et al., 2008). When the pool of progenitor neurons have reached a sufficient size they switch from the symmetrical to an asymmetrical division, making one neural progenitor and one neuron (Bystron et al., 2008; Stiles and Jernigan, 2010). The progenitors stay in the VZ and continue dividing while the newborn neurons migrate to its destination in the developing brain. The VZ can be subdivided into different subregions that give rise to different brain regions and neuron types (Bystron et al., 2008). Cortical excitatory neurons migrate from the cortical VZ along a single radial glial cell whereas hippocampal excitatory neurons migrate from the medial VZ in a climbing mode switching between multiple radial glial cells (Hayashi et al., 2015). Interneurons originate from two dorsal located subregions of the VZ, medial ganglionic eminence (MGE) and lateral ganglionic eminence (LGE), where they migrate tangentially throughout the whole brain (Nadarajah and Parnavelas, 2002; Wonders and Anderson, 2006; Bystron et al., 2008).

The first wave of neurons to migrate away from the proliferative zone to form the cortex gives rise to the preplate. The preplate is further separated into two regions, the marginal zone (MZ) and the subplate (SP) by the following wave of

migrating neurons. Both these regions are transient layers that are critical for the development of cortex. The MZ contains Cajal-Retzius cells that guide the migrating neurons to the correct layer. They do this by producing reelin that signals the neurons to stop migrating. Through this mechanism the layers of the cortex form in an inside-out pattern where the deeper cortical layers is established first followed by each of the more superficial layers in consecutive order (Frotscher, 1998; Hack et al., 2002). The SP guides the long-range connections arriving from thalamus by serving as a relay station (Hanganu et al., 2001; 2002) and is important for the correct formation of cortical columns (Dupont et al., 2006; Tolner et al., 2012). Similar functions have been identified for the formation of the HP. Here, newborn excitatory neurons from the medial VZ migrate towards the hippocampal plate that later give rise to stratum pyramidale. Contrary to the inside-out development of the cortex, it is still debated whether the HP form in a similar way (Hayashi et al., 2015).

In rodents, the migration and formation of axons and dendrites are completed towards the end of the first postnatal week and is followed by the growth of blood vessels, astrocytes and oligodendrocytes (Cirelli and Tononi, 2015). During this period an increase in the amount of chemical synapses and spines occur, as well as a reduction of gap junction connections (Peinado et al., 1993; Ashby and Isaac, 2011). During the early first postnatal period most glutamatergic synapses are silent due to only containing N-Methyl-D-aspartic acid (NMDA) receptors while α-amino-3-hydroxy-5-methyl-4-isoxazolepropioic acid (AMPA) receptors get incorporated in the second postnatal period (Isaac et al., 1997; Rumpel et al., 1998). Similarly, GABAergic neurons undergo profound changes during this period switching from being depolarizing to becoming hyperpolarizing by downregulating sodium-potassium cotransporter 1 (NKCC1) and upregulating of potassium-chloride cotransporter 2 (KCC2) leading to reduced intracellular chloride concentration (Khazipov et al., 2004a; Dehorter et al., 2012). Moreover, during the second postnatal period a switch in the rules of synaptic plasticity occurs, changing from always inducing long-term potentiation (LTP) independent of the timing of spikes in the presynaptic and postsynaptic neurons to spike-time dependent plasticity with long-term depression (LTD) or LTP depending of the timing of spikes (Feldman et al., 1999; Itami et al., 2016).

Neurons generate patterns of coordinated electrical activity. The question arise whether these patterns are relevant for refining and maturing developing neuronal networks (Hanganu-Opatz, 2010).

2.4 Electrophysiological patterns of early brain activity

The oscillatory activity observed during early development are distinct from the patterns observed in the mature adult brain. Early electrophysiological recordings of premature born human infants show brief spindle-like activity called “delta brushes”. Newborn rodents are born altricial and their developmental stage corresponds to the second gestational trimester in humans. They show similar activity patterns as observed in premature born humans and therefore serve as an ideal model for the investigation of early network activity (Khazipov and Luhmann, 2006; Hanganu-Opatz, 2010).

Early activity patterns are discontinuous, consisting of periods of silence with intermittent periods of oscillatory burst activity. As the brain matures, the discontinuous activity switches into the continuous activity observed in the adult brain (Brockmann et al., 2011; Shen and Colonnese, 2016). The early activity has been found to influence various developmental processes such as neuronal differentiation, plasticity and migration (Katz and Shatz, 1996; Khazipov and Luhmann, 2006; Page et al., 2017), and is believed to be an early functional template for setting later cortical topography (Dupont et al., 2006; Hanganu et al., 2006; Tolner et al., 2012).

2.4.1 Oscillatory activity in the developing sensory cortices

The most prominent electrophysiological patterns in the neonatal rodent cerebral cortex is (i) the spindle burst, the rodent correlate of the human delta brush activity, (ii) gamma bursts and (iii) long oscillations (Yang et al., 2009). The rodent spindle burst has been observed in multiple cortical regions of the neonatal brain; somatosensory (Khazipov et al., 2004b), visual (Hanganu et al., 2006; Hanganu et al., 2007) and motor (An et al., 2014). Spindle bursts are brief events of 0.5 – 3 s duration consisting primarily of theta activity and occasionally superimposed with beta-gamma activity (Khazipov et al., 2004b; An et al., 2014).

The rodent spindle bursts have been mostly studied in the sensory cortices. They are present at birth and can be triggered by peripheral stimulations such as

tactile (Khazipov et al., 2004b; Yang et al., 2009), visual (Hanganu et al., 2006) or spontaneous limb movement (Khazipov et al., 2004b; An et al., 2014). Notably, after removal of sensory inputs, a reduction, but not elimination, of the occurrence of spindle bursts, indicating that they can be generated endogenously within the cortex (Khazipov et al., 2004b; Hanganu et al., 2006; An et al., 2014). Generation of spindle bursts in the barrel cortex was found to be completely suppressed following pharmacological blockage of AMPA receptors whereas blockage of NMDA receptor show moderate effect on occurrence and duration of the spindle burst (Minlebaev et al., 2007; 2009; Yang et al., 2009). GABAergic neurons are not crucial for the generation of spindle bursts but appear to be important for their compartmentalization, as blockage of $GABA_A$ receptors disrupted the spatial confinement of spindle bursts but did not affect their generation (Minlebaev et al., 2007; Kirmse et al., 2015). These results indicate that excitatory neurons to be important for the generation of the neonatal spindle burst activity. Additionally, removal of the SP neurons at birth prevented the emergence of both spontaneous and evoked spindle bursts in the somatosensory cortex illustrating an important role of the thalamo-cortical network for the emergence of generation of spindle bursts in sensory cortices (Tolner et al., 2012).

2.4.2 Oscillatory activity in the developing hippocampal-prefrontal network

Spindle bursts are not confined to sensory cortical regions but have also been observed in PFC (Brockmann et al., 2011; Cichon et al., 2014; Hartung et al., 2016a). Contrary to sensory cortical regions they first appear a couple of days after birth in the rodent brain (Brockmann et al., 2011). Two distinct types of spindle bursts activity have been reported in PFC, one containing theta with little or no gamma activity, the second type primarily occur in PL, termed nested gamma spindle burst, containing beta-gamma activity superimposed on the theta rhythm. The cellular substrate giving rise to these oscillations is still poorly understood. Recent investigation of the cellular substrate underlying oscillatory activity in layer V/VI using *in vivo* patch-clamp recordings found that glutamatergic inputs on pyramidal neurons are correlated with theta activity, whereas the glutamatergic inputs on interneurons are correlated with beta-gamma activity (Bitzenhofer et al., 2015). Two primary sources for the glutamatergic inputs to layer V/VI neurons are layer II/III pyramidal neurons and CA1 pyramidal neurons in i/vHP. Simultaneous local field potential (LFP) recordings of

both layer II/III and layer V/VI showed that theta are primarily synchronized within layers and does not cross into other layers, indicating HP as the most likely candidate for the glutamatergic inputs to layer V/VI pyramidal neurons (Brockmann et al., 2011; Cichon et al., 2014). As functional connections from layer II/II pyramidal neurons to layer V/VI interneurons are present during this period (Zhang, 2004; Anastasiades et al., 2016) and the fact that beta-gamma activity is highly synchronous between layer II/III and layer V/VI (Brockmann et al., 2011; Cichon et al., 2014), indicates layer II/II pyramidal neurons as a likely candidate for the glutamatergic inputs to layer V/VI interneurons and the generation of beta-gamma activity.

At birth, uni-directional glutamatergic projections from i/vHP to PFC is already present (Brockmann et al., 2011) while projections from PFC back to i/vHP is relayed through the ventral medial thalamus (Hartung et al., 2016a). Similar to cortical regions, HP show discontinuous oscillatory patterns consisting of theta burst activity and SPWs that are already present at birth. Gamma and ripple activity emerges toward the end of the first postnatal week (Lahtinen et al., 2002; Leinekugel et al., 2002; Karlsson and Blumberg, 2003; Mohns and Blumberg, 2010; Brockmann et al., 2011). The drive and temporal coordination within the neonatal PFC is likely through theta burst oscillations originating from i/vHP (Brockmann et al., 2011; Hartung et al., 2016a), whereas the role of SPWs in entraining the neonatal PFC is still unknown. Disruption of i/vHP at birth impaired the oscillatory entrainment in PFC throughout the neonatal and juvenile period and led to poor performance in object recognition tasks (Brockmann et al., 2011; Kruger et al., 2012). The theta entrainment within the prefrontal-hippocampal network was found to be independent of GABAergic neurons in i/vHP, whereas SPWs was found to occur less often following depletion of local GABAergic neurons (Bitzenhofer and Hanganu-Opatz, 2014). Since prefrontal-hippocampal entrainment was not modulated by GABAergic neurons it most likely relies on hippocampal excitatory neurons. The role of dHP in the prefrontal-hippocampal network during development is still unknown.

The present thesis aimed to further characterize the cellular substrates involved in the emergence of oscillatory activity in the PFC and HP regions during the

neonatal period. The specific contribution of pyramidal neurons layer II/III and layer V/VI in PFC for the generation of local oscillatory activity is still unknown. To solve this question we established a protocol that enabled area-, layer-, and cell-type specific transfection of optogenetic tools to PFC. By simultaneously recording electrophysiological activity in combination with optogenetic stimulation of excitatory pyramidal neurons confined in either Layer II/III or Layer V/VI in postnatal (P)8 to P10 day old mice *in vivo* we aim to elucidate their role in the generation of oscillatory activity *(**Bitzenhofer et al., 2017**)*. We next sought to further characterize the prefrontal-hippocampal coupling to PFC. While in the adult brain different roles of dHP and i/vHP has been shown, it is still not known if such differences are also present during development. To meet this aim, simultaneous electrophysiological recordings of either dHP or i/vHP in combination with PFC in P8 to P10 day old mice was performed *in vivo*. Furthermore, the cellular substrate underlying the prefrontal-hippocampal coupling during development is unknown. To investigate the role of CA1 pyramidal neurons for the hippocampal drive to PFC, we simultaneous performed electrophysiological recordings and optogenetic stimulation of pyramidal neurons confined to stratum pyramidale of CA1 area of either dHP or i/vHP in combination with electrophysiological recordings of PFC in P8 to P10 day old mice *in vivo (**Ahlbeck et al., in preparation**)*. Furthermore, a review and a method paper are presented. The review discusses the similarities and differences between the adult sleep spindle and the neonatal spindle burst (**Lindemann et al., 2016**). The method paper introduces *in utero* electroporation (IUE) as a key method to achieve reliable expression of optogenetic tools during the neonatal period as well as a discussion of different patterns of light stimulation to induce electrophysiological activity in neonatal networks (**Bitzenhofer et al., *accepted***).

3 Methods

3.1 *In utero* electroporation

IUE enables area-, layer, and cell type specific transfection of genetic material (Baumgart and Grebe, 2015; Szczurkowska et al., 2016). By taking advantage of the unique way of neuronal generation and migration during embryonal development it allows for selective insertion of genetic material into specific neuronal populations.

Following injection of deoxyribonucleic acid (DNA) construct into the VZ, an electrical field is applied around the head of the embryo that leads to neural progenitor cells located towards the positive pole of the electrical field in taking up the DNA construct. The DNA construct includes coding segments for a promoter that initiates transcription of the genetic material, a gene coding for a specific protein of interest, and a subsequent gene coding for a fluorescent reporter that enables identification of the transfected neurons post-mortem. By varying the position of the electrical field, one can guide the DNA into specific compartments of the VZ thereby spatially confining the transfection to specific brain regions such as the PFC or HP. Similarly, specificity for glutamatergic excitatory neurons can be achieved by confining the electrical field to the upper regions of VZ whereas interneurons are originating from the MGE and LGE subregions of the VZ. This makes neuron type specific promotes obsolete as neuron specificity can be achieved solely by the spatial confinement of the electrical field. Due to the inside-out formation of the cortical layers during development one can achieve layer-specific transfection by temporally confining the IUE to specific time point such as embryonic (E)12.5 for targeting layer V/VI and E15.5 for layer II/III in the PFC of mice.

3.2 Optogenetics

As the typical techniques such as electrical stimulation and pharmacological substances for manipulation of neuronal activity are lacking in spatial and temporal resolution we applied the recently developed technique of optogenetics (Zhang et al., 2010). Optogenetics enables cell-type specific excitation or inhibition of neuronal activity by use of optical stimulation at a high temporal and spatial resolution (Boyden et al., 2005; Yizhar et al., 2011). Selective populations of neurons can be transfected through genetic modification such as viral gene delivery, transgenic breeding, or IUE

(Mei and Zhang, 2012; Packer et al., 2013). Different light-activated microbial opsins can be used such as channelrhodopsins for neural activation (Nagel et al., 2003; Boyden et al., 2005) or halorhopdopsins and archaerhodopsins for neural silencing (Zhang et al., 2007; Chow et al., 2010; Gradinaru et al., 2010; Han et al., 2011). In the experiments conducted here a double mutated form of channelrhodopsin-2 (ChR2) was used ChR2 E123T T159C (ET/TC) that has faster-kinetics and larger photocurrents than the original ChR2 that enables stimulation of up to 60 Hz (Berndt et al., 2011).

3.3 Electrophysiological recordings in neonatal mice

The combination of electrophysiology and optogenetics enables the elucidation of cell-type specific contributions in the generation of oscillatory activity. Acute extracellular recordings in combination with optogenetic stimulation were performed in urethane anesthetized neonatal mice from P8 to P10 containing ChR2(ET/TC) or an opsinfree construct confined to either PFC or HP. Urethane anesthesia show similar oscillatory rhythms and neuronal firing as in sleeping non-anesthetized neonatal rodents (Bitzenhofer et al., 2015). The surgical preparation for acute recording was performed under isoflurane anesthesia. As the skull of neonatal mice is uncalcified, two plastic bars were mounted on the nasal and occipital bones with dental cement to make it possible to fixate the mouse in a stereotaxic apparatus. Holes in the skull were drilled over the regions of interest and following a 15 minute recovery period the mouse was fixed in the recording setup. Depending on the experiment conducted multichannel electrodes and/or multichannel optoelectrodes were inserted into PFC and either dHP or i/vHP. Following a 10 minute recovery period the recording session started and spontaneous (that is, not induced by light stimulation) activity was recorded for 15 min at the beginning and end of each recording session as baseline activity. Three different light stimulations, pulsed (laser on-off), sinusoidal and ramp (linearly increasing light power over time), were used between the two baseline recordings.

4 Articles

4.1 Article 1

The full article can be found at the end of the thesis

4.1.1 Information

Nature Communications, 2017**,** 14563, DOI: 10.1038/ncomms14563

Layer-specific optogenetic activation of pyramidal neurons causes beta gamma entrainment of neonatal networks

Bitzenhofer SH[1*], **Ahlbeck J**[1*], Amy Wolff[1], J. Simon Wiegert[2], Christine E. Gee[2], Thomas G. Oertner[2] & Hanganu-Opatz IL[1].

[1] Developmental Neurophysiology, Institute of Neuroanatomy, University Medical Center Hamburg-Eppendorf, 20251 Hamburg, Germany
[2] Institute for Synaptic Physiology, University Medical Center Hamburg-Eppendorf, 20251 Hamburg, Germany
* These authors contributed equally to this work.

4.1.2 Abstract

Coordinated activity patterns in the developing brain may contribute to the wiring of neuronal circuits underlying future behavioural requirements. However, causal evidence for this hypothesis has been difficult to obtain owing to the absence of tools for selective manipulation of oscillations during early development. We established a protocol that combines optogenetics with electrophysiological recordings from neonatal mice *in vivo* to elucidate the substrate of early network oscillations in the prefrontal cortex. We show that light-induced activation of layer II/III pyramidal neurons that are transfected by *in utero* electroporation with a high-efficiency channelrhodopsin drives frequency-specific spiking and boosts network oscillations within beta–gamma frequency range. By contrast, activation of layer V/VI pyramidal neurons causes nonspecific network activation. Thus, entrainment of neonatal prefrontal networks in fast rhythms relies on the activation of layer II/III pyramidal neurons. This approach used here may be useful for further interrogation of developing circuits, and their behavioural readout.

4.1.3 Personal contribution

I.L.H.-O. designed the experiments, S.H.B. and J.A. carried out the experiments, S.H.B. and J.A. analyzed the data, A.W., C.E.G., J.S.W. and T.G.O.

contributed to the establishment of experimental protocols and provided the constructs, I.L.H.-O., S.H.B. and J.A. interpreted the data and wrote the paper. All authors discussed and commented on the manuscript.

4.2 Article 2

The full article can be found at the end of the thesis

4.2.1 Information

In preparation

Intermediate but not dorsal hippocampal CA1 projection neurons drive the oscillatory entrainment of prefrontal circuits in the neonatal mouse

Ahlbeck J[1], Candela A[1], Chini M[1], Bitzenhofer SH[1] & Hanganu-Opatz IL[1].

[1] Developmental Neurophysiology, Institute of Neuroanatomy, University Medical Center Hamburg-Eppendorf, 20251 Hamburg, Germany

4.2.2 Abstract

The long-range coupling within prefrontal-hippocampal networks that account for cognitive performance emerges early in life. The discontinuous hippocampal theta bursts have been proposed to drive the generation of neonatal prefrontal oscillations, yet causal testing of this hypothesis is missing. Here, we selectively target optogenetic manipulation of glutamatergic projection neurons in the CA1 area of either dorsal or intermediate/ventral hippocampus at neonatal age to prove their contribution to the emergence of prefrontal oscillatory entrainment. We show that despite stronger theta and ripples activation of dorsal hippocampus, the prefrontal cortex is mainly coupled with intermediate/ventral hippocampus by phase-locking of neuronal firing via dense direct axonal projections. Light-induced activation of pyramidal neurons in the intermediate/ventral but not dorsal CA1 that are transfected by *in utero* electroporation with high-efficiency channelrhodopsins boosts theta-band prefrontal oscillations. Our data causally prove the long-range coupling in the developing brain and identify the cellular origin of specific neonatal network states.

4.2.3 Personal contribution

I.L.H.-O. designed the experiments, J.A., S.H.B. and A.C. carried out the experiments, J.A., M.C., and A.C. analyzed the data, I.L.H.-O. and J.A. interpreted the data and wrote the paper. All authors discussed and commented on the manuscript.

4.3 Article 3

The full article can be found at the end of the thesis

4.3.1 Information

Neural Plasticity, 2016**,** 5787423, DOI: 10.1155/2016/5787423

Spindle Activity Orchestrates Plasticity during Development and Sleep

Lindemann C[1], **Ahlbeck J**[1], Bitzenhofer SH[1] & Hanganu-Opatz IL[1].

[1] Developmental Neurophysiology, Institute of Neuroanatomy, University Medical Center Hamburg-Eppendorf, 20251 Hamburg, Germany

4.3.2 Abstract

Spindle oscillations have been described during early brain development and in the adult brain. Besides similarities in temporal patterns and involved brain areas, neonatal spindle bursts (NSBs) and adult sleep spindles (ASSs) show differences in their occurrence, spatial distribution, and underlying mechanisms. While NSBs have been proposed to coordinate the refinement of the maturating neuronal network, ASSs are associated with the implementation of acquired information within existing networks. Along with these functional differences, separate synaptic plasticity mechanisms seem to be recruited. Here, we review the generation of spindle oscillations in the developing and adult brain and discuss possible implications of their differences for synaptic plasticity. The first part of the review is dedicated to the generation and function of ASSs with a particular focus on their role in healthy and impaired neuronal networks. The second part overviews the present knowledge of spindle activity during development and the ability of NSBs to organize immature circuits. Studies linking abnormal maturation of brain wiring with neurological and neuropsychiatric disorders highlight the importance to better elucidate neonatal plasticity rules in future research.

4.3.3 Personal contribution

I.L.H.-O. designed the review. C.L., J.A. and S.H.B. wrote the first draft of the manuscript. I.L.H.-O., C.L., J.A. and S.H.B finalized the manuscript.

4.4 Article 4

The full article can be found at the end of the thesis

4.4.1 Information

Frontiers in Cellular Neuroscience, accepted

Methodological approach for optogenetic manipulation of neonatal neuronal networks

Bitzenhofer SH[1], **Ahlbeck J**[1] & Hanganu-Opatz IL[1].

[1] Developmental Neurophysiology, Institute of Neuroanatomy, University Medical Center Hamburg-Eppendorf, 20251 Hamburg, Germany

4.4.2 Abstract

Coordinated patterns of electrical activity are critical for the functional maturation of neuronal networks, yet their interrogation has proven difficult in the developing brain. Optogenetic manipulations strongly contributed to the mechanistic understanding of network activation in the adult brain, but difficulties to specifically and reliably express opsins at neonatal age hampered similar interrogation of developing circuits. Here, we introduce a protocol that enables to control the activity of specific neuronal populations by light, starting from early postnatal development. We show that brain area-, layer-, and cell type-specific expression of opsins by in utero electroporation, as exemplified for the medial prefrontal cortex and hippocampus, permits the manipulation of neuronal activity in vitro and in vivo. Both individual and population responses to different patterns of light stimulation are monitored by extracellular multi-site recordings in the medial prefrontal cortex of neonatal mice. The expression of opsins via in utero electroporation provides a flexible approach to disentangle the cellular mechanism underlying early rhythmic network activity, and to elucidate the role of early neuronal activity for brain maturation, as well as its contribution to neurodevelopmental disorders.

4.4.3 Personal contribution

I.L.H.-O. designed the experiments. S.H.B and J.A. developed the protocol and carried out the experiments, S.H.B. and J.A. analyzed the data. I.L.H.-O., S.H.B., J.A. interpreted the data and wrote the manuscript.

5 Discussion

It has been proposed that the oscillatory patterns observed during early development are important for the establishment and maturation of functioning neuronal networks (Hanganu-Opatz, 2010). Recent evidence has revealed that neuropsychiatric disorders such as schizophrenia have a disrupted prefrontal-hippocampal network (Meyer-Lindenberg et al., 2005; Sigurdsson et al., 2010) and disturbances are already present during development, long before clinical symptoms appear (Cannon et al., 2003; Uhlhaas and Singer, 2011; Hartung et al., 2016b). Elucidation of prefrontal-hippocampal network during development is mandatory as it opens up new opportunities for diagnosis and treatment of patients with neuropsychiatric disorders.

We established a protocol using IUE for area-, layer, and cell-type specific expression of optogenetic tools in the neonatal mouse brain *in vivo*. This enabled the causal investigation of the relationship between specific neuronal populations and their role in the generation of oscillatory activity (**Bitzenhofer et al., 2017; Bitzenhofer et al., *accepted*; Ahlbeck et al., *in preparation***). By combining optogenetic stimulations of excitatory neurons in either layer II/III or layer V/VI of PL with electrophysiological recordings of LFP and SUA during early development, we show that excitation of pyramidal neurons in layer II/III entrains beta-gamma activity whereas excitation of pyramidal neurons in layer V/VI causes non-specific entrainment **(Bitzenhofer et al., 2017**). We then investigated the structural and functional coupling between PFC and the CA1 area of either dHP or i/vHP in neonatal mice. We found that i/vHP is significantly stronger coupled to PFC than dHP. Furthermore, selective activation of CA1 pyramidal neurons in i/vHP but not dHP strengthen oscillatory coupling by synchrony within prefrontal-hippocampal networks in frequency specific manner (**Ahlbeck et al., *in preparation***).

5.1 Optogenetic manipulation of neonatal neuronal networks

By application of optogenetics it is possible to investigate the causal relationship between specific group of neurons and the entrainment of oscillatory activity at a high temporal and spatial resolution. Optogenetics have been extensively used in the adult brain for the elucidation of specific neuronal populations and their role in sensory processing (Lepousez and Lledo, 2013; Olcese et al., 2013), memory

(Johansen et al., 2014; Liu et al., 2014; Spellman et al., 2015) and neuropsychiatric disorders (Tye and Deisseroth, 2012; Steinberg et al., 2015).

5.1.1 Area-, layer- and cell-type specific targeting during development

The application of optogenetics for the investigation of the neonatal brain activity have been hindered by the lack of methods for selectively targeting specific groups of neurons already shortly after birth. The most common used methods for expressing optogenetic tools in the adult brain are viral transduction and genetically modified mouse lines, both techniques requiring cell-type specific promoters (Yizhar et al., 2011; Madisen et al., 2015). During early development many promoters undergo qualitative and quantitative changes that can lead to unspecific expression of the optogenetic tool (Sanchez et al., 1992; Kwakowsky et al., 2007; Wang et al., 2013). Most viruses require at least 10-14 days until reliable transfection which makes them redundant for the investigation of neuronal activity during the neonatal period (Zhang et al., 2010) and the fast-acting viruses have been reported to reach toxic levels after a brief period (Klein et al., 2006). We tested two fast-expressing viruses, adeno-associated virus 8 and canine adenovirus, which have been reported to lead to expression within 2-6 days. Both viruses led to weak and insufficient expression at P8-P10 following injection at P1 (**Bitzenhofer et al., 2017**). Application of transgenic lines is hindered by the lack of area-specificity and the number of reporter lines with optogenetic tools. Even though area-specificity can be achieved by limiting the area of light illumination it does not prevent the activation of projections passing through that region. Additionally, maintenance of transgenic lines is costly and time-consuming. A third and rarely applied method is IUE that allows for area-, layer- and cell-type specific expression already at birth. It has been extensively used for the investigation of neuronal migration during development (Tabata and Nakajima, 2001; Borrell et al., 2005; Page et al., 2017). This makes IUE a superior method for the selective expression of optogenetic tools during early development.

We developed a protocol using IUE for application of optogenetics in investigation of neuronal activity in the neonatal brain *in vivo*. We first tested three different promoters, synapsin, eukaryotic translation elongation factor 1 alpha (EF1α) or cytomegalovirus enhancer fused to chicken beta-actin (CAG) in achieving expression of optogenetic tools in neonatal mice. While the promoters synapsin and

EF1α only achieved sparse expression, the CAG promoter led to a strong robust expression that was confirmed functional by *in vitro* patch-clamp recordings (**Bitzenhofer et al., 2017; Bitzenhofer et al., *accepted***). To confirm area-, layer, and cell-type specific expression we performed immunohistochemistry analysis of the transfected animals. Within PFC about 35 % of the pyramidal neurons confined in either layer II/III or layer V/VI was transfected (**Bitzenhofer et al., 2017**) whereas about 20 % hippocampal CA1 pyramidal neurons was transfected (**Ahlbeck et al., *in preparation***).

5.1.2 Entrainment of neuronal activity using optogenetics during development

Electrophysiological recordings of LFP and SUA in combination with light-stimulation of transfected neurons using multi-site silicon probes were performed at P8 to P10 *in vivo.* We observed that the common used light pulses induced large artifacts in the region stimulated making analysis of local LFP impossible. We therefore characterized three different types of light patterns, pulsed, sinusoidal and ramp stimulations **(Bitzenhofer et al., 2017; Bitzenhofer et al., *accepted***). We found that both pulsed and sinusoidal light stimulation induced large peaks in the power spectrum at the frequency stimulated, with pulsed stimulation additionally having harmonics due to its non-sinusoidal shape of the light pattern used. Further elucidation of this effect by comparing it before and after a lethal injection of ketamine-xylazine, we found that it consisted of two components, a fast, low amplitude photoelectric artifact and a second slow, large amplitude deflection that was only present in animals expressing the ChR2(ET/TC) representing opening of the ChR2. Even after reduction of the photoelectric artifact by aligning the optical fiber away from the recording sites or using glass capillary electrodes the second slow deflection will always be present, as it is the physiological response of opening and closing channels (Cardin et al., 2010; **Bitzenhofer et al., *accepted***). As we wished to interrogate the local generation of network activity in the PFC during stimulation we applied a ramp stimulation that did not have the deflections as reported for pulsed and sinusoidal stimulation. Ramp stimulation does not force a specific rhythm but rather leads the neuronal population to generate its own through driving the neurons at their intrinsic or preferred rhythm (Adesnik and Scanziani, 2010; Bitzenhofer et al., 2017). Therefore, ramp stimulation is preferential when studying the role of a specific group of neurons in generating local network activity.

In the second part, we investigated the contribution of CA1 pyramidal neurons in either dHP or i/vHP for the generation of local activity in the PFC. For this, the deflections induced locally in CA1 by pulsed stimulation could be ignored and the frequency-specific response in PFC could be investigated as the photoelectric artifact did not reach the second recording electrode (**Ahlbeck et al., *in preparation***).

5.2 Layer-specific contribution of pyramidal neurons in the developing prefrontal cortex

Coordinated and synchronous interplay of excitatory pyramidal and inhibitory interneurons give rise to the distinct oscillatory activity critical for various behavioral and cognitive tasks (Buzsaki and Draguhn, 2004; Harris and Mrsic-Flogel, 2013). In the adult brain, cell-type specific activation using optogenetics have provided causal evidence for underlying cellular mechanisms in generating oscillatory activity (Cardin et al., 2009; Adesnik and Scanziani, 2010; Siegle et al., 2014). Similar understanding of the cellular substrates underlying the generation of oscillatory activity in the developing cortex is missing. Adult gamma oscillations in cortical regions have been found to be dependent on pyramidal neurons in layer II/III that spreads to deeper layers (Adesnik and Scanziani, 2010). As connections from superficial layer pyramidal neurons to deeper layer interneurons is established towards the end of the first postnatal week (Zhang, 2004; Anastasiades and Butt, 2012; Anastasiades et al., 2016), beta-gamma oscillatory activity spread between layers in the PFC (Cichon et al., 2014) and PFC layer V/VI interneurons receive glutamatergic inputs locked to beta rhythm (Bitzenhofer et al., 2015), suggests that layer II/III pyramidal neurons might be critical for the entrainment of beta-gamma rhythms in the developing PFC.

We expressed the highly efficient light sensitive channelrhodopsin ChR2(ET/TC) specifically to pyramidal neurons confined in either layer II/III or layer V/VI of the PFC. Upon light stimulation, we found that neurons in layer II/III concentrated their firingrate around 16 Hz whereas neurons in layer V/VI did not show any preferred firingrate. This layer specific difference was further confirmed when investigating the induced oscillatory activity. Whereas stimulation of layer V/VI pyramidal neurons caused a broad unspecific increase of oscillatory activity at all frequencies, stimulation of layer II/III pyramidal neurons resulted in confined entrainment of beta-gamma activity that spread to layer V/VI. These results indicate

layer II/III pyramidal neurons to be a key element in the generation of beta-gamma rhythms in PFC during the neonatal period (**Bitzenhofer et al., 2017**).

The different responses upon exciting pyramidal neurons in either layer II/III or layer V/VI most likely represent different wiring schemes. As previously mentioned, layer II/III pyramidal neurons form local intra- and interlaminar connections in the adult brain (Adesnik and Scanziani, 2010) that are also formed and functional during the developmental period (Anastasiades and Butt, 2012; Anastasiades et al., 2016) whereas layer V/VI pyramidal neurons are primarily output neurons that project to other brain regions (Adesnik and Scanziani, 2010; Harris and Shepherd, 2015). In accordance with this, we found that the beta-gamma induced activity in layer II/III pyramidal neurons spread to layer V/VI, whereas the broadband activity induced by activating layer V/VI pyramidal neurons did not spread to layer II/III.

Adult gamma oscillations in cortical regions have been shown to emerge from feedforward inhibitory networks involving fast-spiking PV-positive interneurons (Bartos et al., 2007; Cardin et al., 2009; Buzsaki and Wang, 2012; Womelsdorf et al., 2014). A similar mechanism might underlie the entrainment of beta-gamma activity during development. Despite the lack of PV-positive interneurons, fast-spiking interneurons innervating pyramidal neurons perisomatically have been identified during early development (Sanchez et al., 1992; Chattopadhyaya et al., 2004). As functional coupling between interneurons and pyramidal neurons in PFC emerge during the postnatal period (Yang et al., 2014), a similar feedforward inhibitory network mechanisms for entrainment of beta-gamma rhythms might also be present during development. However, as GABAergic interneurons have been found to be excitatory during the developmental period (Rheims et al., 2008; Ben-Ari, 2014), a different mechanism might underlie the entrainment of oscillatory rhythms than via feed-forward inhibition networks. Recent *in vivo* studies in the developing cortex found that GABAergic interneurons do have an inhibitory effect on network activity by controlling the spatial spread of spindle bursts, possibly through shunting inhibition (Minlebaev et al., 2007; Kirmse et al., 2015). Alternatively, as numerous neurons are connected through gap junctions during the first 2 postnatal weeks (Peinado et al., 1993) and the fact that electrically coupled pairs of interneurons can give rise to gamma oscillations (Beierlein et al., 2000; Hormuzdi et al., 2001; Mancilla et al.,

2007), a gap junction mediated mechanism could give rise to the beta-gamma activity during development. Application of gap junction blockers show a weak increase in the occurrence of spindle bursts activity during development (Hanganu et al., 2006; Minlebaev et al., 2007; Yang et al., 2009) but its effect on the spectral composition of early activity were not tested. Further characterization of inhibitory neurons and their role during the neonatal period is needed to clarify their purpose for the entrainment of activity during development.

As targeting interneurons by IUE only provide a very sparse transfection, alternative methods is needed if one wish to apply optogenetics for their interrogation during development (Borrell et al., 2005). This is further complicated by the lack of expression markers such as PV (Sanchez et al., 1992) making many virus and transgenic lines obsolete. Recently, new markers such as distalless homeobox 5 and 6 (Dlx5/6) have been found that enable transfection of interneurons already during embryonic development by using transgenetic lines (Taniguchi et al., 2011; Dimidschstein et al., 2016).

5.3 Role of CA1 pyramidal neurons within the developing prefrontal-hippocampal network

Directed oscillatory coupling within prefrontal-hippocampal networks underlies cognitive processing in adults (Preston and Eichenbaum, 2013; Sigurdsson and Duvarci, 2015). This communication emerges early in life, long before the maturation of mnemonic abilities. Discontinuous hippocampal theta bursts have been proposed to be driving the initial oscillatory entrainment of local prefrontal networks but causal evidence is missing (Brockmann et al., 2011; Bitzenhofer and Hanganu-Opatz, 2014; Hartung et al., 2016a). While the theta coupling within the developing prefrontal-hippocampal network are modulated by GABAergic and cholinergic inputs from the medial septum (Brockmann et al., 2011; Janiesch et al., 2011) it was found to be independent of local GABAergic neurons in i/vHP (Bitzenhofer and Hanganu-Opatz, 2014), leading to the hypothesis that the drive from HP to PFC relies on hippocampal pyramidal neurons. Here, we provide the causal evidence that pyramidal neurons in CA1 area of i/vHP, but not dHP are capable of entraining oscillatory activity in the PFC of neonatal mice (**Ahlbeck et al., *in preparation***).

Previous studies have shown that i/vHP and PFC are coupled during the neonatal period (Brockmann et al., 2011; Bitzenhofer and Hanganu-Opatz, 2014; Hartung et al., 2016a) but the role of dHP was until now not known. In compliance with results from the adult brain we found stronger theta coupling to PFC from i/vHP than dHP during development (Adhikari et al., 2010; O'Neill et al., 2013; Tamura et al., 2016). This is shown by increased coherence, phaselocking and strength of directed interactions for i/vHP and PFC than dHP and PFC. An inherent issue when using LFP for analysis of functional coupling between regions is the risk of false synchrony due to volume conduction throughout the brain. To ensure that the interactions observed is not the result of instantaneous non-specific volume conduction we used the imaginary component of the coherence spectrum excluding any zero time-lag synchronization (Nolte et al., 2004). Furthermore, if volume conduction was contaminating the results one would expect a stronger coherence between regions localized closer to each other. Since we find stronger coupling and strength of directed interactions for i/vHP, a region farther away than dHP, argues that the coupling observed is a physiological feature and not due to volume conduction. Even though dHP is lacking direct projections to PFC it still shows significant theta coupling as seen in the adult brain, most likely through an intermediary brain region such as nucleus reunions of thalamus or entorhinal cortex (Ito et al., 2015; Eichenbaum, 2017). Bi-directional projections between reunions and PFC as well as PFC and i/vHP is already established during the neonatal period (Hartung et al., 2016a). Although the authors did not investigate dHP, projections from dHP to reunions were observed (personal communication), indicating that an anatomical circuit for dHP to communicate with PFC through the reunions is established during the neonatal period.

During development, hippocampal SPWs have been observed to occur in a sequential manner, with muscle twitches leading to spindle burst activity in sensory cortices followed by SPWs in HP (Karlsson et al., 2006; Mohns and Blumberg, 2010). Following separation of sensory inputs to the brainstem or lesion of the parahippocampal connections between sensory cortex and hippocampus, the synchronous order of spindle burst activity and SPWs was disrupted and instead occurred independently of each other (Karlsson et al., 2006; Mohns and Blumberg, 2010). As hippocampal sharpwaves and theta burst activity often co-occur

(Brockmann et al., 2011; Bitzenhofer and Hanganu-Opatz, 2014) we sought to investigate whether a correlation between spindle burst activity in PFC and SPWs in HP is present during development. In line with results from the adult brain, we observe that hippocampal SPWs precedes activity in PFC by ≈100 ms (Siapas and Wilson, 1998; Siapas et al., 2005; Molle et al., 2006; Sirota et al., 2008). We also observed that SPWs originating in i/vHP lead to a larger power and spiking response in PFC than SPWs from dHP indicating that i/vHP is providing a stronger drive on PFC activity. While SPWs is known as a mechanism for memory consolidation by transferring information from HP to the neocortex (Colgin, 2011; Buzsaki, 2015), it is still not clear whether they serve a similar purpose during development or whether instead they are involved in the maturation and refinement of the neuronal networks (Karlsson et al., 2006; Mohns and Blumberg, 2010; Buzsaki, 2015). The neonatal SPW might serve in linking HP and PFC, enabling the induction of activity-dependent plasticity. As LTP is always induced independent of the spike-time during the neonatal period (Feldman et al., 1999; Itami et al., 2016), SPW might serve as a mechanism for synchronizing the firing between i/vHP and PL strengthening their coupling thereby given rise to a functional network enabling the adult memory consolidation. In line with this we observed that spiking activity in both HP and PFC was centered around the peak of a hippocampal SPW.

The cellular substrate underlying the theta communication with in the developing prefrontal-hippocampal network is still unknown. The most likely candidate is the excitatory CA1 pyramidal neurons as depletion of GABAergic interneurons in i/vHP did not affect theta coupling to PFC (Bitzenhofer and Hanganu-Opatz, 2014). To causally investigate whether CA1 neurons in i/vHP are mandatory for the entrainment of PFC we selectively expressed ChR2(ET/TC) to excitatory neurons confined to the CA1 area of dHP and i/vHP by IUE. Timing the firing of pyramidal neurons confined to CA1 area of i/vHP at theta range caused a broad entrainment of oscillatory activity in PFC. This oscillatory entrainment was not observed neither when we stimulated at a frequency below or above theta in i/vHP, stimulated dHP at any frequency, or in our control animals containing no ChR2(ET/TC). These results shows that the rhythmic firing of pyramidal neurons at theta frequency in CA1 area of i/vHP are capable of driving the coupling within the i/vHP-PFC network leading to the emergence of oscillatory activity in PFC.

Interestingly, entrainment of PFC was frequency specific to the light stimulation at 8 Hz, and not to light stimulations at 4 or 16 Hz. Some neurons have been found to exhibit a membrane resonance frequency making them more likely to elicit action potentials when activated at this frequency (Buzsaki, 2002). Both pyramidal neurons and interneurons in PFC receive monosynaptic glutamatergic inputs from i/vHP (Gabbott et al., 2002; Tierney et al., 2004) and paired recordings of both types found that interneurons consistently respond before the pyramidal neurons (Tierney et al., 2004), indicating a local feedforward inhibitory network. As previously mentioned, such a local feedforward inhibitory network is capable of entraining gamma activity in sensory cortices (Swadlow, 2003; Cardin et al., 2009) leading to the speculation that such a network is underlying the hippocampal entrainment of PFC. Recently, an *in vivo* study showed that spike transmission of cortical fast-spiking PV-positive interneurons was enhanced selectively at the theta rhythm (Stark et al., 2013). By optogenetically stimulation using a chirp pattern, a sinusoidal stimulation with increasing frequency, they found that cortical PV-positive interneurons resonate selectively at the theta frequency leading to higher spiking probability when driven at this frequency. Such theta-centered spiking resonance might contribute to the observed frequency-specific entrainment of PFC in our experiments. Activation of the excitatory pyramidal neurons from i/vCA1 specifically at 8 Hz but not 4 or 16 Hz, would lead to feedforward excitation of fast spiking interneurons in PFC at their resonant frequency leading to the entrainment of oscillatory activity by the local feedforward inhibition. Although, as previously mentioned, the contribution of GABAergic interneurons in such a feed-forward network during development is still unclear and further elucidation of the underlying role of interneurons in the emergence of oscillatory activity is needed. One method to elucidate whether fast-spiking interneurons are mandatory for the entrainment of activity PFC during development can be performed by the combined use of transgenic lines and IUE. Expressing two different opsins that have a non-overlapping excitation spectrum allows simultaneous manipulation of two different neuronal groups (Inagaki et al., 2014). Targeting Dlx5/6 positive interneurons through transgenic breeding and following transfecting pyramidal neurons using IUE is possible. This enables the elucidation of the role of interneurons by simultaneously manipulating interneurons and pyramidal neurons with light. This method can be applied both for interrogating

the local generation of activity within PFC as well as the coupling in the prefrontal-hippocampal network.

5.4 Comparison of adult sleep spindles and neonatal spindle bursts

The neonatal spindle bursts is a hallmark of the developing brain and disappears as the brain matures into the adult state (Cirelli and Tononi, 2015; Tiriac and Blumberg, 2016; Yang et al., 2016). Despite having similar features to the adult sleep spindle such as their temporal patterns and the brain regions involved, they still differentiate in their occurrence, spatial distribution and underlying mechanisms, and are believed to be two distinct types of activity (**Lindemann et al., 2016**). A clear difference is the fact that neonatal spindle bursts are present already at birth and disappear towards the end of the second postnatal week, whereas sleep spindles first emerges after the second postnatal week (Gramsbergen, 1976; Cirelli and Tononi, 2015; Yang et al., 2016). These changes might occur due to the maturation of the neuromodulatory system that becomes functional during the postnatal week (Nakamura et al., 1987; Latsari et al., 2002; Reboreda et al., 2007; Janiesch et al., 2011). Another distinct feature is the fact that the neonatal spindle bursts occurs both during sleep and awake stages, and can be evoked by sensory stimulus (Khazipov et al., 2004b; Hanganu et al., 2006; Yang et al., 2009) whereas the adult sleep spindle occur during sleep, a period of where the cortex is decoupled from sensory inputs (Cirelli and Tononi, 2015; Tiriac and Blumberg, 2016). The neonatal spindle burst also has a confined spatial spread of a few columns (Kirmse et al., 2015; Kirmse et al., 2017) whereas sleep spindles spread over large cortical regions (Contreras et al., 1996). As the rules of synaptic plasticity favors LTP during development (Feldman et al., 1999; Itami et al., 2016), one could speculate that spindle bursts are mainly functioning on establishing and refining the neuronal networks, whereas sleep spindles are involved in memory consolidation and homeostatic scaling of synaptic strengths involving the classic rules of synaptic plasticity with spike-time dependent plasticity (Cirelli and Tononi, 2015).

The elucidation of cellular substrates underlying oscillatory activity in the developing prefrontal-hippocampal network is mandatory for our understanding for the ontogeny of cognitive function. Multiple developmental processes such as

neuronal migration, differentiation, axon growth, synapse formation, programmed cell death, and myelination is shaped by neuronal activity (Spitzer, 2002; Heck et al., 2008; De Marco Garcia et al., 2011; Kirkby et al., 2013; Mitew et al., 2016) and early network activity has been shown to be crucial for the maturation and refinement of neuronal networks such as the importance of endogenous generated retinal waves for the development of the visual cortex (Hubel et al., 1977; Huberman et al., 2006) or thalamic interactions for the formation of barrel fields in the somatosensory cortex (Dupont et al., 2006; Kanold and Luhmann, 2010). The prefrontal-hippocampal network is important for cognitive processing (Sigurdsson and Duvarci, 2015; Eichenbaum, 2017) and early network activity has been proposed to shape and refine this network during the developmental period (Brockmann et al., 2011; Bitzenhofer and Hanganu-Opatz, 2014; Hartung et al., 2016a; **Bitzenhofer et al., 2017; Ahlbeck et al., *in preparation***). Disruptions within the developing prefrontal-hippocampal network have shown to affect local network activity within PFC and leads to impairments of cognitive function at juvenile age (Brockmann et al., 2011; Kruger et al., 2012). Various neuropsychiatric disorders such as schizophrenia have been found to have a disrupted prefrontal-hippocampal network (Meyer-Lindenberg et al., 2005; Sigurdsson et al., 2010) that are already present during development (Hartung et al., 2016b; Tamura et al., 2016). Furthermore, the distribution of prefrontal layer II/III pyramidal neurons has been found to be regulated in an activity-dependent manner where altered activity leads to pathological formation of layer II/III as seen in autism and schizophrenia (Page et al., 2017). Whether the disturbances observed in PFC in neuropsychiatric disorders are due to a local malfunction or a disrupted drive from hippocampus could be investigated using the techniques developed here.

Further studies on the role of early network activity for the establishment of neuronal networks is crucial for our understanding of the ontogeny of cognitive function in health and disease leading to possible new ways of detecting disturbances before clinical onset and the development of new therapeutic interventions.

6 Conclusions

Entrainment of neuronal activity within the prefrontal-hippocampal is mandatory for the emergence of later cognitive function. Here we established a protocol that enables area-, cell-type and layer-specific expression of optogenetic tools that enables the dissection of the neural substrates involved in the emergence of oscillatory activity. We show that layer II/III and not layer V/VI pyramidal neurons to be a key element for the entrainment of local beta-gamma oscillations in the neonatal PFC. Furthermore, the roles of dHP and i/vHP in driving PFC activity was characterized. We show that i/vHP is the main contributor for the entrainment of activity in PFC and further show that frequency specific entrainment at theta rhythm of i/vHP CA1 pyramidal neurons leads to entrainment of the neonatal PFC. The established protocol and the results presented here opens up new paths for investigation of network oscillations during development and could further aid our understanding of neurodevelopmental disorders.

7 List of abbreviations

AMPA	α-amino-3-hydroxy-5-methyl-4-isoxazolepropioic acid
CA	Cornu ammonis
CAG	Cytomegalovirus enhancer fused to chicken beta-actin
Cg	Anterior cingulate cortex
ChR2	Channelrhodopsin-2
ChR2(ET/TC)	Channelrhodopsin-2 E123T T159C
DG	Dentata gyrus
dHP	Dorsal hippocampus
Dlx5/6	Distalless homeobox 5 and 6
DNA	Deoxyribonucleic acid
E	Embryonic
EF1α	Eukaryotic translation elongation factor 1 alpha
GABA	γ-aminobutyric acid
HP	Hippocampus
i/vHP	Intermediate-ventral hippocampus
IL	Infralimbic
IUE	*In utero* electroporation
KCC2	Potassium-chloride cotransporter 2
LGE	Lateral ganglionic eminence
LTD	Long-term depression
LTP	Long-term potentiation
MGE	Medial ganglionic eminence
MZ	Marginal zone
NKCC1	Sodium-potassium cotransporter 1
NMDA	N-Methyl-D-aspartic acid
P	Postnatal
PFC	Prefrontal cortex
PL	Prelimbic
PV	Parvalbumin
SOM	Somatostatin
SP	Subplate
SPW	Sharp wave
SUA	Single unit activity
VZ	Ventricular zone

8 Acknowledgements

First of all, I want to thank my supervisor Prof. Dr. Ileana L. Hanganu-Opatz for giving me the opportunity to write my thesis within her working group. I am grateful for her great support and close supervision over my stay. Moreover, I wish to thank my co-authors for their contributions to the studies. I would also like to thank my co-supervisors Prof. Dr. med. Andreas. K. Engel and Prof. Dr. med. Christoph Mulert for their helpful insights and support.

I am grateful for the support I received from my current and former colleagues at the department of developmental neurophysiology during the last 4 years. In particularly, I would like to thank Sebastian H. Bitzenhofer for being my close collaborator and always available for helpful discussions of the results.

Finally I wish to thank my family and my close friends for their loving support, interest and encouragement.

9 References

Adesnik, H., and Scanziani, M. (2010). Lateral competition for cortical space by layer-specific horizontal circuits. *Nature* 464(7292)**,** 1155-1160. doi: 10.1038/nature08935.

Adhikari, A., Topiwala, M.A., and Gordon, J.A. (2010). Synchronized activity between the ventral hippocampus and the medial prefrontal cortex during anxiety. *Neuron* 65(2)**,** 257-269. doi: 10.1016/j.neuron.2009.12.002.

Agster, K.L., and Burwell, R.D. (2009). Cortical efferents of the perirhinal, postrhinal, and entorhinal cortices of the rat. *Hippocampus* 19(12)**,** 1159-1186. doi: 10.1002/hipo.20578.

Ahlbeck, J., Candela, A., Chini, M., Bitzenhofer, S.H., and Hanganu-Opatz, I.L. (in preparation). Intermediate but not dorsal hippocampal CA1 projection neurons drive the oscillatory entrainment of prefrontal circuits in the neonatal mouse.

Amaral, D.G., and Witter, M.P. (1989). The three-dimensional organization of the hippocampal formation: a review of anatomical data. *Neuroscience* 31(3)**,** 571-591.

An, S., Kilb, W., and Luhmann, H.J. (2014). Sensory-evoked and spontaneous gamma and spindle bursts in neonatal rat motor cortex. *J Neurosci* 34(33)**,** 10870-10883. doi: 10.1523/JNEUROSCI.4539-13.2014.

Anastasiades, P.G., and Butt, S.J. (2012). A role for silent synapses in the development of the pathway from layer 2/3 to 5 pyramidal cells in the neocortex. *J Neurosci* 32(38)**,** 13085-13099. doi: 10.1523/JNEUROSCI.1262-12.2012.

Anastasiades, P.G., Marques-Smith, A., Lyngholm, D., Lickiss, T., Raffiq, S., Katzel, D., et al. (2016). GABAergic interneurons form transient layer-specific circuits in early postnatal neocortex. *Nat Commun* 7**,** 10584. doi: 10.1038/ncomms10584.

Ashby, M.C., and Isaac, J.T. (2011). Maturation of a recurrent excitatory neocortical circuit by experience-dependent unsilencing of newly formed dendritic spines. *Neuron* 70(3)**,** 510-521. doi: 10.1016/j.neuron.2011.02.057.

Bartos, M., Vida, I., and Jonas, P. (2007). Synaptic mechanisms of synchronized gamma oscillations in inhibitory interneuron networks. *Nat Rev Neurosci* 8(1)**,** 45-56. doi: 10.1038/nrn2044.

Baumgart, J., and Grebe, N. (2015). C57BL/6-specific conditions for efficient in utero electroporation of the central nervous system. *J Neurosci Methods* 240**,** 116-124. doi: 10.1016/j.jneumeth.2014.11.004.

Beierlein, M., Gibson, J.R., and Connors, B.W. (2000). A network of electrically coupled interneurons drives synchronized inhibition in neocortex. *Nat Neurosci* 3(9)**,** 904-910. doi: 10.1038/78809.

Ben-Ari, Y. (2014). The GABA excitatory/inhibitory developmental sequence: a personal journey. *Neuroscience* 279**,** 187-219. doi: 10.1016/j.neuroscience.2014.08.001.

Benchenane, K., Peyrache, A., Khamassi, M., Tierney, P.L., Gioanni, Y., Battaglia, F.P., et al. (2010). Coherent theta oscillations and reorganization of spike timing in the hippocampal- prefrontal network upon learning. *Neuron* 66(6)**,** 921-936. doi: 10.1016/j.neuron.2010.05.013.

Berndt, A., Schoenenberger, P., Mattis, J., Tye, K.M., Deisseroth, K., Hegemann, P., et al. (2011). High-efficiency channelrhodopsins for fast neuronal stimulation at low light levels. *Proc Natl Acad Sci U S A* 108(18)**,** 7595-7600. doi: 10.1073/pnas.1017210108.

Bitzenhofer, S.H., Ahlbeck, J., and Hanganu-Opatz, I.L. (accepted). Optogenetic manipulation of neonatal neuronal networks.

Bitzenhofer, S.H., Ahlbeck, J., Wolff, A., Wiegert, J.S., Gee, C.E., Oertner, T.G., et al. (2017). Layer-specific optogenetic activation of pyramidal neurons causes beta-gamma entrainment of neonatal networks. *Nat Commun* 8**,** 14563. doi: 10.1038/ncomms14563.

Bitzenhofer, S.H., and Hanganu-Opatz, I.L. (2014). Oscillatory coupling within neonatal prefrontal-hippocampal networks is independent of selective removal of GABAergic neurons in the hippocampus. *Neuropharmacology* 77**,** 57-67. doi: 10.1016/j.neuropharm.2013.09.007.

Bitzenhofer, S.H., Sieben, K., Siebert, K.D., Spehr, M., and Hanganu-Opatz, I.L. (2015). Oscillatory activity in developing prefrontal networks results from theta-gamma-modulated synaptic inputs. *Cell Rep* 11(3)**,** 486-497. doi: 10.1016/j.celrep.2015.03.031.

Borrell, V., Yoshimura, Y., and Callaway, E.M. (2005). Targeted gene delivery to telencephalic inhibitory neurons by directional in utero electroporation. *J Neurosci Methods* 143(2)**,** 151-158. doi: 10.1016/j.jneumeth.2004.09.027.

Boyden, E.S., Zhang, F., Bamberg, E., Nagel, G., and Deisseroth, K. (2005). Millisecond-timescale, genetically targeted optical control of neural activity. *Nat Neurosci* 8(9)**,** 1263-1268. doi: 10.1038/nn1525.

Brockmann, M.D., Poschel, B., Cichon, N., and Hanganu-Opatz, I.L. (2011). Coupled oscillations mediate directed interactions between prefrontal cortex and hippocampus of the neonatal rat. *Neuron* 71(2)**,** 332-347. doi: 10.1016/j.neuron.2011.05.041.

Burwell, R.D., and Amaral, D.G. (1998). Cortical afferents of the perirhinal, postrhinal, and entorhinal cortices of the rat. *The Journal of Comparative Neurology* 398(2)**,** 179-205. doi: 10.1002/(sici)1096-9861(19980824)398:2<179::aid-cne3>3.0.co;2-y.

Buzsaki, G. (2002). Theta oscillations in the hippocampus. *Neuron* 33(3)**,** 325-340.

Buzsaki, G. (2015). Hippocampal sharp wave-ripple: A cognitive biomarker for episodic memory and planning. *Hippocampus*. doi: 10.1002/hipo.22488.

Buzsaki, G., Anastassiou, C.A., and Koch, C. (2012). The origin of extracellular fields and currents--EEG, ECoG, LFP and spikes. *Nat Rev Neurosci* 13(6)**,** 407-420. doi: 10.1038/nrn3241.

Buzsaki, G., and Draguhn, A. (2004). Neuronal oscillations in cortical networks. *Science* 304(5679)**,** 1926-1929. doi: 10.1126/science.1099745.

Buzsáki, G., Lai-Wo S, L., and Vanderwolf, C.H. (1983). Cellular bases of hippocampal EEG in the behaving rat. *Brain Research Reviews* 6(2)**,** 139-171. doi: 10.1016/0165-0173(83)90037-1.

Buzsaki, G., and Silva, F.L. (2012). High frequency oscillations in the intact brain. *Prog Neurobiol* 98(3)**,** 241-249. doi: 10.1016/j.pneurobio.2012.02.004.

Buzsaki, G., and Wang, X.J. (2012). Mechanisms of gamma oscillations. *Annu Rev Neurosci* 35**,** 203-225. doi: 10.1146/annurev-neuro-062111-150444.

Bystron, I., Blakemore, C., and Rakic, P. (2008). Development of the human cerebral cortex: Boulder Committee revisited. *Nat Rev Neurosci* 9(2)**,** 110-122. doi: 10.1038/nrn2252.

Cannon, T.D., van Erp, T.G.M., Bearden, C.E., Loewy, R., Thompson, P., Toga, A.W., et al. (2003). Early and late neurodevelopmental influences in the prodrome to schizophrenia, contributions of genes, environment, and their interactions. *Schizophrenia Bulletin* 29(4)**,** 653-669.

Cardin, J.A., Carlen, M., Meletis, K., Knoblich, U., Zhang, F., Deisseroth, K., et al. (2009). Driving fast-spiking cells induces gamma rhythm and controls sensory responses. *Nature* 459(7247)**,** 663-667. doi: 10.1038/nature08002.

Cardin, J.A., Carlen, M., Meletis, K., Knoblich, U., Zhang, F., Deisseroth, K., et al. (2010). Targeted optogenetic stimulation and recording of neurons in vivo using cell-type-specific expression of Channelrhodopsin-2. *Nat Protoc* 5(2)**,** 247-254. doi: 10.1038/nprot.2009.228.

Chattopadhyaya, B., Di Cristo, G., Higashiyama, H., Knott, G.W., Kuhlman, S.J., Welker, E., et al. (2004). Experience and activity-dependent maturation of perisomatic GABAergic innervation in primary visual cortex during a postnatal critical period. *J Neurosci* 24(43)**,** 9598-9611. doi: 10.1523/JNEUROSCI.1851-04.2004.

Chow, B.Y., Han, X., Dobry, A.S., Qian, X., Chuong, A.S., Li, M., et al. (2010). High-performance genetically targetable optical neural silencing by light-driven proton pumps. *Nature* 463(7277)**,** 98-102. doi: 10.1038/nature08652.

Cichon, N.B., Denker, M., Grun, S., and Hanganu-Opatz, I.L. (2014). Unsupervised classification of neocortical activity patterns in neonatal and pre-juvenile rodents. *Front Neural Circuits* 8**,** 50. doi: 10.3389/fncir.2014.00050.

Cirelli, C., and Tononi, G. (2015). Cortical development, electroencephalogram rhythms, and the sleep/wake cycle. *Biol Psychiatry* 77(12)**,** 1071-1078. doi: 10.1016/j.biopsych.2014.12.017.

Colgin, L.L. (2011). Oscillations and hippocampal-prefrontal synchrony. *Curr Opin Neurobiol* 21(3), 467-474. doi: 10.1016/j.conb.2011.04.006.

Colgin, L.L. (2016). Rhythms of the hippocampal network. *Nat Rev Neurosci* 17(4), 239-249. doi: 10.1038/nrn.2016.21.

Contreras, D., Destexhe, A., Sejnowski, T.J., and Steriade, M. (1996). Control of Spatiotemporal Coherence of a Thalamic Oscillation by Corticothalamic Feedback. *Science* 274(5288), 771-774. doi: 10.1126/science.274.5288.771.

Csicsvari, J., Hirase, H., Czurko, A., Mamiya, A., and Buzsaki, G. (1999). Fast network oscillations in the hippocampal CA1 region of the behaving rat. *J Neurosci* 19(16), RC20.

De Marco Garcia, N.V., Karayannis, T., and Fishell, G. (2011). Neuronal activity is required for the development of specific cortical interneuron subtypes. *Nature* 472(7343), 351-355. doi: 10.1038/nature09865.

Dehorter, N., Vinay, L., Hammond, C., and Ben-Ari, Y. (2012). Timing of developmental sequences in different brain structures: physiological and pathological implications. *Eur J Neurosci* 35(12), 1846-1856. doi: 10.1111/j.1460-9568.2012.08152.x.

Dimidschstein, J., Chen, Q., Tremblay, R., Rogers, S.L., Saldi, G.A., Guo, L., et al. (2016). A viral strategy for targeting and manipulating interneurons across vertebrate species. *Nat Neurosci* 19(12), 1743-1749. doi: 10.1038/nn.4430.

Dolleman-van Der Weel, M.J., and Witter, M.P. (1996). Projections from the nucleus reuniens thalami to the entorhinal cortex, hippocampal field CA1, and the subiculum in the rat arise from different populations of neurons. *The Journal of Comparative Neurology* 364(4), 637-650. doi: 10.1002/(sici)1096-9861(19960122)364:4<637::aid-cne3>3.0.co;2-4.

Dupont, E., Hanganu, I.L., Kilb, W., Hirsch, S., and Luhmann, H.J. (2006). Rapid developmental switch in the mechanisms driving early cortical columnar networks. *Nature* 439(7072), 79-83. doi: 10.1038/nature04264.

Eichenbaum, H. (2017). Prefrontal-hippocampal interactions in episodic memory. *Nat Rev Neurosci*. doi: 10.1038/nrn.2017.74.

Engel, A.K., Fries, P., and Singer, W. (2001). Dynamic predictions: oscillations and synchrony in top-down processing. *Nat Rev Neurosci* 2(10), 704-716. doi: 10.1038/35094565.

Feldman, D.E., Nicoll, R.A., and Malenka, R.C. (1999). Synaptic plasticity at thalamocortical synapses in developing rat somatosensory cortex: LTP, LTD, and silent synapses. *Journal of Neurobiology* 41(1), 92-101. doi: 10.1002/(sici)1097-4695(199910)41:1<92::aid-neu12>3.0.co;2-u.

Freund, T.F., and Antal, M. (1988). GABA-containing neurons in the septum control inhibitory interneurons in the hippocampus. *Nature* 336(6195), 170-173. doi: 10.1038/336170a0.

Fries, P. (2015). Rhythms for Cognition: Communication through Coherence. *Neuron* 88(1), 220-235. doi: 10.1016/j.neuron.2015.09.034.

Frotscher, M. (1998). Cajal-Retzius cells, Reelin, and the formation of layers. *Curr Opin Neurobiol* 8(5), 570-575.

Gabbott, P., Headlam, A., and Busby, S. (2002). Morphological evidence that CA1 hippocampal afferents monosynaptically innervate PV-containing neurons and NADPH-diaphorase reactive cells in the medial prefrontal cortex (Areas 25/32) of the rat. *Brain Research* 946(2), 314-322. doi: 10.1016/s0006-8993(02)02487-3.

Goutagny, R., Jackson, J., and Williams, S. (2009). Self-generated theta oscillations in the hippocampus. *Nat Neurosci* 12(12), 1491-1493. doi: 10.1038/nn.2440.

Gradinaru, V., Zhang, F., Ramakrishnan, C., Mattis, J., Prakash, R., Diester, I., et al. (2010). Molecular and cellular approaches for diversifying and extending optogenetics. *Cell* 141(1), 154-165. doi: 10.1016/j.cell.2010.02.037.

Gramsbergen, A. (1976). The development of the EEG in the rat. *Dev Psychobiol* 9(6), 501-515. doi: 10.1002/dev.420090604.

Hack, I., Bancila, M., Loulier, K., Carroll, P., and Cremer, H. (2002). Reelin is a detachment signal in tangential chain-migration during postnatal neurogenesis. *Nat Neurosci* 5(10)**,** 939-945. doi: 10.1038/nn923.

Han, X., Chow, B.Y., Zhou, H., Klapoetke, N.C., Chuong, A., Rajimehr, R., et al. (2011). A high-light sensitivity optical neural silencer: development and application to optogenetic control of non-human primate cortex. *Front Syst Neurosci* 5**,** 18. doi: 10.3389/fnsys.2011.00018.

Hanganu-Opatz, I.L. (2010). Between molecules and experience: role of early patterns of coordinated activity for the development of cortical maps and sensory abilities. *Brain Res Rev* 64(1)**,** 160-176. doi: 10.1016/j.brainresrev.2010.03.005.

Hanganu, I.L., Ben-Ari, Y., and Khazipov, R. (2006). Retinal waves trigger spindle bursts in the neonatal rat visual cortex. *J Neurosci* 26(25)**,** 6728-6736. doi: 10.1523/JNEUROSCI.0752-06.2006.

Hanganu, I.L., Kilb, W., and Luhmann, H.J. (2001). Spontaneous synaptic activity of subplate neurons in neonatal rat somatosensory cortex. *Cereb Cortex* 11(5)**,** 400-410. doi: 10.1093/cercor/11.5.400.

Hanganu, I.L., Kilb, W., and Luhmann, H.J. (2002). Functional synaptic projections onto subplate neurons in neonatal rat somatosensory cortex. *J Neurosci* 22(16)**,** 7165-7176. doi: 20026716.

Hanganu, I.L., Staiger, J.F., Ben-Ari, Y., and Khazipov, R. (2007). Cholinergic modulation of spindle bursts in the neonatal rat visual cortex in vivo. *J Neurosci* 27(21)**,** 5694-5705. doi: 10.1523/JNEUROSCI.5233-06.2007.

Harris, K.D., and Mrsic-Flogel, T.D. (2013). Cortical connectivity and sensory coding. *Nature* 503(7474)**,** 51-58. doi: 10.1038/nature12654.

Harris, K.D., and Shepherd, G.M. (2015). The neocortical circuit: themes and variations. *Nat Neurosci* 18(2)**,** 170-181. doi: 10.1038/nn.3917.

Hartung, H., Brockmann, M.D., Poschel, B., De Feo, V., and Hanganu-Opatz, I.L. (2016a). Thalamic and Entorhinal Network Activity Differently Modulates the Functional Development of Prefrontal-Hippocampal Interactions. *Journal of Neuroscience* 36(13)**,** 3676-3690. doi: 10.1523/jneurosci.3232-15.2016.

Hartung, H., Cichon, N., De Feo, V., Riemann, S., Schildt, S., Lindemann, C., et al. (2016b). From Shortage to Surge: A Developmental Switch in Hippocampal-Prefrontal Coupling in a Gene-Environment Model of Neuropsychiatric Disorders. *Cereb Cortex*. doi: 10.1093/cercor/bhw274.

Hartwich, K., Pollak, T., and Klausberger, T. (2009). Distinct firing patterns of identified basket and dendrite-targeting interneurons in the prefrontal cortex during hippocampal theta and local spindle oscillations. *J Neurosci* 29(30)**,** 9563-9574. doi: 10.1523/JNEUROSCI.1397-09.2009.

Hayashi, K., Kubo, K., Kitazawa, A., and Nakajima, K. (2015). Cellular dynamics of neuronal migration in the hippocampus. *Front Neurosci* 9**,** 135. doi: 10.3389/fnins.2015.00135.

Heck, N., Golbs, A., Riedemann, T., Sun, J.J., Lessmann, V., and Luhmann, H.J. (2008). Activity-dependent regulation of neuronal apoptosis in neonatal mouse cerebral cortex. *Cereb Cortex* 18(6)**,** 1335-1349. doi: 10.1093/cercor/bhm165.

Heidbreder, C.A., and Groenewegen, H.J. (2003). The medial prefrontal cortex in the rat: evidence for a dorso-ventral distinction based upon functional and anatomical characteristics. *Neuroscience & Biobehavioral Reviews* 27(6)**,** 555-579. doi: 10.1016/j.neubiorev.2003.09.003.

Hormuzdi, S.G., Pais, I., LeBeau, F.E.N., Towers, S.K., Rozov, A., Buhl, E.H., et al. (2001). Impaired Electrical Signaling Disrupts Gamma Frequency Oscillations in Connexin 36-Deficient Mice. *Neuron* 31(3)**,** 487-495. doi: 10.1016/s0896-6273(01)00387-7.

Hubel, D.H., Wiesel, T.N., and LeVay, S. (1977). Plasticity of Ocular Dominance Columns in Monkey Striate Cortex. *Philosophical Transactions of the Royal Society B: Biological Sciences* 278(961)**,** 377-409. doi: 10.1098/rstb.1977.0050.

Huberman, A.D., Speer, C.M., and Chapman, B. (2006). Spontaneous retinal activity mediates development of ocular dominance columns and binocular receptive fields in v1. *Neuron* 52(2), 247-254. doi: 10.1016/j.neuron.2006.07.028.

Hyman, J.M., Zilli, E.A., Paley, A.M., and Hasselmo, M.E. (2005). Medial prefrontal cortex cells show dynamic modulation with the hippocampal theta rhythm dependent on behavior. *Hippocampus* 15(6), 739-749. doi: 10.1002/hipo.20106.

Inagaki, H.K., Jung, Y., Hoopfer, E.D., Wong, A.M., Mishra, N., Lin, J.Y., et al. (2014). Optogenetic control of Drosophila using a red-shifted channelrhodopsin reveals experience-dependent influences on courtship. *Nat Methods* 11(3), 325-332. doi: 10.1038/nmeth.2765.

Isaac, J.T., Crair, M.C., Nicoll, R.A., and Malenka, R.C. (1997). Silent synapses during development of thalamocortical inputs. *Neuron* 18(2), 269-280.

Itami, C., Huang, J.Y., Yamasaki, M., Watanabe, M., Lu, H.C., and Kimura, F. (2016). Developmental Switch in Spike Timing-Dependent Plasticity and Cannabinoid-Dependent Reorganization of the Thalamocortical Projection in the Barrel Cortex. *J Neurosci* 36(26), 7039-7054. doi: 10.1523/JNEUROSCI.4280-15.2016.

Ito, H.T., Zhang, S.J., Witter, M.P., Moser, E.I., and Moser, M.B. (2015). A prefrontal-thalamo-hippocampal circuit for goal-directed spatial navigation. *Nature* 522(7554), 50-55. doi: 10.1038/nature14396.

Janiesch, P.C., Kruger, H.S., Poschel, B., and Hanganu-Opatz, I.L. (2011). Cholinergic control in developing prefrontal-hippocampal networks. *J Neurosci* 31(49), 17955-17970. doi: 10.1523/JNEUROSCI.2644-11.2011.

Jay, T.M., Glowinski, J., and Thierry, A.M. (1989). Selectivity of the hippocampal projection to the prelimbic area of the prefrontal cortex in the rat. *Brain Res* 505(2), 337-340.

Jay, T.M., Thierry, A.-M., Wiklund, L., and Glowinski, J. (1992). Excitatory Amino Acid Pathway from the Hippocampus to the Prefrontal Cortex. Contribution of AMPA Receptors in Hippocampo-prefrontal Cortex Transmission. *European Journal of Neuroscience* 4(12), 1285-1295. doi: 10.1111/j.1460-9568.1992.tb00154.x.

Johansen, J.P., Diaz-Mataix, L., Hamanaka, H., Ozawa, T., Ycu, E., Koivumaa, J., et al. (2014). Hebbian and neuromodulatory mechanisms interact to trigger associative memory formation. *Proc Natl Acad Sci U S A* 111(51), E5584-5592. doi: 10.1073/pnas.1421304111.

Jones, M.W., and Wilson, M.A. (2005). Theta rhythms coordinate hippocampal-prefrontal interactions in a spatial memory task. *PLoS Biol* 3(12), e402. doi: 10.1371/journal.pbio.0030402.

Kanold, P.O., and Luhmann, H.J. (2010). The subplate and early cortical circuits. *Annu Rev Neurosci* 33, 23-48. doi: 10.1146/annurev-neuro-060909-153244.

Karlsson, K.A., Mohns, E.J., di Prisco, G.V., and Blumberg, M.S. (2006). On the co-occurrence of startles and hippocampal sharp waves in newborn rats. *Hippocampus* 16(11), 959-965. doi: 10.1002/hipo.20224.

Karlsson, K.A.E., and Blumberg, M.S. (2003). Hippocampal theta in the newborn rat is revealed under conditions that promote REM sleep. *Journal of Neuroscience* 23(4), 1114-1118.

Katz, L.C., and Shatz, C.J. (1996). Synaptic Activity and the Construction of Cortical Circuits. *Science* 274(5290), 1133-1138. doi: 10.1126/science.274.5290.1133.

Khazipov, R., Khalilov, I., Tyzio, R., Morozova, E., Ben-Ari, Y., and Holmes, G.L. (2004a). Developmental changes in GABAergic actions and seizure susceptibility in the rat hippocampus. *Eur J Neurosci* 19(3), 590-600.

Khazipov, R., and Luhmann, H.J. (2006). Early patterns of electrical activity in the developing cerebral cortex of humans and rodents. *Trends Neurosci* 29(7), 414-418. doi: 10.1016/j.tins.2006.05.007.

Khazipov, R., Sirota, A., Leinekugel, X., Holmes, G.L., Ben-Ari, Y., and Buzsaki, G. (2004b). Early motor activity drives spindle bursts in the developing somatosensory cortex. *Nature* 432(7018), 758-761. doi: 10.1038/nature03132.

Kirkby, L.A., Sack, G.S., Firl, A., and Feller, M.B. (2013). A role for correlated spontaneous activity in the assembly of neural circuits. *Neuron* 80(5)**,** 1129-1144. doi: 10.1016/j.neuron.2013.10.030.

Kirmse, K., Hubner, C.A., Isbrandt, D., Witte, O.W., and Holthoff, K. (2017). GABAergic Transmission during Brain Development: Multiple Effects at Multiple Stages. *Neuroscientist***,** 1073858417701382. doi: 10.1177/1073858417701382.

Kirmse, K., Kummer, M., Kovalchuk, Y., Witte, O.W., Garaschuk, O., and Holthoff, K. (2015). GABA depolarizes immature neurons and inhibits network activity in the neonatal neocortex in vivo. *Nat Commun* 6**,** 7750. doi: 10.1038/ncomms8750.

Klein, R.L., Dayton, R.D., Leidenheimer, N.J., Jansen, K., Golde, T.E., and Zweig, R.M. (2006). Efficient neuronal gene transfer with AAV8 leads to neurotoxic levels of tau or green fluorescent proteins. *Mol Ther* 13(3)**,** 517-527. doi: 10.1016/j.ymthe.2005.10.008.

Kruger, H.S., Brockmann, M.D., Salamon, J., Ittrich, H., and Hanganu-Opatz, I.L. (2012). Neonatal hippocampal lesion alters the functional maturation of the prefrontal cortex and the early cognitive development in pre-juvenile rats. *Neurobiol Learn Mem* 97(4)**,** 470-481. doi: 10.1016/j.nlm.2012.04.001.

Kvitsiani, D., Ranade, S., Hangya, B., Taniguchi, H., Huang, J.Z., and Kepecs, A. (2013). Distinct behavioural and network correlates of two interneuron types in prefrontal cortex. *Nature* 498(7454)**,** 363-366. doi: 10.1038/nature12176.

Kwakowsky, A., Schwirtlich, M., Zhang, Q., Eisenstat, D.D., Erdelyi, F., Baranyi, M., et al. (2007). GAD isoforms exhibit distinct spatiotemporal expression patterns in the developing mouse lens: correlation with Dlx2 and Dlx5. *Dev Dyn* 236(12)**,** 3532-3544. doi: 10.1002/dvdy.21361.

Lahtinen, H., Palva, J.M., Sumanen, S., Voipio, J., Kaila, K., and Taira, T. (2002). Postnatal development of rat hippocampal gamma rhythm in vivo. *J Neurophysiol* 88(3)**,** 1469-1474.

Latsari, M., Dori, I., Antonopoulos, J., Chiotelli, M., and Dinopoulos, A. (2002). Noradrenergic innervation of the developing and mature visual and motor cortex of the rat brain: a light and electron microscopic immunocytochemical analysis. *J Comp Neurol* 445(2)**,** 145-158.

Leinekugel, X., Khazipov, R., Cannon, R., Hirase, H., Ben-Ari, Y., and Buzsaki, G. (2002). Correlated bursts of activity in the neonatal hippocampus in vivo. *Science* 296(5575)**,** 2049-2052. doi: 10.1126/science.1071111.

Lepousez, G., and Lledo, P.M. (2013). Odor discrimination requires proper olfactory fast oscillations in awake mice. *Neuron* 80(4)**,** 1010-1024. doi: 10.1016/j.neuron.2013.07.025.

Lindemann, C., Ahlbeck, J., Bitzenhofer, S.H., and Hanganu-Opatz, I.L. (2016). Spindle Activity Orchestrates Plasticity during Development and Sleep. *Neural Plast* 2016**,** 5787423. doi: 10.1155/2016/5787423.

Liu, X., Ramirez, S., Redondo, R.L., and Tonegawa, S. (2014). Identification and Manipulation of Memory Engram Cells. *Cold Spring Harb Symp Quant Biol* 79**,** 59-65. doi: 10.1101/sqb.2014.79.024901.

Madisen, L., Garner, A.R., Shimaoka, D., Chuong, A.S., Klapoetke, N.C., Li, L., et al. (2015). Transgenic mice for intersectional targeting of neural sensors and effectors with high specificity and performance. *Neuron* 85(5)**,** 942-958. doi: 10.1016/j.neuron.2015.02.022.

Maingret, N., Girardeau, G., Todorova, R., Goutierre, M., and Zugaro, M. (2016). Hippocampo-cortical coupling mediates memory consolidation during sleep. *Nat Neurosci*. doi: 10.1038/nn.4304.

Mancilla, J.G., Lewis, T.J., Pinto, D.J., Rinzel, J., and Connors, B.W. (2007). Synchronization of electrically coupled pairs of inhibitory interneurons in neocortex. *J Neurosci* 27(8)**,** 2058-2073. doi: 10.1523/JNEUROSCI.2715-06.2007.

Maviel, T., Durkin, T.P., Menzaghi, F., and Bontempi, B. (2004). Sites of neocortical reorganization critical for remote spatial memory. *Science* 305(5680)**,** 96-99. doi: 10.1126/science.1098180.

Mei, Y., and Zhang, F. (2012). Molecular tools and approaches for optogenetics. *Biol Psychiatry* 71(12)**,** 1033-1038. doi: 10.1016/j.biopsych.2012.02.019.

Meyer-Lindenberg, A.S., Olsen, R.K., Kohn, P.D., Brown, T., Egan, M.F., Weinberger, D.R., et al. (2005). Regionally specific disturbance of dorsolateral prefrontal-hippocampal functional connectivity in schizophrenia. *Arch Gen Psychiatry* 62(4)**,** 379-386. doi: 10.1001/archpsyc.62.4.379.

Minlebaev, M., Ben-Ari, Y., and Khazipov, R. (2007). Network mechanisms of spindle-burst oscillations in the neonatal rat barrel cortex in vivo. *J Neurophysiol* 97(1)**,** 692-700. doi: 10.1152/jn.00759.2006.

Minlebaev, M., Ben-Ari, Y., and Khazipov, R. (2009). NMDA receptors pattern early activity in the developing barrel cortex in vivo. *Cereb Cortex* 19(3)**,** 688-696. doi: 10.1093/cercor/bhn115.

Mitew, S., Xing, Y.L., and Merson, T.D. (2016). Axonal activity-dependent myelination in development: Insights for myelin repair. *J Chem Neuroanat* 76(Pt A)**,** 2-8. doi: 10.1016/j.jchemneu.2016.03.002.

Mohns, E.J., and Blumberg, M.S. (2010). Neocortical activation of the hippocampus during sleep in infant rats. *J Neurosci* 30(9)**,** 3438-3449. doi: 10.1523/JNEUROSCI.4832-09.2010.

Molle, M., Yeshenko, O., Marshall, L., Sara, S.J., and Born, J. (2006). Hippocampal sharp wave-ripples linked to slow oscillations in rat slow-wave sleep. *J Neurophysiol* 96(1)**,** 62-70. doi: 10.1152/jn.00014.2006.

Nadarajah, B., and Parnavelas, J.G. (2002). Modes of neuronal migration in the developing cerebral cortex. *Nat Rev Neurosci* 3(6)**,** 423-432. doi: 10.1038/nrn845.

Nagel, G., Szellas, T., Huhn, W., Kateriya, S., Adeishvili, N., Berthold, P., et al. (2003). Channelrhodopsin-2, a directly light-gated cation-selective membrane channel. *Proc Natl Acad Sci U S A* 100(24)**,** 13940-13945. doi: 10.1073/pnas.1936192100.

Nakamura, S., Kimura, F., and Sakaguchi, T. (1987). Postnatal development of electrical activity in the locus ceruleus. *J Neurophysiol* 58(3)**,** 510-524.

Nolte, G., Bai, O., Wheaton, L., Mari, Z., Vorbach, S., and Hallett, M. (2004). Identifying true brain interaction from EEG data using the imaginary part of coherency. *Clin Neurophysiol* 115(10)**,** 2292-2307. doi: 10.1016/j.clinph.2004.04.029.

O'Leary, D.D., and Nakagawa, Y. (2002). Patterning centers, regulatory genes and extrinsic mechanisms controlling arealization of the neocortex. *Curr Opin Neurobiol* 12(1)**,** 14-25.

O'Neill, P.K., Gordon, J.A., and Sigurdsson, T. (2013). Theta oscillations in the medial prefrontal cortex are modulated by spatial working memory and synchronize with the hippocampus through its ventral subregion. *J Neurosci* 33(35)**,** 14211-14224. doi: 10.1523/JNEUROSCI.2378-13.2013.

Olcese, U., Iurilli, G., and Medini, P. (2013). Cellular and synaptic architecture of multisensory integration in the mouse neocortex. *Neuron* 79(3)**,** 579-593. doi: 10.1016/j.neuron.2013.06.010.

Packer, A.M., Roska, B., and Hausser, M. (2013). Targeting neurons and photons for optogenetics. *Nat Neurosci* 16(7)**,** 805-815. doi: 10.1038/nn.3427.

Padilla-Coreano, N., Bolkan, S.S., Pierce, G.M., Blackman, D.R., Hardin, W.D., Garcia-Garcia, A.L., et al. (2016). Direct Ventral Hippocampal-Prefrontal Input Is Required for Anxiety-Related Neural Activity and Behavior. *Neuron* 89(4)**,** 857-866. doi: 10.1016/j.neuron.2016.01.011.

Page, S.C., Hamersky, G.R., Gallo, R.A., Rannals, M.D., Calcaterra, N.E., Campbell, M.N., et al. (2017). The schizophrenia- and autism-associated gene, transcription factor 4 regulates the columnar distribution of layer 2/3 prefrontal pyramidal neurons in an activity-dependent manner. *Mol Psychiatry*. doi: 10.1038/mp.2017.37.

Peinado, A., Yuste, R., and Katz, L.C. (1993). Extensive dye coupling between rat neocortical neurons during the period of circuit formation. *Neuron* 10(1)**,** 103-114. doi: 10.1016/0896-6273(93)90246-n.

Preston, A.R., and Eichenbaum, H. (2013). Interplay of hippocampus and prefrontal cortex in memory. *Curr Biol* 23(17)**,** R764-773. doi: 10.1016/j.cub.2013.05.041.

Reboreda, A., Raouf, R., Alonso, A., and Seguela, P. (2007). Development of cholinergic modulation and graded persistent activity in layer v of medial entorhinal cortex. *J Neurophysiol* 97(6)**,** 3937-3947. doi: 10.1152/jn.01233.2006.

Rheims, S., Minlebaev, M., Ivanov, A., Represa, A., Khazipov, R., Holmes, G.L., et al. (2008). Excitatory GABA in rodent developing neocortex in vitro. *J Neurophysiol* 100(2)**,** 609-619. doi: 10.1152/jn.90402.2008.

Riga, D., Matos, M.R., Glas, A., Smit, A.B., Spijker, S., and Van den Oever, M.C. (2014). Optogenetic dissection of medial prefrontal cortex circuitry. *Front Syst Neurosci* 8**,** 230. doi: 10.3389/fnsys.2014.00230.

Robinson, J., Manseau, F., Ducharme, G., Amilhon, B., Vigneault, E., El Mestikawy, S., et al. (2016). Optogenetic Activation of Septal Glutamatergic Neurons Drive Hippocampal Theta Rhythms. *J Neurosci* 36(10)**,** 3016-3023. doi: 10.1523/JNEUROSCI.2141-15.2016.

Rumpel, S., Hatt, H., and Gottmann, K. (1998). Silent synapses in the developing rat visual cortex: evidence for postsynaptic expression of synaptic plasticity. *J Neurosci* 18(21)**,** 8863-8874.

Sanchez, M.P., Frassoni, C., Alvarez-Bolado, G., Spreafico, R., and Fairen, A. (1992). Distribution of calbindin and parvalbumin in the developing somatosensory cortex and its primordium in the rat: an immunocytochemical study. *J Neurocytol* 21(10)**,** 717-736.

Schnitzler, A., and Gross, J. (2005). Normal and pathological oscillatory communication in the brain. *Nat Rev Neurosci* 6(4)**,** 285-296. doi: 10.1038/nrn1650.

Shen, J., and Colonnese, M.T. (2016). Development of Activity in the Mouse Visual Cortex. *J Neurosci* 36(48)**,** 12259-12275. doi: 10.1523/JNEUROSCI.1903-16.2016.

Siapas, A.G., Lubenov, E.V., and Wilson, M.A. (2005). Prefrontal phase locking to hippocampal theta oscillations. *Neuron* 46(1)**,** 141-151. doi: 10.1016/j.neuron.2005.02.028.

Siapas, A.G., and Wilson, M.A. (1998). Coordinated interactions between hippocampal ripples and cortical spindles during slow-wave sleep. *Neuron* 21(5)**,** 1123-1128. doi: Doi 10.1016/S0896-6273(00)80629-7.

Siegle, J.H., Pritchett, D.L., and Moore, C.I. (2014). Gamma-range synchronization of fast-spiking interneurons can enhance detection of tactile stimuli. *Nat Neurosci* 17(10)**,** 1371-1379. doi: 10.1038/nn.3797.

Sigurdsson, T., and Duvarci, S. (2015). Hippocampal-Prefrontal Interactions in Cognition, Behavior and Psychiatric Disease. *Front Syst Neurosci* 9**,** 190. doi: 10.3389/fnsys.2015.00190.

Sigurdsson, T., Stark, K.L., Karayiorgou, M., Gogos, J.A., and Gordon, J.A. (2010). Impaired hippocampal-prefrontal synchrony in a genetic mouse model of schizophrenia. *Nature* 464(7289)**,** 763-767. doi: 10.1038/nature08855.

Sirota, A., Montgomery, S., Fujisawa, S., Isomura, Y., Zugaro, M., and Buzsaki, G. (2008). Entrainment of neocortical neurons and gamma oscillations by the hippocampal theta rhythm. *Neuron* 60(4)**,** 683-697. doi: 10.1016/j.neuron.2008.09.014.

Spellman, T., Rigotti, M., Ahmari, S.E., Fusi, S., Gogos, J.A., and Gordon, J.A. (2015). Hippocampal-prefrontal input supports spatial encoding in working memory. *Nature* 522(7556)**,** 309-314. doi: 10.1038/nature14445.

Spitzer, N.C. (2002). Activity-dependent neuronal differentiation prior to synapse formation: the functions of calcium transients. *Journal of Physiology-Paris* 96(1-2)**,** 73-80. doi: 10.1016/s0928-4257(01)00082-1.

Stark, E., Eichler, R., Roux, L., Fujisawa, S., Rotstein, H.G., and Buzsaki, G. (2013). Inhibition-induced theta resonance in cortical circuits. *Neuron* 80(5)**,** 1263-1276. doi: 10.1016/j.neuron.2013.09.033.

Steinberg, E.E., Christoffel, D.J., Deisseroth, K., and Malenka, R.C. (2015). Illuminating circuitry relevant to psychiatric disorders with optogenetics. *Curr Opin Neurobiol* 30**,** 9-16. doi: 10.1016/j.conb.2014.08.004.

Stiles, J., and Jernigan, T.L. (2010). The basics of brain development. *Neuropsychol Rev* 20(4)**,** 327-348. doi: 10.1007/s11065-010-9148-4.

Swadlow, H.A. (2003). Fast-spike Interneurons and Feedforward Inhibition in Awake Sensory Neocortex. *Cerebral Cortex* 13(1)**,** 25-32. doi: 10.1093/cercor/13.1.25.

Swanson, L.W. (1981). A direct projection from Ammon's horn to prefrontal cortex in the rat. *Brain Res* 217(1)**,** 150-154.

Szczurkowska, J., Cwetsch, A.W., dal Maschio, M., Ghezzi, D., Ratto, G.M., and Cancedda, L. (2016). Targeted in vivo genetic manipulation of the mouse or rat brain by in utero electroporation with a triple-electrode probe. *Nat Protoc* 11(3)**,** 399-412. doi: 10.1038/nprot.2016.014.

Tabata, H., and Nakajima, K. (2001). Efficient in utero gene transfer system to the developing mouse brain using electroporation: Visualization of neuronal migration in the developing cortex. *Neuroscience* 103(4)**,** 865-872. doi: Doi 10.1016/S0306-4522(01)00016-1.

Takehara, K., Kawahara, S., and Kirino, Y. (2003). Time-dependent reorganization of the brain components underlying memory retention in trace eyeblink conditioning. *J Neurosci* 23(30)**,** 9897-9905.

Tamura, M., Mukai, J., Gordon, J.A., and Gogos, J.A. (2016). Developmental Inhibition of Gsk3 Rescues Behavioral and Neurophysiological Deficits in a Mouse Model of Schizophrenia Predisposition. *Neuron*. doi: 10.1016/j.neuron.2016.01.025.

Taniguchi, H., He, M., Wu, P., Kim, S., Paik, R., Sugino, K., et al. (2011). A resource of Cre driver lines for genetic targeting of GABAergic neurons in cerebral cortex. *Neuron* 71(6)**,** 995-1013. doi: 10.1016/j.neuron.2011.07.026.

Thierry, A.M., Gioanni, Y., Degenetais, E., and Glowinski, J. (2000). Hippocampo-prefrontal cortex pathway: anatomical and electrophysiological characteristics. *Hippocampus* 10(4)**,** 411-419. doi: 10.1002/1098-1063(2000)10:4<411::AID-HIPO7>3.0.CO;2-A.

Tierney, P.L., Degenetais, E., Thierry, A.M., Glowinski, J., and Gioanni, Y. (2004). Influence of the hippocampus on interneurons of the rat prefrontal cortex. *Eur J Neurosci* 20(2)**,** 514-524. doi: 10.1111/j.1460-9568.2004.03501.x.

Tiriac, A., and Blumberg, M.S. (2016). The Case of the Disappearing Spindle Burst. *Neural Plast* 2016**,** 8037321. doi: 10.1155/2016/8037321.

Tolner, E.A., Sheikh, A., Yukin, A.Y., Kaila, K., and Kanold, P.O. (2012). Subplate neurons promote spindle bursts and thalamocortical patterning in the neonatal rat somatosensory cortex. *J Neurosci* 32(2)**,** 692-702. doi: 10.1523/JNEUROSCI.1538-11.2012.

Tye, K.M., and Deisseroth, K. (2012). Optogenetic investigation of neural circuits underlying brain disease in animal models. *Nat Rev Neurosci* 13(4)**,** 251-266. doi: 10.1038/nrn3171.

Uhlhaas, P.J., and Singer, W. (2011). The development of neural synchrony and large-scale cortical networks during adolescence: relevance for the pathophysiology of schizophrenia and neurodevelopmental hypothesis. *Schizophr Bull* 37(3)**,** 514-523. doi: 10.1093/schbul/sbr034.

Uylings, H.B.M., Groenewegen, H.J., and Kolb, B. (2003). Do rats have a prefrontal cortex? *Behavioural Brain Research* 146(1-2)**,** 3-17. doi: 10.1016/j.bbr.2003.09.028.

Vertes, R.P. (2006). Interactions among the medial prefrontal cortex, hippocampus and midline thalamus in emotional and cognitive processing in the rat. *Neuroscience* 142(1)**,** 1-20. doi: 10.1016/j.neuroscience.2006.06.027.

Vertes, R.P., Hoover, W.B., Szigeti-Buck, K., and Leranth, C. (2007). Nucleus reuniens of the midline thalamus: link between the medial prefrontal cortex and the hippocampus. *Brain Res Bull* 71(6)**,** 601-609. doi: 10.1016/j.brainresbull.2006.12.002.

Wang, X., Zhang, C., Szabo, G., and Sun, Q.Q. (2013). Distribution of CaMKIIalpha expression in the brain in vivo, studied by CaMKIIalpha-GFP mice. *Brain Res* 1518**,** 9-25. doi: 10.1016/j.brainres.2013.04.042.

Wang, X.J. (2010). Neurophysiological and computational principles of cortical rhythms in cognition. *Physiol Rev* 90(3)**,** 1195-1268. doi: 10.1152/physrev.00035.2008.

Wierzynski, C.M., Lubenov, E.V., Gu, M., and Siapas, A.G. (2009). State-dependent spike-timing relationships between hippocampal and prefrontal circuits during sleep. *Neuron* 61(4)**,** 587-596. doi: 10.1016/j.neuron.2009.01.011.

Womelsdorf, T., Valiante, T.A., Sahin, N.T., Miller, K.J., and Tiesinga, P. (2014). Dynamic circuit motifs underlying rhythmic gain control, gating and integration. *Nat Neurosci* 17(8)**,** 1031-1039. doi: 10.1038/nn.3764.

Wonders, C.P., and Anderson, S.A. (2006). The origin and specification of cortical interneurons. *Nat Rev Neurosci* 7(9)**,** 687-696. doi: 10.1038/nrn1954.

Xu, W., and Sudhof, T.C. (2013). A neural circuit for memory specificity and generalization. *Science* 339(6125)**,** 1290-1295. doi: 10.1126/science.1229534.

Yang, J.M., Zhang, J., Yu, Y.Q., Duan, S., and Li, X.M. (2014). Postnatal development of 2 microcircuits involving fast-spiking interneurons in the mouse prefrontal cortex. *Cereb Cortex* 24(1)**,** 98-109. doi: 10.1093/cercor/bhs291.

Yang, J.W., Hanganu-Opatz, I.L., Sun, J.J., and Luhmann, H.J. (2009). Three patterns of oscillatory activity differentially synchronize developing neocortical networks in vivo. *J Neurosci* 29(28)**,** 9011-9025. doi: 10.1523/JNEUROSCI.5646-08.2009.

Yang, J.W., Reyes-Puerta, V., Kilb, W., and Luhmann, H.J. (2016). Spindle Bursts in Neonatal Rat Cerebral Cortex. *Neural Plast* 2016**,** 3467832. doi: 10.1155/2016/3467832.

Yizhar, O., Fenno, L.E., Davidson, T.J., Mogri, M., and Deisseroth, K. (2011). Optogenetics in neural systems. *Neuron* 71(1)**,** 9-34. doi: 10.1016/j.neuron.2011.06.004.

Ylinen, A., Bragin, A., Nadasdy, Z., Jando, G., Szabo, I., Sik, A., et al. (1995). Sharp Wave-Associated High-Frequency Oscillation (200-Hz) in the Intact Hippocampus - Network and Intracellular Mechanisms. *Journal of Neuroscience* 15(1)**,** 30-46.

Young, C.K., and McNaughton, N. (2009). Coupling of theta oscillations between anterior and posterior midline cortex and with the hippocampus in freely behaving rats. *Cereb Cortex* 19(1)**,** 24-40. doi: 10.1093/cercor/bhn055.

Zhang, F., Gradinaru, V., Adamantidis, A.R., Durand, R., Airan, R.D., de Lecea, L., et al. (2010). Optogenetic interrogation of neural circuits: technology for probing mammalian brain structures. *Nat Protoc* 5(3)**,** 439-456. doi: 10.1038/nprot.2009.226.

Zhang, F., Wang, L.P., Brauner, M., Liewald, J.F., Kay, K., Watzke, N., et al. (2007). Multimodal fast optical interrogation of neural circuitry. *Nature* 446(7136)**,** 633-639. doi: 10.1038/nature05744.

Zhang, Z.W. (2004). Maturation of layer V pyramidal neurons in the rat prefrontal cortex: intrinsic properties and synaptic function. *J Neurophysiol* 91(3)**,** 1171-1182. doi: 10.1152/jn.00855.2003.

10 Summary of the thesis

10.1 English summary:

Directed oscillatory coupling within prefrontal-hippocampal networks underlies cognitive processing in adults. This communication emerges early in life, long before the maturation of mnemonic abilities, with discontinuous hippocampal theta bursts driving the initial oscillatory entrainment of local prefrontal networks via direct axonal projections. During development, the cellular substrates underlying the local entrainment of activity in prefrontal cortex as well as the directed long-range coupling within the prefrontal-hippocampal network is still poorly understood. To fill this knowledge gap we established a protocol that enables area-, layer, and cell-type specific transfection of optogenetic tools enabling the dissection of cellular interactions underlying network activity during the neonatal period.

The contribution of pyramidal neurons within the prefrontal cortex in generating local oscillatory activity was investigated by simultaneously recording electrophysiological activity in combination with optogenetic stimulation of excitatory pyramidal neurons confined in either Layer II/III or Layer V/VI in postnatal day 8 to 10 day old mice *in vivo*. We identified layer II/III pyramidal neurons in as a key component for the local entrainment of beta-gamma activity.

Further elucidation of the cellular components involved in the excitatory drive with prefrontal-hippocampal networks was also performed. We found that intermediate-ventral hippocampus is stronger coupled than dorsal hippocampus to prefrontal cortex. Furthermore, we show that the theta coupling within prefrontal-hippocampus networks are driven by CA1 area pyramidal neurons projecting to PFC, as frequency-specific activation at theta rhythm of intermediate-ventral CA1 area pyramidal neurons leads to entrainment of activity in prefrontal cortex.

Elucidation of the cellular substrates underlying the entrainment of oscillations during development is crucial for our understanding of their role in maturation and refinement of neural networks. The established protocol and the results presented here opens up new paths for investigation of network oscillations during development and could further aid our understanding of neurodevelopmental disorders.

10.2 German summary:

Im Erwachsenenalter unterliegen gerichtete oszillatorische Kopplungen innerhalb des präfrontal-hippokampalen Netzwerks kognitiven Prozessen. Diese Kommunikation entwickelt sich im frühen Leben, lang vor der Reifung der Gedächtnisfunktion, durch diskontinuierliche hippokampale Theta Ausbrüche von Aktivität, die das erste oszillatorische Entrainment von lokalen präfrontalen Netzwerken einer gerichteten axionalen Projektion vorantreiben. Während der Entwicklung sind die zellulären Mechanismen, die dem lokalen Entrainment der Aktivität im präfrontalen Kortex und der gerichteten weitreichenden Kopplung der präfrontal-hippokampalen Netzwerke unterliegen, immer noch kaum bekannt. Um diese Wissenslücke zu füllen haben wir ein Protokoll etabliert, das bereichs-, schicht- und zelltypspezifische Transfektionen von optogenetischen Methoden erlaubt, die wiederum die Analyse von zellulären Interaktionen ermöglichen, welche der neonatalen Netzwerkaktivität unterliegen.

Die Mitwirkung der Pyramidalneuronen bei der Generierung von lokaler oszillatorischer Aktivität innerhalb des präfrontalen Kortex wurde durch Ableitungen von elektrophysiologischer Aktivität in Kombination mit optogenetischer Stimulation von exzitatorischer Pyramidalneuronen in Schicht II/III oder V/VI an den postnatalen Tagen 8 bis 10 in vivo untersucht. Wir identifizierten Schicht II/III Pyramidalneuronen als Schlüsselkomponenten für das lokale Entrainment von Beta-Gamma Aktivität.

Weiterhin wurden zellulären Komponenten, die in die exzitatorische Steuerung innerhalb des präfrontal-hippokampalen Netzwerks involviert sind, untersucht. Wir fanden, dass der intermedial-ventrale Hippokampus stärker mit dem präfrontalen Kortex verbunden ist als der dorsale Hippokampus. Weiterhin zeigten wir, dass Theta Kopplung innerhalb des präfrontal-hippokampalen Netzwerks von CA1-Pyramidalneuronen gesteuert wird, die durch frequenzspezifische Aktivierung des Theta Rhythmus der intermedial-ventralen CA1-Pyramidalneuronen zum präfrontalen Kortex projizieren und das Entrainment der Aktivierung im präfrontalen Kortex steuern.

Die Untersuchung des zellulären Substrats, das dem Entrainment der Oszillation während der Entwicklung unterliegt, ist grundlegend für das Verständnis ihrer Rolle in der Entwicklung und der Verfeinerung neuronaler Netzwerke. Das

etablierte Protokoll und die präsentierten Ergebnisse eröffnen einen neuen Weg um Netzwerkoszillationen während der Entwicklung zu untersuchen und können dem Verständnis von neuronalen Entwicklungsstörungen beitragen.

11 Curriculum Vitae

Personal Data:

Joachim Ahlbeck
Scheideholzweg 63b
21149 Hamburg
Germany
Email: joachimahlbeck@gmail.com
Born May 23rd, 1988, Aalborg, Denmark

Academic Education

2013 – Present:	Ph.D. student at Department of Developmental Neurophysiology
2010 – 2012:	MSc Medicine with Industrial Specialization (MedIS) in Translational Medicine, Department of Health Science and Technology, Aalborg University, Aalborg, Denmark.
2007 – 2010:	BSc MedIS, Department of Health Science and Technology, Aalborg University, Aalborg, Denmark

12 Reprints of articles

Article 1:

Bitzenhofer SH, **Ahlbeck J**, Wolff A, Wiegert JS, Gee CE, Oertner TG, Hanganu-Opatz IL (2017). Layer-specific optogenetic activation of pyramidal neurons causes beta-gamma entrainment of neonatal networks. Nat Commun. 20;8:14563.

Article 2

Ahlbeck J, Candela A, Chini M, Bitzenhofer SH, Hanganu-Opatz IL (*In preparation*). Intermediate but not dorsal hippocampal CA1 projection neurons drive the oscillatory entrainment of prefrontal circuits in the neonatal mouse

Article 3

Lindemann C, **Ahlbeck J**, Bitzenhofer SH, Hanganu-Opatz IL (2016). Spindle Activity Orchestrates Plasticity during Development and Sleep. Neural Plast. 2016:5787423.

Article 4

Bitzenhofer SH, **Ahlbeck J**, Hanganu-Opatz IL (*Accepted*). Methodological approach for optogenetic manipulation of neonatal neuronal networks

nature COMMUNICATIONS

ARTICLE

Received 19 Apr 2016 | Accepted 12 Jan 2017 | Published 20 Feb 2017

DOI: 10.1038/ncomms14563 OPEN

Layer-specific optogenetic activation of pyramidal neurons causes beta–gamma entrainment of neonatal networks

Sebastian H. Bitzenhofer[1,*], Joachim Ahlbeck[1,*], Amy Wolff[1], J. Simon Wiegert[2], Christine E. Gee[2], Thomas G. Oertner[2] & Ileana L. Hanganu-Opatz[1]

Coordinated activity patterns in the developing brain may contribute to the wiring of neuronal circuits underlying future behavioural requirements. However, causal evidence for this hypothesis has been difficult to obtain owing to the absence of tools for selective manipulation of oscillations during early development. We established a protocol that combines optogenetics with electrophysiological recordings from neonatal mice *in vivo* to elucidate the substrate of early network oscillations in the prefrontal cortex. We show that light-induced activation of layer II/III pyramidal neurons that are transfected by *in utero* electroporation with a high-efficiency channelrhodopsin drives frequency-specific spiking and boosts network oscillations within beta–gamma frequency range. By contrast, activation of layer V/VI pyramidal neurons causes nonspecific network activation. Thus, entrainment of neonatal prefrontal networks in fast rhythms relies on the activation of layer II/III pyramidal neurons. This approach used here may be useful for further interrogation of developing circuits, and their behavioural readout.

[1] Developmental Neurophysiology, Institute of Neuroanatomy, University Medical Center Hamburg-Eppendorf, 20251 Hamburg, Germany. [2] Institute for Synaptic Physiology, University Medical Center Hamburg-Eppendorf, 20251 Hamburg, Germany. * These authors contributed equally to this work. Correspondence and requests for materials should be addressed to I.L.H.-O. (email: hangop@zmnh.uni-hamburg.de) or to S.H.B. (email: sebbitz@zmnh.uni-hamburg.de).

The developing brain functions according to unique processing rules. The highly discontinuous and fragmented temporal organization of the network activity[1–4], the depolarizing action of GABA (γ-aminobutyric acid)[5,6] as well as the patterns of local and long-range network coupling[7,8] relying on specific neuronal subpopulations and their transient connectivity[9,10] profoundly differentiate the developing brain from the adult one. The mechanisms underlying the unique wiring and function of the brain early in life are still poorly understood. It is also still a matter of debate whether the development-specific activity patterns are critical for the adult function and behavioural performance or simply a by-product of maturation processes.

In adulthood, brain function is tightly related to the activity of neuronal circuits. Pyramidal neurons and several classes of inhibitory interneurons dynamically interact to generate network activity in distinct frequency bands and enable diverse behaviours[11,12]. Resolving these circuits by identifying the contribution of each neuronal population to the rhythmic network activity and overall brain function *in vivo* has been recently enabled by the development of technologies to specifically control and manipulate neuronal activity at fast timescales[13,14]. Activation or suppression of action potentials (APs) in distinct neuronal populations by artificial incorporation of diverse light-sensitive proteins has been utilized to decipher the underlying mechanisms of memory[15–18], sensory and multisensory processing[19–21], and neuropsychiatric disorders[22–24].

Similar interrogation of developing circuits is currently missing. Consequently, the origin of neonatal brain rhythms remains unknown. Correlative evidence emphasized the contribution of complex and precisely tuned cellular interactions to the emergence of discontinuous patterns of early oscillatory activity[2,3,8,25,26], but induction of a distinct network state by cell-type-specific activation was not possible.

Here, we introduce a protocol for causal manipulation of neuronal and network activity in the neonatal brain (that is, postnatal day (P) 8–10) *in vivo* using targeted optogenetic stimulation. For this, cell-type- and layer-specific transfection of neurons by *in utero* electroporation (IUE) was combined with head-fixed recordings of local field potential (LFP) and spiking activity in neonatal mice during light stimulation. By these means we identified pyramidal neurons in layer II/III but not layer V/VI of the prelimbic subdivision (PL) of the prefrontal cortex (PFC) as key elements for the generation of beta–gamma oscillations during neonatal development.

Results

Cell-type-specific transfection during early development. The first prerequisite for the interrogation of developing circuits with optogenetics is the selective and effective transfection of neuronal populations with light-sensitive proteins early in life. For this, it is necessary to identify a suitable method of transfection, type of promoter giving the best expression and a light-sensitive protein. The most effective strategy for achieving functional expression of optogenetic tools in the adult brain, viral expression systems, cannot be reliably used for the investigation of developmental networks, because it usually requires 1–3 weeks until the gene expression reaches functional levels and layer specificity is rather poor[27,28]. Our pilot investigation confirmed these findings. Viral vectors based on adeno-associated virus 8 or canine adenovirus that have been described as enabling fast (48 h–6 days) expression *in vitro*[29,30] led to insufficient, if any, expression of channelrhodopsins (ChRs) in the PL of the PFC from P5–10 mice when injected *in vivo* 1–2 days after birth. Moreover, the promoters suitable for targeting neuronal subpopulations in adult mice often lack specificity or promote weak and unstable expression during early development.

To achieve stable gene expression in specific subpopulations of neurons in the neonatal brain, we used IUE as it enables cell-type-, layer- and area-specific transfection of neurons already prenatally without the need of cell-type-specific promoters of a sufficiently small size[31–33]. Pyramidal neurons either in layer II/III or in layer V/VI were addressed by this approach, since our previous investigations identified their activity as temporal correlate of network oscillations in neonatal PL[8,34]. Aiming at targeting pyramidal neurons in layers II/III of the PL, we injected constructs coding for the highly efficient fast-kinetics double mutant ChR2 E123T T159C (ET/TC)[35] and the red fluorescent protein tDimer2 into the right lateral ventricle at embryonic day (E) 14.5–15.5. Subsequenty, we applied an electrical field to the embryo's head to transfect neural precursor cells in the subventricular zone (Fig. 1a,b). This protocol is intended to selectively transfect pyramidal neurons in upper cortical layers (layer II/III) due to the distinct timing, origin and migration paths (that is, radial vs. tangential) of cortical pyramidal neurons and interneurons[36]. The procedure for targeting pyramidal neurons in layer V/VI was similar in its settings (for example, angle, electrical field), but performed at E12.5. To reach a high transfection rate, we tested the efficiency of several promoters in the neonatal brain. While human elongation factor 1α (EF1α) and synapsin promoters led to few or no tDimer2-positive neurons in the PL, the cytomegalovirus enhancer fused to chicken β-actin (CAG) promoter led to a robust expression in both upper and deeper layers that remained constant throughout the entire period of postnatal development (P5–25).

Analysis of consecutive coronal sections from IUE-transfected P8–10 mice revealed that tDimer2-positive neurons are mainly present in the PL, cingulate and infralimbic cortices and to a lesser extent in motor cortex (2 out of 9 for IUE at E15.5 and 2 out of 12 for IUE at E12.5) (Fig. 1c,f and Supplementary Fig. 8a). Staining for NeuN showed that $34.7 \pm 0.8\%$ ($n = 7$ pups) of neurons in prelimbic layer II/III and $33.1 \pm 1.2\%$ ($n = 5$ pups, $P = 0.288$) of neurons in layer V/VI were transfected by IUE at E15.5 or E12.5, respectively. The pyramidal-like shape and orientation of primary dendrites as well as the expression of Ca^{2+}/calmodulin-dependent protein kinase II (CaMKII) and the absence of positive staining for GABA confirmed that the expression constructs are exclusively integrated into cell lineages of pyramidal neurons (Fig. 1d,e,g,h). In line with the timing of migration[37], IUE at E15.5 selectively targeted neurons in the upper prelimbic layers II/III ($99.3 \pm 0.2\%$). Only $<0.5\%$ of tDimer2-positive neurons were detected in layer I or deep layers V/VI. Targeting of neurons in layer V/VI was less precisely confined, due to ongoing migration of a small fraction of neurons transfected at early age. However, the majority of transfected neurons were located in layer V/VI ($87.7 \pm 0.9\%$). Omission of ChR2(ET/TC) from the expression construct (that is, opsin-free) yields similar expression rates and distribution of tDimer2-positive neurons (Fig. 1e,h). Moreover, the success rate of transfection by IUE was similar in both groups of mice (Supplementary Fig. 1a,d).

To exclude nonspecific effects of the transfection procedure by IUE on the overall development of animals, we assessed the developmental milestones and reflexes of electroporated opsin-expressing and opsin-free mice as well as of non-electroporated mice (Supplementary Fig. 1). While IUE caused significant reduction of litter size (non-electroporated: 7.7 ± 0.3 pups per litter; IUE: 5 ± 0.2 pups per litter; $P = 0.004$), all investigated pups had similar body length, tail length and weight during the early postnatal period. Vibrissa placing, surface righting and cliff aversion reflexes were also not affected by IUE or transfection of

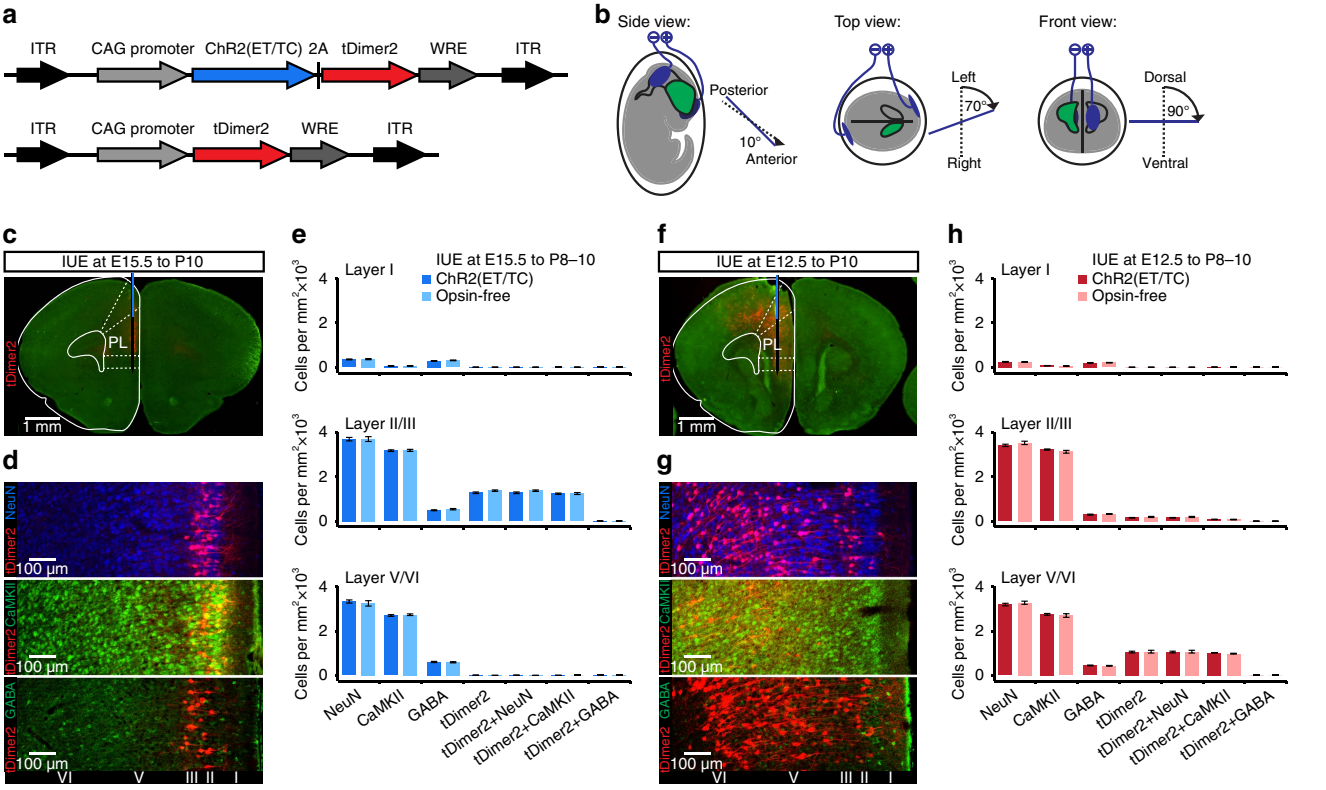

Figure 1 | Cell- and layer-specific transfection of neonatal prelimbic cortex by site-directed *in utero* electroporation. (**a**) Structure of the ChR2(ET/TC)-containing and opsin-free constructs. (**b**) Schematic drawing illustrating the orientation of electrode paddles for specific targeting of pyramidal neurons in layer II/III and V/VI of PL. (**c**) tDimer2-expressing cells (red) in a 50-µm-thick coronal section of a P10 mouse at the level of the prefrontal cortex after IUE at E15.5. (**d**) Photographs displaying NeuN (blue), Ca^{2+}/calmodulin-dependent protein kinase II (CaMKII) (green) and GABA (green) immunohistochemistry in relationship to tDimer2 expression (red) at P10 after IUE at E15.5. Note that the transfection is restricted to CaMKII-positive and GABA-negative neurons in layer II/III. (**e**) Bar diagrams displaying the mean density of NeuN-, CaMKII-, GABA-, tDimer2-, tDimer2 + NeuN-, tDimer2 + CaMKII- as well as tDimer2 + GABA-positive cells in layer I (top), II/III (middle) and V/VI (bottom) of PL from P8 to P10 mice after IUE with constructs containing CAG-ChR2(ET/TC)-2A-tDimer2 (dark blue bars, $n = 28$ slices from 7 pups for tDimer2, NeuN, GABA; $n = 20$ slices from 5 pups for CaMKII) or opsin-free constructs (light blue bars, $n = 28$ slices from 7 pups for tDimer2, NeuN, GABA; $n = 20$ slices from 5 pups for CaMKII). (**f**–**h**) Same as (**c**–**e**) for IUE at E12.5 with constructs containing CAG-ChR2(ET/TC)-2A-tDimer2 (dark red bars, $n = 20$ slices from 5 pups for tDimer2, NeuN, GABA; $n = 20$ slices from 5 pups for CaMKII) or opsin-free constructs (light red bars, $n = 20$ slices from 5 pups for tDimer2, NeuN, GABA; $n = 16$ slices from 4 pups for CaMKII). Note that the transfection is restricted to CaMKII-positive and GABA-negative cells mainly located in layer V/VI. Data are presented as mean ± s.e.m. ITR, inverted terminal repeat. WRE, woodchuck hepatitis virus posttranscriptional regulatory element.

neurons with opsins. These data indicate that the overall somatic development during embryonic and postnatal stage of ChR2 (ET/TC)-transfected mice is normal.

Light-induced spiking of neonatal neurons *in vitro*. We first assessed the efficiency of light stimulation in evoking APs in neonatal neurons. For this, whole-cell patch-clamp recordings were performed from tDimer2-positive pyramidal neurons in layer II/III ($n = 14$ cells) and layer V/VI ($n = 12$ cells) in coronal slices containing the PL from P8 to 10 mice after IUE at E15.5 and E12.5, respectively (Figs 2a and 3a). In line with the previously reported 'inside-out' pattern of cortical maturation[38], layer II/III and V/VI pyramidal neurons significantly differed in their passive membrane properties such as resting membrane potential (RMP) (layer II/III -73.3 ± 1.8 mV; layer V/VI -65.8 ± 2.3 mV; $P = 0.012$) and input resistance (layer II/III 1,067.5 ± 135.0 MΩ; layer V/VI 614.3 ± 98.6 MΩ; $P = 0.024$). These data confirm the more mature profile of neurons in deep layers of the PL compared with superficial layers. All investigated neurons fired overshooting APs in response to sustained depolarization by intracellular current injection (Figs 2b and 3b). The passive and active properties of ChR2(ET/TC)-transfected neurons were similar to those previously reported for age-matched rats[8]. However, the active properties of layer II/III pyramidal neurons differed from those of layer V/VI neurons (AP threshold: layer II/III -38.2 ± 1 mV, layer V/VI -43.2 ± 0.9 mV, $P = 0.002$; AP half-width: layer II/III 3.2 ± 0.2 ms, layer V/VI 2.3 ± 0.3 ms, $P = 0.013$). To gain insights whether early oscillations in the neonatal PL are the result of intrinsic neuronal properties or of network activation, we tested the resonance profile of transfected neurons. The impedance profile in response to chirp current injection with linearly increasing frequency from 1 to 50 Hz did not indicate a preferred membrane resonance frequency of layer II/III and V/VI pyramidal neurons (Figs 2c and 3c).

Blue light pulses (473 nm, 5.2 mW mm^{-2}) depolarized all fluorescently labelled neurons, yet the suprathreshold activation critically depended on the promoter used as well as the intensity and duration of light pulses. Consistent with the rather weak fluorescence of neurons transfected with ChR2(ET/TC) under the control of EF1α, AP firing was evoked when the duration of light pulses exceeded 100 ms. In contrast, the use of the CAG promoter resulted in reliable firing of single APs in response to 3-ms-long

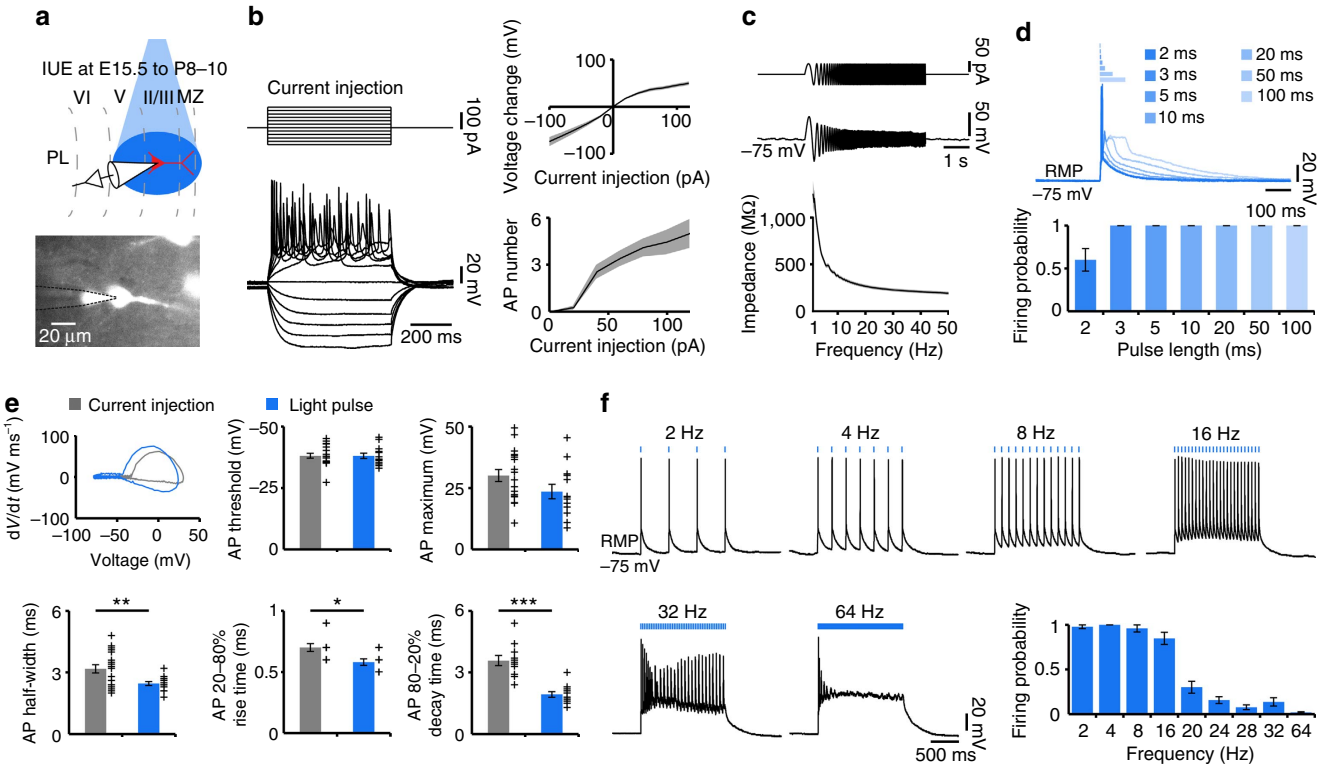

Figure 2 | Optogenetic activation of prelimbic layer II/III pyramidal neurons *in vitro*. (**a**) Experimental approach for combined light stimulation and whole-cell recordings from IUE-transfected layer II/III pyramidal neurons in coronal slices of P8–10 mice. (**b**) Left, voltage responses of a representative neuron to hyper- and depolarizing current pulses. The RMP was −73.7 mV. Right, averaged plots of the current–voltage relationship (top) and current-firing rate relationship (bottom) ($n=20$ neurons). (**c**) Top, waveform of subthreshold chirp current injection with increasing frequency from 1 to 50 Hz. Middle, voltage response of a representative neuron. Bottom, averaged plots of the impedance ($n=16$ neurons). (**d**) Top, voltage responses of a representative ChR2(ET/TC)-transfected neuron to blue light pulses (473 nm, 5.2 mW mm^{-2}) of 1 (dark blue) to 100 ms (light blue) duration. Bottom, bar diagram displaying the mean firing probabilty of transfected neurons in response to blue light pulses of variable duration ($n=14$ neurons). (**e**) Top, representative phase plot of APs elicited in a transfected neuron by depolarizing current injection (grey) or a 3-ms-long light pulse (473 nm, 5.2 mW mm^{-2}, blue). Bottom, bar diagrams displaying the mean active membrane properties after depolarizing current injections (grey, $n=18$ neurons) and after light stimulation (blue, $n=14$ neurons). Individual values are displayed as black crosses. (**f**) Representative voltage responses of a transfected neuron to repetitive trains of 3-ms-long light stimuli at variable frequencies. Bar diagram displaying the mean firing probability of transfected neurons in response to repetitive light stimuli ($n=14$ neurons). Data are presented as mean ± s.e.m. $^{*}P<0.05$, $^{**}P<0.01$ and $^{***}P<0.001$, two-sided *t*-tests. MZ, marginal zone.

light pulses (Figs 2d and 3d). APs evoked by light and by current injection were similar in their threshold (layer II/III—light triggered: −38.1 ± 1.1 mV, current triggered: −38.2 ± 1 mV, $P=0.98$; layer V/VI—light triggered: −41.5 ± 1 mV, current triggered: −43.2 ± 0.9 mV, $P=0.22$) and peak voltage (layer II/III—light triggered: 23.6 ± 2.9 mV, current triggered: 30.1 ± 2.5 mV, $P=0.09$; layer V/VI—light triggered: 34.3 ± 5 mV, current triggered: 37 ± 5.1 mV, $P=0.72$) (Figs 2e and 3e), indicating that light stimulation causes physiological activation of ChR2(ET/TC)-transfected neurons. However, half-width of light-triggered APs was significantly reduced for layer II/III (current triggered 3.2 ± 0.2 ms; light triggered 2.5 ± 0.1 ms; $P=0.009$), but not for layer V/VI (current triggered 2.3 ± 0.3 ms; light triggered 2.0 ± 0.2 ms; $P=0.358$) pyramidal cells (Figs 2e and 3e). To mechanistically explain these differences, we modelled the effect of Na^+/K^+ conductances on the AP time course with the Hodgkin–Huxley model[39] (Supplementary Fig. 2). Modelled AP half-width was modulated by the strength of the current injection for neurons with low (that is, immature), but not high (that is, mature) Na^+/K^+ conductances, suggesting a strong inward current after stimulation. A similar dependence was experimentally detected for current injections only for layer II/III pyramidal neurons (Supplementary Fig. 2f).

Precise induction of APs over a broad range of frequencies, corresponding to those of neonatal network oscillations, requires the use of ChRs with fast kinetics that deliver large photocurrents. Adult ChR2(ET/TC)-expressing neurons have been reported to reliably follow stimulation frequencies up to 60 Hz (ref. 35). We stimulated neonatal ChR2(ET/TC)-expressing neurons with trains of 3-ms-long light pulses at frequencies ranging from 2 to 64 Hz. Robust firing was evoked in all neurons throughout stimulation up to 32 Hz, but the probability of triggering APs by trains of light stimuli decreased with increasing stimulation frequency (2 Hz: layer II/III 0.97 ± 0.02, layer V/VI 1 ± 0, $P=0.328$; 4 Hz: layer II/III 1 ± 0, layer V/VI 0.94 ± 0.06, $P=0.289$; 8 Hz: layer II/III 0.96 ± 0.04, layer V/VI 0.80 ± 0.09, $P=0.103$; 16 Hz: layer II/III 0.85 ± 0.07, layer V/VI 0.46 ± 0.11, $P=0.004$; 20 Hz: layer II/III 0.3 ± 0.07, layer V/VI 0.3 ± 0.1, $P=0.975$; 24 Hz: layer II/III 0.16 ± 0.04, layer V/VI 0.26 ± 0.11, $P=0.399$; 28 Hz: layer II/III 0.08 ± 0.03, layer V/VI 0.24 ± 0.11, $P=0.192$; 32 Hz: layer II/III 0.14 ± 0.05, layer V/VI 0.2 ± 0.09, $P=0.561$; 64 Hz: layer II/III 0.02 ± 0.01, layer V/VI 0.04 ± 0.01, $P=0.18$) (Figs 2f and 3f). These data show that only

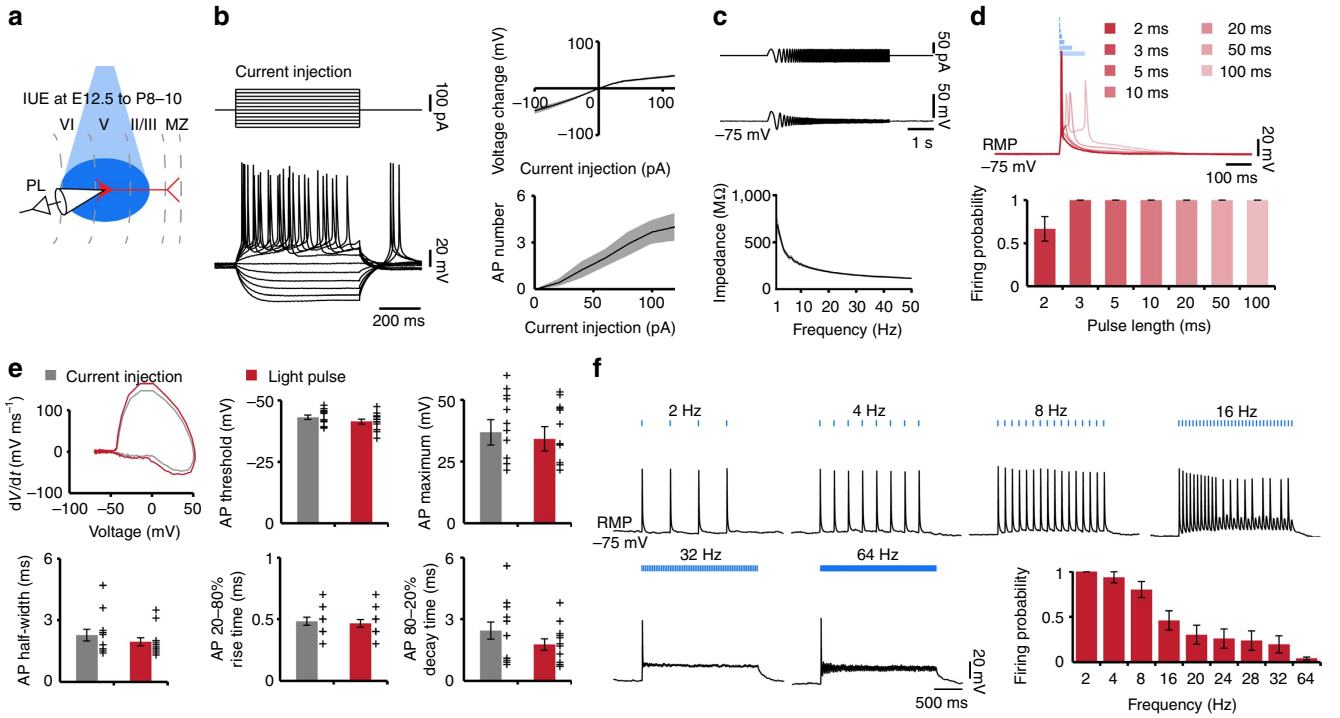

Figure 3 | Optogenetic activation of prelimbic layer V/VI pyramidal neurons *in vitro*. (**a**) Experimental approach for combined light stimulation and whole-cell recordings from IUE-transfected layer V/VI pyramidal neurons in coronal slices of P8–10 mice. (**b**) Left, voltage responses of a representative neuron to hyper- and depolarizing current pulses. The RMP was −68.6 mV. Right, averaged plots of the current–voltage relationship (top) and current-firing rate relationship (bottom) ($n=12$ neurons). (**c**) Top, waveform of subthreshold chirp current injection with increasing frequency from 1 to 50 Hz. Middle, voltage response of a representative neuron. Bottom, averaged plots of the impedance ($n=12$ neurons). (**d**) Top, voltage responses of a representative ChR2(ET/TC)-transfected neuron to blue light pulses (473 nm, 5.2 mW mm^{-2}) of 1 (dark red) to 100 ms (light red) duration. Bottom, bar diagram displaying the mean firing probabilty of transfected neurons in response to blue light pulses of variable duration ($n=12$ neurons). (**e**) Top, representative phase plot of APs elicited in a transfected neuron by depolarizing current injection (grey) or a 3-ms-long light pulse (473 nm, 5.2 mW mm^{-2}, red). Bottom, bar diagrams displaying the mean active membrane properties after depolarizing current injections (grey, $n=12$ neurons) and after light stimulation (red, $n=12$ neurons). Individual values are displayed as black crosses. (**f**) Representative voltage responses of a transfected neuron to repetitive trains of 3-ms-long light stimuli at variable frequencies. Bar diagram displaying the mean firing probability of transfected neurons in response to repetitive light stimuli ($n=12$ neurons). Data are presented as mean ± s.e.m. Two-sided *t*-tests. MZ, marginal zone.

for 16 Hz the firing probability was significantly higher for layer II/III when compared to layer V/VI pyramidal neurons. At stimulation frequencies >32 Hz the firing probability strongly decreased and the few APs triggered at the beginning of the stimulation train were followed by a prominent plateau depolarization. These values are consistent with the maximal firing rate (layer II/III 10.0 ± 0.4 Hz; layer V/VI 8.0 ± 0.4 Hz) of these pyramidal neurons in response to depolarizing current injection.

In addition to identifying intrinsic differences in the activation of layer II/III and V/VI pyramidal neurons by light, the results of *in vitro* experiments were instrumental for setting light stimulation *in vivo*. All further manipulation of neonatal ChR2(ET/TC)-expressing pyramidal neurons were performed with 3-ms-long light pulses at frequencies up to 32 Hz.

Layer II/III pyramidal neurons tend to fire in beta-rhythm. To determine whether layer II/III and layer V/VI pyramidal neurons have distinct functions for the emergence of prelimbic network activity at neonatal age, we monitored the effects of their light activation *in vivo*. If these neurons contribute to the generation of oscillatory activity in the developing PL, then light stimulation should cause a concentration of their firing within a specific frequency band. Multisite recordings of the LFP and multiunit activity (MUA) were performed from layer II/III or layer V/VI of the PL in urethane-anesthetized P8–10 mouse pups before, during and after repetitive stimulation with pulse trains or ramp light stimuli (Supplementary Fig. 3a). Our previous data revealed that network oscillations and neuronal firing are similar in urethane-anesthetized and asleep non-anesthetized neonatal rodents[8]. For each pup, the intensity of light stimulation was set to evoke reliable MUA activity <15 ms after stimulus onset (Supplementary Fig. 3b,c) and ranged between 20 and 40 mW mm^{-2}. Stimulation efficacy increased with light power, yet the onset of evoked spiking remained constant (Supplementary Fig. 3d). To exclude that light-evoked effects are due to local tissue heating during illumination, we estimated the temperature change during stimulation using a recently developed model[40]. Stimulation with the illumination parameters set *in vitro* (3-ms-long light pulses, frequencies ranging from 2 to 32 Hz) led to a temperature increase of max. 0.2 °C (Supplementary Fig. 3e–h). These values are below those that have been reported to augment neuronal firing[40,41], indicating that the neonatal brain activity is not affected by light-induced tissue heating.

Trains of pulse stimuli (3-ms-long pulses at 2–32 Hz, total duration 3 s) and ramp light stimuli (total duration 3 s) increased the neuronal firing of ChR2(ET/TC)-transfected pyramidal neurons in both upper and deeper layers, but not of neurons tranfected with opsin-free constructs (Fig. 4a,d, Supplementary

Fig. 4 and Supplementary Fig. 5). The effects were more prominent in layer II/III than in layer V/VI neurons. Similar to the *in vitro* results, the firing of deeper layer pyramidal neurons was not reliably detected after trains of light pulses. In the upper layers, MUA discharge and the firing of 34 out of 69 single units (SUA) augmented in a frequency-dependent manner when trains of stimuli were applied. Although for low stimulation frequencies (2–16 Hz), the spiking increase was similar after each light pulse, at higher frequencies (16–32 Hz) the stimulation efficacy strongly decreased during the train, confirming the *in vitro* findings (Supplementary Fig. 4b–f). The onset of light-evoked spiking (6.2 ± 0.5 ms, $n = 29$ recording sites from 10 mice) was similar to the onset of APs recorded in prelimbic neurons in slices (7.9 ± 0.4 ms, $n = 14$ cells). To exclude the possibility that the layer-specific firing patterns induced by light stimulation resulted from activation of a different number of neurons, we assessed the number of activated neurons by using the model of spatiotemporal propagation of light[40]. Taking into account the density of transfected and all neurons (layer II/III $3{,}698.8 \pm 108.7$ NeuN$^+$ per mm^2, layer V/VI $3{,}245.2 \pm 121$ NeuN$^+$ per mm^2, $P = 0.007$), similar numbers of neurons were estimated to be activated (illumination > 10 mW mm^{-2}) in layer II/III (363 neurons) and layer V/VI (303 neurons). This suggests a comparable light activation for both layers; however, a contribution of minor differences in the activated number of neurons for superficial and deep layers to the observed differences remains possible.

Ramp stimulation of transfected neurons in upper and deeper layers led to sustained increase of spike discharge that was initiated once the power exceeded a certain threshold (Fig. 4a,d). For some neurons the activity dropped towards the end of ramp stimulation, suggesting that, similar to *in vitro* recordings, their membrane potential reached a depolarized plateau potential preventing further spiking. However, for the majority of neurons the mean firing rate for 1 s after stimulus remained significantly higher than before stimulus (layer II/III—before: 1.0 ± 0.1 Hz, after: 2.9 ± 0.5 Hz, $P = 0.048$, $n = 21$ recording sites; layer V/VI—before: 1.1 ± 0.1 Hz, after: 3.9 ± 0.3 Hz, $P < 0.001$, $n = 61$ recording sites), suggesting that short-term plasticity has been induced by light stimulation in developing circuits. Ramp stimulation revealed major differences between the firing of upper and deeper layers. While layer II/III neurons did not fire randomly, but had a preferred interspike interval of ~ 60 ms, equivalent to a concentration of individual and population firing at 16.7 Hz (Fig. 4b,c), layer V/VI neurons lack this coordinated firing (Fig. 4e,f). The beta band concentration of firing in upper prelimbic layers was detected solely during ramp stimulus and was absent before and afterwards. The absence of a preferred membrane resonance of layer II/III pyramidal neurons (Fig. 2c) suggests that this firing pattern is not intrinsic, but emerges from cellular interactions within local networks. In line with the persistent poststimulus augmentation of firing rates, the proportion of short interspike intervals was larger after ramp light stimulus than before (Fig. 4b,c,e,f).

These results indicate that on light activation pyramidal neurons in layer II/III but not layer V/VI of neonatal PL concentrate their firing in beta frequency range.

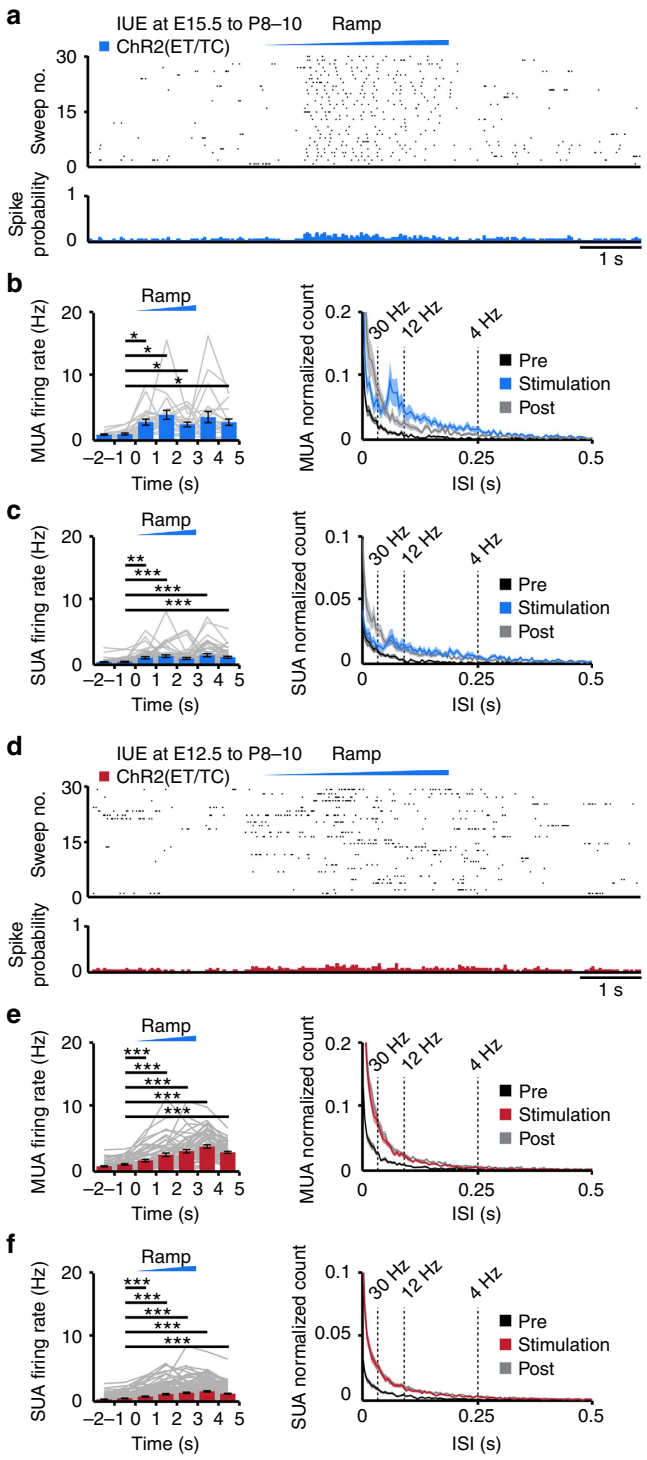

Figure 4 | Optogenetic activation of layer II/III and layer V/VI pyramidal neurons *in vivo*. (**a**) Representative raster plot and corresponding spike probability histogram displaying the firing of transfected layer II/III pyramidal neurons in response to 30 sweeps of ramp illumination (473 nm, 3 s). (**b**) Left, bar diagram displaying the mean MUA frequency in ChR2(ET/TC)-transfected neurons from P8 to P10 mice in response to ramp illumination. Right, occurrence rate of interspike intervals averaged for 3 s before light stimulation (pre, black), 3 s during ramp stimulation (stimulation, blue) and 3 s after light stimulation (post, grey, $n = 21$ recording sites from 9 pups). Note the prominent increase in the rate of interspike intervals between 12 and 30 Hz peaking at 16.7 Hz during ramp stimulation. (**c**) Same as (**b**) for SUA ($n = 50$ units from 9 pups). Note that the peak between 12 and 30 Hz is present, but less pronounced due to the incorporation of non-triggered units. (**d–f**) Same as (a–c) for layer V/VI pyramidal neurons (red, $n = 12$ pups; MUA of $n = 61$ recording sites; SUA of $n = 152$ units). For (**b**,**c**,**e**,**f**) grey lines correspond to firing of individual neurons. Data are presented as mean ± s.e.m. $^*P < 0.05$, $^{**}P < 0.01$ and $^{***}P < 0.001$), one-way repeated-measures analysis of variance (ANOVA) with Bonferoni-corrected *post hoc* analysis.

Layer II/III pyramidal neurons drive beta–gamma oscillations. Activation of pyramidal neurons in upper layers has been proposed to underlie the emergence of network oscillations in beta–gamma frequency range in the neonatal PL[8]. To causally prove this hypothesis, we tested whether the frequency-specific synchronization of layer II/III pyramidal neurons on light stimulation boosts the generation of discontinuous oscillatory activity in P8–10 mice. As previously reported[7,34], the first patterns of network activity in the neonatal PL are discontinuous, that is, spindle-shaped oscillations switching between theta and beta–gamma frequency components alternated with long periods of silence (Supplementary Fig. 6a,d). Selective expression of ChR2(ET/TC) in pyramidal neurons of prelimbic upper or deeper layers did not perturb the spontaneous discontinuous oscillatory events. In particular, their duration, amplitude, occurrence and spectral composition as well as their temporal relationship with the neuronal firing as quantified by phase locking were similar in pups transfected with ChR2(ET/TC)-containing constructs (layer II/III $n=28$ pups, layer V/VI $n=17$ pups) and pups transfected with opsin-free constructs (layer II/III $n=11$ pups, layer V/VI $n=12$ pups) (Supplementary Fig. 6b,c,e,f).

In a first step, we used trains of light pulses (3-ms-long, total duration of 3 s) to drive the spiking of either layer II/III or layer V/VI neurons in the PL of mice transfected with ChR2(ET/TC) at different frequencies (2, 4, 8, 16 and 32 Hz) (Supplementary Fig. 7a,b). Simultaneously, we recorded the LFP in PL. As previously reported, scattered photons hitting the recording sites of LFP electrodes led to prominent light artefacts[42]. They were measured at the end of the recordings in pups that were killed (see Methods) and eliminated by subtraction after corresponding scaling (Supplementary Fig. 7c,d). In opsin-free pups the procedure led to abolishment of the light-induced response, which consisted only of the photoelectric artefact. In contrast, in ChR2(ET/TC)-transfected pups, large negative voltage deflections with slower kinetics persisted after elimination of the photoelectric artefact. They seem to reflect physiological current sinks created in the extracellular space by simultaneous opening of the light-activated channels[43]. These large light-triggered responses precluded the assessment of induced oscillations when analysing the LFP, since due to their periodicity they are prominently reflected in the LFP power (Supplementary Fig. 7a,c). Therefore, we compared the power of network oscillations in the upper PL layers before and after, but not during each train of light pulses that activates layer II/III pyramidal neurons. Stimulation at 2, 4 as well as 32 Hz did not significantly modify the LFP. In contrast, 8 and 16 Hz stimulation augmented the power of oscillatory activity in theta (4–12 Hz) (post/pre theta: 2 Hz: 1.20 ± 0.15 $P=0.228$; 4 Hz: 1.02 ± 0.12 $P=0.860$; 8 Hz: 1.32 ± 0.12 $P=0.021$; 16 Hz: 1.31 ± 0.08 $P=0.004$; 32 Hz: 1.17 ± 0.17 $P=0.333$), beta (12–30 Hz) (post/pre beta: 2 Hz: 1.27 ± 0.13 $P=0.069$; 4 Hz: 1.10 ± 0.08 $P=0.265$; 8 Hz: 1.23 ± 0.07 $P=0.012$; 16 Hz: 1.30 ± 0.06 $P=0.001$; 32 Hz: 1.21 ± 0.15 $P=0.202$) and gamma (30–100 Hz) (post/pre gamma: 2 Hz: 1.11 ± 0.08 $P=0.189$; 4 Hz: 1.04 ± 0.04 $P=0.354$; 8 Hz: 1.11 ± 0.04 $P=0.030$; 16 Hz: 1.17 ± 0.05 $P=0.006$; 32 Hz: 1.05 ± 0.06 $P=0.385$) frequency bands (Supplementary Fig. 7b). The strongest effects were observed when layer II/III pyramidal neurons were driven at 16 Hz. To examine the time course of network activation during stimulation, we applied ramp stimulations. When compared with pulse train stimulations, they had the advantage of not inducing power contamination by repetitive and fast large-amplitude voltage deflections (Figs 5a and 6a) and to trigger more physiological and not artificially synchronous firing patterns. The LFP power in beta frequency component significantly increased on ramp stimulation of layer II/III pyramidal neurons, whereas the prominent theta component remained unaffected during stimulation (Fig. 5b). At higher light intensity gamma band activity was also boosted. Even after stimulus, the augmented network activation persisted, yet lacked frequency specificity. To assess the influence of light-induced network activity on prelimbic firing, we calculated the phase locking of MUA and clustered SUA to oscillations. The firing of layer II/III neurons was more strongly phase-locked to beta (SUA: baseline: 0.18 ± 0.01; ramp: 0.26 ± 0.03; $P=0.016$) and gamma (SUA: baseline: 0.45 ± 0.02; ramp: 0.58 ± 0.03; $P=0.003$) activity during ramp stimulation when compared to their timing during spontaneous activity (Fig. 5c,d).

In contrast, light activation of layer V/VI pyramidal neurons did not cause frequency-specific boosting of oscillatory activity (Fig. 6a,b). Ramp stimulation of deep layers led to an overall power increase in theta, beta and gamma band that outlasted the stimulus. Consequently, no significant changes of phase-locking of neuronal firing to network oscillations were detected during or after light stimulation of layer V/VI pyramidal neurons (Fig. 6c,d). These layer-specific differences do not result from variant expression of light-sensitive proteins across pups. Two pieces of evidence support this conclusion. First, the fraction of pups with extraprelimbic transfection was similar after IUE at E12.5 and E15.5. Second, no significant correlations between expression strength and the firing rate or oscillatory power were detected (Supplementary Fig. 8).

To examine whether layer-specific stimulation by light differentially entrains the entire PL in oscillatory rhythms of defined frequency, we performed LFP recordings using 4-shank optoelectrodes covering the whole cortical depth. Light stimulation of layer II/III neurons ($n=11$ pups) augmented the coherence and power, especially in beta and gamma band, within and between layers (Fig. 7a and Supplementary Fig. 9). In contrast, stimulation of layer V/VI pyramidal neurons ($n=6$ pups) did not change the synchrony strength during stimulation and was followed by intralayer coupling in beta–gamma range poststimulus (Fig. 7b). Interestingly, no significant changes in theta-band coherence were observed after light stimulation of upper and deeper layers, despite increased theta-band power in the poststimulation period. This suggests that external input, most likely hippocampal drive[7,34,44], is required for theta-band activation of the PL.

These data identify pyramidal neurons in layer II/III of PL as a cellular substrate of beta–gamma network oscillations capable of synchronizing intra- and interlayer the neonatal PL, whereas layer V/VI pyramidal neurons contribute to the overall activation within developing networks (Fig. 8).

Discussion

Combining selective optogenetic activation with extracellular recordings from neonatal mice *in vivo*, we provide causal evidence that cortical oscillations during early development can emerge as result of cell-type-specific activation within local intracortical circuits. Optical stimulation of ChR-expressing pyramidal neurons in layer II/III but not layer V/VI of the PL coordinated the neuronal firing and specifically boosted the emergence of discontinuous oscillatory activity in beta–gamma frequency bands.

Despite limited behavioural abilities, the developing cortex shows complex patterns of discontinuous network activity[45,46]. Their diversity (for example, fast discharge interspersing slow rhythms) and large frequency spectrum (that is, from delta band to high-frequency oscillations) even at such early age lead to the question whether these early network oscillations control the functional maturation of the neocortex. One prerequisite for

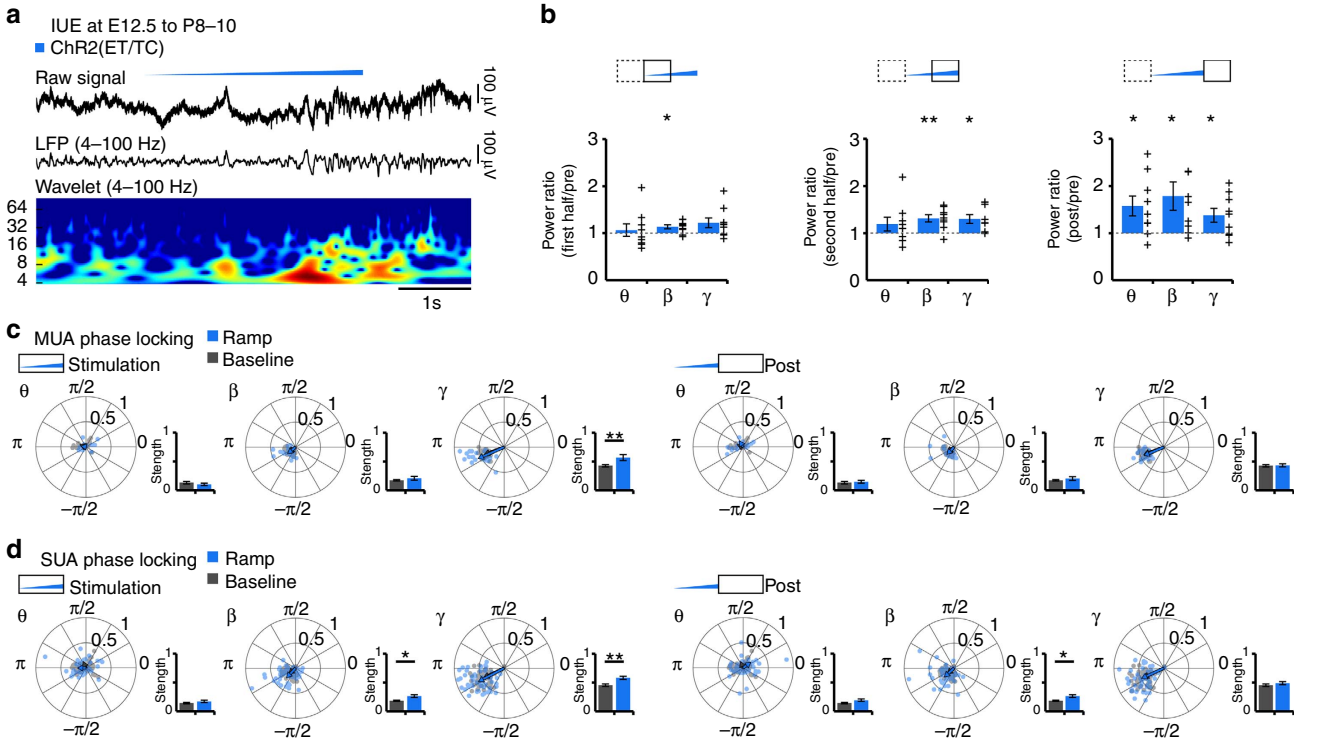

Figure 5 | Generation of discontinuous patterns of oscillatory activity in the neonatal prelimbic cortex in response to optogenetic activation of layer II/III pyramidal neurons *in vivo*. (**a**) Characteristic light-induced (ramp stimulus, 473 nm, 3 s) discontinuous oscillatory activity from a P10 mouse after transfection of layer II/III pyramidal neurons with ChR2(ET/TC) by IUE. The LFP is displayed before (top) and after band-pass filtering (4–100 Hz) (middle) together with the corresponding colour-coded wavelet spectrum at identical timescale. (**b**) Bar diagrams displaying the LFP power during the first half (1.5 s), the second half (1.5 s) and after (post, 1.5 s) ramp stimulus when normalized to the power before stimulation (pre, 1.5 s). Network activity in theta (θ, 4–12 Hz), beta (β, 12–30 Hz) and gamma (γ, 30–100 Hz) frequency bands ($n=9$ pups) was considered. (**c**) Polar plots displaying the phase-locking of light-triggered (blue, stimulation 3 s, post 3 s) and spontaneous (grey) MUA to oscillatory activity from layer II/III ChR2(ET/TC)-transfected mice ($n=21$ recording sites from 9 pups). Bar diagrams display the locking strength. (**d**) Same as (**c**) for SUA ($n=50$ units from 9 pups). For (**b**) individual values corresponding to pups with light-induced oscillations are displayed as black crosses. For (**c**,**d**) the values from individual units are shown as blue and grey dots, whereas the arrows correspond to the mean resulting group vectors. Data are presented as mean ± s.e.m. $^*P<0.05$, $^{**}P<0.01$, two-sided *t*-tests and circular statistics toolbox.

elucidating the function of early oscillations is to understand their mechanisms of generation. Electrical stimulation and *in vivo* pharmacology showed that the early cortical activity is, at least in part, triggered by endogeneous activation of sensory periphery or by theta drive from other cortical and subcortical areas[2,3,7,25,47–49]. However, the partial persistence of early network oscillations after removal or blockade of these extraneocortical sources indicates that local activation of the neocortical circuitry may be sufficient for their generation. Indeed, we recently gained the first insights into the wiring scheme of layer V and showed that external glutamatergic inputs correlate with theta and beta–gamma activity[8]. However, none of these studies could precisely assign a specific neuronal population as generator of early patterns of network oscillations. The present study fills this knowledge gap by taking advantage of the selectivity of optogenetic manipulation and identifies one possible source of neonatal network activity. Using area-, layer- and cell-type-specific expression of a high-efficiency ChR mutant, we provide causal evidence that layer II/III pyramidal neurons, preferentially driven by light to fire at ~16 Hz, can entrain beta-band oscillatory activity in the neonatal PL. In contrast, activation of layer V/VI pyramidal neurons contributes to the overall oscillatory activation of neonatal prelimbic networks. When simultaneously monitored by 4-shank recordings, light activation of layer II/III and V/VI caused distinct synchrony patterns over PL. These data provide evidence for the existence of different wiring schemes in layer II/III and V/VI. Their detailed elucidation will require simultaneous optogenetic targeting of both pyramidal neurons and interneurons in upper and deeper layers of PL. Another aspect that needs clarification in the future is to what extent the emerging mechanisms of early network oscillations are common for limbic and sensory cortices, which at adulthood have distinct structure, connectivity and behavioural relevance (for example, five versus six layers, prominent hippocampal versus thalamic innervation)[50,51].

Several considerations regarding the technical challenges of optogenetic manipulation of neonatal networks need to be made. First, the combination of the CAG promoter and targeting by IUE ensured a sufficiently high level of opsin expression in the neurons and layers of interest. Moreover, the number of transfected pyramidal neurons in the investigated layer II/III was sufficient to specifically induce coordinated fast network oscillations when stimulated with light. One intriguing question is how many pyramidal neurons in these layers must be synchronously activated to affect the network entrainment of the neonatal PL. Further technological development, such as high-density silicon probes combined with micron-sized light-emitting diodes could enable us to address this question in the future[52,53]. Second, the pattern of light stimulation appears critical for dissecting the cellular substrate of early network oscillations. Here we used both trains of pulses at different frequencies and ramp stimulation. Even after light artefacts were

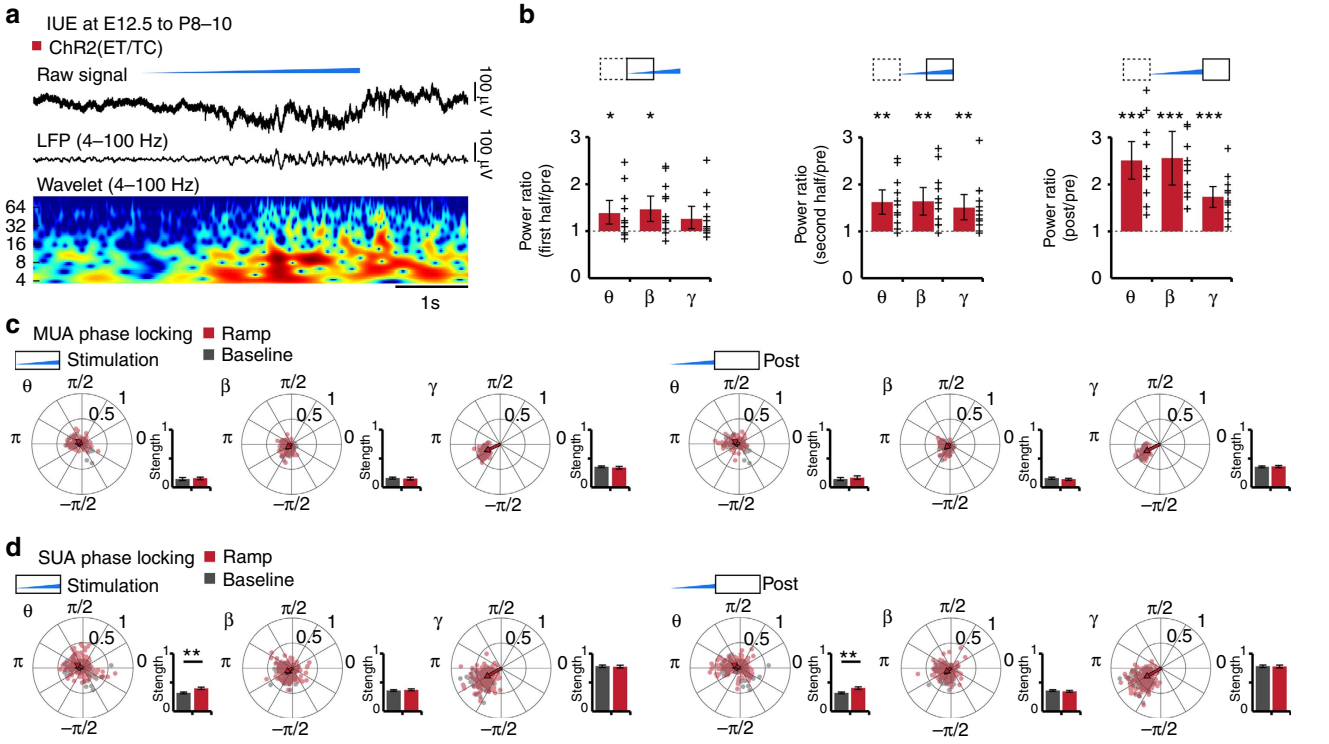

Figure 6 | Generation of discontinuous patterns of oscillatory activity in the neonatal prelimbic cortex in response to optogenetic activation of layer V/VI pyramidal neurons *in vivo*. (**a**) Characteristic light-induced (ramp stimulus, 473 nm, 3 s) discontinuous oscillatory activity from a P10 mouse after transfection of layer V/VI pyramidal neurons with ChR2(ET/TC) by IUE. The LFP is displayed before (top) and after band-pass filtering (4–100 Hz) (middle) together with the corresponding colour-coded wavelet spectrum at identical timescale. (**b**) Bar diagrams displaying the LFP power during the first half (1.5 s), the second half (1.5 s) and after (post, 1.5 s) ramp stimulus when normalized to the power before stimulation (pre, 1.5 s). Network activity in theta (θ, 4–12 Hz), beta (β, 12–30 Hz) and gamma (γ, 30–100 Hz) frequency bands ($n=12$ pups) was considered. (**c**) Polar plots displaying the phase-locking of light-triggered (red, stimulation 3 s, post 3 s) and spontaneous (grey) MUA to oscillatory activity from layer V/VI ChR2(ET/TC)-transfected mice ($n=61$ recording sites from 12 pups). Bar diagrams display the locking strength. (**d**) Same as (**c**) for SUA ($n=152$ units from 12 pups). For (**b**) individual values corresponding to pups with light-induced oscillations are displayed as black crosses. For (**c**,**d**) the values from individual units are shown as red and grey dots, whereas the arrows correspond to the mean resulting group vectors. Data are presented as mean ± s.e.m. $^{*}P<0.05$, $^{**}P<0.01$, and $^{***}P<0.001$, two-sided *t*-tests and circular statistics toolbox.

efficiently eliminated by subtraction[54], stimuli trains caused pronounced current sinks due to simultaneous opening of light-gated channels (large negative deflections of LFP in Supplementary Fig. 7c,d) that masked the induced network activity. This was not the case for ramp stimulation. Neuronal firing and early network oscillations were induced after a critical level of light intensity was reached. The LFP power gradually increased, persisting even after the stimulus. Similar to the activation of the adult brain[55,56], both train and ramp stimulations led to plastic boosting of activation within neuronal networks, as shown by the effects on LFP and MUA outlasting the stimulus. Its consequences for the functional maturation of the cortical circuitry remain to be assessed. Third, the entire investigation was performed on anesthetized neonatal mice. However, we note that previous comparisons of coordinated activity patterns in urethane-anesthetized and -non-anesthetized sleeping rodents identified no differences at neonatal age[8], when rodents sleep 70% of the time[57]. Therefore, we hypothesize that layer II/III and layer V/VI pyramidal neurons of the PL play a similar role as described here in anesthetized animals for the emergence of network oscillations in non-anesthetized naturally sleeping pups, although this remains to be tested directly.

In adults, optogenetic stimulation has been utilized to establish causal links between cell-type-specific activation and specific behavioural performance. By these means, the behavioural readout of fast beta and gamma oscillations has been characterized with relationship to their cellular substrates[58–60]. Modelling work proposed a dual origin of beta oscillations: they emerge either as 'slow gamma' within feedforward inhibitory networks including parvalbumin-expressing inteneurons, which are absent during neonatal development, or from the interplay between interneurons firing in gamma range and pyramidal neurons firing at lower beta frequency[61,62]. During early development, beta oscillations seem to be generated within an intracortical circuit that involves the activation of pyramidal neurons in layer II/III (shown here), which project to interneurons in layer V and boost their local inhibitory action entraining cortical circuits in gamma frequency band[8]. Taking into account the limited behavioural abilities of pups, it has been hypothesized that the complex patterns of early network activity do not have a direct behavioural readout but rather regulate the network wiring and neonatal plasticity, which is mandatory for later cortical function[8,63,64]. The present experimental strategy and findings open new perspectives for directly testing this hypothesis. Chronic optogenetic manipulation during defined developmental time windows (that is, critical/sensitive periods) of cellular elements identified as being necessary for the generation of early network oscillations will reveal, how the early cellular interplay controls circuit function later in life.

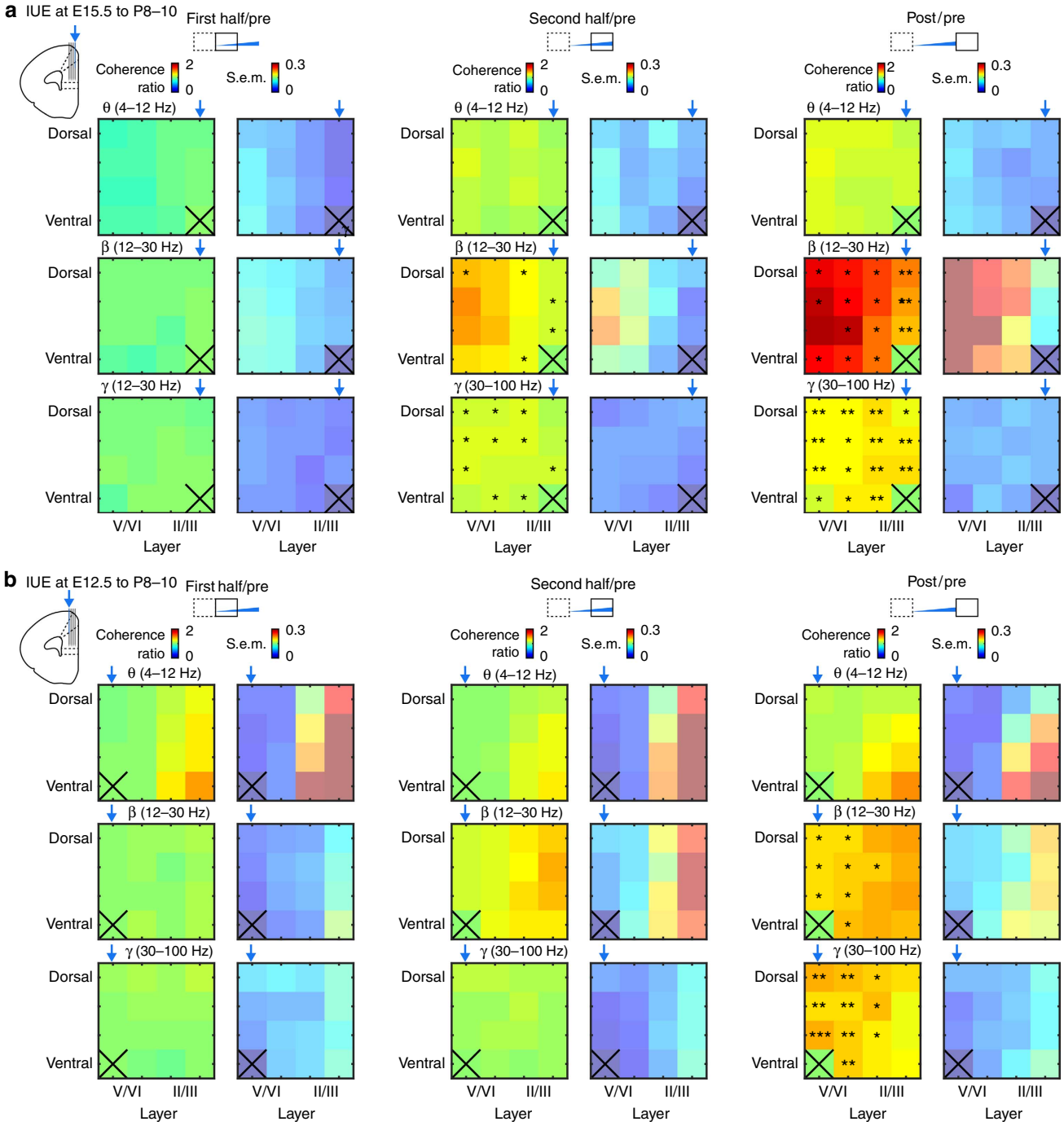

Figure 7 | Frequency-dependent entrainment of neonatal prelimbic cortex in response to layer-specific optogenetic activation *in vivo*. (**a**) Colour-coded images displaying the baseline normalized (pre, 1.5 s) coherence (mean and s.e.m.) between light-stimulated reference recording site in layer II/III (marked by X) and all other sites covering the PL depth during the first half (1.5 s), the second half (1.5 s) and after (post, 1.5 s) ramp stimulus. The coherence was calculated for theta (θ, 4–12 Hz, top), beta (β, 12–30 Hz, middle) and gamma (γ, 30–100 Hz, bottom) frequency bands and values were averaged ($n=11$ pups). (**b**) Same as (**a**) for layer V/VI-expressing P8–10 mice ($n=6$ pups). Reference recording site was located in the light-stimulated layer V/VI (marked by X). Blue arrows indicate the position of the light fibre. $^{*}P<0.05$, $^{**}P<0.01$ and $^{***}P<0.001$, two-sided *t*-tests.

Methods

Animals. All experiments were performed in compliance with the German laws and the guidelines of the European Community for the use of animals in research and were approved by the local ethical committee (111/12, 132/12). Experiments were performed on female and male C57Bl/6J mice at the age of P8–10 after IUE at E12.5 or E15.5.

***In utero* electroporation.** Timed-pregnant C57Bl/6J mice from the animal facility of the University Medical Center Hamburg-Eppendorf were housed individually in breeding cages at a 12 h light/12 h dark cycle and fed *ad libitum*. The day of vaginal plug detection was defined E0.5, while the day of birth was assigned as P0. Additional wet food was provided on a daily basis and was supplemented with 2–4 drops Metacam (0.5 mg ml^{-1}; Boehringer-Ingelheim, Germany) from one day before until two days after surgery. At E12.5 or E14.5–15.5 randomly assigned pregnant mice were injected subcutaneously with buprenorphine (0.05 mg/kg body weight) 30 min before surgery. The surgery was performed on a heating blanket and toe pinch and breathing were monitored throughout. Under isoflurane anesthesia (induction: 5%; maintenance: 3.5%), the eyes of the dam were covered with eye ointment to prevent damage before the uterine horns were exposed and

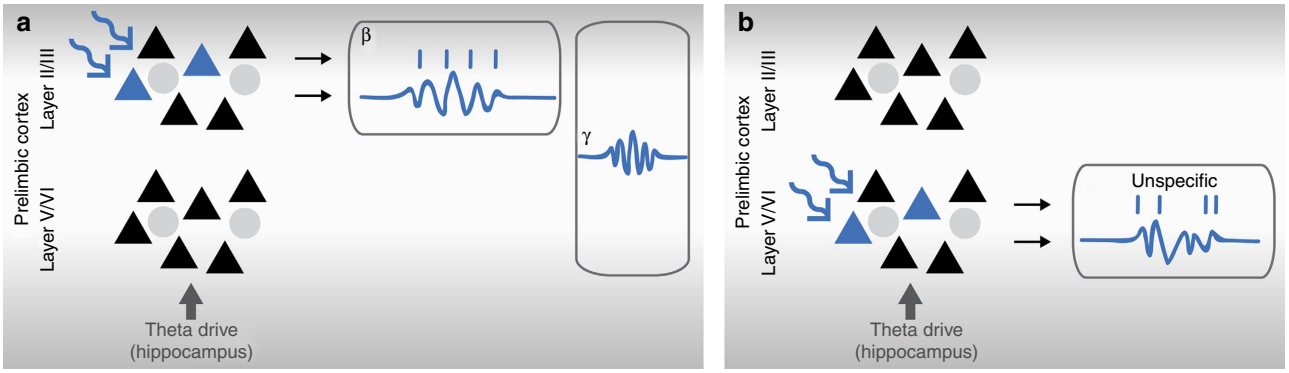

Figure 8 | Schematic diagram depicting the contribution of layer II/III and layer V/VI to the generation of early oscillatory activity in distinct frequency bands investigated by optogenetic manipulation. (**a**) Light stimulation of pyramidal neurons in layer II/III facilitates the generation of beta oscillations and increases the intra- (beta band) and interlayer (gamma band) synchrony. (**b**) Stimulation of pyramidal neurons in layer V/VI leads to network activation in all frequency bands and synchronizes solely deeper layers. Blue triangle, ChR2(ET/TC)-transfected pyramidal neurons; black triangle, non-transfected pyramidal neurons; grey circles, interneurons.

moistened with warm sterile PBS (37 °C). Solution containing 1.25 μg μl^{-1} DNA (pAAV-EF1α-ChR2(E123T/T159C)-2A-tDimer2, pAAV-synapsin-ChR2(E123T/T159C)-2A-tDimer2, pAAV-CAG-ChR2(E123T/T159C)-2AtDimer2 or pAAV-CAG-tDimer2)) and 0.1% fast green dye at a volume of 0.75–1.25 μl were injected into the right lateral ventricle of individual embryos using pulled borosilicate glass capillaries with a sharp and long tip. Plasmid DNA was purified with NucleoBond (Macherey-Nagel, Germany). 2A encodes for a ribosomal skip sentence, splitting the fluorescent protein tDimer2 from the opsin during gene translation. Each embryo within the uterus was placed between the electroporation tweezer-type paddles (3 mm diameter for E12.5, 5 mm diameter for E14.5–15.5; Protech, TX, USA) that were oriented at a rough 20° leftward angle from the midline and a rough 10° angle downward from anterior to posterior. By these means, neural precursor cells from the subventricular zone, which radially migrate into the medial PFC, were transfected. Electrode pulses (35 V, 50 ms) were applied five times at intervals of 950 ms controlled by an electroporator (CU21EX; BEX, Japan). Most caudal embryos were not electroporated to minimize lethality. Uterine horns were placed back into the abdominal cavity after electroporation. The abdominal cavity was filled with warm sterile PBS (37 °C) and abdominal muscles and skin were sutured individually with absorbable and non-absorbable suture thread, respectively. The surgery was performed on a heating blanket, and toe pinch reflex and breathing were monitored. After recovery, pregnant mice were returned to their home cages, which were half placed on a heating blanket for two days after surgery. For most of the pups, opsin expression was assessed with a portable fluorescent flashlight (Nightsea, MA, USA) through the intact skull and skin at P2–3 and confirmed post mortem by fluorescence microscopy in brain slices. Pups without expression in the PFC were excluded from the analysis. Mice of both sexes were used.

Behavioural examination. Mouse pups were tested for their somatic development and reflexes at P2, P5 and P8. Weight, body and tail length were assessed. Surface righting reflex was quantified as time (max 30 s) until the pup turned over with all four feet on the ground after being placed on its back. Cliff aversion reflex was quantified as time (max 30 s) until the pup withdrew after snout and forepaws were positioned over an elevated edge. Vibrissa placing was rated positive if the pup turned its head after gently touching the whiskers with a toothpick.

Histology and immunohistochemistry. To quantify the transfection, P8–10 mice were anesthetized with 10% ketamine (aniMedica, Germany)/2% xylazine (WDT, Germany) in 0.9% NaCl solution (10 μg/g body weight, intraperitoneally (i.p.)) and transcardially perfused with Histofix (Carl Roth, Germany) containing 4% paraformaldehyde. Brains were postfixed in 4% paraformaldehyde for 24 h and sectioned coronally at 50 μm. Free-floating slices were permeabilized and blocked with PBS containing 0.8% Triton X-100 (Sigma-Aldrich, MO, USA), 5% normal bovine serum (Jackson Immuno Research, PA, USA) and 0.05% sodium azide. Subsequently, slices were incubated overnight with mouse monoclonal Alexa Fluor-488-conjugated antibody against NeuN (1:100, MAB377X; Merck Millipore, MA, USA), rabbit polyclonal primary antibody against CaM kinase II (1:200, PA5-38239; Thermo Fisher Scientific, MA, USA) or rabbit polyclonal primary antibody against GABA (1:1,000, no. A2052; Sigma-Aldrich), followed by 2 h incubation with Alexa Fluor-488 goat anti-rabbit IgG secondary antibody (1:500, A11008; Merck Millipore). Slices were transferred to glass slides and covered with Fluoromount (Sigma-Aldrich). Wide field fluorescence images were acquired to reconstruct the recording electrode position in brain slices of electrophysiologically investigated pups and to localize tDimer2 expression in pups after IUE. High magnification images were acquired with a confocal microscope (DM IRBE, Leica, Germany) to quantify tDimer2 expression and immunopositive cells (4 brain slices per investigated mouse). All images were similarly analysed with ImageJ.

***In vitro* electrophysiology paired with optogenetic stimulation.** Whole-cell patch-clamp recordings were performed from fluorescently labelled layer II/III and layer V/VI prelimbic neurons in brain slices of P8–10 mice after IUE at E15.5 and E12.5, respectively. Pups were decapitated, brains were removed and immediately sectioned coronally at 300 μm in ice-cold oxygenated high sucrose-based artificial cerebral spinal fluid (ACSF) (in mM: 228 sucrose, 2.5 KCl, 1 NaH_2PO_4, 26.2 $NaHCO_3$, 11 glucose, 7 $MgSO_4$; 320 mOsm) with a vibratome. Slices were incubated in oxygenated ACSF (in mM: 119 NaCl, 2.5 KCl, 1 NaH_2PO_4, 26.2 $NaHCO_3$, 11 glucose, 1.3 $MgSO_4$; 320 mOsm) at 37 °C for 45 min before cooling to room temperature and superfused with oxygenated ACSF in the recording chamber. tDimer2-positive neurons were patched under optical control using pulled borosilicate glass capillaries (tip resistance of 4–7 MΩ) filled with pipette solution (in mM: 130 K-gluconate, 10 HEPES, 0.5 EGTA, 4 Mg-ATP, 0.3 Na-GTP, 8 NaCl; 285 mOsm, pH 7.4). Recordings were controlled with the Ephus software[65] in the Matlab environment (MathWorks, MA, USA). Capacitance artefacts and series resistance were minimized using the built-in circuitry of the patch-clamp amplifier (Axopatch 200B; Molecular devices, CA, USA). Responses of neurons to hyper- and depolarizing current injections, as well as blue light pulses (473 nm, 5.2 mW mm^{-1}) were digitized at 5 kHz in current-clamp mode. Linearly increasing chirp current injections were applied for membrane resonance measurements. Impedance was calculated as ratio of Fourier transforms of the measured voltage response to chirp current injections.

***In vivo* electrophysiology combined with optogenetic stimulation.** Multisite extracellular recordings were performed in the PL of P8–10 mice. Mice were injected i.p. with urethane (1 mg/g body weight; Sigma-Aldrich) before surgery. Under isoflurane anesthesia (induction: 5%; maintenance: 2.5%), the head of the pup was fixed into a stereotaxic apparatus using two plastic bars mounted on the nasal and occipital bones with dental cement. The bone above the PFC (0.5 mm anterior to bregma, 0.1 mm right to the midline for layer II/III, 0.5 mm for layer V/VI) was carefully removed by drilling a hole of <0.5 mm in diameter. After a 10–20 min recovery period on a heating blanket, one- or four-shank multisite optoelectrodes (NeuroNexus, MI, USA) were inserted 2–2.4 mm deep into PFC perpendicular to the skull surface. One-shank optoelectrodes contained 1×16 recordings sites (0.4–0.8 MΩ impedance, 100 μm spacing) aligned with an optical fibre (105 μm diameter) ending 200 μm above the top recording site. Four-shank optoelectrodes contained 4×4 recording sites (0.4–0.8 MΩ impedance, 100 μm spacing, 125 μm intershank spacing) aligned with optical fibres (50 μm diameter) ending 200 μm above the top recording sites. A silver wire was inserted into the cerebellum and served as ground and reference electrode. Extracellular signals were band-pass filtered (0.1–9,000 Hz) and digitized (32 kHz) with a multichannel extracellular amplifier (Digital Lynx SX; Neuralynx, Bozeman, MO, USA) and the Cheetah acquisition software (Neuralynx). Spontaneous (that is, not induced by light stimulation) activity was recorded for 15 min at the beginning and end of each recording session as baseline activity. Pulsed (laser on-off) and ramp (linearly increasing power) light stimulations were performed with an arduino uno (Arduino, Italy) controlled diode laser (473 nm; Omicron, Austria). Laser power was adjusted to trigger neuronal spiking in response to $>25\%$ of 3-ms-long light pulses at 16 Hz. Resulting light power was in the range of 20–40 mW mm^{-1} at the fibre tip. Light-induced LFP artefacts were measured at the end of the experiment.

For this, mice were killed with an injection of 10% ketamine/2% xylazine in 0.9% NaCl solution (20 µg/g body weight, i.p.) abolishing brain activity while maintaining the optoelectrode position. Stimulation protocols were repeated 15 min after the lethal injection and the photoelectric artefacts were eliminated from alive recordings by subtraction after scaling to the immediate downstroke (that is, negative deflection 0–1.5 ms after the start of the light pulse) of the alive recordings in response to light pulses.

Estimation of light and heat propagation. The spatiotemporal propagation of light and heat were estimated using a recently developed model for *in vivo* data[40] for pulsed illumination (473 nm, 3 s, 3 ms pulses) at 2 to 32 Hz and 1 to 10 mW light power at the fibre tip (105 µm, numerical aperture 0.22) with optical absorption parameters for brain tissue[66]. Measured light power at the fibre tip before inserting the optoelectrode was in the range from 1 to 5 mW.

AP Action potential modelling. The conductance-based Hodgkin–Huxley model solved with the Euler method was used to investigate the influence of Na^+/K^+ conductance changes during development on AP properties in response to current injections[39]. APs were modelled with different levels of Na^+/K^+ conductance (Na^+: 0.6 mS cm^{-2}; K^+: 0.18 mS cm^{-2} multiplied by 1.0 to 3.0) and AP properties in response to current injections were calculated.

Data analysis. Data were imported and analysed offline using custom-written tools in the Matlab software (MathWorks). For *in vitro* data, all potentials were corrected for liquid junction potentials with −10 mV for the gluconate-based electrode solution[67]. The RMP was measured immediately after obtaining the whole-cell configuration. For the determination of the input resistance, hyperpolarizing current pulses of 200 ms duration were applied. Active membrane properties and current–voltage relationships were assessed by unsupervised analysis of responses to a series of 600 ms long hyper- and depolarizing current pulses. Amplitude of APs was measured from threshold to peak.

In vivo data were processed as following: band-pass filtered (500–5,000 Hz) to analyse MUA and low-pass filtered (<1,500 Hz) using a third-order Butterworth filter before downsampling to 3.2 kHz to analyse LFP. All filtering procedures were performed in a manner preserving phase information. MUA was detected as the peak of negative deflections greater than five times the standard deviation of filtered signals. SUA was detected and clustered using Offline Sorter (Plexon, TC, USA) and 1–4 single units were detected at each recording site. Spikes occurring in a 15 ms time window after the start of a light pulse were considered to be light-evoked. Stimulation efficacy was calculated as the probability of at least one spike occurring in this period. Discontinuous network oscillations in the LFP were detected using a previously developed unsupervised algorithm[34]. Briefly, deflections of the root mean square of band-pass filtered signals (1–100 Hz) exceeding a variance-depending threshold were assigned as network oscillations. The threshold was determined by a Gaussian fit to the values ranging from 0 to the global maximum of the root-mean-square histogram. Only oscillations lasting >1 s were considered for further analysis. Time–frequency plots were calculated by transforming the data using Morlet continuous wavelet. For periods with light stimulations, photoelectric artefacts recorded post mortem were filtered (1–400 Hz), averaged, scaled to the immediate downstroke (0–1.5 ms after light onset) of the alive recordings and subtracted from the alive recordings. This immediate downstroke reflects the photoelectric artefact and is largely independent of currents sinks created by synchronized opening of ChRs. MUA band was not contaminated by light artefacts.

Statistical analyses were performed using SPSS Statistics 21 (IBM, NY, USA) or Matlab. Data were tested for normal distribution by the Shapiro–Wilk test. Normally distributed data were tested for significant differences ($^*P<0.05$, $^{**}P<0.01$ and $^{***}P<0.001$) using paired *t*-test, unpaired *t*-test or one-way repeated-measures analysis of variance with Bonferoni-corrected *post hoc* analysis. Not normally distributed data were tested with the nonparametric Mann–Whitney *U*-test. The circular statistics toolbox was used to test for significant differences in the phase locking data. Data are presented as mean ± s.e. of the mean. No statistical measures were used to estimate sample size since effect size was unknown. Investigators were not blinded to the group allocation during the experiments. Unsupervised analysis software was used if possible to preclude investigator biases.

Data availability. The authors declare that all data and code supporting the findings of this study are included in the manuscript and its Supplementary Information or are available from the corresponding authors on request.

References

1. Lamblin, M. D. *et al.* Électroencéphalographie du nouveau-né prématuré et à terme. Aspects maturatifs et glossaire. *Clin. Neurophysiol.* **29,** 123–219 (1999).
2. Khazipov, R. *et al.* Early motor activity drives spindle bursts in the developing somatosensory cortex. *Nature* **432,** 758–761 (2004).
3. Hanganu, I. L., Ben-Ari, Y. & Khazipov, R. Retinal waves trigger spindle bursts in the neonatal rat visual cortex. *J. Neurosci.* **26,** 6728–6736 (2006).
4. Blumberg, M. S. *et al.* Development of twitching in sleeping infant mice depends on sensory experience. *Curr. Biol.* **25,** 656–662 (2015).
5. Kirmse, K. *et al.* GABA depolarizes immature neurons and inhibits network activity in the neonatal neocortex *in vivo*. *Nat. Commun.* **6,** 7750 (2015).
6. Ben-Ari, Y. The GABA excitatory/inhibitory developmental sequence: a personal journey. *Neuroscience* **279,** 187–219 (2014).
7. Brockmann, M. D., Poschel, B., Cichon, N. & Hanganu-Opatz, I. L. Coupled oscillations mediate directed interactions between prefrontal cortex and hippocampus of the neonatal rat. *Neuron* **71,** 332–347 (2011).
8. Bitzenhofer, S. H., Sieben, K., Siebert, K. D., Spehr, M. & Hanganu-Opatz, I. L. Oscillatory activity in developing prefrontal networks results from theta–gamma-modulated synaptic inputs. *Cell Rep.* **11,** 486–497 (2015).
9. Tuncdemir, S. N. *et al.* Early somatostatin interneuron connectivity mediates the maturation of deep layer cortical circuits. *Neuron* **89,** 521–535 (2016).
10. Kanold, P. O. & Shatz, C. J. Subplate neurons regulate maturation of cortical inhibition and outcome of ocular dominance plasticity. *Neuron* **51,** 627–638 (2006).
11. Markram, H. *et al.* Interneurons of the neocortical inhibitory system. *Nat. Rev. Neurosci.* **5,** 793–807 (2004).
12. Harris, K. D. & Mrsic-Flogel, T. D. Cortical connectivity and sensory coding. *Nature* **503,** 51–58 (2013).
13. Fenno, L., Yizhar, O. & Deisseroth, K. The development and application of optogenetics. *Annu. Rev. Neurosci.* **34,** 389–412 (2011).
14. Williams, S. C. & Deisseroth, K. Optogenetics. *Proc. Natl Acad. Sci. USA* **110,** 16287 (2013).
15. Liu, X., Ramirez, S. & Tonegawa, S. Inception of a false memory by optogenetic manipulation of a hippocampal memory engram. *Philos. Trans. R. Soc. Lond. Ser. B* **369,** 20130142 (2014).
16. Johansen, J. P. *et al.* Hebbian and neuromodulatory mechanisms interact to trigger associative memory formation. *Proc. Natl Acad. Sci. USA* **111,** E5584–E5592 (2014).
17. Siegle, J. H. & Wilson, M. A. Enhancement of encoding and retrieval functions through theta phase-specific manipulation of hippocampus. *eLife* **3,** e03061 (2014).
18. Spellman, T. *et al.* Hippocampal–prefrontal input supports spatial encoding in working memory. *Nature* **522,** 309–314 (2015).
19. Lepousez, G. & Lledo, P. M. Odor discrimination requires proper olfactory fast oscillations in awake mice. *Neuron* **80,** 1010–1024 (2013).
20. Olcese, U., Iurilli, G. & Medini, P. Cellular and synaptic architecture of multisensory integration in the mouse neocortex. *Neuron* **79,** 579–593 (2013).
21. Peron, S. P., Freeman, J., Iyer, V., Guo, C. & Svoboda, K. A cellular resolution map of barrel cortex activity during tactile behavior. *Neuron* **86,** 783–799 (2015).
22. Tye, K. M. & Deisseroth, K. Optogenetic investigation of neural circuits underlying brain disease in animal models. *Nat. Rev. Neurosci.* **13,** 251–266 (2012).
23. Kim, I. H. *et al.* Spine pruning drives antipsychotic-sensitive locomotion via circuit control of striatal dopamine. *Nat. Neurosci.* **18,** 883–891 (2015).
24. Steinberg, E. E., Christoffel, D. J., Deisseroth, K. & Malenka, R. C. Illuminating circuitry relevant to psychiatric disorders with optogenetics. *Curr. Opin. Neurobiol.* **30,** 9–16 (2015).
25. Minlebaev, M., Colonnese, M., Tsintsadze, T., Sirota, A. & Khazipov, R. Early gamma oscillations synchronize developing thalamus and cortex. *Science* **334,** 226–229 (2011).
26. Gireesh, E. D. & Plenz, D. Neuronal avalanches organize as nested theta- and beta/gamma-oscillations during development of cortical layer 2/3. *Proc. Natl Acad. Sci. USA* **105,** 7576–7581 (2008).
27. Taymans, J. M. *et al.* Comparative analysis of adeno-associated viral vector serotypes 1, 2, 5, 7, and 8 in mouse brain. *Hum. Gene. Ther.* **18,** 195–206 (2007).
28. Zhang, F. *et al.* Optogenetic interrogation of neural circuits: technology for probing mammalian brain structures. *Nat. Protoc.* **5,** 439–456 (2010).
29. Klein, R. L. *et al.* Efficient neuronal gene transfer with AAV8 leads to neurotoxic levels of tau or green fluorescent proteins. *Mol. Ther.* **13,** 517–527 (2006).
30. Bru, T., Salinas, S. & Kremer, E. J. An update on canine adenovirus type 2 and its vectors. *Viruses* **2,** 2134–2153 (2010).
31. Tabata, H. & Nakajima, K. Efficient *in utero* gene transfer system to the developing mouse brain using electroporation: visualization of neuronal migration in the developing cortex. *Neuroscience* **103,** 865–872 (2001).
32. Borrell, V., Yoshimura, Y. & Callaway, E. M. Targeted gene delivery to telencephalic inhibitory neurons by directional *in utero* electroporation. *J. Neurosci. Methods* **143,** 151–158 (2005).
33. Niwa, M. *et al.* Knockdown of DISC1 by *in utero* gene transfer disturbs postnatal dopaminergic maturation in the frontal cortex and leads to adult behavioral deficits. *Neuron* **65,** 480–489 (2010).

34. Cichon, N. B., Denker, M., Grun, S. & Hanganu-Opatz, I. L. Unsupervised classification of neocortical activity patterns in neonatal and pre-juvenile rodents. *Front. Neural Circuits* **8,** 50 (2014).
35. Berndt, A. *et al.* High-efficiency channelrhodopsins for fast neuronal stimulation at low light levels. *Proc. Natl Acad. Sci. USA* **108,** 7595–7600 (2011).
36. Marin, O. & Rubenstein, J. L. Cell migration in the forebrain. *Annu. Rev. Neurosci.* **26,** 441–483 (2003).
37. Greig, L. C., Woodworth, M. B., Galazo, M. J., Padmanabhan, H. & Macklis, J. D. Molecular logic of neocortical projection neuron specification, development and diversity. *Nat. Rev. Neurosci.* **14,** 755–769 (2013).
38. Rakic, P., Ayoub, A. E., Breunig, J. J. & Dominguez, M. H. Decision by division: making cortical maps. *Trends. Neurosci.* **32,** 291–301 (2009).
39. Hodgkin, A. L. & Huxley, A. F. A quantitative description of membrane current and its application to conduction and excitation in nerve. *J. Physiol.* **117,** 500–544 (1952).
40. Stujenske, J. M., Spellman, T. & Gordon, J. A. Modeling the spatiotemporal dynamics of light and heat propagation for *in vivo* optogenetics. *Cell Rep.* **12,** 525–534 (2015).
41. Reig, R., Mattia, M., Compte, A., Belmonte, C. & Sanchez-Vives, M. V. Temperature modulation of slow and fast cortical rhythms. *J. Neurophysiol.* **103,** 1253–1261 (2010).
42. Cardin, J. A. *et al.* Targeted optogenetic stimulation and recording of neurons *in vivo* using cell-type-specific expression of Channelrhodopsin-2. *Nat. Protoc.* **5,** 247–254 (2010).
43. Han, X. *In vivo* application of optogenetics for neural circuit analysis. *ACS Chem. Neurosci.* **3,** 577–584 (2012).
44. Hartung, H., Brockmann, M. D., Poschel, B., De Feo, V. & Hanganu-Opatz, I. L. Thalamic and entorhinal network activity differently modulates the functional development of prefrontal–hippocampal interactions. *J. Neurosci.* **36,** 3676–3690 (2016).
45. Hanganu-Opatz, I. L. Between molecules and experience: role of early patterns of coordinated activity for the development of cortical maps and sensory abilities. *Brain Res. Rev.* **64,** 160–176 (2010).
46. Khazipov, R., Minlebaev, M. & Valeeva, G. Early gamma oscillations. *Neuroscience* **250,** 240–252 (2013).
47. Hanganu, I. L., Staiger, J. F., Ben-Ari, Y. & Khazipov, R. Cholinergic modulation of spindle bursts in the neonatal rat visual cortex *in vivo*. *J. Neurosci.* **27,** 5694–5705 (2007).
48. Janiesch, P. C., Kruger, H. S., Poschel, B. & Hanganu-Opatz, I. L. Cholinergic control in developing prefrontal–hippocampal networks. *J. Neurosci.* **31,** 17955–17970 (2011).
49. Yang, J. W. *et al.* Thalamic network oscillations synchronize ontogenetic columns in the newborn rat barrel cortex. *Cereb. Cortex* **23,** 1299–1316 (2013).
50. DeNardo, L. A., Berns, D. S., DeLoach, K. & Luo, L. Connectivity of mouse somatosensory and prefrontal cortex examined with trans-synaptic tracing. *Nat. Neurosci.* **18,** 1687–1697 (2015).
51. Beul, S. F. & Hilgetag, C. C. Towards a 'canonical' agranular cortical microcircuit. *Front. Neuroanat.* **8,** 165 (2014).
52. Buzsaki, G. *et al.* Tools for probing local circuits: high-density silicon probes combined with optogenetics. *Neuron* **86,** 92–105 (2015).
53. Wu, F. *et al.* Monolithically integrated muLEDs on silicon neural probes for high-resolution optogenetic studies in behaving animals. *Neuron* **88,** 1136–1148 (2015).
54. Beltramo, R. *et al.* Layer-specific excitatory circuits differentially control recurrent network dynamics in the neocortex. *Nat. Neurosci.* **16,** 227–234 (2013).
55. Li, N. *et al.* Optogenetic-guided cortical plasticity after nerve injury. *Proc. Natl Acad. Sci. USA* **108,** 8838–8843 (2011).
56. Alonso, M. *et al.* Activation of adult-born neurons facilitates learning and memory. *Nat. Neurosci.* **15,** 897–904 (2012).
57. Cirelli, C. & Tononi, G. Cortical development, electroencephalogram rhythms, and the sleep/wake cycle. *Biol. Psychiatry* **77,** 1071–1078 (2015).
58. Cardin, J. A. *et al.* Driving fast-spiking cells induces gamma rhythm and controls sensory responses. *Nature* **459,** 663–667 (2009).
59. Siegle, J. H., Pritchett, D. L. & Moore, C. I. Gamma-range synchronization of fast-spiking interneurons can enhance detection of tactile stimuli. *Nat. Neurosci.* **17,** 1371–1379 (2014).
60. Lu, Y. *et al.* Optogenetically induced spatiotemporal gamma oscillations and neuronal spiking activity in primate motor cortex. *J. Neurophysiol.* **113,** 3574–3587 (2015).
61. Whittington, M. A., Traub, R. D., Kopell, N., Ermentrout, B. & Buhl, E. H. Inhibition-based rhythms: experimental and mathematical observations on network dynamics. *Int. J. Psychophysiol.* **38,** 315–336 (2000).
62. Womelsdorf, T., Valiante, T. A., Sahin, N. T., Miller, K. J. & Tiesinga, P. Dynamic circuit motifs underlying rhythmic gain control, gating and integration. *Nat. Neurosci.* **17,** 1031–1039 (2014).
63. Khazipov, R., Valeeva, G. & Khalilov, I. Depolarizing GABA and developmental epilepsies. *CNS Neurosci. Ther.* **21,** 83–91 (2015).
64. Winnubst, J., Cheyne, J. E., Niculescu, D. & Lohmann, C. Spontaneous activity drives local synaptic plasticity *in vivo*. *Neuron* **87,** 399–410 (2015).
65. Suter, B. A. *et al.* Ephus: multipurpose data acquisition software for neuroscience experiments. *Front. Neural Circuits* **4,** 100 (2010).
66. Johansson, J. D. Spectroscopic method for determination of the absorption coefficient in brain tissue. *J. Biomed. Opt.* **15,** 057005 (2010).
67. Mienville, J. M. & Pesold, C. Low resting potential and postnatal upregulation of NMDA receptors may cause Cajal–Retzius cell death. *J. Neurosci.* **19,** 1636–1646 (1999).

Acknowledgements

We thank Annette Marquardt, Iris Ohmert and Achim Dahlmann for technical assistance. This work was funded by grants from the European Research Council (ERC-2015-CoG 681577 to I.L.H.-O.) and the German Research Foundation (SPP 1665 to I.L.H.-O. and T.G.O., SFB 936 B5 to I.L.H.-O. and B7 to T.G.O., FOR 2419 P7 to J.S.W. and C.E.G., FOR 2419 P4 to T.G.O. and SPP 1926 to J.S.W.).

Author contributions

I.L.H.-O. designed the experiments, S.H.B. and J.A. carried out the experiments, S.H.B. and J.A. analysed the data, A.W., C.E.G., J.S.W. and T.G.O. contributed to the establishment of experimental protocols and provided the constructs, I.L.H.-O., S.H.B. and J.A. interpreted the data and wrote the paper. All authors discussed and commented on the manuscript.

Additional information

Supplementary Information accompanies this paper at http://www.nature.com/naturecommunications

Competing financial interests: The authors declare no competing financial interests.

Reprints and permission information is available online at http://npg.nature.com/reprintsandpermissions/

How to cite this article: Bitzenhofer, S. H. *et al.* Layer-specific optogenetic activation of pyramidal neurons causes beta-gamma entrainment of neonatal networks. *Nat. Commun.* **8,** 14563 doi: 10.1038/ncomms14563 (2017).

Publisher's note: Springer Nature remains neutral with regard to jurisdictional claims in published maps and institutional affiliations.

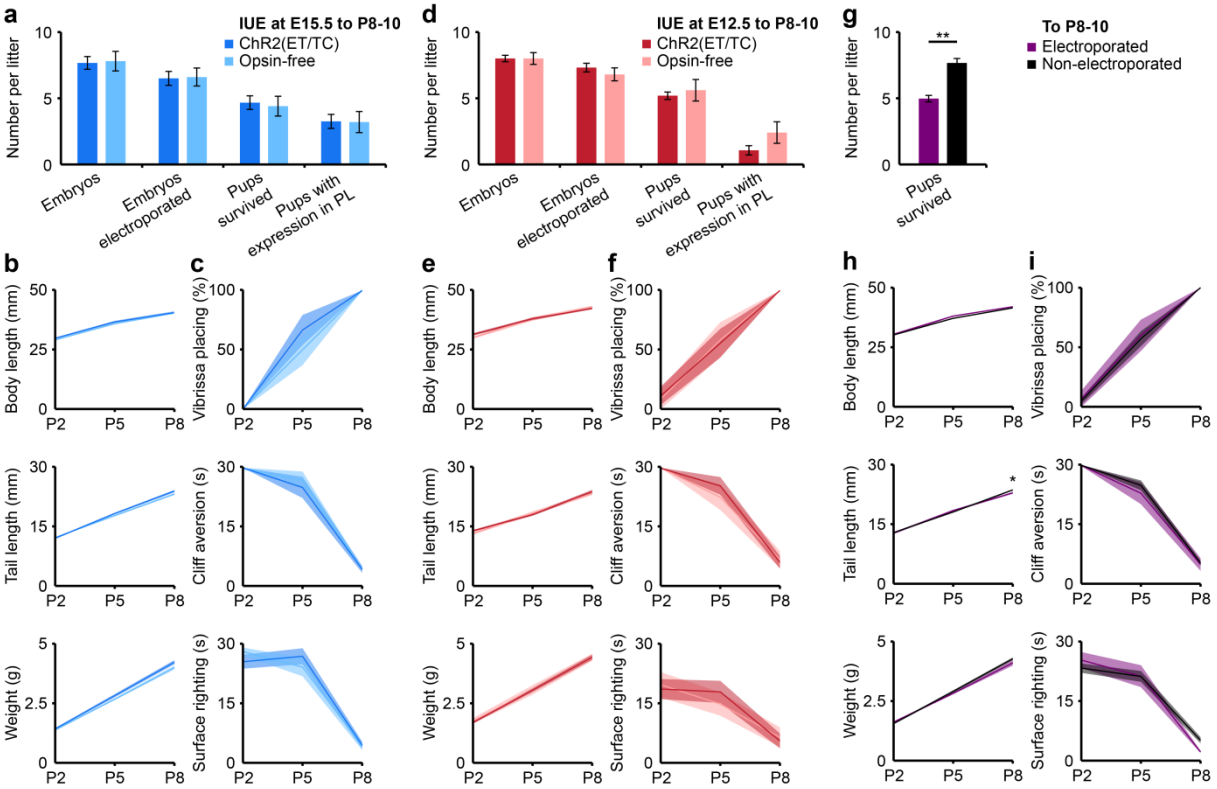

Supplementary Figure 1 (related to Figure 1): Somatic and reflex development of mouse pups transfected by *in utero* electroporation. **(a)** Bar diagram displaying the mean number of embryos, electroporated embryos, surviving pups, and positively transfected pups when ChR2(ET/TC)-containing (dark blue, n=12 litter) and opsin-free constructs (light blue, n=5 litter) were tranfected by IUE at E15.5. **(b)** Line plots displaying the developmental profile of somatic growth [body length (top), tail length (middle), weight (bottom)] of P2-8 pups expressing ChR2(ET/TC) (dark blue, n=17 pups) or opsin-free constructs (light blue, n=16 pups) in layer II/III pyramidal neurons. **(c)** Line plots displaying the development profile of reflexes [vibrissa placing (top), cliff aversion (middle) and surface righting reflexes (bottom)] of P2-8 pups expressing ChR2(ET/TC) (n=17, dark blue) or opsin-free constructs (n=16, light blue) in layer II/III pyramidal neurons. **(d)-(f)** Same as (a)-(c) for pups expressing ChR2(ET/TC)-containing (dark red, n=16 litter, n=18 pups) or opsin-free constructs (light red, n=5 litter, n=12 pups) in layer V/VI pyramidal neurons. **(g)** Bar diagram displaying the survival rate of electroporated (violet) and non-electroporated litters (black). **(h)-(i)** Same as (b)-(c) for electroporated (violet, n=63 pups) and non-electroporated pups (black, n=15 pups). Data are displayed as mean ± SEM. *p < 0.05, **p < 0.01, and ***p < 0.001, two-sided t-tests.

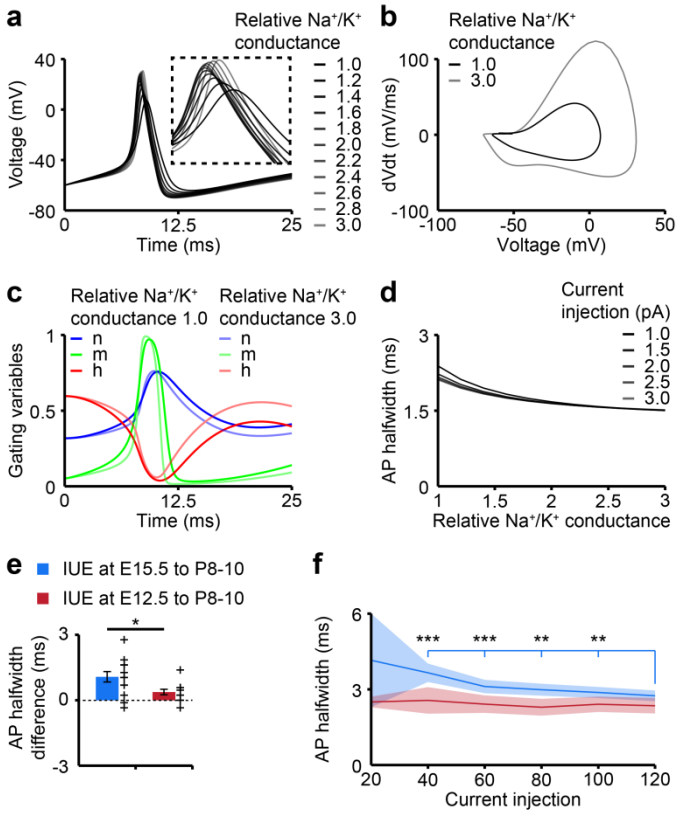

Supplementary Figure 2 (related to Figure 2,3): Control of AP shape by Na^+/K^+ conductance and input strength. **(a)** Dependence of AP time course on augmenting Na^+/K^+ conductance as modeled by the Hodgkin-Huxley conductance based model. **(b)** Phase plots of modeled APs for low (Na^+: 0.6 mS/cm²; K^+: 0.18 mS/cm²) and high (Na^+: 1.8 mS/cm²; K^+: 0.54 mS/cm²) Na^+/K^+ conductance. **(c)** Time course of the gating variables m, n and h of the differential equations of the Hodgkin-Huxley model. **(d)** Line plots displaying the relationship between AP half-width and current input for different Na^+/K^+ conductances. **(e)** Bar plot displaying the difference between half-width of APs triggered by current and by light for layer II/III (blue, n=13 neurons) and layer V/VI (red, n=12 neurons) pyramidal neurons. **(f)** Line plots displaying the relationship between APs half-width and injected current for transfected layer II/III (blue, n=13) and V/VI (red, n=12) pyramidal neurons. Data are presented as mean ± SEM. *p < 0.05, **p < 0.01, and ***p < 0.001, two-sided t-test.

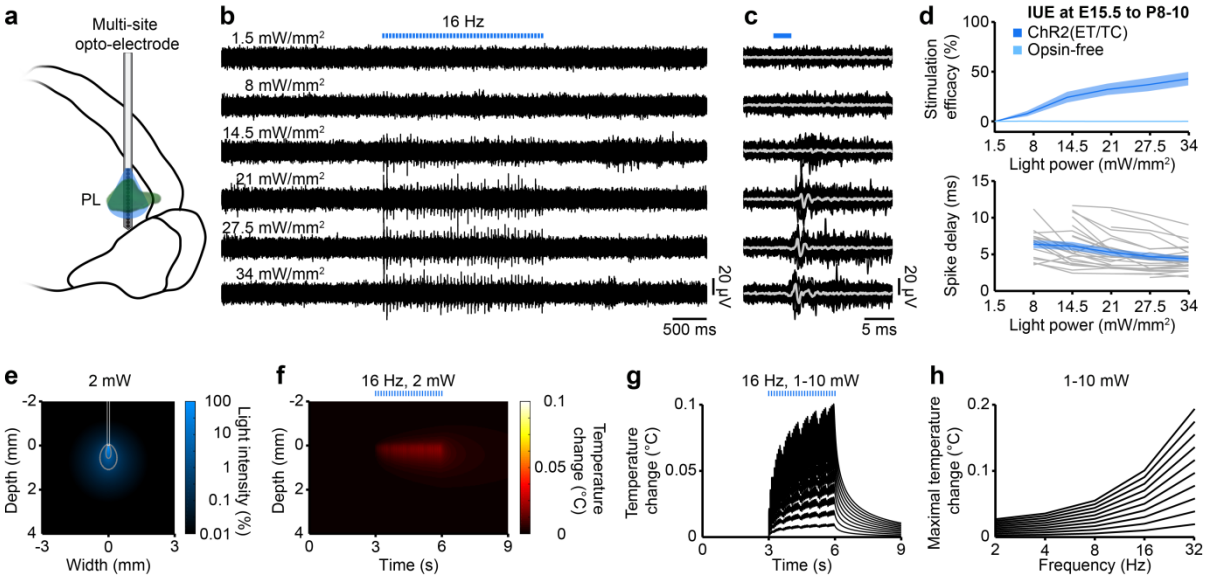

Supplementary Figure 3 (related to Figure 4): Assessment of spatiotemporal dynamics of light and heat propagation for *in vivo* optogenetics in the neonatal brain. **(a)** Schematic representation of combined light stimulation and extracellular recordings in the neonatal PL *in vivo*. **(b)** Representative MUA (band-pass filter: 500 to 5000 Hz) at one recording site in response to trains of light stimuli (473 nm, 3 ms-long, 16 Hz, total duration 3 s) at six levels of light intensity. **(c)** Superimposed single (black) and mean (gray) traces of representative MUA evoked by 30 individual light pulses (473 nm, 3 ms) at six levels of light intensity aligned at stimulus onset. **(d)** Mean stimulation efficacy (top) and spike delay (bottom) in response to trains of light stimuli (473 nm, 3 ms, 16 Hz) at six levels of light intensity when averaged for ChR2(ET/TC)-transfected (n=29 recording sites from 10 pups) and opsin-free (n=11 recording sites from 11 pups) pups. Gray lines correspond to individual recording channels. **(e)** Propagation of light intensity in the brain as predicted by Monte Carlo simulations for the used optical fiber (diameter 105 µm, numerical aperture 0.22, light parameters: 473 nm, 2 mW). Gray lines correspond to the iso-contour lines for 1 and 10 mW/mm². **(f)** Color-coded map of predicted heat-changes over time and tissue depth for trains of light pulses (473 nm, 3 ms) at 16 Hz for 3 s and 2 mW. **(g)** Line plot displaying the temperature change below the fiber tip over time for light pulses (473 nm, 3 ms, 16 Hz) with increasing power (1 to 10 mW). **(h)** Line plot displaying the relationship between maximal temperature change and frequency of light stimulation for increasing light power (1 to 10 mW). Data were obtained from pups expressing ChR2(ET/TC) in layer II/III pyramidal neurons and are displayed as mean ± SEM.

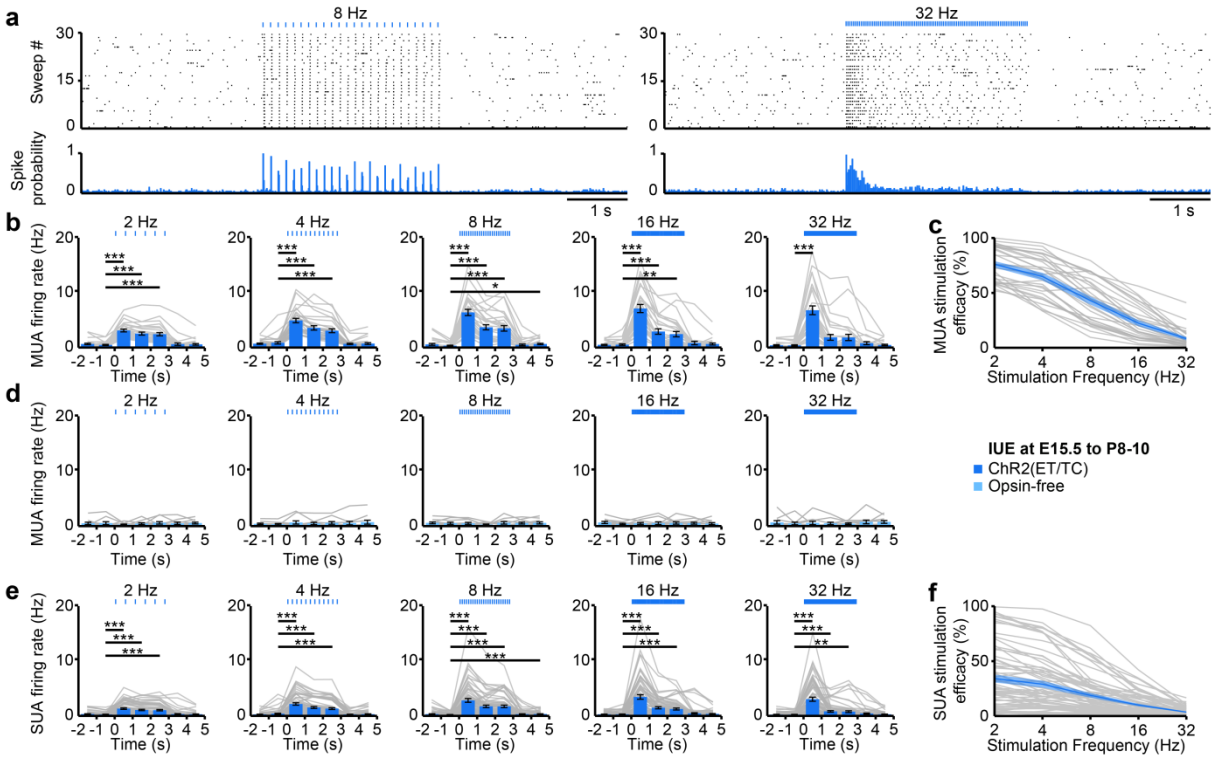

Supplementary Figure 4 (related to Figure 4): Optogenetic activation of layer II/III pyramidal neurons in response to pulse train stimulation *in vivo*. **(a)** Representative raster plots and corresponding spike probability histograms displaying the firing of ChR2(ET/TC) transfected layer II/III pyramidal neurons in response to 30 sweeps of illumination (473 nm, 3 ms) at 8 Hz (left) and 32 Hz (right). **(b)** Bar diagrams displaying the mean MUA firing rate of ChR2(ET/TC)-transfected neurons from P8-10 mice before, during and after trains of pulsed light stimulation (473 nm, 3 ms) at 2, 4, 8, 16, and 32 Hz (n=29 recording sites from 10 mice). **(c)** Mean (dark blue) and individual (gray) stimulation efficacy of MUA in response to pulsed light stimulation (473 nm, 3 ms) at the six different frequencies (n=29 recording sites from 10 pups). **(d)** Same as (b) averaged for P8-10 mice expressing opsin-free constructs in layer II/III pyramidal neurons (light blue, n=11 recording sites from 11 pups). **(e)** Bar diagrams displaying the mean SUA firing rate of ChR2(ET/TC)-transfected neurons from P8-10 mice before, during and after trains of pulsed light stimulation (473 nm, 3 ms) at 2, 4, 8, 16, and 32 Hz (n=69 recording sites from 10 pups). **(f)** Mean (dark blue) and individual (gray) stimulation efficacy of SUA in response to pulsed light stimulation (473 nm, 3 ms) at the six different frequencies (n=69 recording sites from 10 pups). Data are presented as mean ± SEM. *p < 0.05, **p < 0.01, and ***p < 0.001, one-way repeated measures ANOVA with Bonferoni corrected post hoc analysis.

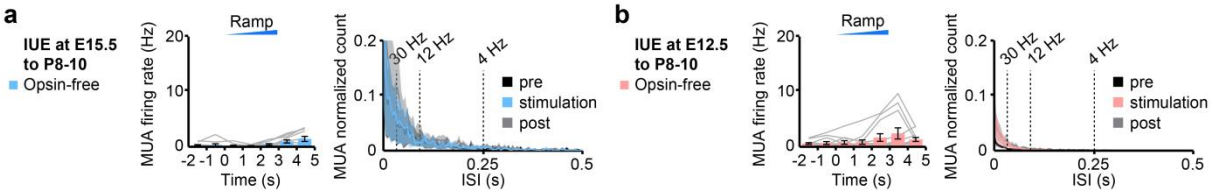

Supplementary Figure 5 (related to Figure 4): *In vivo* spiking of layer II/III and layer V/VI pyramidal neurons transfected by IUE with opsin-free constructs. **(a)** Left, bar diagram displaying the mean MUA frequency in response to ramp illumination averaged for mice expressing opsin-free constructs in layer II/III pyramidal neurons (light blue). Right, occurrence rate of inter-spike intervals averaged for 3 s before (pre, black), 3 s during (stimulation, blue), and 3 s after ramp stimulation (post, gray) (n=11 recording sites of 11 pups). **(b)** Same as (a) for mice expressing opsin-free constructs in layer V/VI (light red, n=12 recording sites of 12 pups). Gray lines correspond to individual firing rates. Data are presented as mean ± SEM. *p < 0.05, **p < 0.01, and ***p < 0.001, one-way repeated measures ANOVA with Bonferoni corrected post hoc analysis.

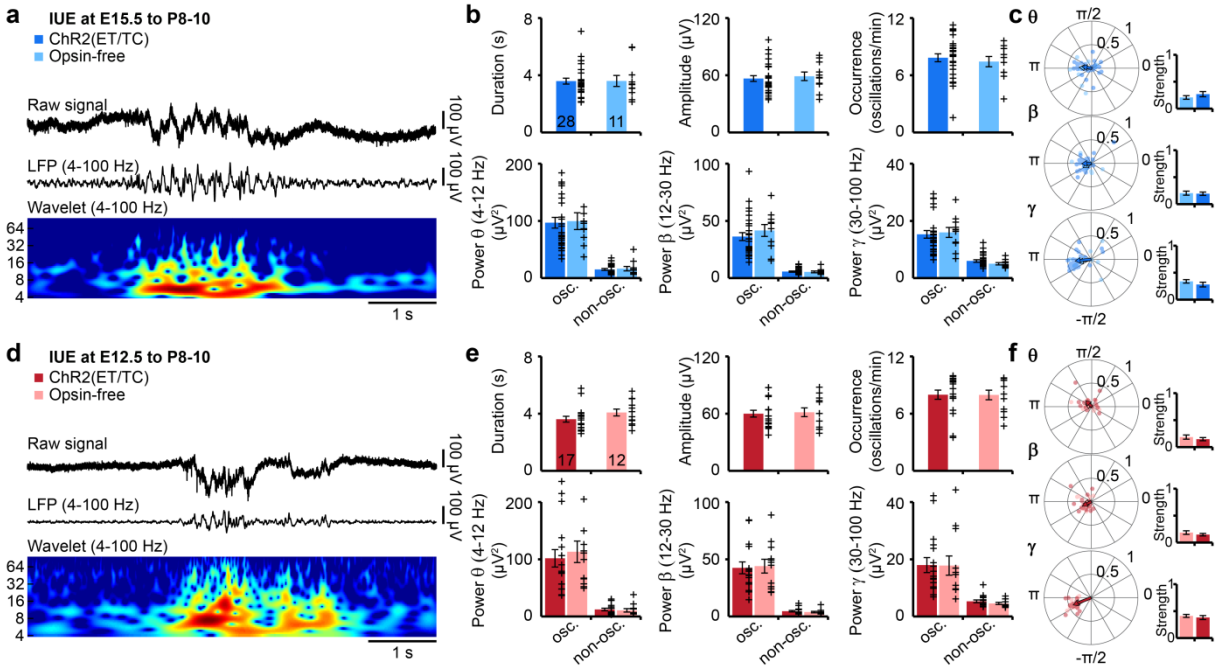

Supplementary Figure 6 (related to Figure 5,6): Spontaneous oscillatory activity of ChR2(ET/TC) and opsin-free transfected mice. **(a)** Characteristic burst of spontaneous discontinuous oscillatory activity from a P10 mouse after transfection of layer II/III pyramidal neurons with ChR2(ET/TC) by IUE. The nested gamma spindle burst is displayed before (top) and after band pass filtering (4-100 Hz) (middle) together with the corresponding color-coded wavelet spectrum at identical time scale. **(b)** Bar diagrams displaying the properties of spontaneous oscillatory activity averaged for layer II/III ChR2(ET/TC)-transfected (dark blue, n=28 pups) and opsin-free mice (light blue, n=11 pups). Note the different scaling for theta (θ, 4-12 Hz), beta (β, 12-30 Hz), and gamma (ɣ, 30-100 Hz) power. Individual values corresponding to pups with light-induced network oscillations are displayed as black crosses. **(c)** Polar plots displaying the phase locking of spontaneous MUA to oscillatory activity (top: θ; middle: β; bottom: ɣ frequency band) from layer II/III ChR2(ET/TC)-transfected (dark blue, n=28 pups) and opsin-free mice (light blue, n=11 pups). The values from individual pups with light-induced network oscillations are shown as dark and light blue dots, whereas the arrows correspond to the mean resulting group vectors. Bar diagrams display the mean locking strength. **(d)-(f)** Same as (a)-(c) for layer V/VI ChR2(ET/TC)-transfected (dark red, n=17 pups) and opsin-free mice (light red, n=12 pups). For (b) and (e) osc = oscillations, non-osc = time windows without oscillatory activity. Data are presented as mean ± SEM. *p < 0.05, **p < 0.01, and ***p < 0.001, two-sided t-tests and circular statistics toolbox.

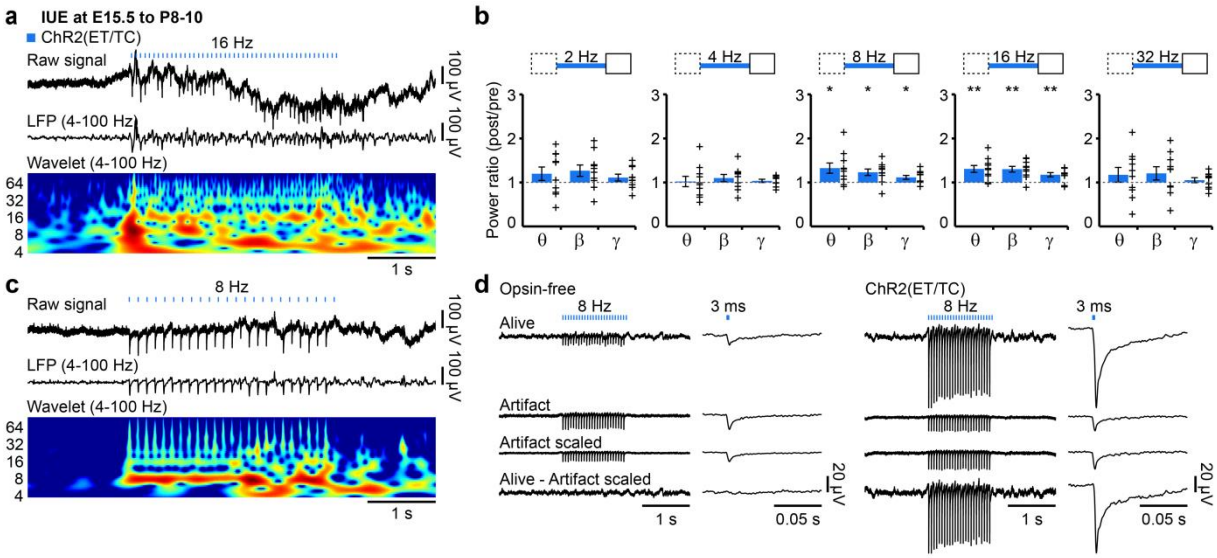

Supplementary Figure 7 (related to Figure 5): Methodological approach for elimination of photoelectric artifacts. **(a)** Characteristic LFP in the PL of a layer II/III expressing P10 mouse in response to a train of light stimuli at 16 Hz (473 nm, 3 ms). The LFP is displayed before (top) and after band-pass filtering (4-100 Hz) (middle) together with the corresponding color-coded wavelet spectrum at identical time scale. **(b)** Bar diagrams displaying the LFP power ratio before (pre, 1.5 s) and after (post, 1.5 s) trains of light stimuli (473 nm, 3 ms-long, total duration 3 s) at 2, 4, 8, 16 or 32 Hz for the main frequency bands of neonatal oscillatory activity (θ, β, ɣ) (n=10 pups). Individual values corresponding to pups with light-induced network oscillations are displayed as black crosses. **(c)** Characteristic LFP in the PL of a P10 mouse transfected by IUE at E15.5 with ChR2(ET/TC) in response to a train of light stimuli (473 nm, 3 ms) at 8 Hz. The LFP is displayed before (top) and after band-pass filtering (4-100 Hz) (middle) together with the corresponding color-coded wavelet spectrum at identical time scale. **(d)** Representative band-pass filtered (1-400 Hz) averaged LFP recorded in response to 30 trains of light stimuli (473 nm, 3 ms, 8 Hz) or single stimuli before (Alive, top) and after (Artifact, Artifact scaled, middle) a lethal injection of ketamine-xylazine from a mouse transfected by IUE with the opsin-free construct (left) and from a mouse transfected with ChR2(ET/TC) (right). The LFP trace after removal of photoelectric artifacts was obtained by subtraction of the scaled artifact (Alive-Artifact scaled, bottom). Note the presence of prominent current sinks generated by the simultaneous opening of light-activated channels only in the ChR2(ET/TC)-expressing animal. Data are presented as mean ± SEM. *p < 0.05, **p < 0.01, and ***p < 0.001, two-sided t-tests.

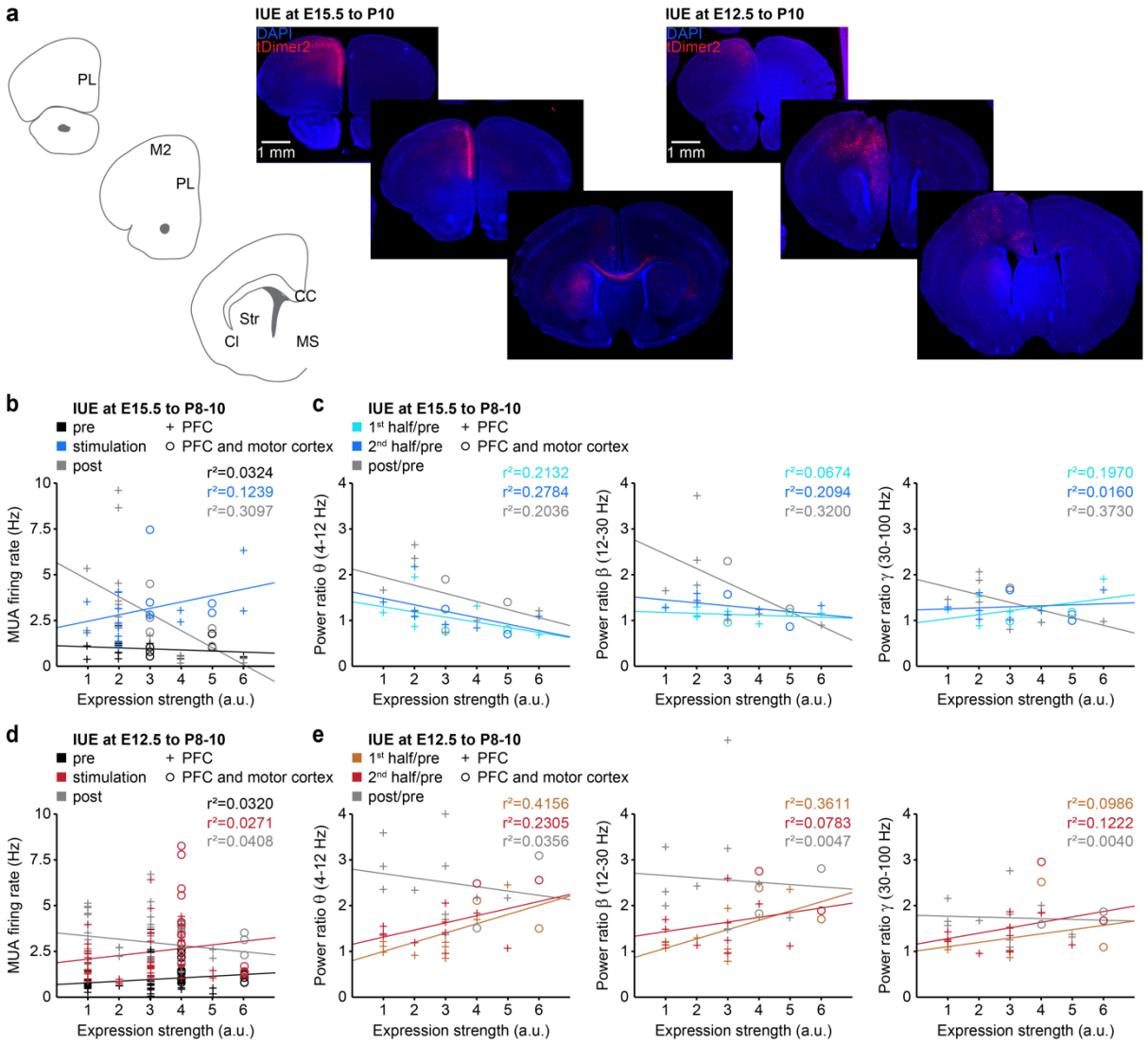

Supplementary Figure 8 (related to Figure 5,6): Impact of light stimulation on neuronal and network activity in relationship to expression strength of ChR2(ET/TC). **(a)** tDimer2-expressing cells (red) in DAPI-stained (blue) coronal sections (50 µm-thick) of two P10 mice after E15.5 (left) and E12.5 (right) IUE, respectively. Note the presence of transfected neurons in PFC and motor cortex as well as the presence of positive fibers (e.g. in striatum). **(b)** Scatter plot with linear regression displaying the MUA firing rate before (pre 3 s, black), during (stimulation 3 s, blue) and after (post 3 s, gray) ramp stimulation in relation to the expression strength for layer II/III expressing P8-10 mice. Values of individual recording sites are displayed as crosses for pups expressing the construct only in the PFC (n=16 recording sites, n=7 pups) and as circles for pups with expression both in the PFC and motor cortex (n=5 recording sites, n=2 pups). **(c)** Scatter plots with linear regressions displaying baseline-normalized LFP power during first half (1st half), second half (2nd half) and after (post) ramp stimulus in relation to the expression strength in layer II/III of P8-10 mice Theta (θ), beta (β) and gamma (ɣ) frequency bands were considered for analysis. Values corresponding to pups with PFC-confined expression (n=7 pups) are displayed as crosses, whereas values from pups with expression both in PFC and motor cortex (n=2 pups) are shown as circles. **(d)-(e)** Same as (b)-(c) for layer V/VI neurons (PFC n=49 recording sites, n=10 pups; PFC and motor cortex n=12 recording sites, n=2 pups). Data are presented as mean for each recording site.

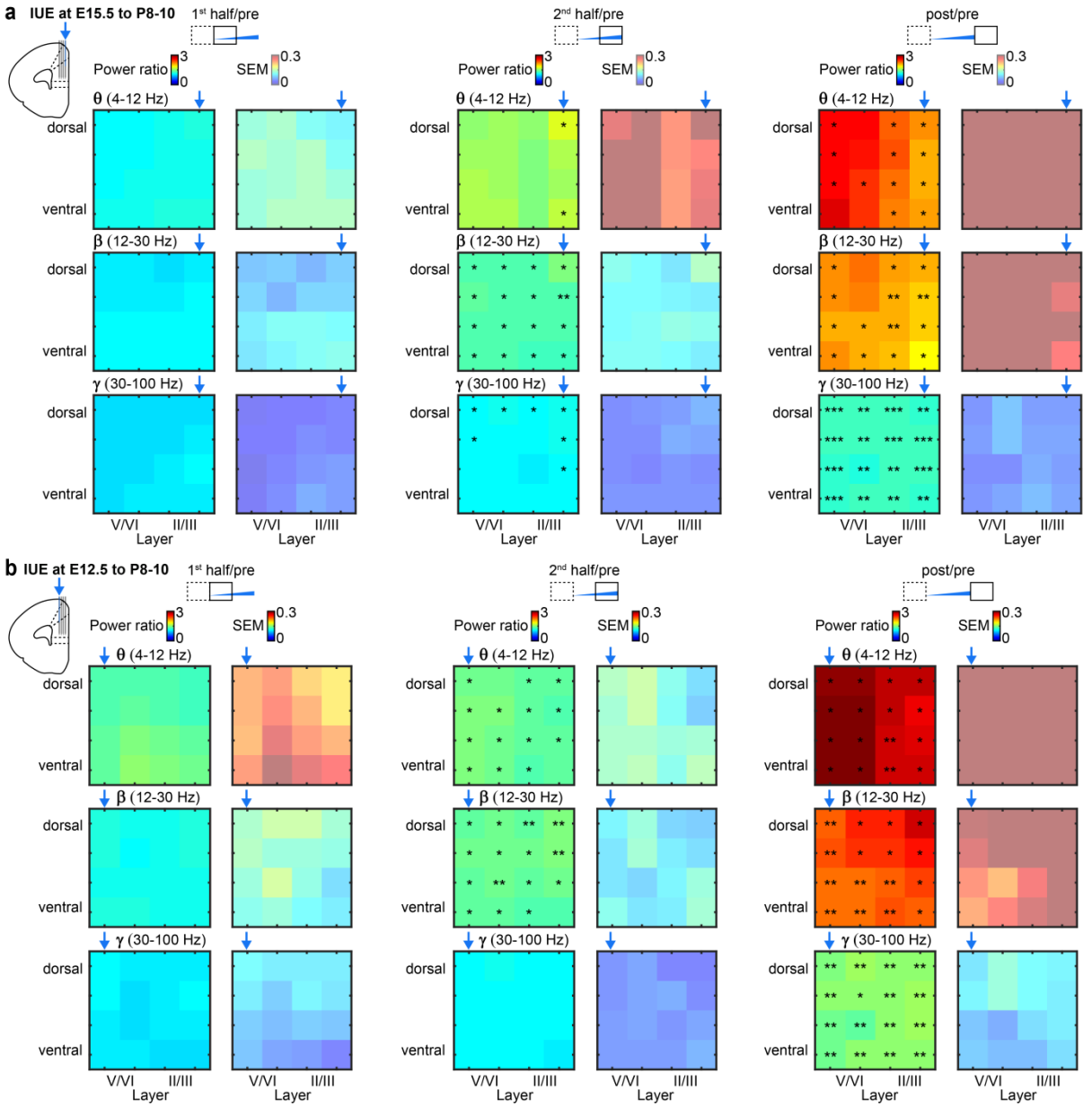

Supplementary Figure 9 (related to Figure 7): Frequency-dependent activation of neonatal prelimbic cortex in response to layer-specific optogenetic activation *in vivo*. **(a)** Color-coded images displaying the baseline normalized (pre, 1.5 s) power (mean and SEM) in response to light stimulation of layer II/III pyramidal neurons for recording sites spanning the PL depth during the first half (1st half, 1.5 s), the second half (2nd half, 1.5 s), and after (post, 1.5 s) ramp stimulus. The power was calculated for theta (θ, 4-12 Hz, top), beta (β, 12-30 Hz, middle) and gamma (ɣ, 30-100 Hz, bottom) frequency bands and values were averaged (n=11 pups). **(b)** Same as (a) for layer V/VI expressing P8-10 mice (n=6). Blue arrows indicate the position of the light fiber. *p < 0.05, **p < 0.01, and ***p < 0.001, two-sided t-tests.

Intermediate but not dorsal hippocampal CA1 projection neurons drive the oscillatory entrainment of prefrontal circuits in the neonatal mouse

Joachim Ahlbeck, Antonio Candela, Mattia Chini, Sebastian H. Bitzenhofer & Ileana L. Hanganu-Opatz

Developmental Neurophysiology, Institute of Neuroanatomy, University Medical Center Hamburg-Eppendorf, 20251 Hamburg, Germany

Corresponding author:
Ileana L. Hanganu-Opatz
Dev. Neurophysiology
Center for Molecular Neurobiology (ZMNH)
University Medical Center Hamburg-Eppendorf
Falkrenried 94
20251 Hamburg
Germany
phone: +49 40 7410 58966
fax: +49 40 7410 58925
e-mail: hangop@zmnh.uni-hamburg.de

SUMMARY

The long-range coupling within prefrontal-hippocampal networks that account for cognitive performance emerges early in life. The discontinuous hippocampal theta bursts have been proposed to drive the generation of neonatal prefrontal oscillations, yet causal testing of this hypothesis is missing. Here, we selectively target optogenetic manipulation of glutamatergic projection neurons in the CA1 area of either dorsal or intermediate/ventral hippocampus at neonatal age to prove their contribution to the emergence of prefrontal oscillatory entrainment. We show that despite stronger theta and ripples activation of dorsal hippocampus, the prefrontal cortex is mainly coupled with intermediate/ventral hippocampus by phase-locking of neuronal firing via dense direct axonal projections. Light-induced activation of pyramidal neurons in the intermediate/ventral but not dorsal CA1 that are transfected by *in utero* electroporation with high-efficiency channelrhodopsins boosts theta-band prefrontal oscillations. Our data causally prove the long-range coupling in the developing brain and identify the cellular origin of specific neonatal network states.

Running title: Optogenetic interrogation of early long-range coupling

Highlights:

- At neonatal age theta bursts, sharp waves and ripples vary along septal-temporal axis
- Prefrontal oscillations and firing are timed by intermediate/ventral hippocampus
- Projections from intermediate/ventral hippocampus target neonatal prefrontal cortex
- Selective targeting of neonatal hippocampus causes precise neuronal firing
- Light stimulation of hippocampal neurons at 8 Hz boosts prefrontal oscillations

eTOC Blurb:

Ahlbeck et al. use optogenetic activation and multi-site neurophysiology to demonstrate cell type- and frequency-specific drive along long-range axonal projections to the prefrontal cortex from the intermediate/ventral but not dorsal hippocampus during neonatal development.

INTRODUCTION

In the adult rodent brain, coordinated patterns of oscillatory activity code in a frequency specific manner for sensory and cognitive performance. For example, learning and memory critically depend on oscillations within theta frequency band (4-12 Hz) that functionally couple the medial prefrontal cortex (PFC) and hippocampus (HP) (Backus et al., 2016; Benchenane et al., 2010; Brincat and Miller, 2015; Siapas and Wilson, 1998; Wirt and Hyman, 2017). These frequency-tuned brain states are present already during early development, long before the emergence of cognitive abilities, and have been extensively characterized and categorized according to their spatial and temporal structure (Lindemann et al., 2016). Network oscillations during development have a highly discontinuous and fragmented organization resulting from the alternation between bursts of activity and “silent” periods (Hanganu et al., 2009; Luhmann and Khazipov, 2017; Seelke and Blumberg, 2010; Shen and Colonnese, 2016). The most common oscillatory pattern, the spindle bursts, synchronizes large cortical and subcortical networks within theta-alpha frequency range. It is accompanied by slow delta waves as well as by faster discharges (beta and gamma oscillations) that account for local activation of circuits.

In the absence of direct behavioral correlates, a mechanistic understanding of oscillatory rhythms in the developing brain is currently lacking. In the sensory systems, spindle bursts have been proposed to act as a template facilitating the formation of cortical maps (Dupont et al., 2006; Hanganu et al., 2006; Tolner et al., 2012), whereas early gamma oscillations seem to control the organization of thalamocortical topography (Khazipov et al., 2013; Minlebaev et al., 2011). In limbic systems dedicated to mnemonic and executive abilities, the knowledge on the relevance of early network oscillations is even sparser. Few lesion studies, yet without selectivity for specific activity patterns, suggested that prefrontal-hippocampal communication during development might be necessary for the maturation of episodic memory (Kruger et al., 2012). Temporal associations between the firing and synaptic discharges of individual neurons and network oscillations in different frequency bands gave first insights into the cellular substrate of coordinated activity in neonates. Whereas in sensory systems endogenous activation of sensory periphery drives entrainment of local circuitry through gap junction coupling as well as glutamatergic and GABAergic transmission (Dupont et al., 2006; Hanganu et al., 2006; Minlebaev et al., 2009), in prefrontal-hippocampal networks, the excitatory drive from the intermediate / ventral HP has been proposed to activate a complex layer- and frequency-specific interplay in the PFC (Bitzenhofer and Hanganu-Opatz, 2014; Bitzenhofer et al., 2015; Brockmann et al., 2011).

While most of these correlative evidences put forward the relevance of early oscillations beyond a simple epiphenomenal signature of developing networks, direct evidence for their causal contribution to circuit maturation is still missing. This is mainly due

to the absence of a causal interrogation of developing networks, similarly to the investigations done in adult ones. Only recently the methodological difficulties related to area-, layer- and cell type-specific manipulations at neonatal age have been overcome (Bitzenhofer et al., 2017). By these means, the local neuronal interplay generating beta-gamma oscillations in the PFC has been elucidated. However, the long-range coupling causing the activation of local prefrontal circuits is still unresolved. We previously proposed that the hippocampal CA1 area drives the oscillatory entrainment of PFC at neonatal age (Brockmann et al., 2011). Here, we provide the causal evidence that activation of pyramidal neurons in the CA1 area of intermediate / ventral (i/vHP), but not of dorsal HP (dHP) elicits theta band oscillations in the PFC of neonatal mice via dense axonal projections.

RESULTS

Neonatal dorsal and intermediate / ventral hippocampus are differently entrained in discontinuous patterns of oscillatory activity

While the different organization and function of the dorsal vs. intermediate/ventral hippocampus of adults have been extensively characterized (Dong et al., 2009; Patel et al., 2013; Thompson et al., 2008), their patterns of structural and functional maturation are still poorly understood. To fill this knowledge gap, we firstly examined the network oscillatory and firing activity of CA1 area of either dHP and i/vHP by performing extracellular recordings of the local field potential (LFP) and multiple unit activity (MUA) in neonatal [postnatal day (P) 8-10] urethane-anesthetized mice (n=144). Our previous data revealed that network oscillations and neuronal firing are similar in urethane-anesthetized and asleep non-anesthetized neonatal rodents (Bitzenhofer et al., 2015). Independently of the position along dorsal-ventral axis, the CA1 area was characterized by discontinuous oscillations with main frequency in theta frequency band (4-12 Hz) and irregular low amplitude beta-gamma components, which have been categorize as theta oscillations. They were accompanied by prominent sharp-waves (SPWs) reversing across pyramidal layer (str pyramidale) and by strong MUA discharge (Figure 1A, E). While the general patterns of activity are similar in dHP and i/vHP, their properties significantly differ between the sub-divisions. The theta bursts in i/vHP had significantly higher occurrence (8.1 ± 0.2 oscillations/min, n=103 mice vs. dCA1: 5.2 ± 0.3 oscillations/min, n=41 mice; $p<0.001$), larger amplitude (110.6 ± 5.6 µV vs. dHP: 92.9 ± 2.6 µV; $p=0.015$), and shorter duration (3.5 ± 0.1 s vs. dHP: 4.3 ± 0.1 s, $p<0.001$) when compared with dHP (Figure 1B, supplementary figure 1A). Investigation of the spectral composition of theta bursts revealed significant differences within theta band (relative power: dHP: 13.0 ± 1.3, n=41 mice; i/vHP: 10.3±0.5, n = 103 mice; $p=0.026$), whereas the faster frequency components remained unaffected (relative power: 12-30 Hz: dHP, 15.0±1.6, n = 41 mice; i/vHP, 13.2 ± 0.7 n = 103 mice, $p = 0.22$; 30-100 Hz: dHP, 6.3 ±

0.6, n = 41 mice; i/vHP: 5.2±0.3, n=103 mice; p=0.073) (Figure 1C, Supplementary figure 1B).

Differences along the dorsal-ventral axis were detected both in the hippocampal spiking and the population events SPWs. Overall, pyramidal neurons in i/vHP fire at higher rates (0.45 ± 0.01 Hz, n = 557 units from 103 mice) than in the dHP (0.35 ± 0.02 Hz, n=158 units from 41 mice; p=0.025) (Figure 1D). Similar to adult HP (Kouvaros and Papatheodoropoulos, 2017), SPW in neonatal HP were more prominent in the dHP (712.8 ± 31.5 μV, n=41 mice) when compared with the i/vHP (223.8 ± 6.3 μV, n=103 mice), yet their occurrence increased along the dorsal-ventral axis (dHP: 6.6 ± 0.5, n=41 mice; i/vHP: 8.6 ± 0.2, n=103 mice, p<0.001) (Figure 1E,F). In line with our previous results (Brockmann et al., 2011), SPWs are accompanied by prominent firing (dHP: 232 Units; i/vHP 670 units) phase-locked to hippocampal ripples (Supplementary Fig. 1C). The power of ripples decreased along dorsal-ventral axis (relative power: dHP, 24.4±3.3, n=41 mice; i/vHP, 6.1±0.60 n=103 mice, P<0.001) (Figures 1G, H). Similarly, the ripple-related spiking was stronger in dHP when compared with i/vHP (Figures 1I, J).

These data show that the activity patterns in the dorsal and intermediate / ventral CA1 area differ in their properties and spectral structure.

Theta activation within dorsal and intermediate/ventral hippocampus differently entrains the neonatal prelimbic cortex

The different properties of network and neuronal activity in dHP vs. i/vHP led us to question their outcome for the long-range coupling in the developing brain. Past studies identified tight interactions between HP and PFC, which emerge already at neonatal age (Brockmann et al., 2011; Hartung et al., 2016) and are in support of memory at adulthood (Kruger et al., 2012; Place et al., 2016; Spellman et al., 2015). The discontinuous theta oscillations in HP have been proposed to drive the activation of local circuits in the PFC. To assess the coupling of dHP and i/vHP with PFC, we recorded simultaneously the LFP and MUA in the corresponding hippocampal CA1 area and the prelimbic subdivision (PL) of the PFC of P8-10 mice. The entire investigation focused on PL, since it is the prefrontal subdivision with the most dense innervation from HP (Jay and Witter, 1991; Vertes et al., 2007). In a first step, we examined the temporal correspondence of discontinuous oscillations recorded simultaneously in the PL and dHP as well as in the PL and i/vHP. We previously characterized the network activity in the PL and showed that spindle-shaped oscillations switching between theta (4-12 Hz) and beta-gamma (12-40 Hz) frequency components alternated with periods of silence (Bitzenhofer et al., 2015; Brockmann et al., 2011). The majority of prelimbic and hippocampal oscillations co-occurred within a narrow time window (Figure 2A). The temporal synchrony between prelimbic and hippocampal oscillations was assessed by performing spectral coherence analysis (Figure 2B). The results revealed a

stronger coupling PL-i/vHP (4-12 Hz: 0.17 ± 0.0069; 12-30 Hz: 0.31 ± 0.011; 30-100 Hz: 0.11 ± 0.0069, n=103 mice) when compared with PL-dHP (4-12 Hz: 0.12 ± 0.0081; 12-30 Hz: 0.18 ± 0.0094; 30-100 Hz: 0.084 ± 0.004, n=41 mice). In line with previous investigations, this level of coherence is a genuine feature of investigated neonatal networks and not the result of non-specific and conduction synchrony, since only the imaginary component of the coherence spectrum, which excludes zero time-lag synchronization (Nolte et al., 2004), was used.

Due to the symmetric interdependence of coherence, it does not offer reliable insights into the information flow between two brain areas. Therefore, in a second step, we estimated the strength of directed interactions between PL and HP by calculating the generalized partial directed coherence (gPDC) (Baccala et al., 2007; Rodrigues and Baccala, 2016) (Figure 2C). The method bases on the notion of Granger causality (Granger, 1980) and avoids distorted connectivity results due to different scaling of data in HP and PL (Baccala et al., 2007; Taxidis et al., 2010). Independently on the position along the dorsal-ventral axis, the information flow in theta or beta frequency band from either dorsal or intermediate/ventral HP to PL is significantly stronger than in the opposite direction. However, mean gDPC values for i/vHP → PL were significantly ($p<0.001$) higher (0.069 ± 0.003, n=103 mice) when compared with those for dHP → PL (0.053 ± 0.003, n=41 mice). The stronger information flow from i/vHP to PL was confined to theta frequency range and was not detected for 12-30 Hz frequencies (i/vHP → PL: 0.048 ± 0.001; dHP → PL: 0.043 ± 0.002, $p=0.16$). Correspondingly, the firing of individual prelimbic neurons was precisely timed by the phase of oscillations in i/vHP but not dHP (Figure 2D). Almost 20% of clustered units (52 out of 310 units) were locked to theta phase in i/vHP, whereas only 3 out of 36 units were timed by dHP. The low number of locked cells in dHP precluded the comparison of coupling strength between the two hippocampal sub-divisions.

These results indicate that the distinct activity patterns in dHP and i/vHP at neonatal age have different outcomes in their coupling with the PL. Despite higher power, theta oscillations in dHP do not account for activity in the PL. In contrast, i/vHP seems to drive neuronal firing and network entrainment in the PL.

SPWs-mediated output of intermediate/ventral but not dorsal hippocampus induces network oscillations and spiking response in the neonatal prelimbic cortex

The prominent differences between SPWs and ripples in dHP and i/vHP suggest their distinct impact in affecting the PFC during neonatal development. While abundant literature documented the contribution of SPWs-spindles complex to memory-relevant processing in downstream targets, such as PFC (for review (Buzsaki, 2015; Colgin, 2011, 2016)), it is fully unknown how these complexes affect the development of cortical activation. Simultaneous recordings from neonatal CA1 area either in dHp or i/vHP and PL show that already at

neonatal age cortical oscillations are generated shortly (~100 ms) after the hippocampal SPWs and ripples. This prelimbic activation is significantly stronger when induced by SPWs-ripples emerging in i/vHP than in dHP as reflected by the significantly higher power of oscillatory activity in theta (PL for dHP: 186.9 ± 12.5 μV^2; PL for i/vHP: 249.5 ± 14.5 μV^2 , p=0.0088), beta (PL for dHP: 34.3 ± 3.3 μV^2; PL for i/vHP: 48.1 ± 2.8 μV^2, p = 0.0049), and gamma (PL for dHP: 11.3 ± 0.9 μV^2; PL for i/vHP: 17.4 ± 1.2 μV^2, p = 0.0026) frequency band (Figure 3A). The SPWs-ripple-induced oscillatory activity in the PL of neonatal mice was accompanied by augmentation of firing rates. While the induced firing following SPW-ripples in i/vHP peaked (≈90 ms) after SPWs-ripples and stayed higher for several seconds, no prominent peak was observed following SPW-ripples in dHP. (Figures 3B, C).

These data reveal that SPWs-ripples from intermediate / ventral but less from the dorsal part of hippocampal CA1 correlate with pronounced neuronal firing and local entrainment in the PL of neonatal mice.

Pyramidal neurons in intermediate / ventral but not dorsal hippocampus densely project to the prefrontal cortex at neonatal age

To identify the anatomical substrate of different coupling strength between i/vHP - PL and dHP - PL, we monitored the projections targeting the PFC from CA1 area in both hippocampal subdivisions. The direct unilateral projection from hippocampal CA1 area to PL, which has been extensively investigated in adult brain (Jay and Witter, 1991; Swanson, 1981; Vertes et al., 2007) and is present already at neonatal age (Brockmann et al., 2011; Hartung et al., 2016). We tested for sub-division specific differences by using retrograde and anterograde stainings. First, we injected unilaterally small amounts of the retrograde tracer Fluorogold (FG) into the PL of the P7 mice (n=8 mice). Three days after FG injections, labeled cells were found in str. pyramidale of CA1 in dHP and i/vHP (Figure 4A). However, their density was significantly different ($p<0.001$). Whereas in dHP very few, if any cells were retrogradely labeled ($0.15*10^3 \pm 0.074*10^3$ cells/mm^2), in the i/vHP a large proportion of cells projects to PL ($3.29*10^3 \pm 0.19*10^3$ cells/mm^2).

Second, the preferential innervation of PL by pyramidal neurons from CA1 area of i/vHP was confirmed by anterograde staining with BDA (n=2 mice). Single injections of small amounts of BDA were injected into the CA1 area of i/vHP (Figure 4B). They led to labeling of the soma and arborized dendritic tree of pyramidal neurons in str. pyramidal with the characteristic orientation of axons. Anterogradely-labeled axons were found in the PL with no discernible layer-specific preference.

Thus, the dense axonal projections from CA1 area of i/vHP may relay the hippocampal activation to the PFC, causing oscillatory entrainment of prelimbic circuits.

Selective light activation of pyramidal neurons in CA1 area of intermediate/ventral but not dorsal hippocampus causes frequency-specific entrainment of neonatal prelimbic circuits

The tight coupling by synchrony and the directed information flow from hippocampal CA1 area to PL via direct axonal projections suggest that the HP acts as a drive for prelimbic activation. Moreover, the differences identified between the communication dHP – PL and i/vHP – PL argue for prominent augmentation of driving force along the dorso-ventral hippocampal axis. To causally confirm these correlative evidences, we selectively activated by light the pyramidal neurons in the CA1 area of either dHP or i/vHP that have been transfected with a highly efficient fast-kinetics double mutant ChR2 E123T T159C (ET/TC) (Berndt et al., 2011) and the red fluorescent protein tDimer2 by *in utero* electroporation (IUE) (Supplementary Figure 2A) (Baumgart and Grebe, 2015; Szczurkowska et al., 2016). This method enables stable area and cell type-specific transfection of neurons already at prenatally without the need of cell-type specific promotors of a sufficiently small size. Analysis of consecutive coronal sections from IUE-transfected P8-10 mice revealed that tDimer-positive neurons are mainly present in the CA1 area of the dHP, when the IUE was performed with two paddles placed 25° leftward angle from the midline and a 0° angle downward from anterior to posterior, or of i/vHP, when three paddles located at 90° leftward angle from the midline for the tweezer-type paddle (both poles negative) and a 0° angle downward from anterior to posterior for the third positive pole (Figure 5A, Supplementary Fig. 2B). Staining with NeuN showed that a large proportion of neurons in str pyramidale of CA1 area (dHP: 18.3 ± 1.0; n=36 slices from 13 mice; i/vHP: 14.5 ± 1.5, n=12 slices from 11 mice) were transfected by IUE. The shape of tDimer2-positive neurons, the orientation of primary dendrites, and the absence of positive staining for GABA confirmed that the light-sensitive protein ChR2(ET/TC) is integrated exclusively into cell lineages of pyramidal neurons (Figure 5A). Omission of ChR2(ET/TC) from the expression construct (that is, opsin-free) yielded similar expression rates and distribution of tDimer2-positive neurons (Supplementary Fig. 2C).

To exclude non-specific effects of transfection procedure by IUE on the overall development of mice, we assessed the developmental milestones and reflexes of electroporated opsin-expressing and opsin-free mice (Supplementary Fig. 2D). While IUE caused significant reduction of litter size (non-electroporated 6.5 ± 0.7, electroporated: 4.5 ± 0.5, p=0.017), all investigated pups had similar body length, tail length, and weight during early postnatal period. Vibrissa placing, surface righting and cliff aversion reflexes were also not affected by IUE or transfection of neurons with opsins. These data indicate that the overall somatic development during embryonic and postnatal stage of ChR2(ET/TC)-transfected mice is normal.

We first assessed the efficiency of light stimulation in evoking action potentials in neonatal hippocampal neurons in vivo. Blue light pulses (473 nm, 20-40 mW/mm^2) at different frequencies (4, 8, 16 Hz) led to precisely timed firing of transfected neurons in dHP as well as i/vHP. Our previous experimental data and modeling work showed that the used light power does not cause local tissue heating that might interfere with neuronal spiking (Bitzenhofer et al., 2017; Stujenske et al., 2015). For both hippocampal sub-divisions the efficiency of firing similarly decreased with augmenting frequency (Figure 5B). For stimulation frequencies >16 Hz, the firing lost the precise timing by light, most likely due to the immaturity of neurons and their projections.

To decide whether activation of HP drives frequency-specific oscillatory activity and boosts the entrainment of prelimbic circuits, we simultaneously performed multi-site recordings of LFP and MUA in PL and HP during pulsed light stimulation of dorsal (n = 22 mice) or intermediate/ventral CA1 (n = 9 mice) (Figure 5C). The firing in i/vHP timed by light at 8 Hz caused significant (theta: p = 0.039, beta: p=0.030, gamma: p=0.0036) augmentation of oscillatory activity in all frequency bands as reflected by the higher power in the PL during the stimulation when compared with the time window before the train of pulses (Figure 5D,table 1). In contrast, stimulation by light of dHP led the prelimbic activity unaffected. In opsin-free animals, stimulation of dHP and i/vHP led to no significant changes in the oscillatory activity (Table 1).

These data represent the experimental proof of the role of theta activity in the CA1 area of i/vHP for driving the emergence of oscillatory activity in the neonatal PL.

DISCUSSION

Combining selective optogenetic activation with extracellular recordings and tracing of projections in neonatal mice in vivo, we provide causal evidence that theta activity in the CA1 area of intermediate / ventral but not dorsal HP drives network oscillations within developing prefrontal cortex. Despite stronger theta entrainment of dorsal HP, solely optical activation of the pyramidal neurons in the intermediate / ventral HP at theta frequency range (8 Hz) boosted the emergence of discontinuous oscillatory activity in theta and beta-gamma bands. These data causally confirm the proposed directed interactions between neonatal prefrontal cortex and hippocampus and offer new perspectives for the interrogation of long-range coupling in the developing brain.

Distinct patterns of functional maturation in dorsal and intermediate / ventral hippocampus

The abundant literature dedicated to the adult hippocampus mainly deals with a single cortical module (Amaral et al., 2007). However, an increasing number of studies in recent

years revealed distinct organization, processing mechanisms and behavioral relevance for dorsal vs. intermediate / ventral hippocampus (Bannerman et al., 2014; Fanselow and Dong, 2010; Strange et al., 2014). For example, the dorsal HP with dense projections from the entorhinal cortex (Witter and Amaral, 2004) is mainly involved in spatial navigation (Moser, 1998; Moser et al., 1995; O'Keefe and Nadel, 1978), whereas the ventral part of HP receives strong cholinergic and dopaminergic innervation (Pitkanen et al., 2000; Witter et al., 1989) and is involved in processing of non-spatial information (Bannerman et al., 2003; Bast et al., 2009). Correspondingly, the network and neuronal activity changes along dorsal-ventral (septo-temporal) axis. The power of the most prominent activity pattern in the adult HP, the theta oscillations, as well as the theta timing of the neuronal firing was substantially reduced in the ventral compared with dorsal HP (Royer et al., 2010). By these means the precise spatial representation deteriorates along the septo-temporal axis, since theta activity is directly linked to place cell representation (Geisler et al., 2007; O'Keefe and Recce, 1993). In contrast, SPWs are more prominent and the ripples have higher amplitude and frequency in the ventral than in the dorsal HP (Kouvaros and Papatheodoropoulos, 2017).

Our data uncovered that some of these differences in the activity patterns along septo-temporal axis emerge already during early neonatal development. Similar to findings from adult rodents, the power of theta bursts at neonatal age was lower in dHP than in the i/vHP. However, the amplitude of SPWs and the power of ripples were larger in the dorsal when compared with the intermediate / ventral subdivision of HP. The developmental profile of activity patterns along septo-temporal axis gives insights into the mechanisms underlying the differences between dHP and i/vHP. It has been proposed that the differences in theta dynamics result from distinct innervation and intrinsic properties of hippocampal neurons. First, cholinergic innervation of dHP mainly originates from the medial septum, whereas the ventral part from the horizontal limb of the diagonal band (Amaral et al., 2007; Stewart and Fox, 1990). These projections already targeted the corresponding hippocampal regions during embryonic development (Linke and Frotscher, 1993) and contribute to the generation of discontinuous theta oscillations during the first postnatal week (Janiesch et al., 2011). Consequently, these projections of different origin may indeed contribute to the more prominent theta oscillations in the dorsal part of HP. Second, maturational differences in the intrinsic resonant properties of hippocampal neurons along the septo-temporal axis may equally cause theta changes in dHP vs. i/vHP. Third, notable gradients of parvalbumin immunoreactivity along the septo-temporal axis detected during development of HP (Honeycutt et al., 2016) might represent an additional source of theta differences, similarly to the lower density of parvalbumin-expressing interneurons in the i/vHP when compared to dHP at adulthood (Ribak and Seress, 1983).

While theta oscillations similarly change along the septal-temporal axis at neonatal and adult age, the properties of SPWs and ripples in dHP vs. i/vHP change over age. Taking into account that these events are self-organized and generated independently of hippocampal inputs (Buzsaki, 2015), the age-dependent switch might mirror profound reorganization of local circuitry in the hippocampus along the septal-temporal axis. While at both neonatal and adult age, the occurrence of SPWs was higher in the i/vHP when compared with the dHP, their amplitude was higher in the neonatal dHP and adult vHP (Kouvaros and Papatheodoropoulos, 2017). The most prominent age-dependent changes were observed for ripples, the power of which was higher in the neonatal dHP and adult vHP. Similarly, their ability to time the neuronal firing was stronger in neonatal dHP and adult vHP. It is still an issue of debate when exactly ripples emerge in the developing hippocampus, although it is obvious that they appear later than theta bursts and SPWs, most likely during the second-thrid postnatal week (Brockmann et al., 2011; Buhl and Buzsaki, 2005). Their underlying mechanisms remain largely unknown. It has been hypothesized that gap junctional coupling and the developmental switch of GABA-induced chloride depolarization to hyperpolarization play an important role, yet these speculations mainly result from the fact that the maturation of ripples parallels the peak of junctional coupling and GABA switch (Ben-Ari et al., 1989; Yuste et al., 1995; Zhang et al., 1990). If these mechanisms contribute to the emergence of ripples, their developmental profile is expected to match the differences along septal-temporal axis that were detected by the present results. However, experimental data mirroring the gap junctional distribution and GABA switch in the dHP and i/vHP over age are fully missing.

Thus, during development the stronger activation of dHP, most likely resulting from external inputs, is accompanied by a higher excitability of local circuits in the i/vHP.

Optogenetic interrogation of long-range coupling in the developing brain

At adult age the communication between PFC and HP has been investigated in relationship with memory tasks both under physiological and disease-related conditions (Adhikari et al., 2010; Eichenbaum, 2017; Sigurdsson et al., 2010; Sirota et al., 2008). Depending on the phase of memory processing, the prefrontal-hippocampal coupling via oscillatory synchrony has been found to be either unidirectional from the HP to PFC or bidirectional (Hallock et al., 2016; Place et al., 2016; Siapas et al., 2005). Both theta and gamma network oscillations contribute to the functional long-range coupling. The model of prefrontal-hippocampal communication has been initially built based on experimental evidence correlating the temporal organization of neuronal and network activity in the two brain areas. The time delay between spike trains and oscillatory phase or between oscillations enabled to propose that the information flows in one direction or the other via mono- or polysynaptic axonal projections. More recently, a direct causal assessment of the coupling became possible

through the optogenetic interrogation of neural circuits. In a seminal study Spellman and colleagues used light-driven inhibition of axonal terminals for dissecting the directionality of interactions between PFC and HP during different phases of memory retrieval (Spellman et al., 2015).

We previously showed that the discontinuous theta bursts in i/vHP are temporally correlated to the network oscillations in the PFC and time the prefrontal firing (Brockmann et al., 2011; Hartung et al., 2016). Moreover, the temporal delay of 10-20 ms between the prefrontal and hippocampal spike trains as well as the computed directionality of information flow between the two areas suggested that hippocampal theta drives the oscillatory entrainment of the local circuits in the PFC. The present data directly confirm this hypothesis using the advantage of the recently developed protocol for optogenetic manipulation of neuronal network at neonatal age (Bitzenhofer et al., 2017).

Several considerations regarding the technical challenges of optogenetic manipulation of different regions of the HP along the septal-temporal axis need to be made. Besides the inherent difficulties related to the specificity of promoters for selective transfection and the targeting procedure that are ubiquitary for all developing networks, confinement of light-sensitive proteins to pyramidal neurons of either dHP or i/vHP required special attention. In a previous study (Bitzenhofer et al., 2017), we developed a selective targeting protocol of neonatal neurons that relies on the combination of CAG promoter and IUE. By these means, the expression of light-sensitive proteins in the neurons located in the neocortical layer and area of interest was sufficiently high to ensure their reliable activation. Similarly, the expression of ChR2(ET/TC) in the pyramidal neurons of hippocampal CA1 area under the promoter CAG was high. Taking into account that viral transduction usually requiring 10-14 days for stable expression is only of limited usability to investigate local network interactions during development, the IUE seems to represent the method of choice for manipulating circuits at this early age. IUE enables targeting of precursor cells of neuronal and glial subpopulations, based on their distinct spatial and temporal patterns of generation in the ventricular zone (Borrell et al., 2005; Hoerder-Suabedissen and Molnar, 2015; Niwa et al., 2010; Tabata and Nakajima, 2001). While IUE based on 2 electrode paddles enabled selective targeting of pyramidal neurons in the CA1 area of dHP in about 60 % of pups per litter (supplementary figure 2(i)), it completely failed (0 out of 32 mice) to target these neurons in i/vHP. Therefore, it was necessary to adapt the IUE to three electrodes. This protocol, although more complicated and time consuming, allows easy and exceedingly reliable transfection at brain locations that are only able to be sporadically targeted by two electrodes (Szczurkowska et al., 2016). It led to efficient targeting of intermediate and ventral CA1 area in about 50 % of pups per litter (supplementary figure 2(ii)) without substantially augmenting the negative side effects (non-electroporated 6.5±0.7, electroporated: 4.5±0.5,

p=0.017). The high IUE-induced expression of light sensitive proteins underlies the reliable firing of neurons in both dHP and i/vHP in response to light pulses. One intriguing question is how many pyramidal neurons in str. pyramidale of CA1 area must be synchronously activated to drive the oscillatory entrainment of prelimbic circuitry. The coupling between i/vHP in contrast to dHP seems to rely on the dense projections of these neurons to PL, as revealed here by both retrograde and anterograde tracing. Light activation / inhibition of hippocampal axonal terminals targeting prefrontal neurons paired with monitoring of network oscillations in the PFC might offer valuable insights into the patterns of coupling sufficient for activation.

Functional relevance of frequency-specific drive within developing prefrontal-hippocampal networks

A long literature links theta frequency coupling within prefrontal-hippocampal networks to cognitive performance and emotional states of adults (Adhikari et al., 2010; Hallock et al., 2016; Place et al., 2016; Spellman et al., 2015; Xu and Sudhof, 2013; Ye et al., 2017). The emergence of directed communication between PFC and i/vHP but not dHP already at neonatal age raises the question of functional relevance of this early coupling.

The maturation of cognitive abilities is a process even more protected than sensory development that takes place during second-third postnatal weeks (Cirelli and Tononi, 2015; Hanganu-Opatz, 2010). As one of the first, recognition memory can be monitored at this age and critically relies on structurally and functionally intact prefrontal-hippocampal networks (Kruger et al., 2012). Assessing directly the role of neonatal communication for the memory as performed for adult circuits is impossible due to the temporal delay of the two processes. The alternative is to manipulate the activity of either PFC, HP or the connectivity between them during defined developmental time windows and monitor the juvenile and adult changes at structural, functional and behavioral level. The present data and the optogenetic protocol described here represent the pre-requisite of this investigating, opening new perspective for assessing the adult behavioral readout of long-range projections in the developing brain.

Several functions have been previously proposed for the oscillatory coupling within prefrontal-hippocampal networks. First, the theta drive from the HP to PFC might facilitate the wiring of local circuitry in the PFC and enable the refinement of the behaviorally relevant communication scaffold between the two regions. By these means, the prefrontal maturation would follow the general rules of activity-dependent plasticity that have been proposed and partially demonstrated for the development of sensory systems (Hubel et al., 1977; Huberman et al., 2006). The instructive role of theta timed inputs from the projections neurons of CA1 area of i/vHP in the refinement of prefrontal circuits needs to be proven by manipulation of temporal structure of the hippocampal drive without affecting the overall level

of activity. Activity-dependent mechanisms have been reported to shape both hippocampal and retinal circuitry (Xu et al., 2011; Yasuda et al., 2011). Second, the prefrontal activity driven by projection neurons in the HP might act as a template, having a pre-adaptive function that facilitates the tuning of circuits with regard to future conditions.

STAR*METHODS

KEY RESOURCE TABLE

REAGENT or RESOURCE	SOURCE	IDENTIFIER
Antibodies		
mouse monoclonal Alexa Fluor-488 conjugated antibody against NeuN	Merck Millipore	MAB377X
rabbit polyclonal primary antibody against GABA	Sigma-Aldrich	A2052
Alexa Fluor-488 goat anti-rabbit IgG secondary antibody	Merck Millipore	A11008
Chemicals, Peptides, and Recombinant Proteins		
Isoflurane	Abbott	B506
Urethane	Fluka analytical	94300
Fluorogold	Fluorochome, LLC	52-9400
Biotinylated dextran amine, 10.000 MW	Thermo Fisher Scientific	D1956
Critical Commercial Assays		
NucleoBond PC 100	Macherey-Nagel	740573
Experimental Models: Organisms/Strains		
Mouse: C57Bl/6J	Universitätsklinikum Hamburg-Eppendorf – Animal facility	N/A
Recombinant DNA		
pAAV-CAG-ChR2(E123T/T159C)-2AtDimer2	T. G. Oertner	http://www.oertner.com/
pAAV-CAG-tDimer2	T. G. Oertner	http://www.oertner.com/
Software and Algorithms		
Matlab R2015a	MathWorks	https://www.mathworks.com
Offline Sorter	Plexon	http://www.plexon.com/
ImageJ 1.48c	ImageJ	https://imagej.nih.gov/ij/
SPSS Statistics 21	IBM	https://www.ibm.com/analytics/us/en/technology/spss/
Cheetah 6	Neuralynx	http://neuralynx.com/
Other		
Arduino Uno SMD	Arduino	A000073
Digital Lynx 4SX	Neuralynx	http://neuralynx.com/
Diode laser (473 nm)	Omicron	LuxX® 473-100
Electroporation device	BEX	CUY21EX
Electroporation tweezer-type paddles	Protech	CUY650-P5
Recording electrode (1 shank, 16 channels)	Neuronexus	A1x16-3mm-703-A16
Recording optrode (1 shank, 16 channels)	Neuronexus	A1x16-5mm-703-OA16LP
Digital midgard precision current source	Stoelting	51595

CONTACT FOR REAGENT AND RESOURCE SHARING

Further information and requests for resources should be directed to and will be fulfilled by the Lead Contact, Prof. Dr. Ileana L. Hanganu-Opatz (hangop@zmnh.uni-hamburg.de)

EXPERIMENTAL MODEL AND SUBJECT DETAILS

Mice

All experiments were performed in compliance with the German laws and the guidelines of the European Community for the use of animals in research and were approved by the local ethical committee (111/12, 132/12). Timed-pregnant C57Bl/6J mice from the animal facility of the University Medical Center Hamburg-Eppendorf were housed individually in breeding cages at a 12 h light / 12 h dark cycle and fed *ad libitum*. The day of vaginal plug detection was defined E0.5, while the day of birth was assigned as P0. Both female and male mice underwent light stimulation and multi-site electrophysiological recordings at P8-10 after after transfection with light-sensitive proteins by IUE at E15.5. For monitoring of projections, tracers were injected at P7 and monitored in their distribution along the axonal tracts at P10.

METHOD DETAILS

Surgical procedures

***In utero electroporation*.** One day before until two days after surgery timed-pregnant C57Bl/6J mice received on a daily basis additional wet food supplemented with 2-4 drops Metacam (0.5 mg/ml, Boehringer-Ingelheim, Germany). At E15.5 randomly assigned pregnant mice were injected subcutaneously with buprenorphine (0.05 mg/kg body weight) 30 min before surgery. The surgery was performed on a heating blanket and toe pinch and breathing were monitored throughout. Under isoflurane anesthesia (induction: 5%, maintenance: 3.5%) the eyes of the dam were covered with eye ointment to prevent damage before the uterine horns were exposed and moistened with warm sterile phosphate buffered saline (PBS, 37°C). Solution containing 1.25 µg/µl DNA [pAAV-CAG-ChR2(E123T/T159C)-2AtDimer2, or pAAV-CAG-tDimer2)] (Supplementary figure 2A) and 0.1% fast green dye at a volume of 0.75-1.25 µl were injected into the right lateral ventricle of individual embryos using pulled borosilicate glass capillaries with a sharp and long tip. Plasmid DNA was purified with NucleoBond (Macherey-Nagel, Germany). 2A encodes for a ribosomal skip sentence, splitting the fluorescent protein tDimer2 from the opsin during gene translation. Two different IUE protocols were used to target either dCA1 or iCA1. For targeting dCA1, each embryo within the uterus was placed between the electroporation tweezer-type paddles (5 mm diameter, Protech, TX, USA) that were oriented at a 25° leftward angle from the midline and a 0° angle downward from anterior to posterior. Electrode pulses (35 V, 50 ms) were applied five times at intervals of 950 ms controlled by an electroporator (CU21EX, BEX, Japan) (Supplementary figure 2B(i)) (Baumgart and Grebe, 2015; Navarro-Quiroga et al., 2007). For

targeting iCA1, a tri-polar approach was used (Szczurkowska et al., 2016). Each embryo within the uterus was placed between the electroporation tweezer-type paddles (5 mm diameter, both positive poles, Protech, TX, USA) that were oriented at 90° leftward angle from the midline and a 0° angle downward from anterior to posterior. A third custom build negative pole was positioned on top of the head roughly between the eyes. Electrode pulses (30 V, 50 ms) were applied six times at intervals of 950 ms controlled by an electroporator (CU21EX, BEX, Japan) (Supplementary figure 2B(ii)). By these means, neural precursor cells from the subventricular zone, which radially migrate into the HP, were transfected. Uterine horns were placed back into the abdominal cavity after electroporation. The abdominal cavity was filled with warm sterile PBS (37°C) and abdominal muscles and skin were sutured individually with absorbable and non-absorbable suture thread, respectively. The surgery was performed on a heating blanket, and toe pinch reflex and breathing were monitored. After recovery, pregnant mice were returned to their home cages, which were half placed on a heating blanket for two days after surgery.

Retrograde and anterograde tracing. For retrograde tracing, mice were injected at P7 with fluorogold (Fluorochrome, LLC, USA) unilaterally into the PFC using iontophoresis. The pups were placed in a stereotactic apparatus and kept under anesthesia with isoflurane (induction: 5%, maintenance: 2.5%) for the entire procedure. A 10 mm incision of the skin on the head was performed with a small scissor. The bone above the PFC (0.5 mm anterior to bregma, 0.3 mm right to the midline) was carefully removed using a syringe. A glass capillary (≈20 µm tip diameter) was filled with ≈1 µL of 5% fluorogold diluted in sterile water by capillary forces, and a silver wire was inserted such that it was in contact with the fluorogold solution. The positive pole from the iontophoresis device was attached to the silver wire. The negative pole was attached to the skin of the neck. The capillary were carefully lowered into the PFC (≈1.5 mm dorsal from the dura). Iontophoretically injection by applying anodal current to the pipette (6s on/off current pulses of 6 µA) was done for 5 min. Following injection, the pipette was left in place for at least 5 min and then slowly retracted. The scalp was closed by application of tissue adhesive glue and the pups were left on a heating pad for 10-15 minutes to fully recover before they were put back to the mother. The pups were perfused at P10.

For anterograde tracing, mice were injected at P7 with the anterograde tracer Biotinylated dextran amine (BDA) (Thermo Fisher Scientific, USA) unilaterally into the intermediate hippocampus using iontophoresis. The pups were placed in a stereotactic apparatus and kept under anesthesia with isoflurane (induction: 5%, maintenance: 2.5%) for the entire procedure. A 10 mm incision of the skin on the head was performed with a small scissor. The bone above the intermediate hippocampus (0.7 mm anterior to lambda, 2.5 mm right to the midline) was carefully removed using a syringe. A glass capillary (≈30 µm tip diameter) was filled with ≈1 µL of 5% BDA diluted in 0.125 M phosphate buffer by capillary forces, and a

silver wire was inserted such that it was in contact with the fluorogold solution. The positive pole from the iontophoresis device was attached to the silver wire. The negative pole was attached to the skin of the neck. The capillary were carefully lowered into the intermediate hippocampus (≈1.5 mm dorsal from the dura). Iontophoretically injection by applying anodal current to the pipette (6s on/off current pulses of 6 µA) was done for 5 min. Following injection, the pipette was left in place for at least 5 min and then slowly retracted. The scalp was closed by application of tissue adhesive glue and the pups were left on a heating pad for 10-15 minutes to fully recover before they were put back to the mother. The pups were perfused at P10.

Surgical preparation for acute electrophysiological recording and light delivery. Mice were injected i.p. with urethane (1 mg/g body weight; Sigma-Aldrich, MO, USA) prior to surgery. Under isoflurane anesthesia (induction: 5%, maintenance: 2.5%) the head of the pup was fixed into a stereotaxic apparatus using two plastic bars mounted on the nasal and occipital bones with dental cement. The bone above the PFC (0.5 mm anterior to bregma, 0.5 mm right to the midline for layer V/VI), hippocampus (2.0 mm posterior to bregma, 1.0 mm right to the midline for dCA1, 3.5 mm posterior to bregma, 3.5 mm right to the midline for iCA1) was carefully removed by drilling a hole of <0.5 mm in diameter. After a 10-20 min recovery period on a heating blanket mice were moved to the setup for electrophysiological recording.

Perfusion. Mice were anesthetized with 10% ketamine (aniMedica, Germany) / 2% xylazine (WDT, Germany) in 0.9% NaCl solution (10 µg/g body weight, i.p.) and transcardially perfused with Histofix (Carl Roth, Germany) containing 4% paraformaldehyde for 30-40 minutes. Brains were postfixed in 4% paraformaldehyde for 24 h.

Behavioral testing

Examination of developmental milestones. Mouse pups were tested for their somatic development and reflexes at P2, P5 and P8. Weight, body and tail length were assessed. Surface righting reflex was quantified as time (max 30 s) until the pup turned over with all four feet on the ground after being placed on its back. Cliff aversion reflex was quantified as time (max 30 s) until the pup withdrew after snout and forepaws were positioned over an elevated edge. Vibrissa placing was rated positive if the pup turned its head after gently touching the whiskers with a toothpick.

Electrophysiology

Electrophysiological recording**.** A one-shank electrode (NeuroNexus, MI, USA) containing 1x16 recording sites (0.4-0.8MΩ impedance, 100 mm spacing) was inserted into the PFC. One-shank optoelectrodes (NeuroNexus, MI, USA) contained 1x16 recordings sites (0.4-0.8 MΩ impedance, 50 mm spacing) aligned with an optical fiber (105 mm diameter) ending 200

µm above the top recording site was inserted into either dCA1 or iCA1. A silver wire was inserted into the cerebellum and served as ground and reference electrode. A recovery period of 10 min following insertion of electrodes before acquisition of data was provided. Extracellular signals were band-pass filtered (0.1-9,000 Hz) and digitized (32 kHz) with a multichannel extracellular amplifier (Digital Lynx SX; Neuralynx, Bozeman, MO, USA) and the Cheetah acquisition software (Neuralynx). Spontaneous (i.e not induced by light stimulation) activity was recorded for 15 min at the beginning and end of each recording session as baseline activity. Only the first baseline was used for data analysis.

Light stimulation. Pulsed (laser on-off) light stimulations were performed with an arduino uno (Arduino, Italy) controlled diode laser (473 nm; Omicron, Austria). Laser power was adjusted to trigger neuronal spiking in response to 425% of 3-ms-long light pulses at 16 Hz. Resulting light power was in the range of 20-40mW/mm^2 at the fiber tip. 30 repetitions of each frequency used (4, 8 and 16 Hz, 3 ms pulse length, 3 s stimulation duration, 6 s inter stimulation interval) in a randomized order were given during the stimulation period.

Histology

Immunohistochemistry**.** Brains were sectioned coronally at 50 µm. Free-floating slices were permeabilized and blocked with PBS containing 0.2 % Triton X 100 (Sigma-Aldrich, MO, USA), 10 % normal bovine serum (Jackson Immuno Research, PA, USA) and 0.02% sodium azide. Subsequently, slices were incubated overnight with mouse monoclonal Alexa Fluor-488 conjugated antibody against NeuN (1:200, MAB377X, Merck Millipore, MA, USA) or rabbit polyclonal primary antibody against GABA (1:1,000, A2052; Sigma-Aldrich), followed by 2 h incubation with Alexa Fluor-488 goat anti-rabbit IgG secondary antibody (1:500, A11008; Merck Millipore). Slices were transferred to glass slides and covered with Fluoromount (Sigma-Aldrich, MO, USA).

Imaging. Wide field fluorescence was performed to reconstruct the recording electrode position in brain slices of electrophysiologically investigated pups and to localize tDimer2 expression in pups after IUE. High magnification images were acquired with a confocal microscope (DM IRBE, Leica, Germany) to quantify tDimer2 expression and immunopositive cells (1-4 brain slices / investigated mouse).

QUANTIFICATION AND STATISTICAL ANALYSIS

Immunohistochemistry quantification. All images were similarly analyzed with ImageJ. For quantification of fluorogold tracing automatic cell counting was done using custom-written tools. For quantifying tDimer2, NeuN and GABA manual counting was performed, since the high neuronal density in str. pyramidale prevented reliable automatic counting.

Spectral analysis of LFP. Data were imported and analyzed offline using custom-written tools in the Matlab software (MathWorks). Data were processed as following: band-pass

filtered (500–5,000 Hz) to analyze MUA and low-pass filtered (<1,500 Hz) using a third-order Butterworth filter before downsampling to 3.2 kHz to analyze LFP. All filtering procedures were performed in a manner preserving phase information.

Detection of oscillatory activity. The detection and of discontinuous patterns of activity in the neonatal PL and hippocampal CA1 area were performed using a modified version of the previously developed algorithm for unsupervised analysis of neonatal oscillations (Cichon et al., 2014) and confirmed by visual inspection. Briefly, deflections of the root mean square of band-pass filtered signals (1–100 Hz) exceeding a variance-depending threshold were assigned as network oscillations. The threshold was determined by a Gaussian fit to the values ranging from 0 to the global maximum of the root-mean-square histogram. If two oscillations occurred within 200 ms of each other they were considered as one. Only oscillations lasting > 1 s was included.

Detection of sharpwaves. Sharpwaves were detected by subtracting the filtered signal (1-300 Hz) from the recording sites 100 µm above and 100 µm below the recording site in stratum pyramidale. Sharpwaves were then detected as peaks above 5 times the standard deviation of the subtracted signal.

Power spectral density. Power spectral density was calculated using the Welch's method. Briefly, segments of the recorded signal were glued together (1 s segments for oscillatory activity; 300 ms segments for sharpwave pre/post comparison; 100 ms segments for ripple comparison; 3 s for light evoked activity) and power were then calculated using non-overlapping windows. Time–frequency plots were calculated by transforming the data using Morlet continuous wavelet.

Coherence. Coherence was calculated using the imaginary coherency method (Nolte et al., 2004). Briefly, the imaginary coherence was calculated by taking the imaginary component of the cross-spectral density between the two signals and normalized by the power spectral density of each. The computation of the imaginary coherence C over frequency (f) for the power spectral density P of signal X and Y was performed according to the formula:

$$C_{XY}(f) = Im\left(\frac{|P_{XY}(f)|^2}{P_{XX}(f)P_{YY}(f)}\right)$$

General partial directed coherence. gPDC is based on linear Granger causality measure. The method attempts to describe the causal relationship between multivariate time series based on the decomposition of multivariate partial coherences computed from multivariate autoregressive models. The LFP signal was divided into segments containing the oscillatory activity. Signal was de-noised using wavelets with the Matlab wavelet toolbox. After de-noising, gPDC was calculated using the gPDC algorithm described by Baccalá et al (Baccala et al., 2007).

Single unit activity analysis. SUA was detected and clustered using Offline Sorter (Plexon, TC, USA). 1–4 single units were detected at each recording site. Data were then imported and analyzed using custom-written tools in the Matlab software (MathWorks). The firingrate temporally related to SPWs was calculated by aligning all units to the detected SPWs. For assessing the phase locking of units to LFP, we firstly used the Rayleigh test for non-uniformity of circular data to identify the units significantly locked to network oscillations. The phase was calculated by extracting the phase component using the Hilbert transform of the filtered signal at each detected spike. Spikes occurring in a 15 ms-long time window after the start of a light pulse were considered to be light-evoked. Stimulation efficacy was calculated as the probability of at least one spike occurring in this period.

Statistical analysis. Statistical analyses were performed using SPSS Statistics 21 (IBM, NY, USA) or Matlab. Data were tested for normal distribution by the Shapiro–Wilk test. Normally distributed data were tested for significant differences (*P<0.05, **P<0.01 and ***P<0.001) using paired t-test, unpaired t-test or one-way repeated-measures analysis of variance with Bonferoni-corrected post hoc analysis. Not normally distributed data were tested with the nonparametric Mann–Whitney U-test. The circular statistics toolbox was used to test for significant differences in the phase locking data. Data are presented as mean±s.e. of the mean. No statistical measures were used to estimate sample size since effect size was unknown. Investigators were not blinded to the group allocation during the experiments. Unsupervised analysis software was used if possible to preclude investigator biases

DATA AND SOFTWARE AVAILABILITY

The authors declare that all data and code supporting the findings of this study are included in the manuscript and its Supplementary Information or are available from the corresponding authors on request.

Author contributions

I.L.H.-O. designed the experiments, J.A., S.H.B. and A.C. carried out the experiments, J.A., M.C., and A.C. analyzed the data, I.L.H.-O. and J.A. interpreted the data and wrote the paper. All authors discussed and commented on the manuscript.

Acknowledgments

We thank Nadine Faesel for help with the development of tracing technique, Drs. S. Wiegert, T. Oertner, and C. Gee for help with the development of opsin constructs as well as A. Marquardt, A. Dahlmann and I. Ohmert for excellent technical assistance. I.L.H.-O. acknowledges support by the ERC (ERC Consolidator Grant 681577) and by the German

Research Foundation (SFB 936 (B5) and SPP 1665 (Ha4466/12-1). I.L.H.-O. is member of the FENS Kavli Network of Excellence.

Competing interests

The authors declare no competing financial interests.

Figure legends

Figure 1. Patterns of discontinuous oscillatory activity in the CA1 area of the neonatal dCA1 and iCA1 *in vivo*. **(A)** Characteristic theta burst activity recorded in the CA1 area of the dHP (left) and i/vHP (right) of a P9 mouse displayed after band-pass filtering (4-100 Hz) and the corresponding MUA (500-5000 Hz). Color-coded frequency plots show the wavelet spectrum of LFP at identical time scale. **(B)** Bar diagram (mean ± SEM) displaying the occurrence of discontinuous theta bursts within dHP (n=41 mice), and iHP (n=103 mice). **(C)** Power analysis of discontinuous oscillatory activity P(f) normalized to the non-oscillatory period $P_0(f)$ in dHP and i/vHP. (i) Power spectra (4-100 Hz) averaged for all investigated mice. (ii) Bar diagrams quantifying the mean power within theta frequency band (4-12 Hz) in dHP (n=41 mice) and i/vHP (n=103 mice) **(D)** Bar diagram displaying the SUA of dHP (n=158 units) and i/vHP (n=557 units) after clustering of spike shapes. **(E)** Characteristic SPWs and ripple events recorded in dHP (left) and i/vHP (right). **(F)** Bar diagrams (mean ± SEM) displaying the SPWs occurrence in dHP and i/vHP. **(G)** Characteristic SPW-ripple events recorded in dHP (left) and i/vHP (right). **(H)** Bar diagram displaying the mean power of ripples in dHP and i/vHP. **(I)** Spike trains from neurons in dHP (left) and neurons in i/vHP (right) aligned to SPWs. **(J)** Histograms of SUA aligned to SPWs (n=232 units for dCA1, n=670 for iCA1).

Figure 2. Dynamic coupling of hippocampal and prefrontal oscillatory activity along septo-temporal axis during neonatal development. **(A)** Simultaneous LFP recordings of discontinuous oscillatory activity in dHP and PL (top) and i/vHP and PL (bottom). **(B)** Long-range synchrony within prefrontal-hippocampal networks. (i) Average coherence spectra for simultaneously recorded oscillatory events in dHP and PL as well as i/vHP and PL. (ii) Bar diagrams (mean ± SEM) displaying the coherence in theta (4-12 Hz), beta (12-30 Hz), and gamma (30-100 Hz) band when averaged for all investigated mice. **(C)** Directed interactions btween PL and either dHP or i/vHP monitored by general Partial Directed Coherence (gPDC) Bar diagrams displaying the gPDC calculated for theta (4-12 Hz, left) and beta (12-30 Hz, right) frequency and averaged for all investigated animals (n=41 mice for dHP and PL, n=103 mice for i/vHP & PL). **(D)** Histograms displaying the phase-locking of prelimbic spikes to theta oscillations in dHP (left) and i/vHP (right). Note the different proportion of spikes significantly locked along the septo-temporal axis (dHP, 3 of 46 units; i/vHP, 52 of 310 units).

Figure 3. Coupling between neonatal PFC and HP during hippocampal SPWs**. (A)** Power changes in the PL during hippocampal SPWs. (i) Color-coded frequency plot showing the relative power in the PL aligned to the onset of SPWs detected in i/vHP when normalized to the power change caused by SPWs in the dHP. All other colors than green represent power augmentation (red) or decrease (blue). (ii) Bar diagrams displaying mean power changes of

prelimbic activity in different frequency bands (left, theta; middle, beta; right, gamma) before (pre) and after (post) hippocampal SPWs in the dHP and i/vHP (n=41 mice for dHP, n=103 mice for i/vHP). **(B)** Spike trains recorded in the PL before and after SPWs occurring either in the dHP (left) or i/vHP (right). **(C)** Histograms of prelimbic spiking in relationship with hippocampal SPWs (n=148 units for dHP, n=560 units for i/vHP).

Figure 4. Long-range monosynaptic axonal projections connecting the neonatal PFC and hippocampal CA1 area along the septo-temporal axis. **(A)** Photomicrographs depicting dense retrogradely labelled neurons in the CA1 area of i/vHP (right) but not dHP (middle) after FG injection into PL at P1 (left). Bar diagram displays the overall density of retrogradely stained neurons when averaged for all investigated pups (n=8 mice). **(B)** Photomicrographs depicting anterogradely labeled axons targeting the PL of a P10 mouse (right) after iontophoretic BDA injection into the CA1 area of i/vHP at P7 (left). The site of injection and the area with the highest axonal density are depicted at higher magnification.

Figure 5. Optogenetic activation of pyramidal neurons in the CA1 area of dHP and i/vHP selectively transfected with CAG-ChR2(ET/TC)-2A-tDimer2 by IUE has different effects on the network activity of neonatal PL. **(A)** Cell- and layer-specific transfection of dCA1 or iCA1 by site-directed IUE. (i) Photomicrographs depicting tDimer2-expressing pyramidal neurons (red) in the CA1 region of dHP (left) and i/vHP (right) when stained for NeuN (green, top panels) or GABA (green, bottom panels). (ii) Photomicrographs depicting the transfected hippocampal neurons when co-stained for NeuN and displayed at larger magnification. (iii) Photomicrographs depicting transfected hippocampal neurons when co-stained for GABA and sisplayed at larger magnification. **(B)** Optogenetic activation of pyramidal neurons in CA1 area along septo-temporal axis. (i) Representative raster plot and corresponding spike probability histogram for dHP (left) and i/vHP (right) in response to 30 sweeps of 8 Hz pulse stimulation (3 ms pulse length, 473 nm). (ii) Bar diagram displaying the efficacy of inducing spiking in dHP and i/vHP of different stimulation frequencies. **(C)** Characteristic light-induced discontinuous oscillatory activity in the PL of a P10 mouse after transfection of pyramidal neurons in the CA1 area of the dHP (left) or i/vHP (right) with ChR2(ET/TC) by IUE. The LFP is displayed after band-pass filtering (4-100 Hz) together with the corresponding color-coded wavelet spectrum at identical time scale. **(D)** Bar diagrams displaying the power changes in PL during light stimulation of pyramidal neurons in the CA1 area of dHP (top panels) or i/vHP (bottom panels) when normalized to the values before hippocampal stimulation.

Supplementary figure 1. Properties of network and neuronal activity in the dHP vs. i/vHP of neonatal mice. **(A)** Bar diagrams displaying the amplitude and duration of discontinuous

oscillatory events in dHP (n=41 mice) and i/vHP (n=103 mice). **(B)** Bar diagrams displaying the power spectrum of discontinuous oscillatory activity P(f) normalized to the non-oscillatory period P_0(f) when averaged for beta (12-30 Hz) and gamma (30-100 Hz) frequency bands in dHP (left, n=41 mice) and i/vHP (right, n=103 mice). **(C)** Histograms displaying the phase-locking of hippocampal spikes to ripple activity in dHP (left) and i/vHP (right)

Supplementary figure 2. Experimental protocol for *in utero* electroporation of the hippocampus. **(A)** Structure of the ChR2(ET/TC)-containing and opsinfree constructs. **(B)** Schematic drawing illustrating the orientation of electrode paddles for specific targeting of either (i) dHPor (ii) i/vHP pyramidal neurons. **(C)** Bar diagram displaying the mean number of embryos, electroporated embryos, surviving pups, and positively transfected pups when ChR2(ET/TC)-containing and opsin-free constructs for (i) dHP (n = 8 litters for opsin-containing group, n = 5 for opsinfree group) and (ii) i/vHP (n = 8 litters for opsin-containing group, n = 3 litters for opsinfree group). **(D)** Line plots displaying the developmental profile of somatic growth [body length, tail length, weight] and reflexes [vibrissa placing, cliff aversion and surface righting reflexes] of P2-8 pups expressing ChR2(ET/TC) or opsin-free constructs in (i) dHP (n = 17 for opsin-containing pups, n = 14 for opsinfree pups) and (ii) i/vHP (n = 9 for opsin-containing pups, n = 5 for opsinfree pups).

Supplementary figure 3.

Bar diagrams displaying the power changes in PL during light stimulation of pyramidal neurons in the CA1 area of dHP (top panels) or i/vHP (bottom panels) when normalized to the values before hippocampal stimulation for opsinfree animals.

Table legends

Table 1.

Table containing mean power changes in PL after stimulation in hippocampus for ChR2(ET/TC)-containing and opsinfree animals.

References

Adhikari, A., Topiwala, M.A., and Gordon, J.A. (2010). Synchronized activity between the ventral hippocampus and the medial prefrontal cortex during anxiety. Neuron 65, 257-269.

Amaral, D.G., Scharfman, H.E., and Lavenex, P. (2007). The dentate gyrus: fundamental neuroanatomical organization (dentate gyrus for dummies). 163, 3-790.

Baccala, L.A., Sameshima, K., and Takahashi, D.Y. (2007). Generalized Partial Directed Coherence. 163-166.

Backus, A.R., Schoffelen, J.M., Szebenyi, S., Hanslmayr, S., and Doeller, C.F. (2016). Hippocampal-Prefrontal Theta Oscillations Support Memory Integration. Curr Biol 26, 450-457.

Bannerman, D.M., Grubb, M., Deacon, R.M.J., Yee, B.K., Feldon, J., and Rawlins, J.N.P. (2003). Ventral hippocampal lesions affect anxiety but not spatial learning. Behavioural Brain Research 139, 197-213.

Bannerman, D.M., Sprengel, R., Sanderson, D.J., McHugh, S.B., Rawlins, J.N., Monyer, H., and Seeburg, P.H. (2014). Hippocampal synaptic plasticity, spatial memory and anxiety. Nat Rev Neurosci 15, 181-192.

Bast, T., Wilson, I.A., Witter, M.P., and Morris, R.G. (2009). From rapid place learning to behavioral performance: a key role for the intermediate hippocampus. PLoS Biol 7, e1000089.

Baumgart, J., and Grebe, N. (2015). C57BL/6-specific conditions for efficient in utero electroporation of the central nervous system. J Neurosci Methods 240, 116-124.

Ben-Ari, Y., Cherubini, E., Corradetti, R., and Gaiarsa, J.L. (1989). Giant synaptic potentials in immature rat CA3 hippocampal neurones. J Physiol 416, 303-325.

Benchenane, K., Peyrache, A., Khamassi, M., Tierney, P.L., Gioanni, Y., Battaglia, F.P., and Wiener, S.I. (2010). Coherent theta oscillations and reorganization of spike timing in the hippocampal- prefrontal network upon learning. Neuron 66, 921-936.

Berndt, A., Schoenenberger, P., Mattis, J., Tye, K.M., Deisseroth, K., Hegemann, P., and Oertner, T.G. (2011). High-efficiency channelrhodopsins for fast neuronal stimulation at low light levels. Proc Natl Acad Sci U S A 108, 7595-7600.

Bitzenhofer, S.H., Ahlbeck, J., Wolff, A., Wiegert, J.S., Gee, C.E., Oertner, T.G., and Hanganu-Opatz, I.L. (2017). Layer-specific optogenetic activation of pyramidal neurons causes beta-gamma entrainment of neonatal networks. Nat Commun 8, 14563.

Bitzenhofer, S.H., and Hanganu-Opatz, I.L. (2014). Oscillatory coupling within neonatal prefrontal-hippocampal networks is independent of selective removal of GABAergic neurons in the hippocampus. Neuropharmacology 77, 57-67.

Bitzenhofer, S.H., Sieben, K., Siebert, K.D., Spehr, M., and Hanganu-Opatz, I.L. (2015). Oscillatory activity in developing prefrontal networks results from theta-gamma-modulated synaptic inputs. Cell Rep 11, 486-497.

Borrell, V., Yoshimura, Y., and Callaway, E.M. (2005). Targeted gene delivery to telencephalic inhibitory neurons by directional in utero electroporation. J Neurosci Methods 143, 151-158.

Brincat, S.L., and Miller, E.K. (2015). Frequency-specific hippocampal-prefrontal interactions during associative learning. Nat Neurosci 18, 576-581.

Brockmann, M.D., Poschel, B., Cichon, N., and Hanganu-Opatz, I.L. (2011). Coupled oscillations mediate directed interactions between prefrontal cortex and hippocampus of the neonatal rat. Neuron 71, 332-347.

Buhl, D.L., and Buzsaki, G. (2005). Developmental emergence of hippocampal fast-field "ripple" oscillations in the behaving rat pups. Neuroscience 134, 1423-1430.

Buzsaki, G. (2015). Hippocampal sharp wave-ripple: A cognitive biomarker for episodic memory and planning. Hippocampus.

Cichon, N.B., Denker, M., Grun, S., and Hanganu-Opatz, I.L. (2014). Unsupervised classification of neocortical activity patterns in neonatal and pre-juvenile rodents. Front Neural Circuits 8, 50.
Cirelli, C., and Tononi, G. (2015). Cortical development, electroencephalogram rhythms, and the sleep/wake cycle. Biol Psychiatry 77, 1071-1078.
Colgin, L.L. (2011). Oscillations and hippocampal-prefrontal synchrony. Curr Opin Neurobiol 21, 467-474.
Colgin, L.L. (2016). Rhythms of the hippocampal network. Nat Rev Neurosci 17, 239-249.
Dong, H.W., Swanson, L.W., Chen, L., Fanselow, M.S., and Toga, A.W. (2009). Genomic-anatomic evidence for distinct functional domains in hippocampal field CA1. Proc Natl Acad Sci U S A 106, 11794-11799.
Dupont, E., Hanganu, I.L., Kilb, W., Hirsch, S., and Luhmann, H.J. (2006). Rapid developmental switch in the mechanisms driving early cortical columnar networks. Nature 439, 79-83.
Eichenbaum, H. (2017). Prefrontal-hippocampal interactions in episodic memory. Nat Rev Neurosci.
Fanselow, M.S., and Dong, H.W. (2010). Are the dorsal and ventral hippocampus functionally distinct structures? Neuron 65, 7-19.
Geisler, C., Robbe, D., Zugaro, M., Sirota, A., and Buzsaki, G. (2007). Hippocampal place cell assemblies are speed-controlled oscillators. Proc Natl Acad Sci U S A 104, 8149-8154.
Granger, C.W.J. (1980). Testing for causality. Journal of Economic Dynamics and Control 2, 329-352.
Hallock, H.L., Wang, A., and Griffin, A.L. (2016). Ventral Midline Thalamus Is Critical for Hippocampal-Prefrontal Synchrony and Spatial Working Memory. J Neurosci 36, 8372-8389.
Hanganu-Opatz, I.L. (2010). Between molecules and experience: role of early patterns of coordinated activity for the development of cortical maps and sensory abilities. Brain Res Rev 64, 160-176.
Hanganu, I.L., Ben-Ari, Y., and Khazipov, R. (2006). Retinal waves trigger spindle bursts in the neonatal rat visual cortex. J Neurosci 26, 6728-6736.
Hanganu, I.L., Okabe, A., Lessmann, V., and Luhmann, H.J. (2009). Cellular mechanisms of subplate-driven and cholinergic input-dependent network activity in the neonatal rat somatosensory cortex. Cereb Cortex 19, 89-105.
Hartung, H., Brockmann, M.D., Poschel, B., De Feo, V., and Hanganu-Opatz, I.L. (2016). Thalamic and Entorhinal Network Activity Differently Modulates the Functional Development of Prefrontal-Hippocampal Interactions. Journal of Neuroscience 36, 3676-3690.
Hoerder-Suabedissen, A., and Molnar, Z. (2015). Development, evolution and pathology of neocortical subplate neurons. Nat Rev Neurosci 16, 133-146.
Honeycutt, J.A., Keary Iii, K.M., Kania, V.M., and Chrobak, J.J. (2016). Developmental Age Differentially Mediates the Calcium-Binding Protein Parvalbumin in the Rat: Evidence for a Selective Decrease in Hippocampal Parvalbumin Cell Counts. Dev Neurosci 38, 105-114.
Hubel, D.H., Wiesel, T.N., and LeVay, S. (1977). Plasticity of Ocular Dominance Columns in Monkey Striate Cortex. Philosophical Transactions of the Royal Society B: Biological Sciences 278, 377-409.
Huberman, A.D., Speer, C.M., and Chapman, B. (2006). Spontaneous retinal activity mediates development of ocular dominance columns and binocular receptive fields in v1. Neuron 52, 247-254.
Janiesch, P.C., Kruger, H.S., Poschel, B., and Hanganu-Opatz, I.L. (2011). Cholinergic control in developing prefrontal-hippocampal networks. J Neurosci 31, 17955-17970.

Jay, T.M., and Witter, M.P. (1991). Distribution of hippocampal CA1 and subicular efferents in the prefrontal cortex of the rat studied by means of anterograde transport of Phaseolus vulgaris-leucoagglutinin. J Comp Neurol 313, 574-586.
Khazipov, R., Minlebaev, M., and Valeeva, G. (2013). Early gamma oscillations. Neuroscience 250, 240-252.
Kouvaros, S., and Papatheodoropoulos, C. (2017). Prominent differences in sharp waves, ripples and complex spike bursts between the dorsal and the ventral rat hippocampus. Neuroscience 352, 131-143.
Kruger, H.S., Brockmann, M.D., Salamon, J., Ittrich, H., and Hanganu-Opatz, I.L. (2012). Neonatal hippocampal lesion alters the functional maturation of the prefrontal cortex and the early cognitive development in pre-juvenile rats. Neurobiol Learn Mem 97, 470-481.
Lindemann, C., Ahlbeck, J., Bitzenhofer, S.H., and Hanganu-Opatz, I.L. (2016). Spindle Activity Orchestrates Plasticity during Development and Sleep. Neural Plast 2016, 5787423.
Linke, R., and Frotscher, M. (1993). Development of the rat septohippocampal projection: tracing with DiI and electron microscopy of identified growth cones. J Comp Neurol 332, 69-88.
Luhmann, H.J., and Khazipov, R. (2017). Neuronal activity patterns in the developing barrel cortex. Neuroscience.
Minlebaev, M., Ben-Ari, Y., and Khazipov, R. (2009). NMDA receptors pattern early activity in the developing barrel cortex in vivo. Cereb Cortex 19, 688-696.
Minlebaev, M., Colonnese, M., Tsintsadze, T., Sirota, A., and Khazipov, R. (2011). Early gamma oscillations synchronize developing thalamus and cortex. Science 334, 226-229.
Moser, E.I. (1998). Impaired Spatial Learning after Saturation of Long-Term Potentiation. Science 281, 2038-2042.
Moser, M.B., Moser, E.I., Forrest, E., Andersen, P., and Morris, R.G. (1995). Spatial learning with a minislab in the dorsal hippocampus. Proc Natl Acad Sci U S A 92, 9697-9701.
Navarro-Quiroga, I., Chittajallu, R., Gallo, V., and Haydar, T.F. (2007). Long-term, selective gene expression in developing and adult hippocampal pyramidal neurons using focal in utero electroporation. J Neurosci 27, 5007-5011.
Niwa, M., Kamiya, A., Murai, R., Kubo, K., Gruber, A.J., Tomita, K., Lu, L., Tomisato, S., Jaaro-Peled, H., Seshadri, S., *et al.* (2010). Knockdown of DISC1 by in utero gene transfer disturbs postnatal dopaminergic maturation in the frontal cortex and leads to adult behavioral deficits. Neuron 65, 480-489.
Nolte, G., Bai, O., Wheaton, L., Mari, Z., Vorbach, S., and Hallett, M. (2004). Identifying true brain interaction from EEG data using the imaginary part of coherency. Clin Neurophysiol 115, 2292-2307.
O'Keefe, J., and Nadel, L. (1978). The Hippocampus as a Cognitive Map (New York: Oxford University Press).
O'Keefe, J., and Recce, M.L. (1993). Phase relationship between hippocampal place units and the EEG theta rhythm. Hippocampus 3, 317-330.
Patel, J., Schomburg, E.W., Berenyi, A., Fujisawa, S., and Buzsaki, G. (2013). Local generation and propagation of ripples along the septotemporal axis of the hippocampus. J Neurosci 33, 17029-17041.
Pitkanen, A., Pikkarainen, M., Nurminen, N., and Ylinen, A. (2000). Reciprocal connections between the amygdala and the hippocampal formation, perirhinal cortex, and postrhinal cortex in rat - A review. Ann Ny Acad Sci 911, 369-391.
Place, R., Farovik, A., Brockmann, M., and Eichenbaum, H. (2016). Bidirectional prefrontal-hippocampal interactions support context-guided memory. Nat Neurosci.
Ribak, C.E., and Seress, L. (1983). Five types of basket cell in the hippocampal dentate gyrus: a combined Golgi and electron microscopic study. J Neurocytol 12, 577-597.

Rodrigues, P.L., and Baccala, L.A. (2016). Statistically significant time-varying neural connectivity estimation using generalized partial directed coherence. Conf Proc IEEE Eng Med Biol Soc 2016, 5493-5496.
Royer, S., Sirota, A., Patel, J., and Buzsaki, G. (2010). Distinct representations and theta dynamics in dorsal and ventral hippocampus. J Neurosci 30, 1777-1787.
Seelke, A.M., and Blumberg, M.S. (2010). Developmental appearance and disappearance of cortical events and oscillations in infant rats. Brain Res 1324, 34-42.
Shen, J., and Colonnese, M.T. (2016). Development of Activity in the Mouse Visual Cortex. J Neurosci 36, 12259-12275.
Siapas, A.G., Lubenov, E.V., and Wilson, M.A. (2005). Prefrontal phase locking to hippocampal theta oscillations. Neuron 46, 141-151.
Siapas, A.G., and Wilson, M.A. (1998). Coordinated interactions between hippocampal ripples and cortical spindles during slow-wave sleep. Neuron 21, 1123-1128.
Sigurdsson, T., Stark, K.L., Karayiorgou, M., Gogos, J.A., and Gordon, J.A. (2010). Impaired hippocampal-prefrontal synchrony in a genetic mouse model of schizophrenia. Nature 464, 763-767.
Sirota, A., Montgomery, S., Fujisawa, S., Isomura, Y., Zugaro, M., and Buzsaki, G. (2008). Entrainment of neocortical neurons and gamma oscillations by the hippocampal theta rhythm. Neuron 60, 683-697.
Spellman, T., Rigotti, M., Ahmari, S.E., Fusi, S., Gogos, J.A., and Gordon, J.A. (2015). Hippocampal-prefrontal input supports spatial encoding in working memory. Nature 522, 309-314.
Stewart, M., and Fox, S.E. (1990). Do septal neurons pace the hippocampal theta rhythm? Trends in Neurosciences 13, 163-169.
Strange, B.A., Witter, M.P., Lein, E.S., and Moser, E.I. (2014). Functional organization of the hippocampal longitudinal axis. Nat Rev Neurosci 15, 655-669.
Stujenske, J.M., Spellman, T., and Gordon, J.A. (2015). Modeling the Spatiotemporal Dynamics of Light and Heat Propagation for In Vivo Optogenetics. Cell Rep 12, 525-534.
Swanson, L.W. (1981). A direct projection from Ammon's horn to prefrontal cortex in the rat. Brain Res 217, 150-154.
Szczurkowska, J., Cwetsch, A.W., dal Maschio, M., Ghezzi, D., Ratto, G.M., and Cancedda, L. (2016). Targeted in vivo genetic manipulation of the mouse or rat brain by in utero electroporation with a triple-electrode probe. Nat Protoc 11, 399-412.
Tabata, H., and Nakajima, K. (2001). Efficient in utero gene transfer system to the developing mouse brain using electroporation: Visualization of neuronal migration in the developing cortex. Neuroscience 103, 865-872.
Taxidis, J., Coomber, B., Mason, R., and Owen, M. (2010). Assessing cortico-hippocampal functional connectivity under anesthesia and kainic acid using generalized partial directed coherence. Biol Cybern 102, 327-340.
Thompson, C.L., Pathak, S.D., Jeromin, A., Ng, L.L., MacPherson, C.R., Mortrud, M.T., Cusick, A., Riley, Z.L., Sunkin, S.M., Bernard, A., *et al.* (2008). Genomic anatomy of the hippocampus. Neuron 60, 1010-1021.
Tolner, E.A., Sheikh, A., Yukin, A.Y., Kaila, K., and Kanold, P.O. (2012). Subplate neurons promote spindle bursts and thalamocortical patterning in the neonatal rat somatosensory cortex. J Neurosci 32, 692-702.
Vertes, R.P., Hoover, W.B., Szigeti-Buck, K., and Leranth, C. (2007). Nucleus reuniens of the midline thalamus: link between the medial prefrontal cortex and the hippocampus. Brain Res Bull 71, 601-609.
Wirt, R.A., and Hyman, J.M. (2017). Integrating Spatial Working Memory and Remote Memory: Interactions between the Medial Prefrontal Cortex and Hippocampus. Brain Sci 7.
Witter, M.P., and Amaral, D.G. (2004). Hippocampal Formation. 635-704.

Witter, M.P., Van Hoesen, G.W., and Amaral, D.G. (1989). Topographical organization of the entorhinal projection to the dentate gyrus of the monkey. J Neurosci 9, 216-228.
Xu, H.P., Furman, M., Mineur, Y.S., Chen, H., King, S.L., Zenisek, D., Zhou, Z.J., Butts, D.A., Tian, N., Picciotto, M.R., and Crair, M.C. (2011). An instructive role for patterned spontaneous retinal activity in mouse visual map development. Neuron 70, 1115-1127.
Xu, W., and Sudhof, T.C. (2013). A neural circuit for memory specificity and generalization. Science 339, 1290-1295.
Yasuda, M., Johnson-Venkatesh, E.M., Zhang, H., Parent, J.M., Sutton, M.A., and Umemori, H. (2011). Multiple forms of activity-dependent competition refine hippocampal circuits in vivo. Neuron 70, 1128-1142.
Ye, X., Kapeller-Libermann, D., Travaglia, A., Inda, M.C., and Alberini, C.M. (2017). Direct dorsal hippocampal-prelimbic cortex connections strengthen fear memories. Nat Neurosci 20, 52-61.
Yuste, R., Nelson, D.A., Rubin, W.W., and Katz, L.C. (1995). Neuronal domains in developing neocortex: mechanisms of coactivation. Neuron 14, 7-17.
Zhang, L., Spigelman, I., and Carlen, P.L. (1990). Whole-cell patch study of GABAergic inhibition in CA1 neurons of immature rat hippocampal slices. Developmental Brain Research 56, 127-130.

Figure 1

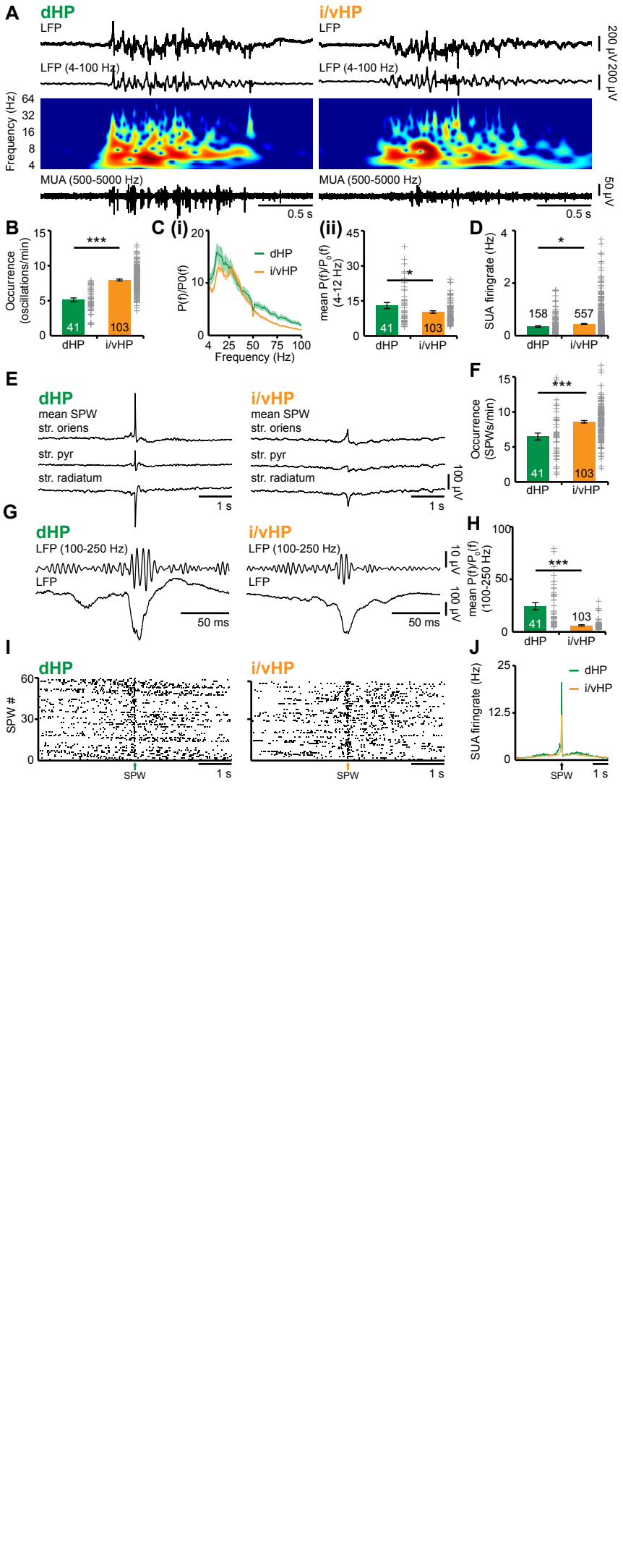
A
dHP
i/vHP
LFP
LFP (4-100 Hz)
200 µV
Frequency (Hz)
64
32
16
8
4
MUA (500-5000 Hz)
0.5 s
50 µV
B
Occurrence (oscillations/min)
***
41
103
dHP
i/vHP
C (i)
P(f)/P0(f)
dHP
i/vHP
Frequency (Hz)
(ii)
mean P(f)/P0(f) (4-12 Hz)
*
D
SUA firingrate (Hz)
158
557
E
mean SPW
str. oriens
str. pyr
str. radiatum
1 s
100 µV
F
Occurrence (SPWs/min)
G
LFP (100-250 Hz)
50 ms
H
mean P(f)/P0(f) (100-250 Hz)
I
SPW #
SPW
J
SUA firingrate (Hz)

Figure 2

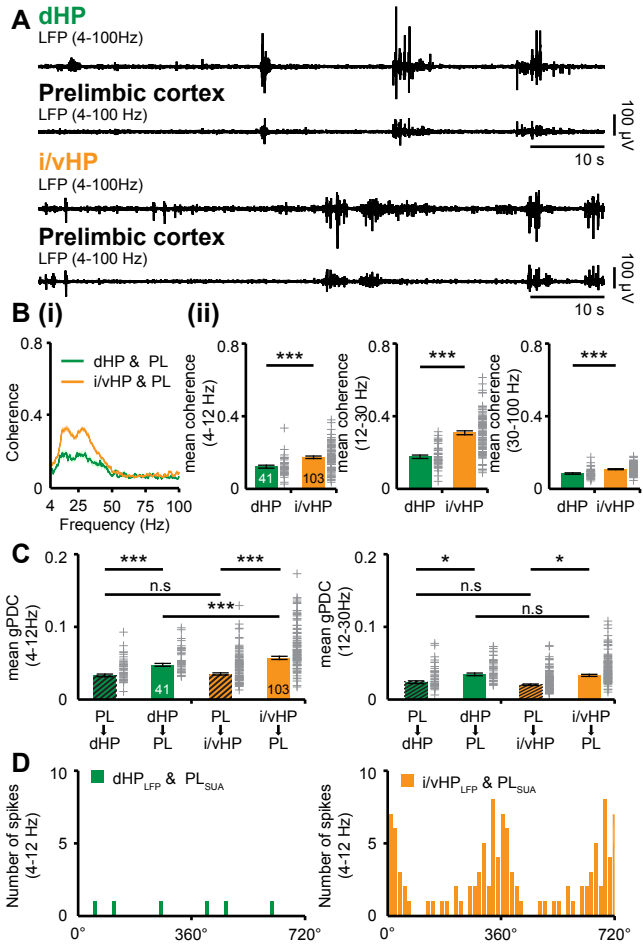
A
dHP
LFP (4-100Hz)
Prelimbic cortex
LFP (4-100 Hz)
100 µV
10 s
i/vHP
LFP (4-100Hz)
Prelimbic cortex
LFP (4-100 Hz)
100 µV
10 s
B (i)
(ii)
dHP & PL
i/vHP & PL
Coherence
Frequency (Hz)
mean coherence (4-12 Hz)
mean coherence (12-30 Hz)
mean coherence (30-100 Hz)
***
41
103
dHP
i/vHP
C
mean gPDC (4-12Hz)
mean gPDC (12-30Hz)
***
n.s
*
PL → dHP
dHP → PL
PL → i/vHP
i/vHP → PL
D
Number of spikes (4-12 Hz)
dHP_LFP & PL_SUA
i/vHP_LFP & PL_SUA
0°
360°
720°

Figure 3


A (i) Prelimbic cortex
Frequency (Hz)
64
32
16
8
4
pre
SPW
post
100 ms
2
1
0
Ratio
(ii)
dHP
i/vHP
mean power (4-12 Hz) (μV²)
1000
500
0
n.s
**
41
103
pre
post
mean power (12-30 Hz) (μV²)
250
125
0
n.s
**
pre
post
mean power (30-100 Hz) (μV²)
100
50
0
*
**
pre
post
B
Spikes in PL (SPW in dHP)
SPW #
60
30
0
SPW
500 ms
Spikes in PL (SPW in i/vHP)
SPW
500 ms
C
SUA firingrate (Hz)
1.5
0.75
0
dHP
i/vHP
SPW
1 s

Figure 4

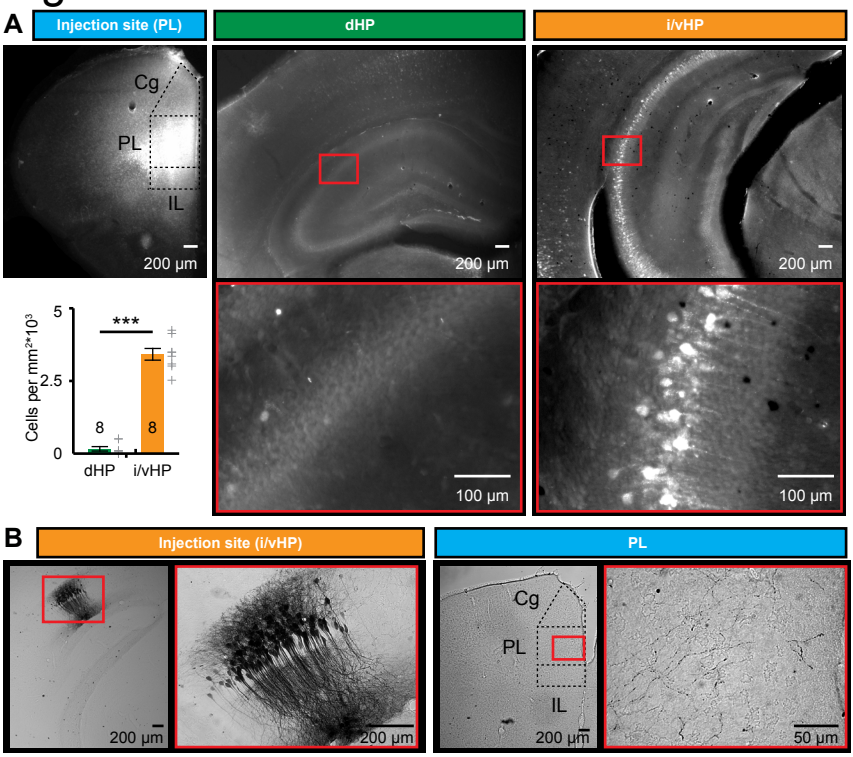
A
Injection site (PL)
dHP
i/vHP
Cg
PL
IL
200 µm
200 µm
200 µm
100 µm
100 µm
Cells per mm²*10³
5
2.5
0
***
8
8
dHP
i/vHP

B
Injection site (i/vHP)
PL
200 µm
200 µm
Cg
PL
IL
200 µm
50 µm

Figure 5

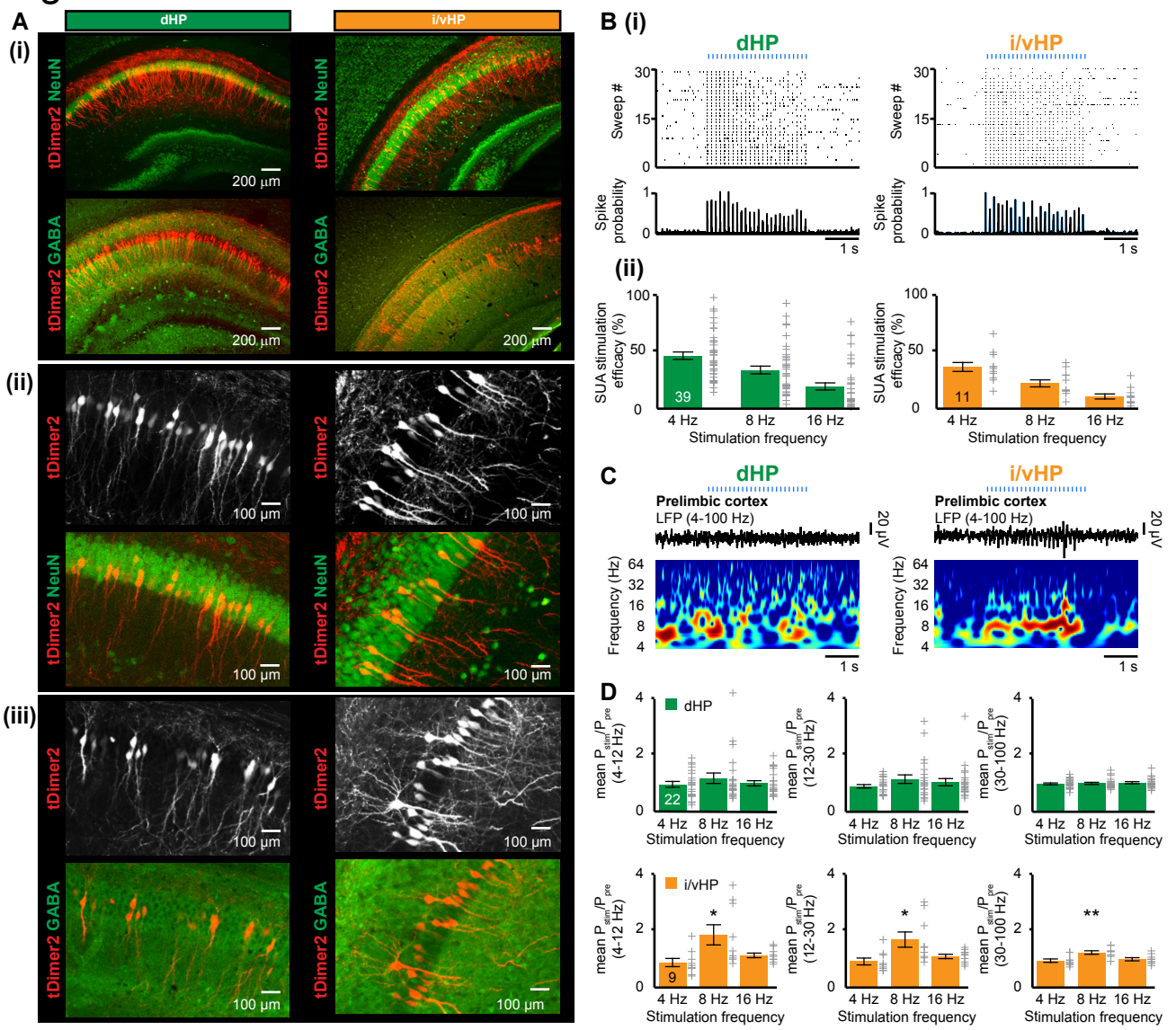
A
dHP
i/vHP
(i)
tDimer2 NeuN
tDimer2 GABA
200 µm
(ii)
tDimer2
tDimer2 NeuN
100 µm
(iii)
tDimer2
tDimer2 GABA
100 µm
B (i)
dHP
i/vHP
Sweep #
Spike probability
1 s
(ii)
SUA stimulation efficacy (%)
39
11
4 Hz
8 Hz
16 Hz
Stimulation frequency
C
dHP
i/vHP
Prelimbic cortex
LFP (4-100 Hz)
20 µV
Frequency (Hz)
64
32
16
8
4
1 s
D
dHP
i/vHP
mean P stim/P pre (4-12 Hz)
mean P stim/P pre (12-30 Hz)
mean P stim/P pre (30-100 Hz)
22
9
*
**
4 Hz
8 Hz
16 Hz
Stimulation frequency

Table 1

	dHP			i/vHP		
	Stimulation Frequency			Stimulation Frequency		
ChR2(ET/TC)	**4 Hz**	**8 Hz**	**16 Hz**	**4 Hz**	**8 Hz**	**16hz**
Theta	0.97±0.10	1.19±0.19	1.0±0.093	0.90±0.15	1.89±0.36 (*)	1.16±0.08
Beta	0.91±0.06	1.17±0.15	1.06±0.13	0.94±0.12	1.72±0.27 (*)	1.12±0.08
Gamma	1.0±0.035	1.00±0.19	1.04±0.38	0.97±0.06	1.26±0.06 (**)	1.02±0.06
Opsinfree						
Theta	1.11±0.14	1.09±0.19	1.14±0.22	1.17±0.27	1.17±0.20	1.06±0.05
Beta	1.13±0.15	0.99±0.16	1.11±0.11	1.05±0.22	0.95±0.18	1.09±0.10
Gamma	1.08±0.06	0.93±0.04	1.03±0.03	0.89±0.09	0.94±0.07	1.04±0.05

Figure S1

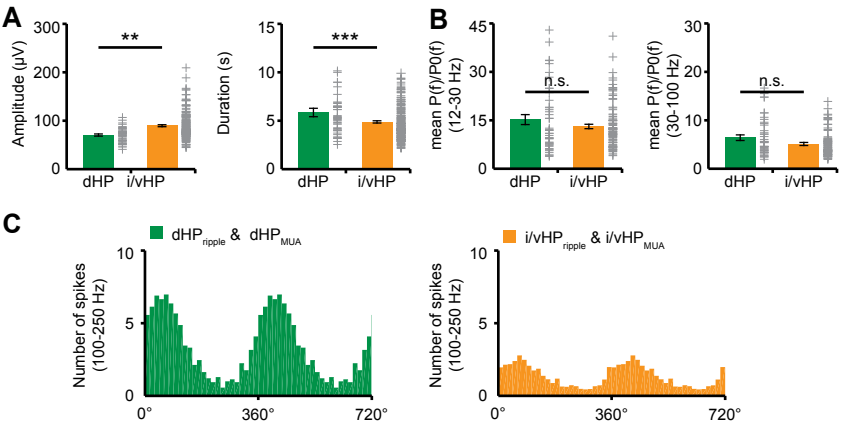
A
Amplitude (μV)
300
200
100
0
**
dHP
i/vHP
Duration (s)
15
10
5
0
***
dHP
i/vHP
B
mean P(f)/P0(f) (12-30 Hz)
45
30
15
0
n.s.
dHP
i/vHP
mean P(f)/P0(f) (30-100 Hz)
30
20
10
0
n.s.
dHP
i/vHP

C
dHP ripple & dHP MUA
Number of spikes (100-250 Hz)
10
5
0
0°
360°
720°
i/vHP ripple & i/vHP MUA
Number of spikes (100-250 Hz)
10
5
0
0°
360°
720°

Figure S2

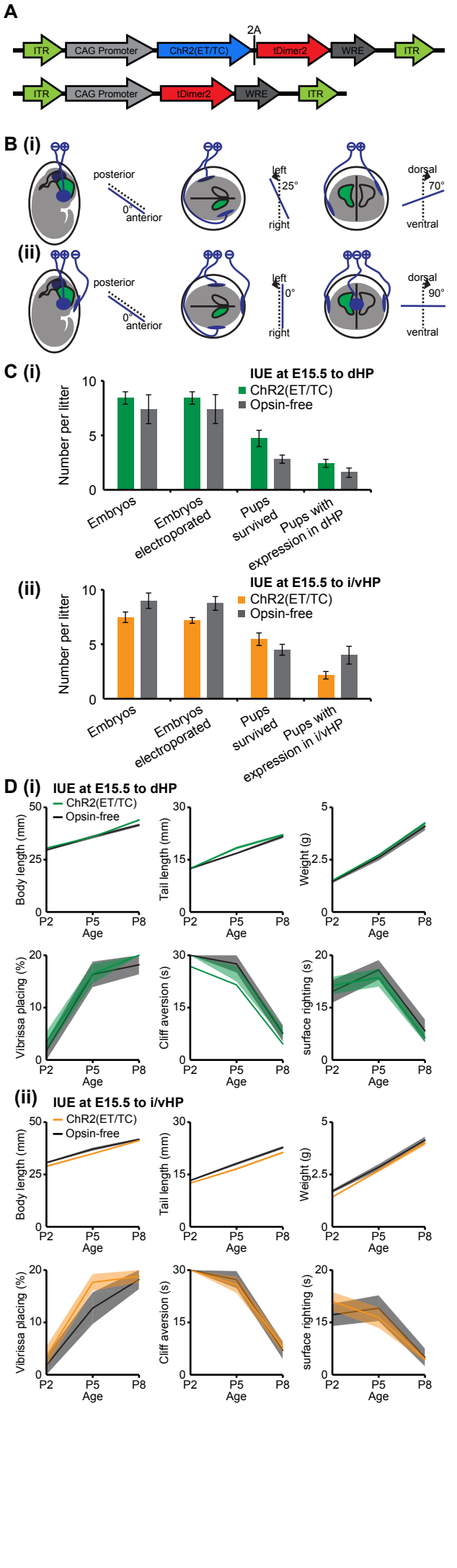
A
2A
ITR
CAG Promoter
ChR2(ET/TC)
tDimer2
WRE
ITR
ITR
CAG Promoter
tDimer2
WRE
ITR
B (i)
posterior
0°
anterior
left
25°
right
dorsal
70°
ventral
(ii)
posterior
0°
anterior
left
0°
right
dorsal
90°
ventral
C (i)
IUE at E15.5 to dHP
ChR2(ET/TC)
Opsin-free
Number per litter
10
5
0
Embryos
Embryos electroporated
Pups survived
Pups with expression in dHP
(ii)
IUE at E15.5 to i/vHP
ChR2(ET/TC)
Opsin-free
Number per litter
10
5
0
Embryos
Embryos electroporated
Pups survived
Pups with expression in i/vHP
D (i)
IUE at E15.5 to dHP
ChR2(ET/TC)
Opsin-free
Body length (mm)
50
25
0
Tail length (mm)
30
15
0
Weight (g)
5
2.5
0
P2
P5
P8
Age
Vibrissa placing (%)
20
10
0
Cliff aversion (s)
30
15
0
surface righting (s)
20
15
0
(ii)
IUE at E15.5 to i/vHP
ChR2(ET/TC)
Opsin-free
Body length (mm)
50
25
0
Tail length (mm)
30
15
0
Weight (g)
5
2.5
0
P2
P5
P8
Age
Vibrissa placing (%)
20
10
0
Cliff aversion (s)
30
15
0
surface righting (s)
20
15
0

Figure S3

A **Response in Prelimbic cortex**

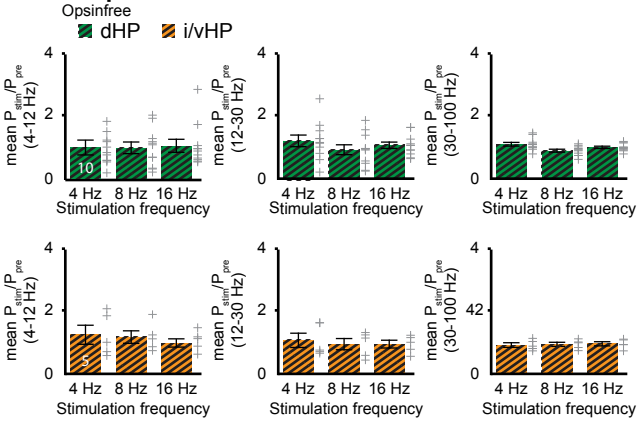

Hindawi Publishing Corporation
Neural Plasticity
Volume 2016, Article ID 5787423, 14 pages
http://dx.doi.org/10.1155/2016/5787423

Review Article

Spindle Activity Orchestrates Plasticity during Development and Sleep

Christoph Lindemann, Joachim Ahlbeck, Sebastian H. Bitzenhofer, and Ileana L. Hanganu-Opatz

Developmental Neurophysiology, Institute of Neuroanatomy, University Medical Center Hamburg-Eppendorf, 20251 Hamburg, Germany

Correspondence should be addressed to Christoph Lindemann; christoph.lindemann@zmnh.uni-hamburg.de

Received 29 January 2016; Accepted 13 April 2016

Academic Editor: Adrien Peyrache

Spindle oscillations have been described during early brain development and in the adult brain. Besides similarities in temporal patterns and involved brain areas, neonatal spindle bursts (NSBs) and adult sleep spindles (ASSs) show differences in their occurrence, spatial distribution, and underlying mechanisms. While NSBs have been proposed to coordinate the refinement of the maturating neuronal network, ASSs are associated with the implementation of acquired information within existing networks. Along with these functional differences, separate synaptic plasticity mechanisms seem to be recruited. Here, we review the generation of spindle oscillations in the developing and adult brain and discuss possible implications of their differences for synaptic plasticity. The first part of the review is dedicated to the generation and function of ASSs with a particular focus on their role in healthy and impaired neuronal networks. The second part overviews the present knowledge of spindle activity during development and the ability of NSBs to organize immature circuits. Studies linking abnormal maturation of brain wiring with neurological and neuropsychiatric disorders highlight the importance to better elucidate neonatal plasticity rules in future research.

1. Introduction

Information processing within the brain critically depends on rhythmic oscillatory activity that synchronizes neuronal networks. Synchronization leads to local and global coupling of network elements and times neuronal firing. By these means, it enables the precise selection of relevant information. Depending on the brain state and the timing of convergent inputs, plastic changes up- or downgrade the importance of new information from the environment [1, 2]. Consolidation of the collected information in long-term memory during sleep guarantees a timely reaction to environmental changes and promotes survival [3–5].

Spindle oscillations are typical representatives of rhythmic network activity that have been monitored in electroencephalographic (EEG) recordings both during early development and at adulthood [6–10]. While the underlying mechanisms of ASSs have been extensively investigated in the past, aiming to identify their role for consolidation of memories [4, 5, 11], NSB-related mechanisms are still largely unresolved and their function remains rather blurry. Only recent experimental evidence indicated that NSBs do not represent a by-product of maturating neuronal networks but important elements for their refinement [12–16]. This review summarizes the different aspects of ASS and NSB plasticity.

2. Adult Sleep Spindles

ASSs are recurrent, short lasting network oscillations (0.5–3 s) characteristic for nonrapid eye movement (NREM) sleep. They have a waxing and waning waveform with the main frequency ranging from 9 to 15 Hz [6, 11]. Spontaneous ASSs synchronize large cortical areas, following defined patterns of spatial distribution that have been monitored in humans both by EEG and magnetoencephalogram (MEG) [17–19]. This distribution depends on different factors, such as spindle peak frequency (slow or fast), sleep stage period (early or late), and age of the investigated person [20–23]. According

to their waveform properties and cortical distribution, two entities of ASSs have been distinguished. On the one hand, prominent slow ASSs (9–13 Hz) emerge as product of spindle generators located in frontal brain regions. On the other hand, low amplitude fast ASSs (13–15 Hz) originate from the thalamic reticular nucleus (TRN) and spread over the whole cortex with strongest occurrence in central and parietal areas [23–27]. However, the exact origin of slow and fast ASSs and whether they share the same generators is still a matter of debate [18, 27–30]. Support for separate underlying generators comes from differential pharmacological modulation of slow and fast ASSs [24].

In contrast to humans, mice show no difference in the frequencies between frontal and centroparietal spindles. Still, ASSs can be divided into three different types based on their anterior, posterior, or global topographical distribution. While anterior ASSs seem to depend mostly on generators within the ventrobasal thalamic nucleus, posterior ASSs appear to be largely initiated by the TRN [20]. This nucleus is also recognized as the main pacemaker for the generation of fast ASSs in humans as detailed below.

2.1. Generation and Origin of Adult Sleep Spindles. The generation of fast ASSs with thalamic origin has been divided into three stages: (i) initiation, (ii) propagation, and (iii) termination.

(i) In line with their ability to initiate rhythmic discharges, neurons in the TRN are the main pacemakers of ASS activity [31]. Reduced excitatory drive from cortical and subcortical afferents, present at the onset of NREM sleep, allows progressive hyperpolarization of TRN cells and a shift of their resting potential to values < -60 mV [32, 33]. At this hyperpolarized membrane potential, selective depolarization of TRN cells by cortical afferents leads to activation of low-voltage gated T-type Ca^{2+} channels that cause dendritic Ca^{2+} accumulation. The rise in Ca^{2+} triggers Ca^{2+}-dependent small-conductance type $2K^{+}$ channels (SK2). As a consequence, burst afterhyperpolarizations are induced and lead to temporal inactivation of earlier triggered T-type channels [34–39]. Such alternations of depolarized and hyperpolarized states in TRN cells shape the typical spindle oscillations.

(ii) Rapid changes of ion concentrations are not sufficient to keep up ASS activity. Additional cellular interplay maintains and particularly propagates ASSs. TRN cells form dense inhibitory connections with thalamocortical (TC) cells in the dorsal thalamus [40]. In reaction to synchronized inhibition by TRN cells, TC cells show paradoxical activation and fire postinhibitory rebound bursts [41, 42]. Excitatory back-projections from TC to TRN cells establish a self-maintaining excitation-inhibition cycle that enables stronger network synchronization and progressive recruitment of further thalamic cells [37]. In addition, coupling of TRN cells by gap junctions facilitates synchronization of the reticular network activity [43, 44]. In line with their nomenclature, TC cells project not only to reticular neurons, but also to different areas of the cortex, primarily targeting fast-spiking interneurons in layer IV [45–47]. Subsequent propagation between cortical layers amplifies the oscillatory activity, whereas deeper cortical layers provide feedback to TC and TRN cells to maintain the thalamic entrainment [48]. The importance of the cortex and the corticothalamic feedback for ASS synchronization and amplification is reflected by reduced ASS synchrony and phase locking after cortical depression and locally restricted synchronization after decortication [49, 50].

(iii) To prevent unrestrained excitation and concomitant development of epileptic seizures, several mechanisms control and terminate ASS activity. First, $GABA_A$-receptor-mediated lateral inhibition between TRN cells prevents the occurrence of hypersynchrony in the thalamocortical network [42]. Second, the strong accumulation of Ca^{2+} in dendrites of TRN cells activates the sarco- (endo-) plasmatic reticulum Ca^{2+} ATPase (SERCA) that pumps Ca^{2+} back into the cellular stores and interrupts the T-SK2 channel interaction [34, 51]. Another effect of the Ca^{2+} accumulation is the persistent upregulation of I_h in TC cells. This upregulation is caused by a Ca^{2+}-induced Ca^{2+} release and a facilitated binding of cAMP to open hyperpolarization-activated, cyclic-nucleotide-gated (HCN) channels. The resulting afterdepolarization prevents the generation of further rebound bursts in TC cells [52, 53]. Finally, reduced synchronization and phase locking of the thalamus and cortex diminishes rebound bursts in TC cells and stops further recurrent entrainment of the network [54].

2.2. Adult Sleep Spindles Boost Plasticity. The mechanisms involved in the initiation, propagation, and termination of ASSs control the synaptic plasticity processes in the corresponding adult networks. Strong and fast increase of local intracellular Ca^{2+} concentration, triggered by NMDA receptor activation after voltage-dependent release of the Mg^{2+} block and opening of voltage gated Ca^{2+} channels (VGCC), activates postsynaptic signaling cascades involving protein kinases, such as PKA and Ca^{2+}/calmodulin-dependent protein kinase II (CaMKII), which represent key players for long-term potentiation (LTP) [55–58]. CaMKII facilitates synaptic potentiation by phosphorylation of AMPA receptors and augmentation of GluR1-containing AMPA receptors at the postsynaptic density [59]. Modelling of plasticity processes in the hippocampus supports a correlation of activated CaMKII with the occurrence of cortical ASSs at the transition between sleep stages [60]. Of note, ASSs occurring outside this transition period did not correlate with the hippocampal CaMKII level.

While strong and fast Ca^{2+} increase contributes to LTP induction, small and long-lasting Ca^{2+} has been shown to generate protein phosphatase dependent long-term depression (LTD) [61]. Furthermore, Ca^{2+}-signaling is important for spike-timing dependent plasticity (STDP) [62]. Dendritic

Ca^{2+} influx through VGCC caused by back-propagating action potentials [63] leads to a supralinear increase of local intracellular Ca^{2+} concentrations and promotes LTP [64–66]. Short-term potentiation and LTP were induced by repetitive pre- and postsynaptic stimulation of cortical layer V pyramidal cells with ASS-associated spike trains, whereas presynaptic stimulation alone led to LTD [67]. Shuffling and mirroring of the ASS spike train used for stimulation failed to induce synaptic potentiation. This indicates that the temporal order of the recorded ASS spike train intervals was ideal to evoke synaptic changes.

2.3. Adult Sleep Spindles in Memory Functions and Network Plasticity. ASSs present during specific sleep phases have been proposed to be beneficial for several forms of memory including declarative [68, 69], procedural [70], and emotional memory [71]. The density of ASSs, especially, has been correlated with the performance in memory retrieval after sleep [72, 73]. However, the exact functions of different sleep stages in relationship with corresponding rhythmic neuronal activity are still poorly understood [3, 5]. Natural sleep in mammals is comprised of about 20% rapid eye movement (REM) and 80% NREM sleep. NREM sleep can be further divided into several stages from drowsiness (N1) over light sleep (N2) to deep, restorative SWS (N3) [11]. EEG and local field potential measurements showed that distinct activity patterns characterize these different stages of natural sleep. On the one hand, REM sleep is characterized by the occurrence of ponto-geniculo-occipital (PGO) waves and hippocampal theta oscillations. On the other hand, cortical slow oscillations, thalamocortical spindle activity, and hippocampal sharp-wave ripples are prominent during NREM sleep [32, 74]. Such rhythmic network activity is supposed to coordinate neuronal activity and to facilitate the integration of information based on the synchrony of convergent inputs, as well as the selection of inputs depending on their timing [1, 2].

The slow oscillations seen in SWS synchronize over large cortical areas and produce alternating depolarized UP and hyperpolarized DOWN states [75]. As common input to neuronal ensembles is relevant for induction of synaptic plasticity, the alternation of UP and DOWN states and, accordingly, long-range network synchronization is thought to provide temporal windows for memory consolidation processes [56, 76]. Furthermore, ASSs might shape memory-related plasticity during NREM sleep on subcellular level. For example, formation of spines on specific dendritic branches of layer V pyramidal neurons in the motor cortex during sleep has been recently observed following a motor learning task [77]. Branch-specific spine formation was shown to depend on reactivation of task-specific synapses and increase of somatic Ca^{2+} levels during subsequent NREM sleep, but not REM sleep [77]. Taking into account the role of ASSs in control of cellular Ca^{2+} concentrations, it is highly likely that ASS activity is involved in the branch-specific spine formation.

However, not all newly encoded memory traces become consolidated during sleep. Sleep favors memories expected to yield future rewards or being relevant for survival. Therefore, the question arises, which mechanisms are responsible for the selection of information for later consolidation? Two major hypotheses have been proposed.

The hypothesis of active system consolidation claims that the active transfer of information is encoded and stored in the neocortex and hippocampus during wakefulness but transferred into cortical long-term memory stores at sleep [78]. To enable this transfer, fast ASSs generated by the thalamus build a unitary complex with cortical slow oscillations and hippocampal sharp-wave ripples (80–200 Hz) [79, 80]. Slow oscillations appear to synchronize the occurrence of ASSs and the repeated accelerated reactivation of memory representations in form of hippocampal ripples during cortical UP states. In both humans and rodents, a clear phase locking between cortical ASS activity and hippocampal ripples can be observed with ripples occurring within the troughs around the peak of ASS activity [81–83]. This suggests the presence of a feedback loop that would enable a precisely timed bidirectional information transfer between cortex and hippocampus promoting synaptic plasticity and consolidation of memory [22].

The synaptic homeostasis hypothesis proposes a different mechanism and suggests that a global downscaling of synapses during sleep counterbalances their strengthening during encoding of new information at wakefulness. The concomitant synaptic potentiation and increase in firing during wakefulness puts the brain under a higher energy demand than continuously sustainable [84, 85]. The resulting progressive increase of glutamate in the extrasynaptic space would lead on the long run to cell intoxication and death [86]. Therefore, a process that resets the catabolic demand and reduces the stress within the brain seems to be mandatory. Likewise, an increasing amount of potentiated synapses reduces the signal-to-noise ratio within networks and prevents flexible responses to changes in the environment [87]. Depending on the actual electric state at the postsynapse recurrent bursts during episodes of ASSs can enable global downscaling of synaptic strength via long-term depression (LTD) [67, 88]. Apart from the attenuation of energy consumption, this global downscaling would also contribute to the emergence of information still concealed by less relevant information during wakefulness [5].

These two hypotheses might complement each other and share mechanisms relevant for memory consolidation. For example, both hypotheses need meaningful strategies to enable the transformation of labile encoded memory traces into long-lasting information during sleep. Recently, Heib and colleagues described a close relationship of event-related increase in hippocampal theta activity during wakefulness and the amount of fast ASS activity in subsequent sleep [89]. Theta oscillations are important for attentional shifts, top-down control of gamma oscillations, and consecutive memory formation [2, 90, 91]. Their correlation with ASS activity allows speculating about a participation of theta activity in the selection and tagging of meaningful memory traces [89]. In support of this, correlation of theta activity and subsequent increase in ASSs during SWS was also shown for theta oscillations occurring in REM sleep [92]. Similar to the

slow oscillations during SWS, theta activity might enable the information transfer between hippocampus and cortex either during performance of a task or during theta replay in REM sleep and prepare selected synapses for further consolidation in SWS episodes.

2.4. Adult Sleep Spindle Pathologies. Deeper understanding of ASS function could be achieved by the investigation of spindle-associated pathologic states. A wealth of studies documents the link between abnormal ASSs and disabilities in neurological disorders. For example, altered ASSs have been related to hypersynchronous activity between thalamus and cortex in different forms of epilepsy [93–95]. Moreover, the occurrence of ASSs is dramatically perturbed in neuropsychiatric disorders, such as schizophrenia or depression [96–98].

In young and adult schizophrenia patients a widespread reduction of ASS occurrence and power has been detected over centroparietal, prefrontal, and temporal areas of the cortex [99, 100]. The overall intelligence of patients is not affected [101], yet lower ASS occurrence correlates with abnormal memory consolidation and the severity of positive symptoms, in particular of auditory hallucinations [98, 101, 102]. The poorer memory consolidation in schizophrenia patients has been correlated with the reduced volume of the left mediodorsal thalamus, including the spindle pacemaker TRN [103–106].

Even if less consistent as for schizophrenia, changes in ASS activity have also been reported for patients with major depression [107]. High-risk individuals and age-matched early-onset depression patients showed reduced ASS density when compared to controls. This decrease was more pronounced in females [108]. With increasing age, the shortage of spindle activity is overcompensated, the ASSs being more frequent in adult female patients when compared to healthy controls [107, 108]. While it cannot be fully excluded that the developmental switch results from methodological differences between studies, it is highly likely that extensive remodeling of brain circuits or hormonal changes during adolescence account for the age-dependent transition from shortage to surge. Males showed milder alterations in ASSs.

The structural and functional substrates of abnormal ASS activity in disease are poorly understood. Brain connectivity in regions relevant for spindle generation and glutamate signaling is disturbed in schizophrenia patients [109–112]. Similarly, in a Disrupted-In-Schizophrenia 1 (DISC1) mouse model of mental illness ^{14}C2-DG imaging revealed pronounced hypometabolism in frontal and hippocampal regions as well as in the TRN. The observed abnormal functional communication between brain areas was accompanied by reduced glutamate release probability [113]. A model with transient interruption of DISC1 signaling showed a loss of plastic compensatory mechanisms. After whisker deprivation during early development, healthy mice usually react with a compensatory expansion of the whisker-corresponding domain into surrounding cortical barrels [114]. This structural modification was absent after transient DISC1 interruption. At adult age, these mice showed a complete absence of intercolumnar LTP and LTD [115]. The impairment of essential mechanisms for learning, like LTP and LTD, might prevent a proper encoding of new information during wakefulness and reduce ASS generation during sleep (see the previously discussed role of ASSs in memory formation). Moreover, studies in calcineurin knockout [116] and dominant-negative DISC1 [117] mouse models of schizophrenia showed a strong increase in power and occurrence of hippocampal sharp-wave ripples. This increase was accompanied by the loss of ripple replay function. Since ripple replay has been proposed as coordinator of cortical ASS activity [83], memory consolidation during SWS might be disturbed in these mice.

In summary, dysfunction of ASS activity seems to be a promising predictive marker for certain neurologic and neuropsychiatric conditions. Future investigations need to strengthen the link between abnormal patterns of activity and disease and unravel associated structural and functional modifications at cellular level. The knowledge gain of such studies will enable the development of therapeutic strategies aiming at improving the cognitive outcome of patients.

3. Neonatal Spindle Burst Oscillations

Oscillatory rhythms are not an exclusive hallmark of the adult brain but emerge already early in life. They have been characterized in EEG recordings from premature human infants [118, 119]. However, technical and ethical limitations precluded the elucidation of mechanisms underlying early oscillatory rhythms in humans. Since rodents are altricial and the stage of their brain development at birth corresponds to the second gestational trimester in humans, they represent an ideal animal model for the investigation of early patterns of activity [120, 121], which are highly reminiscent to those recorded in human preterm babies [13, 122, 123].

Early neuronal activity has a discontinuous structure with alternating periods of oscillatory discharges (2–30 s duration) and network silence [14, 15, 124, 125]. With ongoing maturation, the discontinuous activity is progressively replaced by adult-like continuous discharges. During neonatal development (i.e., first-second postnatal week) a large diversity of discontinuous oscillations have been described in the rodent cortex. The most common pattern is the NSBs [14, 124]. These oscillations have a duration of 1–3 s and a frequency of 7–10 Hz. They can be superimposed with faster beta/gamma activity and high frequency oscillations (HFOs) [126, 127] and are then classified as nested gamma spindle bursts (NGs). For visual areas, slow activity transients of <0.5 Hz, also known as delta waves, seem to coordinate NSBs [128], whereas long-oscillations (20–110 s duration) have been characterized in the primary somatosensory cortex [125]. Ca^{2+} imaging revealed similar activity patterns spreading along the posterior-anterior cortical axis [129, 130]. Brief periods of early gamma oscillations also occur independent of spindles in cortical [125], thalamic [131], and hippocampal networks [132]. Despite the diverse nomenclature, it is likely that the early network oscillations share similar mechanisms of generation.

Synchronization and coupling of neuronal networks in oscillatory rhythms early during development organize the communication of spatially distributed neuronal subsets. They increase the probability of cooccurring pre- and postsynaptic activity and by these means control synaptic plasticity. Each burst recruits a different set of synapses and enforces the potentiation of parallel activated neighboring synapses and dendritic clustering [133–135]. In the following we will focus on the most dominant pattern of discontinuous activity, the NSBs.

3.1. Generation and Origin of Neonatal Spindle Bursts in Sensory Systems. During the last 10–15 years substantial effort has been made to elucidate the mechanisms of NSB generation. Stimulation of the optical nerve, mechanical touch of the limbs, or whisker stimulation reliably triggered NSBs in primary sensory cortices [14, 15, 124]. Correspondingly, interruption of peripheral sensory inputs by brain stem lesion [124], pharmacological blockade [12], or removal of the retina [14] leads to a strong reduction in the occurrence of NSBs. These studies reveal the importance of the sensory periphery/external stimuli for the emergence of NSBs during development. They equally demonstrate that NSBs partially depend on the activity of intrinsic pacemakers [136].

In neonatal rodents an important region for the amplification and integration of information from the periphery turns out to be the subplate. Subplate cells originate in the ventricular and subventricular zone as well as the medial ganglionic eminence. At early developmental stage, they show adult neuronal characteristics with a heterogeneous morphology and neurotransmitter profile as well as dense connectivity [137, 138]. Subplate cells form a transiently expressed layer located between the intermediate zone and the cortical plate [139, 140]. They guide axons from subcortical structures, such as thalamus, to their appropriate targets in the developing neocortex and are ideally positioned to shape neocortical plasticity [141–143]. The early networks, which are organized by subplate neurons, are driven by thalamocortical projections and modulated by cholinergic afferents from the basal forebrain. By these means, spatially confined synchrony (e.g., barrels in the somatosensory cortex, ocular dominance columns in the visual cortex of higher mammals) is established [136, 144–146]. NSBs, which play an important role in this synchronization, emerge within the thalamocortical networks at neonatal age [124, 147]. Removal of subplate neurons in rats at postnatal days (P) 0-1 prevents the emergence of spontaneous and evoked NSBs in the somatosensory cortex at P7–10 together with a weakening of thalamocortical connectivity [16].

The relay of information from the periphery via thalamic nuclei and the subplate to specific areas of the cortex appears to follow a universal scheme and is similar for different sensory modalities. In the primary somatosensory cortex of P0-1 rats, whisker stimulation induced gamma activity in the ventral posteromedial nucleus of the thalamus (VPM) followed by shortly delayed NSBs [136]. Inactivation of the VPM with electrolytic lesion almost abolished NSBs [136]. For the visual system, Mooney and colleagues showed that spontaneous retinal activity elicits bursts in the lateral geniculate nucleus (LGN) of the thalamus. Burst activity in the LGN was suppressed after pharmacological blockade or cut of the optic nerve [148]. In addition, blocking action potential propagation in the optic nerve by TTX injection led to a twofold decrease of the NSB occurrence in the visual cortex [14]. In the auditory system, inner hair cells in the cochlea of neonatal rats (P7) generate discrete bursts of action potentials that propagate along central auditory pathways already before hearing onset [149, 150]. This activity was shown to be crucial for the establishment of precise tonotopy in auditory nuclei, for example, lateral superior olive [151]. Although a clear link of these bursts to activity in higher structures of the auditory pathway is missing, it has been demonstrated that subplate neurons receive input from the medial geniculate nucleus of the auditory thalamic nucleus from P2 on. These subplate cells provide excitatory input to layer IV neurons in the auditory cortex [152]. With the medial geniculate nucleus lying upstream of the lateral superior olive, it is likely that the transfer of information in the auditory system during early development follows similar principles as for visual and somatosensory systems. Altogether, these findings suggest the importance of peripheral input and corticothalamic connectivity for the generation of NSBs in various sensory networks.

Another interesting aspect in the generation of NSBs is their early dependence on neuromodulatory inputs. For example, the cholinergic drive from the basal forebrain profoundly influences the NSB activity at neonatal age. While electrical stimulation of the basal forebrain increases the incidence of NSBs, selective immunotoxic lesion of its cholinergic neurons with antibody-conjugated saporin and pharmacological blockade of cortical muscarinic acetylcholine receptors lead to substantial reduction of NSB occurrence [153]. In contrast, blockade of acetylcholine esterase promoted NSB generation. These data support a facilitating action of the cholinergic system on NSBs. One possible substrate of this function is the cholinergic action on subplate neurons. Ca^{2+} transients induced by muscarine application show high synchronicity in the subplate region, while transients in the cortical plate appear less frequent and more random [143].

NSBs in the sensory cortices are significantly modulated by interhemispheric communication. After callosotomy at P1–6, the presence of spontaneous NSBs in both hemispheres is doubled, indicating that projections via the corpus callosum inhibit developmental activity patterns during the first postnatal week [154]. In contrast, callosotomy at P7–15 does not alter the rate of spontaneous NSBs [155]. Moreover, callosotomy reduced the occurrence of NSBs evoked by forepaw stimulation in the somatosensory cortex during defined developmental periods (i.e., P1–6). It can be hypothesized that a period critical for spindle related plasticity spans the time from birth to P7. Remarkably, this developmental period coincides with an increase of GABAergic and glutamatergic presynaptic terminals in the deeper layers of the somatosensory cortex [155].

The mechanisms generating early network oscillations vary during the course of development [156]. *In vivo* investigations have shown that glutamatergic inputs are critical

for the emergence of NSBs [15, 16, 157, 158]. The slow delta components of NSBs are reliant on both NMDA and AMPA receptors whereas the faster spindle component mainly depends on AMPA receptors [158]. Pharmacological blockade of AMPA receptors using CNQX completely and reversibly blocked the occurrence of spontaneous spindle bursts in S1 indicating the importance of the glutamatergic inputs for the generation of NSBs [15]. As previously mentioned ablation of subplate neurons weakens the thalamocortical connectivity and reduces the occurrence of NSBs suggesting that the glutamatergic inputs important for NSBs are of thalamic origin [16]. Knockout of the NR1 NMDA receptor subunit in the ventrobasal thalamic nucleus resulted in miswiring of the barrel cortex and behavioral deficits supporting a contribution of NMDA receptors to STDP already during early development [157]. Additionally, electrical communication through gap junctions contributes to the generation of NSBs. Inhibition of gap junctions was followed by reduction or abolishment of spindle oscillations both *in vitro* [159] and *in vivo* [125]. These data indicate that an early gap junction syncytium acts as template for later cortical topography [160] and represents an efficient mechanism of communication at a developmental time point of synaptic immaturity [161, 162]. However, due to the side-effects of many gap junction blockers, the contribution of electrical communication to early spindle activity remains a matter of debate and findings are sometimes contradictory. For example, *in vivo* blockade of gap junctions at P1–P3 has been shown to cause an increase in the occurrence of spindle bursts [15].

The generation of NSBs is additionally influenced by GABAergic neurotransmission. During the embryonic stage and the first postnatal week an increased chloride accumulation/extrusion ratio due to high NKCC1 activity and low KCC2 expression causes a depolarizing action of GABA in immature neurons [163, 164]. Early depolarizing GABAergic activity is linked to critical period plasticity in the visual cortex [165]. Interference with early depolarizing $GABA_A$ receptor signaling was shown to persistently reduce the formation of AMPA receptors. Furthermore, the tight interaction of $GABA_A$ and NMDA receptors controls the activation of silent synapses [166]. Blockade of NKCC1 was shown to cause a negative shift in the $GABA_A$ reversal potential but did not affect the occurrence and properties of NSBs [15]. However, $GABA_A$ receptor-mediated depolarization has been recently shown to exert an inhibitory control on network activity *in vivo* [167]. Such early GABAergic inhibition is in line with enhanced NSB activity after GABA receptor blockade, reduced activity after positive modulation of $GABA_A$ receptors [15], and the confinement of early network oscillations by GABAergic surround inhibition [15, 168, 169]. The precise actions of GABA may not only depend on the maturation level of an individual neuron but also on the timing of GABAergic and glutamatergic inputs. Recently, it was shown *in vitro* for adult born neurons in the hippocampus that weak GABAergic input is beneficial for neuronal excitation and strong GABAergic input leads to shunting inhibition [170]. Such a mechanism would contribute to the spatial confinement of NSBs in local cortical networks. Around P12 an increase in KCC2 expression and reduction in NKCC1 activity in cortical neurons shifts the GABAergic transmission to the "classical" hyperpolarizing function [171]. Of note, this switch does not occur at the same time point in the entire cortex, but rather depends on the maturation timeline of individual cortical areas. Even within the same area, the hyperpolarizing action of GABA starts in more mature deeper cortical layers before it reaches the upper cortical layers [172]. However, in general, this time point coincides with the disappearance of NSBs during the end of the second postnatal week. NSBs are gradually replaced by adult-like ongoing oscillations within different frequency bands related to behavioral states. Early GABAergic transmission is also relevant to shape emerging cortical networks. During the first postnatal week layer 5/6 somatostatin interneurons receive transient innervation from the thalamus. This innervation supports the development of parvalbumin interneuron driven perisomatic inhibition of pyramidal neurons, which is crucial for the generation of fast rhythmic activity in the adult cortex [173]. The role of NSBs for the development of this network needs further investigation.

3.2. Generation and Origin of Neonatal Spindle Bursts in Limbic Systems. NSBs are not restricted to sensory cortical areas but also synchronize limbic structures [126, 174]. In line with the developmental delay of the prefrontal cortex (PFC) compared to the sensory areas, NSBs are absent at birth and firstly detected in the PFC at P3 [14, 126]. With ongoing maturation, the power of NSBs augments. In the cingulate subdivision of the medial PFC, NSBs contain little or no gamma activity. In contrast, frequent NGs have been detected in the prelimbic subdivision (PL) of the PFC [126]. NSBs synchronize the activity within prefrontal layers, whereas the faster gamma components of NGs synchronize the coupling between different layers [127]. The distinct activity patterns in prefrontal subdivisions might reflect an adapted maturation in regard to their later functionality.

Similar to the importance of thalamocortical networks for the generation of NSBs in sensory areas, the hippocampal-prefrontal networks appear to be mandatory for the emergence of limbic NSBs. The drive and temporal coordination within these networks is provided by theta oscillations from the hippocampal CA1 area. These are relayed to pyramidal neurons of layer V in the PFC via glutamatergic projections, which in turn trigger local beta/gamma activity in cortical networks [126, 175, 176]. Excitotoxic lesion of the hippocampus led to substantial diminishment of prelimbic oscillatory activity [126]. First correlative evidence suggests that the coherent activity within neonatal prefrontal-hippocampal networks is critical for juvenile cognitive abilities, such as recognition memory [177].

Similar to oscillatory patterns in sensory cortices, NSBs in limbic areas depend on cholinergic modulation. Cholinergic projections from the basal forebrain selectively target interneurons in the neonatal PL [174]. Neurotoxic lesion of cholinergic nuclei in the basal forebrain profoundly affected the activity within prefrontal-hippocampal networks by increasing the occurrence of hippocampal theta oscillations

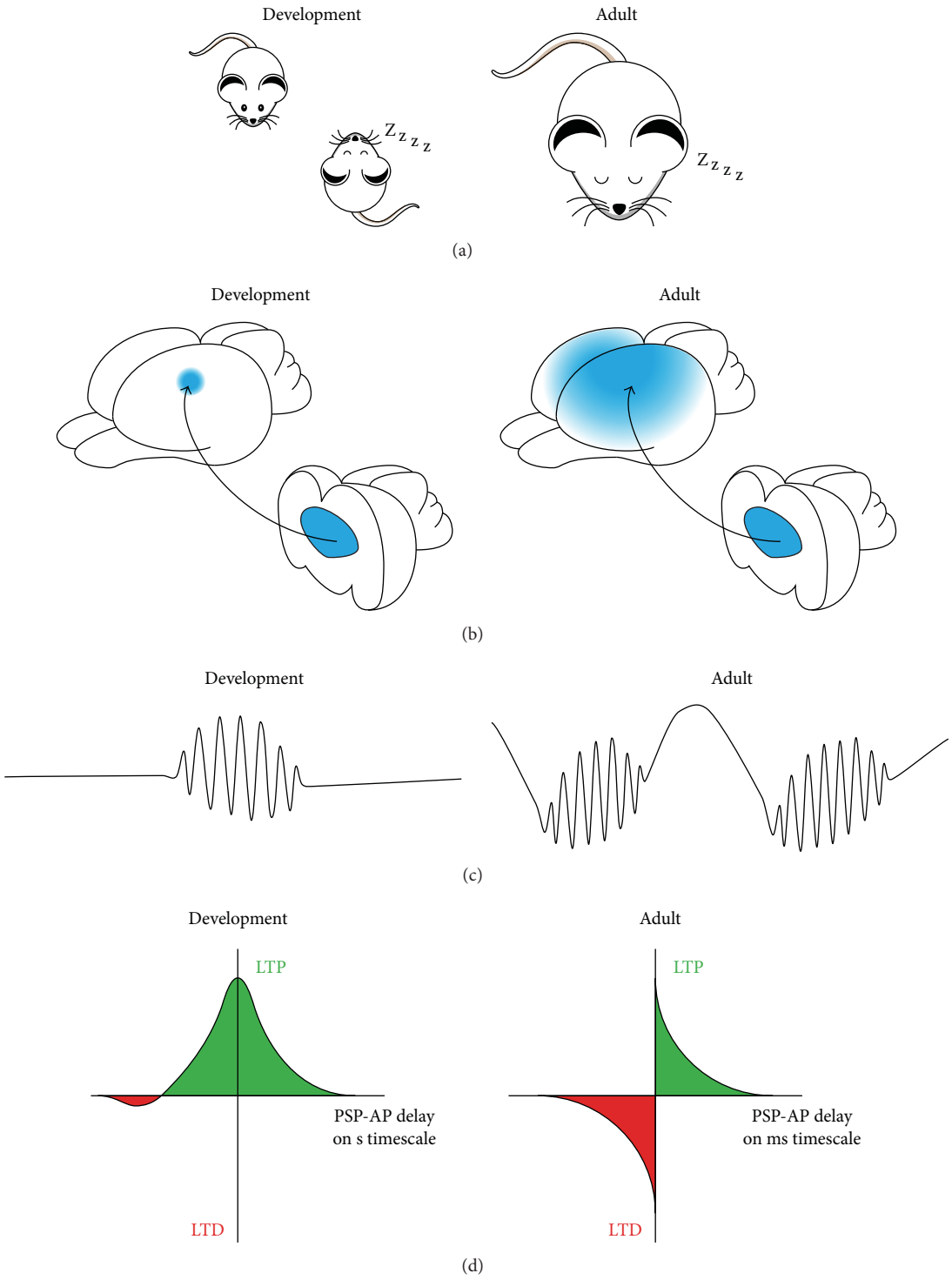

Figure 1: Spindle activity in development and adult sleep. (a) NSBs occur independent of the behavioral state (left), whereas ASSs are confined to SWS (right). (b) Thalamocortical activity locally synchronizes the developing networks (left), whereas ASSs entrain large cortical areas (right). (c) NSBs represent discontinuous patterns of oscillatory activity during early development (left). ASSs are embedded in slow oscillations (right). (d) Synchronized activity during development leads to synaptic potentiation (left). Precise timing of synaptic inputs and action potentials controls synaptic potentiation and depression in mature brains (right).

and the NSB amplitude in the PFC [174]. Thus, NSBs in sensory and limbic cortices share similar properties and mechanisms of generation. While an external drive (e.g., activation of sensory periphery, hippocampus) is mandatory, NSBs additionally emerge from the activation of local circuits and are strongly modulated by subcortical inputs.

4. Comparison of Adult Sleep Spindles and Neonatal Spindle Bursts

Transient bursts of network oscillations are present in cortical networks during early development and at adulthood. They are generated, at least in part, within thalamocortical and hippocampocortical circuits. Several features distinguish NSBs and ASSs (Figure 1). First, NSBs are not restricted to sleep but occur during all behavioral states [124]. Second, NSBs synchronize relatively small cortical patches [124, 125], whereas ASSs spread over large cortical areas. Third, NSBs occur spontaneously at irregular intervals [12, 14, 124], whereas ASSs are generated more regularly.

While synaptic plasticity is present in the brain throughout the whole lifespan, mechanistic differences were described for the developing and the adult brain. In general, synaptic potentiation is more prominent during development and gradually changes towards a balanced potentiation and depression in the mature brain. This phenomenon is probably related to a switch in the mechanisms that mediate LTP. Before P10 the induction of LTP in the rodent hippocampus was shown to be PKA and GluR4-dependent [178–180] and could be induced by random neuronal activity [181]. From P12 on LTP was driven by activation of CaMKII and GluR1 and plasticity started to follow precise STDP rules, including LTD [182, 183]. In the barrel cortex the mechanisms mediating LTP are similar, yet the switch from PKA and GluR4 dependence to CaMKII and GluR1 dependence occurs at P13 [184, 185]. A bias towards potentiation based on the timing of bursts over a second-long time window was also described in the immature thalamus [186].

The switch in plasticity mechanisms is further reflected by the massive increase in the number of synapses and connections during the early postnatal period. During the third postnatal week synaptic pruning causes profound network refinement [187–189]. In other words, a rough connectivity scheme at early development is established long before the emergence of precise topographic maps. Consequently, the occurring plastic processes are constantly modulated by changes in molecular expression and ongoing network activity. While neonatal and adult spindle oscillations demonstrate similarities in shape, frequency distribution, and origin, they are faced with different plasticity conditions and therefore differentially modulate brain circuits.

The knowledge on the role of spindle activity during early development and at adulthood is still sparse. It is accepted that early network oscillations promote the maturation of cortical structure and function, yet reliable causal evidence is still missing. Repetitive coactivation of specific networks during NSBs would create optimal conditions to strengthen and refine synaptic connections [134, 185, 186]. ASSs are implicated in memory consolidation and homeostatic scaling of synaptic strengths. They may coordinate the communication of specific networks in faster frequencies to orchestrate the interplay of synaptic depression and potentiation dependent on the timing of pre- and postsynaptic activity on a millisecond timescale. Thus, NSBs may provide time windows of synchronous activity necessary for the refinement of circuitry, whereas ASSs may help to adapt the mature network to integrate recently acquired information.

5. Conclusions and Perspectives

ASSs and NSBs represent distinct patterns of network synchronization in the adult and developing brain. While ASSs support memory consolidation through synchronous activation of large cortical areas, NSBs coordinate the maturation of local neocortical networks. Both patterns coordinate activity in sensory and limbic systems and modulate local plasticity critical for network refinement. Causal links from specific cellular mechanisms to oscillatory activity need to be established. Knowledge about NSB-related plasticity, especially, is still sparse. Further studies need to elucidate to what extent disturbed NSB activity during cortical maturation affects the pathological changes observed for ASSs, for example, in schizophrenia and depression. This would allow developing new therapeutic approaches to prevent manifestation of neurodevelopmental diseases.

Competing Interests

The authors declare that there is no conflict of interests regarding the publication of this paper.

References

[1] G. Buzsáki and A. Draguhn, "Neuronal oscillations in cortical networks," *Science*, vol. 304, no. 5679, pp. 1926–1929, 2004.

[2] P. Fries, "Rhythms for cognition: communication through coherence," *Neuron*, vol. 88, no. 1, pp. 220–235, 2015.

[3] Y. Dudai, A. Karni, and J. Born, "The consolidation and transformation of memory," *Neuron*, vol. 88, no. 1, pp. 20–32, 2015.

[4] B. Rasch and J. Born, "About sleep's role in memory," *Physiological Reviews*, vol. 93, no. 2, pp. 681–766, 2013.

[5] G. Tononi and C. Cirelli, "Sleep and the price of plasticity: from synaptic and cellular homeostasis to memory consolidation and integration," *Neuron*, vol. 81, no. 1, pp. 12–34, 2014.

[6] P. Andersen and S. A. Andersson, *Physiological Basis of the Alpha Rhythm*, Plenum Publishing Corporation, 1968.

[7] H. Berger, "Das Elektrenkephalogramm des Menschen und seine Deutung," *Naturwissenschaften*, vol. 25, no. 13, pp. 193–196, 1937.

[8] E. Dempsey and R. Morison, "The electrical activity of a thalamocortical relay system," *American Journal of Physiology—Legacy Content*, vol. 138, pp. 283–296, 1943.

[9] S. Vanhatalo and K. Kaila, "Development of neonatal EEG activity: from phenomenology to physiology," *Seminars in Fetal and Neonatal Medicine*, vol. 11, no. 6, pp. 471–478, 2006.

[10] M.-F. Vecchierini, A.-M. d'Allest, and P. Verpillat, "EEG patterns in 10 extreme premature neonates with normal neurological outcome: qualitative and quantitative data," *Brain and Development*, vol. 25, no. 5, pp. 330–337, 2003.

[11] S. Astori, R. D. Wimmer, and A. Lüthi, "Manipulating sleep spindles—expanding views on sleep, memory, and disease," *Trends in Neurosciences*, vol. 36, no. 12, pp. 738–748, 2013.

[12] S. An, W. Kilb, and H. J. Luhmann, "Sensory-evoked and spontaneous gamma and spindle bursts in neonatal rat motor cortex," *The Journal of Neuroscience*, vol. 34, no. 33, pp. 10870–10883, 2014.

[13] I. L. Hanganu-Opatz, "Between molecules and experience: role of early patterns of coordinated activity for the development of cortical maps and sensory abilities," *Brain Research Reviews*, vol. 64, no. 1, pp. 160–176, 2010.

[14] I. L. Hanganu, Y. Ben-Ari, and R. Khazipov, "Retinal waves trigger spindle bursts in the neonatal rat visual cortex," *The Journal of Neuroscience*, vol. 26, no. 25, pp. 6728–6736, 2006.

[15] M. Minlebaev, Y. Ben-Ari, and R. Khazipov, "Network mechanisms of spindle-burst oscillations in the neonatal rat barrel cortex in vivo," *Journal of Neurophysiology*, vol. 97, no. 1, pp. 692–700, 2007.

[16] E. A. Tolner, A. Sheikh, A. Y. Yukin, K. Kaila, and P. O. Kanold, "Subplate neurons promote spindle bursts and thalamocortical patterning in the neonatal rat somatosensory cortex," *Journal of Neuroscience*, vol. 32, no. 2, pp. 692–702, 2012.

[17] W. R. Jankel and E. Niedermeyer, "Sleep spindles," *Journal of Clinical Neurophysiology*, vol. 2, no. 1, pp. 1–35, 1985.

[18] P. Y. Ktonas and E.-C. Ventouras, "Automated detection of sleep spindles in the scalp eeg and estimation of their intracranial current sources: comments on techniques and on related experimental and clinical studies," *Frontiers in Human Neuroscience*, vol. 8, article 998, 2014.

[19] Y. Zerouali, J.-M. Lina, Z. Sekerovic et al., "A time-frequency analysis of the dynamics of cortical networks of sleep spindles from MEG-EEG recordings," *Frontiers in Neuroscience*, vol. 8, article 310, 2014.

[20] D. Kim, E. Hwang, M. Lee, H. Sung, and J. H. Choi, "Characterization of topographically specific sleep spindles in mice," *Sleep*, vol. 38, no. 1, pp. 85–96, 2015.

[21] N. Martin, M. Lafortune, J. Godbout et al., "Topography of age-related changes in sleep spindles," *Neurobiology of Aging*, vol. 34, no. 2, pp. 468–476, 2013.

[22] M. Mölle, T. O. Bergmann, L. Marshall, and J. Born, "Fast and slow spindles during the sleep slow oscillation: disparate coalescence and engagement in memory processing," *Sleep*, vol. 34, no. 10, pp. 1411–1421, 2011.

[23] E. Werth, P. Achermann, D.-J. Dijk, and A. A. Borbély, "Spindle frequency activity in the sleep EEG: individual differences and topographic distribution," *Electroencephalography and Clinical Neurophysiology*, vol. 103, no. 5, pp. 535–542, 1997.

[24] A. Ayoub, D. Aumann, A. Hörschelmann et al., "Differential effects on fast and slow spindle activity, and the sleep slow oscillation in humans with carbamazepine and flunarizine to antagonize voltage-dependent Na^+ and Ca^{2+} channel activity," *Sleep*, vol. 36, no. 6, pp. 905–911, 2013.

[25] N. Dehghani, S. S. Cash, and E. Halgren, "Topographical frequency dynamics within EEG and MEG sleep spindles," *Clinical Neurophysiology*, vol. 122, no. 2, pp. 229–235, 2011.

[26] F. A. Gibbs and E. L. Gibbs, *Atlas of Electroencephalography*, vol. 1, Addison-Wesley, Reading, Mass, USA, 1950.

[27] I. Timofeev and S. Chauvette, "The spindles: are they still thalamic?" *Sleep*, vol. 36, no. 6, pp. 825–826, 2013.

[28] N. Dehghani, S. S. Cash, A. O. Rossetti, C. C. Chen, and E. Halgren, "Magnetoencephalography demonstrates multiple asynchronous generators during human sleep spindles," *Journal of Neurophysiology*, vol. 104, no. 1, pp. 179–188, 2010.

[29] V. Gumenyuk, T. Roth, J. E. Moran et al., "Cortical locations of maximal spindle activity: magnetoencephalography (MEG) study," *Journal of Sleep Research*, vol. 18, no. 2, pp. 245–253, 2009.

[30] Y. Urakami, "Relationships between sleep spindles and activities of cerebral cortex as determined by simultaneous EEG and MEG recording," *Journal of Clinical Neurophysiology*, vol. 25, no. 1, pp. 13–24, 2008.

[31] M. Steriade, L. Domich, G. Oakson, and M. Deschênes, "The deafferented reticular thalamic nucleus generates spindle rhythmicity," *Journal of Neurophysiology*, vol. 57, no. 1, pp. 260–273, 1987.

[32] A. Lüthi, "Sleep spindles: where they come from, what they do," *Neuroscientist*, vol. 20, no. 3, pp. 243–256, 2014.

[33] D. A. McCormick and H.-C. Pape, "Properties of a hyperpolarization-activated cation current and its role in rhythmic oscillation in thalamic relay neurones," *The Journal of Physiology*, vol. 431, pp. 291–318, 1990.

[34] P. Coulon, T. Budde, and H.-C. Pape, "The sleep relay—the role of the thalamus in central and decentral sleep regulation," *Pflügers Archiv*, vol. 463, no. 1, pp. 53–71, 2012.

[35] S. R. Crandall, G. Govindaiah, and C. L. Cox, "Low-threshold Ca^{2+} current amplifies distal dendritic signaling in thalamic reticular neurons," *Journal of Neuroscience*, vol. 30, no. 46, pp. 15419–15429, 2010.

[36] A. Destexhe, D. Contreras, M. Steriade, T. J. Sejnowski, and J. R. Huguenard, "In vivo, in vitro, and computational analysis of dendritic calcium currents in thalamic reticular neurons," *Journal of Neuroscience*, vol. 16, no. 1, pp. 169–185, 1996.

[37] A. Destexhe, M. Neubig, D. Ulrich, and J. Huguenard, "Dendritic low-threshold calcium currents in thalamic relay cells," *Journal of Neuroscience*, vol. 18, no. 10, pp. 3574–3588, 1998.

[38] F. Espinosa, M. A. Torres-Vega, G. A. Marks, and R. H. Joho, "Ablation of Kv3.1 and Kv3.3 potassium channels disrupts thalamocortical oscillations in vitro and in vivo," *The Journal of Neuroscience*, vol. 28, no. 21, pp. 5570–5581, 2008.

[39] J. R. Huguenard, "Low-threshold calcium currents in central nervous system neurons," *Annual Review of Physiology*, vol. 58, pp. 329–348, 1996.

[40] M. E. Scheibel and A. B. Scheibel, "The organization of the nucleus reticularis thalami: a Golgi study," *Brain Research*, vol. 1, no. 1, pp. 43–62, 1966.

[41] M. Steriade, D. A. McCormick, and T. J. Sejnowski, "Thalamocortical oscillations in the sleeping and aroused brain," *Science*, vol. 262, no. 5134, pp. 679–685, 1993.

[42] D. Ulrich and J. R. Huguenard, "$GABA_A$-receptor-mediated rebound burst firing and burst shunting in thalamus," *Journal of Neurophysiology*, vol. 78, no. 3, pp. 1748–1751, 1997.

[43] J. S. Haas, B. Zavala, and C. E. Landisman, "Activity-dependent long-term depression of electrical synapses," *Science*, vol. 334, no. 6054, pp. 389–393, 2011.

[44] C. E. Landisman, M. A. Long, M. Beierlein, M. R. Deans, D. L. Paul, and B. W. Connors, "Electrical synapses in the thalamic reticular nucleus," *The Journal of Neuroscience*, vol. 22, no. 3, pp. 1002–1009, 2002.

[45] Z. Molnár and C. Blakemore, "Lack of regional specificity for connections formed between thalamus and cortex in coculture," *Nature*, vol. 351, no. 6326, pp. 475–477, 1991.

[46] S. M. Sherman and R. W. Guillery, "Functional organization of thalamocortical relays," *Journal of Neurophysiology*, vol. 76, no. 3, pp. 1367–1395, 1996.

[47] N. Yamamoto, T. Kurotani, and K. Toyama, "Neural connections between the lateral geniculate nucleus and visual cortex in vitro," *Science*, vol. 245, no. 4914, pp. 192–194, 1989.

[48] D. Contreras and M. Steriade, "Spindle oscillation in cats: the role of corticothalamic feedback in a thalamically generated rhythm," *The Journal of Physiology*, vol. 490, part 1, pp. 159–179, 1996.

[49] D. Contreras, A. Destexhe, T. J. Sejnowski, and M. Steriade, "Control of spatiotemporal coherence of a thalamic oscillation by corticothalamic feedback," *Science*, vol. 274, no. 5288, pp. 771–774, 1996.

[50] A. Destexhe, D. Contreras, and M. Steriade, "Cortically-induced coherence of a thalamic-generated oscillation," *Neuroscience*, vol. 92, no. 2, pp. 427–443, 1999.

[51] P. Coulon, D. Herr, T. Kanyshkova, P. Meuth, T. Budde, and H.-C. Pape, "Burst discharges in neurons of the thalamic reticular nucleus are shaped by calcium-induced calcium release," *Cell Calcium*, vol. 46, no. 5-6, pp. 333–346, 2009.

[52] A. Lüthi and D. A. McCormick, "Ca^{2+}-mediated up-regulation of I_h in the thalamus: how cell-intrinsic ionic currents may shape network activity," *Annals of the New York Academy of Sciences*, vol. 868, pp. 765–769, 1999.

[53] A. Lüthi and D. A. McCormick, "b. Modulation of a pacemaker current through Ca^{2+}-induced stimulation of cAMP production," *Nature Neuroscience*, vol. 2, pp. 634–641, 1999.

[54] M. Bonjean, T. Baker, M. Lemieux, I. Timofeev, T. Sejnowski, and M. Bazhenov, "Corticothalamic feedback controls sleep spindle duration in vivo," *Journal of Neuroscience*, vol. 31, no. 25, pp. 9124–9134, 2011.

[55] S. J. Aton, J. Seibt, M. Dumoulin et al., "Mechanisms of sleep-dependent consolidation of cortical plasticity," *Neuron*, vol. 61, no. 3, pp. 454–466, 2009.

[56] S. Chauvette, J. Seigneur, and I. Timofeev, "Sleep oscillations in the thalamocortical system induce long-term neuronal plasticity," *Neuron*, vol. 75, no. 6, pp. 1105–1113, 2012.

[57] S.-J. R. Lee, Y. Escobedo-Lozoya, E. M. Szatmari, and R. Yasuda, "Activation of CaMKII in single dendritic spines during long-term potentiation," *Nature*, vol. 458, no. 7236, pp. 299–304, 2009.

[58] M. Mayford, M. E. Bach, Y.-Y. Huang, L. Wang, R. D. Hawkins, and E. R. Kandel, "Control of memory formation through regulated expression of a CaMKII transgene," *Science*, vol. 274, no. 5293, pp. 1678–1683, 1996.

[59] J. Lisman, R. Yasuda, and S. Raghavachari, "Mechanisms of CaMKII action in long-term potentiation," *Nature Reviews Neuroscience*, vol. 13, no. 3, pp. 169–182, 2012.

[60] W. Blanco, C. M. Pereira, V. R. Cota et al., "Synaptic homeostasis and restructuring across the sleep-wake cycle," *PLoS Computational Biology*, vol. 11, no. 5, Article ID e1004241, 2015.

[61] R. J. Cormier, A. C. Greenwood, and J. A. Connor, "Bidirectional synaptic plasticity correlated with the magnitude of dendritic calcium transients above a threshold," *Journal of Neurophysiology*, vol. 85, no. 1, pp. 399–406, 2001.

[62] J. C. Magee and D. Johnston, "A synaptically controlled, associative signal for Hebbian plasticity in hippocampal neurons," *Science*, vol. 275, no. 5297, pp. 209–213, 1997.

[63] B. L. Sabatini and K. Svoboda, "Analysis of calcium channels in single spines using optical fluctuation analysis," *Nature*, vol. 408, no. 6812, pp. 589–593, 2000.

[64] D. A. Hoffman, J. C. Magee, C. M. Colbert, and D. Johnston, "K^+ channel regulation of signal propagation in dendrites of hippocampal pyramidal neurons," *Nature*, vol. 387, no. 6636, pp. 869–875, 1997.

[65] H. J. Koester and B. Sakmann, "Calcium dynamics in single spines during coincident pre- and postsynaptic activity depend on relative timing of back-propagating action potentials and subthreshold excitatory postsynaptic potentials," *Proceedings of the National Academy of Sciences of the United States of America*, vol. 95, no. 16, pp. 9596–9601, 1998.

[66] H. Markram, J. Lübke, M. Frotscher, and B. Sakmann, "Regulation of synaptic efficacy by coincidence of postsynaptic APs and EPSPs," *Science*, vol. 275, no. 5297, pp. 213–215, 1997.

[67] M. Rosanova and D. Ulrich, "Pattern-specific associative long-term potentiation induced by a sleep spindle-related spike train," *Journal of Neuroscience*, vol. 25, no. 41, pp. 9398–9405, 2005.

[68] K. Hoedlmoser, D. P. J. Heib, J. Roell et al., "Slow sleep spindle activity, declarative memory, and general cognitive abilities in children," *Sleep*, vol. 37, no. 9, pp. 1501–1512, 2014.

[69] M. Schabus, G. Gruber, S. Parapatics et al., "Sleep spindles and their significance for declarative memory consolidation," *Sleep*, vol. 27, no. 8, pp. 1479–1485, 2004.

[70] A. Morin, J. Doyon, V. Dostie et al., "Motor sequence learning increases sleep spindles and fast frequencies in post-training sleep," *Sleep*, vol. 31, no. 8, pp. 1149–1156, 2008.

[71] S. A. Cairney, S. J. Durrant, J. Hulleman, and P. A. Lewis, "Targeted memory reactivation during slow wave sleep facilitates emotional memory consolidation," *Sleep*, vol. 37, no. 4, pp. 701–707, 2014.

[72] S. Gais, M. Mölle, K. Helms, and J. Born, "Learning-dependent increases in sleep spindle density," *The Journal of Neuroscience*, vol. 22, no. 15, pp. 6830–6834, 2002.

[73] M. Mölle, O. Eschenko, S. Gais, S. J. Sara, and J. Born, "The influence of learning on sleep slow oscillations and associated spindles and ripples in humans and rats," *European Journal of Neuroscience*, vol. 29, no. 5, pp. 1071–1081, 2009.

[74] S. Diekelmann and J. Born, "The memory function of sleep," *Nature Reviews Neuroscience*, vol. 11, no. 2, pp. 114–126, 2010.

[75] A. Destexhe, S. W. Hughes, M. Rudolph, and V. Crunelli, "Are corticothalamic 'up' states fragments of wakefulness?" *Trends in Neurosciences*, vol. 30, no. 7, pp. 334–342, 2007.

[76] A. Sirota and G. Buzsáki, "Interaction between neocortical and hippocampal networks via slow oscillations," *Thalamus and Related Systems*, vol. 3, no. 4, pp. 245–259, 2005.

[77] G. Yang, C. S. W. Lai, J. Cichon, L. Ma, W. Li, and W.-B. Gan, "Sleep promotes branch-specific formation of dendritic spines after learning," *Science*, vol. 344, no. 6188, pp. 1173–1178, 2014.

[78] P. W. Frankland and B. Bontempi, "The organization of recent and remote memories," *Nature Reviews Neuroscience*, vol. 6, no. 2, pp. 119–130, 2005.

[79] A. Peyrache, M. Khamassi, K. Benchenane, S. I. Wiener, and F. P. Battaglia, "Replay of rule-learning related neural patterns in the prefrontal cortex during sleep," *Nature Neuroscience*, vol. 12, no. 7, pp. 919–926, 2009.

[80] A. G. Siapas and M. A. Wilson, "Coordinated interactions between hippocampal ripples and cortical spindles during slow-wave sleep," *Neuron*, vol. 21, no. 5, pp. 1123–1128, 1998.

[81] Z. Clemens, M. Mölle, L. Eross et al., "Fine-tuned coupling between human parahippocampal ripples and sleep spindles," *European Journal of Neuroscience*, vol. 33, no. 3, pp. 511–520, 2011.

[82] A. Sirota, J. Csicsvari, D. Buhl, and G. Buzsáki, "Communication between neocortex and hippocampus during sleep in rodents," *Proceedings of the National Academy of Sciences of the United States of America*, vol. 100, no. 4, pp. 2065–2069, 2003.

[83] B. P. Staresina, T. O. Bergmann, M. Bonnefond et al., "Hierarchical nesting of slow oscillations, spindles and ripples in the human hippocampus during sleep," *Nature Neuroscience*, vol. 18, no. 11, pp. 1679–1686, 2015.

[84] A. Kostin, D. Stenberg, and T. Porkka-Heiskanen, "Effect of sleep deprivation on multi-unit discharge activity of basal forebrain," *Journal of Sleep Research*, vol. 19, no. 2, pp. 269–279, 2010.

[85] V. V. Vyazovskiy, U. Olcese, Y. M. Lazimy et al., "Cortical firing and sleep homeostasis," *Neuron*, vol. 63, no. 6, pp. 865–878, 2009.

[86] M. B. Dash, C. L. Douglas, V. V. Vyazovskiy, C. Cirelli, and G. Tononi, "Long-term homeostasis of extracellular glutamate in the rat cerebral cortex across sleep and waking states," *The Journal of Neuroscience*, vol. 29, no. 3, pp. 620–629, 2009.

[87] A. Hashmi, A. Nere, and G. Tononi, "Sleep-dependent synaptic down-selection (II): single-neuron level benefits for matching, selectivity, and specificity," *Frontiers in Neurology*, vol. 4, article 148, 2013.

[88] C. M. Werk, H. S. Klein, C. E. Nesbitt, and C. A. Chapman, "Long-term depression in the sensorimotor cortex induced by repeated delivery of 10 Hz trains in vivo," *Neuroscience*, vol. 140, no. 1, pp. 13–20, 2006.

[89] D. P. J. Heib, K. Hoedlmoser, P. Anderer, G. Gruber, J. Zeitlhofer, and M. Schabus, "Oscillatory theta activity during memory formation and its impact on overnight consolidation: a missing link?" *Journal of Cognitive Neuroscience*, vol. 27, no. 8, pp. 1648–1658, 2015.

[90] A. Gazzaley and A. C. Nobre, "Top-down modulation: bridging selective attention and working memory," *Trends in Cognitive Sciences*, vol. 16, no. 2, pp. 129–135, 2012.

[91] K. M. Igarashi, "Plasticity in oscillatory coupling between hippocampus and cortex," *Current Opinion in Neurobiology*, vol. 35, pp. 163–168, 2015.

[92] S. M. Fogel, C. T. Smith, and R. J. Beninger, "Evidence for 2-stage models of sleep and memory: learning-dependent changes in spindles and theta in rats," *Brain Research Bulletin*, vol. 79, no. 6, pp. 445–451, 2009.

[93] J. T. Paz, A. S. Bryant, K. Peng et al., "A new mode of corticothalamic transmission revealed in the *Gria4*$^{-/-}$ model of absence epilepsy," *Nature Neuroscience*, vol. 14, no. 9, pp. 1167–1175, 2011.

[94] J. T. Paz and J. R. Huguenard, "Microcircuits and their interactions in epilepsy: is the focus out of focus?" *Nature Neuroscience*, vol. 18, no. 3, pp. 351–359, 2015.

[95] M. Steriade, "Sleep, epilepsy and thalamic reticular inhibitory neurons," *Trends in Neurosciences*, vol. 28, no. 6, pp. 317–324, 2005.

[96] F. Ferrarelli and G. Tononi, "The thalamic reticular nucleus and schizophrenia," *Schizophrenia Bulletin*, vol. 37, no. 2, pp. 306–315, 2011.

[97] V. Latreille, J. Carrier, M. Lafortune et al., "Sleep spindles in Parkinson's disease may predict the development of dementia," *Neurobiology of Aging*, vol. 36, no. 2, pp. 1083–1090, 2015.

[98] Z. Vukadinovic, "Sleep abnormalities in schizophrenia may suggest impaired trans-thalamic cortico-cortical communication: towards a dynamic model of the illness," *European Journal of Neuroscience*, vol. 34, no. 7, pp. 1031–1039, 2011.

[99] N. Tesler, M. Gerstenberg, M. Franscini, O. G. Jenni, S. Walitza, and R. Huber, "Reduced sleep spindle density in early onset schizophrenia: a preliminary finding," *Schizophrenia Research*, vol. 166, no. 1–3, pp. 355–357, 2015.

[100] Z. Vukadinovic, "Sleep spindle reductions in schizophrenia and its implications for the development of cortical body map," *Schizophrenia Research*, vol. 168, no. 1-2, pp. 589–590, 2015.

[101] F. Ferrarelli, M. J. Peterson, S. Sarasso et al., "Thalamic dysfunction in schizophrenia suggested by whole-night deficits in slow and fast spindles," *American Journal of Psychiatry*, vol. 167, no. 11, pp. 1339–1348, 2010.

[102] R. Göder, A. Graf, F. Ballhausen et al., "Impairment of sleep-related memory consolidation in schizophrenia: relevance of sleep spindles?" *Sleep Medicine*, vol. 16, no. 5, pp. 564–569, 2015.

[103] A. Buchmann, D. Dentico, M. J. Peterson et al., "Reduced mediodorsal thalamic volume and prefrontal cortical spindle activity in schizophrenia," *NeuroImage*, vol. 102, no. 2, pp. 540–547, 2014.

[104] W. Byne, M. S. Buchsbaum, E. Kemether et al., "Magnetic resonance imaging of the thalamic mediodorsal nucleus and pulvinar in schizophrenia and schizotypal personality disorder," *Archives of General Psychiatry*, vol. 58, no. 2, pp. 133–140, 2001.

[105] P. Danos, B. Baumann, A. Krämer et al., "Volumes of association thalamic nuclei in schizophrenia: a postmortem study," *Schizophrenia Research*, vol. 60, no. 2-3, pp. 141–155, 2003.

[106] M. Shimizu, H. Fujiwara, K. Hirao et al., "Structural abnormalities of the adhesio interthalamica and mediodorsal nuclei of the thalamus in schizophrenia," *Schizophrenia Research*, vol. 101, no. 1–3, pp. 331–338, 2008.

[107] D. T. Plante, M. R. Goldstein, E. C. Landsness et al., "Topographic and sex-related differences in sleep spindles in major depressive disorder: a high-density EEG investigation," *Journal of Affective Disorders*, vol. 146, no. 1, pp. 120–125, 2013.

[108] J. Lopez, R. Hoffmann, and R. Armitage, "Reduced sleep spindle activity in early-onset and elevated risk for depression," *Journal of the American Academy of Child and Adolescent Psychiatry*, vol. 49, no. 9, pp. 934–943, 2010.

[109] J. Gallinat, K. McMahon, S. Kuhn, F. Schubert, and M. Schaefer, "Cross-sectional study of glutamate in the anterior cingulate and hippocampus in schizophrenia," *Schizophrenia Bulletin*, vol. 42, no. 2, pp. 425–433, 2016.

[110] T. Gleich, L. Deserno, R. C. Lorenz et al., "Prefrontal and striatal glutamate differently relate to striatal dopamine: potential regulatory mechanisms of striatal presynaptic dopamine function?" *The Journal of Neuroscience*, vol. 35, no. 26, pp. 9615–9621, 2015.

[111] P. J. Uhlhaas and W. Singer, "Oscillations and neuronal dynamics in schizophrenia: the search for basic symptoms and translational opportunities," *Biological Psychiatry*, vol. 77, no. 12, pp. 1001–1009, 2015.

[112] E. J. Wamsley, M. A. Tucker, A. K. Shinn et al., "Reduced sleep spindles and spindle coherence in schizophrenia: mechanisms of impaired memory consolidation?" *Biological Psychiatry*, vol. 71, no. 2, pp. 154–161, 2012.

[113] N. Dawson, M. Kurihara, D. M. Thomson et al., "Altered functional brain network connectivity and glutamate system function in transgenic mice expressing truncated Disrupted-in-Schizophrenia 1," *Translational Psychiatry*, vol. 5, article e569, 2015.

[114] H. Van der Loos and T. A. Woolsey, "Somatosensory cortex: structural alterations following early injury to sense organs," *Science*, vol. 179, no. 4071, pp. 395–398, 1973.

[115] S. D. Greenhill, K. Juczewski, A. M. de Haan, G. Seaton, K. Fox, and N. R. Hardingham, "Adult cortical plasticity depends on an early postnatal critical period," *Science*, vol. 349, no. 6246, pp. 424–427, 2015.

[116] C. Altimus, J. Harrold, H. Jaaro-Peled, A. Sawa, and D. J. Foster, "Disordered ripples are a common feature of genetically distinct mouse models relevant to schizophrenia," *Molecular Neuropsychiatry*, vol. 1, no. 1, pp. 52–59, 2015.

[117] J. Suh, D. J. Foster, H. Davoudi, M. A. Wilson, and S. Tonegawa, "Impaired hippocampal ripple-associated replay in a mouse model of schizophrenia," *Neuron*, vol. 80, no. 2, pp. 484–493, 2013.

[118] C. Dreyfus-Brisac, "The electroencephalogram of the premature infant," *World Neurology*, vol. 3, pp. 5–15, 1962.

[119] M. D. Lamblin, M. André, M. J. Challamel et al., "Electroencephalography of the premature and term newborn. Maturational aspects and glossary," *Neurophysiologie Clinique*, vol. 29, pp. 123–219, 1999.

[120] B. Clancy, R. B. Darlington, and B. L. Finlay, "Translating developmental time across mammalian species," *Neuroscience*, vol. 105, no. 1, pp. 7–17, 2001.

[121] A. D. Workman, C. J. Charvet, B. Clancy, R. B. Darlington, and B. L. Finlay, "Modeling transformations of neurodevelopmental sequences across mammalian species," *The Journal of Neuroscience*, vol. 33, no. 17, pp. 7368–7383, 2013.

[122] M. Colonnese and R. Khazipov, "Spontaneous activity in developing sensory circuits: implications for resting state fMRI," *NeuroImage*, vol. 62, no. 4, pp. 2212–2221, 2012.

[123] R. Khazipov and H. J. Luhmann, "Early patterns of electrical activity in the developing cerebral cortex of humans and rodents," *Trends in Neurosciences*, vol. 29, no. 7, pp. 414–418, 2006.

[124] R. Khazipov, A. Sirota, X. Leinekugel, G. L. Holmes, Y. Ben-Ari, and G. Buzsáki, "Early motor activity drives spindle bursts in the developing somatosensory cortex," *Nature*, vol. 432, no. 7018, pp. 758–761, 2004.

[125] J.-W. Yang, I. L. Hanganu-Opatz, J.-J. Sun, and H. J. Luhmann, "Three patterns of oscillatory activity differentially synchronize developing neocortical networks in vivo," *The Journal of Neuroscience*, vol. 29, no. 28, pp. 9011–9025, 2009.

[126] M. D. Brockmann, B. Pöschel, N. Cichon, and I. L. Hanganu-Opatz, "Coupled oscillations mediate directed interactions between prefrontal cortex and hippocampus of the neonatal rat," *Neuron*, vol. 71, no. 2, pp. 332–347, 2011.

[127] N. B. Cichon, M. Denker, S. Grün, and I. L. Hanganu-Opatz, "Unsupervised classification of neocortical activity patterns in neonatal and pre-juvenile rodents," *Frontiers in Neural Circuits*, vol. 8, article 50, 2014.

[128] M. T. Colonnese and R. Khazipov, "'Slow activity transients' in infant rat visual cortex: a spreading synchronous oscillation patterned by retinal waves," *The Journal of Neuroscience*, vol. 30, no. 12, pp. 4325–4337, 2010.

[129] H. Adelsberger, O. Garaschuk, and A. Konnerth, "Cortical calcium waves in resting newborn mice," *Nature Neuroscience*, vol. 8, no. 8, pp. 988–990, 2005.

[130] O. Garaschuk, J. Linn, J. Eilers, and A. Konnerth, "Large-scale oscillatory calcium waves in the immature cortex," *Nature Neuroscience*, vol. 3, no. 5, pp. 452–459, 2000.

[131] M. Minlebaev, M. Colonnese, T. Tsintsadze, A. Sirota, and R. Khazipov, "Early gamma oscillations synchronize developing thalamus and cortex," *Science*, vol. 334, no. 6053, pp. 226–229, 2011.

[132] X. Leinekugel, R. Khazipov, R. Cannon, H. Hirase, Y. Ben-Ari, and G. Buzsáki, "Correlated bursts of activity in the neonatal hippocampus in vivo," *Science*, vol. 296, no. 5575, pp. 2049–2052, 2002.

[133] T. Kleindienst, J. Winnubst, C. Roth-Alpermann, T. Bonhoeffer, and C. Lohmann, "Activity-dependent clustering of functional synaptic inputs on developing hippocampal dendrites," *Neuron*, vol. 72, no. 6, pp. 1012–1024, 2011.

[134] J. Winnubst, J. E. Cheyne, D. Niculescu, and C. Lohmann, "Spontaneous activity drives local synaptic plasticity in vivo," *Neuron*, vol. 87, no. 2, pp. 399–410, 2015.

[135] J. Winnubst and C. Lohmann, "Synaptic clustering during development and learning: the why, when, and how," *Frontiers in Molecular Neuroscience*, vol. 5, article 70, 2012.

[136] J.-W. Yang, S. An, J.-J. Sun et al., "Thalamic network oscillations synchronize ontogenetic columns in the newborn rat barrel cortex," *Cerebral Cortex*, vol. 23, no. 6, pp. 1299–1316, 2013.

[137] A. Hoerder-Suabedissen and Z. Molnár, "Development, evolution and pathology of neocortical subplate neurons," *Nature Reviews Neuroscience*, vol. 16, no. 3, pp. 133–146, 2015.

[138] M. Marx, G. Qi, I. L. Hanganu-Opatz, W. Kilb, H. J. Luhmann, and D. Feldmeyer, "Neocortical layer 6B as a remnant of the subplate—a morphological comparison," *Cerebral Cortex*, In press.

[139] J. M. Candy, E. K. Perry, R. H. Perry et al., "Evidence for the early prenatal development of cortical cholinergic afferents from the nucleus of Meynert in the human foetus," *Neuroscience Letters*, vol. 61, no. 1-2, pp. 91–95, 1985.

[140] N. Mechawar and L. Descarries, "The cholinergic innervation develops early and rapidly in the rat cerebral cortex: a quantitative immunocytochemical study," *Neuroscience*, vol. 108, no. 4, pp. 555–567, 2001.

[141] I. L. Hanganu, W. Kilb, and H. J. Luhmann, "Functional synaptic projections onto subplate neurons in neonatal rat somatosensory cortex," *The Journal of Neuroscience*, vol. 22, no. 16, pp. 7165–7176, 2002.

[142] I. L. Hanganu and H. J. Luhmann, "Functional nicotinic acetylcholine receptors on subplate neurons in neonatal rat somatosensory cortex," *Journal of Neurophysiology*, vol. 92, no. 1, pp. 189–198, 2004.

[143] I. L. Hanganu, A. Okabe, V. Lessmann, and H. J. Luhmann, "Cellular mechanisms of subplate-driven and cholinergic input-dependent network activity in the neonatal rat somatosensory cortex," *Cerebral Cortex*, vol. 19, no. 1, pp. 89–105, 2009.

[144] C. Chiu and M. Weliky, "Relationship of correlated spontaneous activity to functional ocular dominance columns in the developing visual cortex," *Neuron*, vol. 35, no. 6, pp. 1123–1134, 2002.

[145] A. D. Huberman, M. B. Feller, and B. Chapman, "Mechanisms underlying development of visual maps and receptive fields," *Annual Review of Neuroscience*, vol. 31, pp. 479–509, 2008.

[146] A. D. Huberman, C. M. Speer, and B. Chapman, "Spontaneous retinal activity mediates development of ocular dominance columns and binocular receptive fields in v1," *Neuron*, vol. 52, no. 2, pp. 247–254, 2006.

[147] J. Cang, R. C. Rentería, M. Kaneko, X. Liu, D. R. Copenhagen, and M. P. Stryker, "Development of precise maps in visual cortex requires patterned spontaneous activity in the retina," *Neuron*, vol. 48, no. 5, pp. 797–809, 2005.

[148] R. Mooney, A. A. Penn, R. Gallego, and C. J. Shatz, "Thalamic relay of spontaneous retinal activity prior to vision," *Neuron*, vol. 17, no. 5, pp. 863–874, 1996.

[149] N. X. Tritsch, A. Rodríguez-Contreras, T. T. H. Crins, H. C. Wang, J. G. G. Borst, and D. E. Bergles, "Calcium action potentials in hair cells pattern auditory neuron activity before hearing onset," *Nature Neuroscience*, vol. 13, no. 9, pp. 1050–1052, 2010.

[150] N. X. Tritsch, E. Yi, J. E. Gale, E. Glowatzki, and D. E. Bergles, "The origin of spontaneous activity in the developing auditory system," *Nature*, vol. 450, no. 7166, pp. 50–55, 2007.

[151] A. Clause, G. Kim, M. Sonntag et al., "The precise temporal pattern of prehearing spontaneous activity is necessary for tonotopic map refinement," *Neuron*, vol. 82, no. 4, pp. 822–835, 2014.

[152] C. Zhao, J. P. Y. Kao, and P. O. Kanold, "Functional excitatory microcircuits in neonatal cortex connect thalamus and layer 4," *Journal of Neuroscience*, vol. 29, no. 49, pp. 15479–15488, 2009.

[153] I. L. Hanganu, J. F. Staiger, Y. Ben-Ari, and R. Khazipov, "Cholinergic modulation of spindle bursts in the neonatal rat visual cortex in vivo," *The Journal of Neuroscience*, vol. 27, no. 21, pp. 5694–5705, 2007.

[154] A. J. Marcano-Reik and M. S. Blumberg, "The corpus callosum modulates spindle-burst activity within homotopic regions of somatosensory cortex in newborn rats," *European Journal of Neuroscience*, vol. 28, no. 8, pp. 1457–1466, 2008.

[155] A. J. Marcano-Reik, T. Prasad, J. A. Weiner, and M. S. Blumberg, "An abrupt developmental shift in callosal modulation of sleep-related spindle bursts coincides with the emergence of excitatory-inhibitory balance and a reduction of somatosensory cortical plasticity," *Behavioral Neuroscience*, vol. 124, no. 5, pp. 600–611, 2010.

[156] M. T. Colonnese, A. Kaminska, M. Minlebaev et al., "A conserved switch in sensory processing prepares developing neocortex for vision," *Neuron*, vol. 67, no. 3, pp. 480–498, 2010.

[157] H. Arakawa, A. Suzuki, S. Zhao et al., "Thalamic NMDA receptor function is necessary for patterning of the thalamocortical somatosensory map and for sensorimotor behaviors," *Journal of Neuroscience*, vol. 34, no. 36, pp. 12001–12014, 2014.

[158] M. Minlebaev, Y. Ben-Ari, and R. Khazipov, "NMDA receptors pattern early activity in the developing barrel cortex in vivo," *Cerebral Cortex*, vol. 19, no. 3, pp. 688–696, 2009.

[159] E. Dupont, I. L. Hanganu, W. Kilb, S. Hirsch, and H. J. Luhmann, "Rapid developmental switch in the mechanisms driving early cortical columnar networks," *Nature*, vol. 439, no. 7072, pp. 79–83, 2006.

[160] H. J. Luhmann, W. Kilb, and I. L. Hanganu-Opatz, "Subplate cells: amplifiers of neuronal activity in the developing cerebral cortex," *Frontiers in Neuroanatomy*, vol. 3, article 19, 2009.

[161] J. T. R. Isaac, M. C. Crair, R. A. Nicoll, and R. C. Malenka, "Silent synapses during development of thalamocortical inputs," *Neuron*, vol. 18, no. 2, pp. 269–280, 1997.

[162] S. Rumpel, H. Hatt, and K. Gottmann, "Silent synapses in the developing rat visual cortex: evidence for postsynaptic expression of synaptic plasticity," *The Journal of Neuroscience*, vol. 18, no. 21, pp. 8863–8874, 1998.

[163] K. Kaila, T. J. Price, J. A. Payne, M. Puskarjov, and J. Voipio, "Cation-chloride cotransporters in neuronal development, plasticity and disease," *Nature Reviews Neuroscience*, vol. 15, no. 10, pp. 637–654, 2014.

[164] C. Rivera, J. Voipio, J. A. Payne et al., "The K^+/Cl^- co-transporter KCC2 renders GABA hyperpolarizing during neuronal maturation," *Nature*, vol. 397, no. 6716, pp. 251–255, 1999.

[165] G. Deidda, M. Allegra, C. Cerri et al., "Early depolarizing GABA controls critical-period plasticity in the rat visual cortex," *Nature Neuroscience*, vol. 18, no. 1, pp. 87–96, 2015.

[166] D. D. Wang and A. R. Kriegstein, "GABA regulates excitatory synapse formation in the neocortex via NMDA receptor activation," *Journal of Neuroscience*, vol. 28, no. 21, pp. 5547–5558, 2008.

[167] K. Kirmse, M. Kummer, Y. Kovalchuk, O. W. Witte, O. Garaschuk, and K. Holthoff, "GABA depolarizes immature neurons and inhibits network activity in the neonatal neocortex in vivo," *Nature Communications*, vol. 6, article 7750, 2015.

[168] Y. Ben-Ari, "The developing cortex," *Handbook of Clinical Neurology*, vol. 111, pp. 417–426, 2013.

[169] R. Khazipov, M. Colonnese, and M. Minlebaev, "Neonatal cortical rhythms," in *Neural Circuit Development and Function in the Brain*, pp. 131–153, Elsevier, 2013.

[170] S. Heigele, S. Sultan, N. Toni, and J. Bischofberger, "Bidirectional GABAergic control of action potential firing in newborn hippocampal granule cells," *Nature Neuroscience*, vol. 19, no. 2, pp. 263–270, 2016.

[171] J. Conhaim, C. R. Easton, M. I. Becker et al., "Developmental changes in propagation patterns and transmitter dependence of waves of spontaneous activity in the mouse cerebral cortex," *The Journal of Physiology*, vol. 589, no. 10, pp. 2529–2541, 2011.

[172] J. Yang, V. Reyes-Puerta, W. Kilb, and H. J. Luhmann, "Spindle bursts in neonatal rat cerebral cortex," *Neural Plasticity*, vol. 2016, Article ID 3467832, 11 pages, 2016.

[173] S. N. Tuncdemir, B. Wamsley, F. J. Stam et al., "Early somatostatin interneuron connectivity mediates the maturation of deep layer cortical circuits," *Neuron*, vol. 89, no. 3, pp. 521–535, 2016.

[174] P. C. Janiesch, H.-S. Krüger, B. Pöschel, and I. L. Hanganu-Opatz, "Cholinergic control in developing prefrontal-hippocampal networks," *The Journal of Neuroscience*, vol. 31, no. 49, pp. 17955–17970, 2011.

[175] S. H. Bitzenhofer and I. L. Hanganu-Opatz, "Oscillatory coupling within neonatal prefrontal-hippocampal networks is independent of selective removal of GABAergic neurons in the hippocampus," *Neuropharmacology*, vol. 77, pp. 57–67, 2014.

[176] S. H. Bitzenhofer, K. Sieben, K. D. Siebert, M. Spehr, and I. L. Hanganu-Opatz, "Oscillatory activity in developing prefrontal networks results from theta-gamma-modulated synaptic inputs," *Cell Reports*, vol. 11, no. 3, pp. 486–497, 2015.

[177] H.-S. Krüger, M. D. Brockmann, J. Salamon, H. Ittrich, and I. L. Hanganu-Opatz, "Neonatal hippocampal lesion alters the functional maturation of the prefrontal cortex and the early cognitive development in pre-juvenile rats," *Neurobiology of Learning and Memory*, vol. 97, no. 4, pp. 470–481, 2012.

[178] J. A. Esteban, S.-H. Shi, C. Wilson, M. Nuriya, R. L. Huganir, and R. Malinow, "PKA phosphorylation of AMPA receptor subunits controls synaptic trafficking underlying plasticity," *Nature Neuroscience*, vol. 6, no. 2, pp. 136–143, 2003.

[179] K. Miyazaki, S. Manita, and W. N. Ross, "Developmental profile of localized spontaneous Ca^{2+} release events in the dendrites of rat hippocampal pyramidal neurons," *Cell Calcium*, vol. 52, no. 6, pp. 422–432, 2012.

[180] H. Yasuda, A. L. Barth, D. Stellwagen, and R. C. Malenka, "A developmental switch in the signaling cascades for LTP induction," *Nature Neuroscience*, vol. 6, no. 1, pp. 15–16, 2003.

[181] J. J. Zhu, J. A. Esteban, Y. Hayashi, and R. Malinow, "Postnatal synaptic potentiation: delivery of GluR4-containing AMPA receptors by spontaneous activity," *Nature Neuroscience*, vol. 3, no. 11, pp. 1098–1106, 2000.

[182] H. Sugiura and T. Yamauchi, "Developmental changes in the levels of Ca^{2+}/calmodulin-dependent protein kinase II α and β proteins in soluble and particulate fractions of the rat brain," *Brain Research*, vol. 593, no. 1, pp. 97–104, 1992.

[183] T. Takahashi, K. Svoboda, and R. Malinow, "Experience strengthening transmission by driving AMPA receptors into synapses," *Science*, vol. 299, no. 5612, pp. 1585–1588, 2003.

[184] C. Cirelli and G. Tononi, "Cortical development, electroencephalogram rhythms, and the sleep/wake cycle," *Biological Psychiatry*, vol. 77, no. 12, pp. 1071–1078, 2015.

[185] C. Itami and F. Kimura, "Developmental switch in spike timing-dependent plasticity at layers 4–2/3 in the rodent barrel cortex," *The Journal of Neuroscience*, vol. 32, no. 43, pp. 15000–15011, 2012.

[186] D. A. Butts, P. O. Kanold, and C. J. Shatz, "A burst-based 'Hebbian' learning rule at retinogeniculate synapses links retinal waves to activity-dependent refinement," *PLoS biology*, vol. 5, no. 3, article e61, 2007.

[187] J. Y. Hua and S. J. Smith, "Neural activity and the dynamics of central nervous system development," *Nature Neuroscience*, vol. 7, no. 4, pp. 327–332, 2004.

[188] G. M. Innocenti and D. J. Price, "Exuberance in the development of cortical networks," *Nature Reviews Neuroscience*, vol. 6, no. 12, pp. 955–965, 2005.

[189] P. Rakic, J.-P. Bourgeois, M. F. Eckenhoff, N. Zecevic, and P. S. Goldman-Rakic, "Concurrent overproduction of synapses in diverse regions of the primate cerebral cortex," *Science*, vol. 232, no. 4747, pp. 232–235, 1986.

Methodological approach for optogenetic manipulation of neonatal neuronal networks

Sebastian H. Bitzenhofer*, Joachim Ahlbeck & Ileana L. Hanganu-Opatz

Developmental Neurophysiology, Institute of Neuroanatomy, University Medical Center Hamburg-Eppendorf, Hamburg, Germany

*Corresponding author: Sebastian H. Bitzenhofer
sebbitz@zmnh.uni-hamburg.de

Running title

Interrogation of developing circuits by optogenetics

Abstract

Coordinated patterns of electrical activity are critical for the functional maturation of neuronal networks, yet their interrogation has proven difficult in the developing brain. Optogenetic manipulations strongly contributed to the mechanistic understanding of network activation in the adult brain, but difficulties to specifically and reliably express opsins at neonatal age hampered similar interrogation of developing circuits. Here, we introduce a protocol that enables to control the activity of specific neuronal populations by light, starting from early postnatal development. We show that brain area-, layer-, and cell type-specific expression of opsins by *in utero* electroporation, as exemplified for the medial prefrontal cortex and hippocampus, permits the manipulation of neuronal activity *in vitro* and *in vivo*. Both individual and population responses to different patterns of light stimulation are monitored by extracellular multi-site recordings in the medial prefrontal cortex of neonatal mice. The expression of opsins via *in utero* electroporation provides a flexible approach to disentangle the cellular mechanism underlying early rhythmic network activity, and to elucidate the role of early neuronal activity for brain maturation, as well as its contribution to neurodevelopmental disorders.

Keywords

development, optogenetics, *in utero* electroporation, prefrontal cortex, hippocampus

Introduction

Specific patterns of rhythmic network activity synchronize neuronal networks during early brain development (Hanganu et al., 2006;Khazipov and Luhmann, 2006;Brockmann et al., 2011). Together with genetic programs this electrical activity controls the maturation of neuronal networks (Khazipov and Luhmann, 2006;Hanganu-Opatz, 2010). The initial development of neuronal networks is controlled by molecular cues and largely independent of evoked neurotransmitter release (Molnar et al., 2002;Washbourne et al., 2002). However, subsequently diverse developmental processes such as neuronal migration, differentiation, axon growth, synapse formation, programmed cell death, and myelination are influenced by neuronal activity and mediate the activity-dependent maturation of neuronal networks (Spitzer, 2002;Heck et al., 2008;De Marco Garcia et al., 2011;Kirkby et al., 2013;Mitew et al., 2016). Spontaneous and sensory-triggered discontinuous patterns of oscillatory activity (e.g. spindle bursts, nested gamma spindle bursts, beta and gamma oscillations) have been shown to influence the maturation of cortical and cortico-subcortical networks (Hanganu-Opatz, 2010). However, the cellular mechanisms generating the different patterns of early network activity are still largely unknown. Furthermore, direct evidence for the impact of early activity on the maturation of neuronal networks is still missing.

Specific contributions of distinct neuronal populations to rhythmic network activity in the adult brain and their influence on behavior have been resolved during the last decade using optogenetics approaches (Cardin et al., 2009;Adesnik and Scanziani, 2010). Selective expression of light sensitive membrane channels and pumps in defined neuronal populations allow for precisely timed control of the activity of these neurons in intact networks (Fenno et al., 2011). The optogenetic approach helped to interrogate a large diversity of neural circuits in the adult brain involved in sensory processing (Lepousez and Lledo, 2013;Olcese et al., 2013), memory (Johansen et al., 2014;Liu et al., 2014;Spellman et al., 2015), and neuropsychiatric disorders (Tye and Deisseroth, 2012;Steinberg et al., 2015).

Similar application of optogenetics in the developing brain has been hampered by the lack of flexible methods to selectively and effectively target neurons at early age. The most common strategies to express light-sensitive proteins in the adult rodent brain are viral transduction and genetically modified mouse lines (Zhang et al., 2010;Yizhar et al., 2011). Both techniques require cell-type specific promoters to restrict the expression to a neuronal subpopulation. Most promoters have been shown to undergo qualitative and quantitative transitions during

development that can lead to unspecific and unstable expression (Sanchez et al., 1992;Kwakowsky et al., 2007;Wang et al., 2013). While recently synapsin has been successfully used as promoter for viral injections in neonatal rats and led to reliable activation of neurons in the visual cortex (Murata and Colonnese, 2016), most promoters that specifically label neuronal subpopulations yield only little expression during development. Thereby, viral transduction is only of limited usability to investigate local network interactions during development. Furthermore, most viruses require 10-14 days until reliable and sufficient expression is achieved, too long for the interrogation of neonatal networks. On the other hand, recently engineered viruses yielding fast expression are often toxic to the expressing cells even after short time periods (Klein et al., 2006), limiting their applicability for long-term investigations.

Another strategy for controlling the activity of developing circuits relies on genetically modified mouse lines. By these means the activity of gamma-aminobutyric acid (GABA)ergic interneurons was controlled by light during early postnatal development using the glutamic acid decarboxylase promoter (Valeeva et al., 2016). However, the major drawback of this approach is the lack of area specificity, the light-sensitive opsins being expressed in the entire brain. Attempts to spatially confine the illumination are useful, but cannot avoid that long range projections are co-activated and interfere with the investigation of the area of interest.

Area and cell-type specific transfection of neurons without the need of specific promoters has been achieved by *in utero* electroporation (IUE). This technique, mainly used to investigate neuronal migration during embryonic development, enables targeting of precursor cells of neuronal and glial subpopulations, based on their distinct spatial and temporal patterns of generation in the ventricular zone (Tabata and Nakajima, 2001;Borrell et al., 2005;Niwa et al., 2010;Hoerder-Suabedissen and Molnar, 2015). This makes IUE the method of choice for the selective targeting of neuronal populations during development. In combination with optogenetics and electrophysiology *in vivo* it enables the interrogation of developing circuits and the elucidation of initial cortical wiring. By these means, we recently elucidated the role of pyramidal neurons in layers II/III and V/VI of the medial prefrontal cortex (PFC) for the generation of frequency-tuned patterns of oscillatory activity (Bitzenhofer et al., 2017).

Here, we introduce the protocol for area-, layer-, and cell-type specific manipulation of neurons by light throughout postnatal development in mice and exemplify it for the PFC or hippocampus (HP). We illustrate for the PFC that site-directed IUE of highly efficient opsins

under control of a ubiquitous promoter yields sufficient population-specific expression to trigger action potentials and rhythmic network activity during early development *in vitro* and *in vivo*.

Materials and methods

All experiments were performed in compliance with the German laws and the guidelines of the European Community for the use of animals in research and were approved by the local ethical committee (Behörde für Gesundheit und Verbraucherschutz / Lebensmittelsicherheit und Veterinärwesen) (111/12, 132/12).

Area-, layer-, and cell type-specific expression at neonatal age by *in utero* electroporation

Pregnant C57Bl/6J mice were received from the animal facility of the University Medical Center Hamburg-Eppendorf at 6 days of gestation, housed individually in breeding cages at a 12 h light/dark cycle, and fed *ad libitum*. The day of vaginal plug detection was defined as embryonic day (E) 0.5. Additional wet food was provided on a daily basis from E 6.5 and was supplemented with 2 drops of Metacam (0.5 mg/ml, Boehringer-Ingelheim, Germany) from one day before until two days after IUE.

At E12.5 or E15.5 pregnant dams were injected subcutaneously with buprenorphine (0.05 mg/kg body weight) 30 min before surgery. Surgery was performed under isoflurane anesthesia (induction: 5%, maintenance: 3.5%) on a heating blanket. The eyes of the dam were covered with ointment to prevent damage. The abdomen was shaved, without causing damage to the nipples, and wiped with an ethanol pad. The dam was positioned on its back on a sterile mat and covered with parafilm sparing the abdomen. Toe pinch reflex and breathing were monitored throughout the surgery. The abdomen was sterilized with povidone-iodine solution (100 mg/ml). A 10 mm long incision along the midline was made successively through the abdominal skin and muscle layer. Uterine horns were carefully exposed using ring forceps. Throughout surgery, uterine horns were kept moist with warm sterile phosphate buffered saline (PBS, 37°C). Pulled borosilicate glass capillaries with a sharp and long tip were used to inject 0.75-1.25 µl solution containing 1.25 µg/µl plasmid DNA coding for a channelrhodopsin 2 mutant and red fluorescent protein (RFP), or just the fluorescent reporter (pAAV- cytomegalovirus enhancer fused to chicken beta-actin (CAG) -tDimer2 or pAAV-CAG- channelrhodopsin 2 double mutant E123T T159C (ChR2(ET/TC)) -2A-tDimer2) into the right lateral ventricle of each embryo. The ubiquitous CAG promoter was used to achieve robust expression. 0.1% fast green dye was added to the

solution for visual control of the injection site. Bright illumination helps to detect the lateral ventricles of the embryos (Fig. 1A).

Depending on the orientation of the electroporation paddles, selective transfection of a subset of neuronal precursor cells in the ventricular zone by IUE yielded area-specific expression of light-sensitive proteins. For targeting PFC, the embryo's head was placed between the bipolar electroporation tweezer-type paddles (3 mm diameter for E12.5, 5 mm diameter for E15.5, Protech, TX, USA) at a 20° leftward angle from the midline and a 10° angle downward from anterior to posterior with the positive pole on the hemisphere contralateral to the injection (Fig. 1Bi). Voltage pulses (35 V, 50 ms) were applied five times at intervals of 950 ms controlled by an electroporator (CU21EX, BEX, Japan) to target the transfection of precursor cells of glutamatergic neurons in the specific area of the subventricular zone that migrate into the medial PFC. For targeting HP, tripolar electroporation paddles were used at E15.5 (dal Maschio et al., 2012;Szczurkowska et al., 2016) and the embryo was placed between the electroporation tweezer-type paddles (5 mm diameter, both positive poles, Protech, TX, USA). A third custom build negative pole was positioned on top of the head roughly between the eyes (Fig. 1Ci). Voltage pulses (30 V, 50 ms) were applied six times at intervals of 950 ms. Warm sterile PBS was applied to the embryo's head immediately after the voltage pulses.

Uterine horns were placed back into the abdominal cavity after electroporation. During the entire procedure, damage to the blood vessels surrounding the uterine horns was avoided. The abdominal cavity was filled with warm sterile PBS and the abdominal muscles and skin were sutured individually with absorbable and non-absorbable suture thread, respectively. After recovery from anesthesia, pregnant mice were returned to their home cages, which were half placed on a heating blanket for two days after surgery. After IUE, the recovery of the dam was visually inspected every day and special attention was given to minimize the stress level. The day of birth was defined as postnatal day (P) 0. IUE can be performed by a single person. However, the quality of the surgery can be significantly improved by reducing its duration if a second person assists in positioning the embryos for the construct injections. Surgeries of short duration are desirable, since they improve the survival rate of IUE-manipulated pups.

Fluorophore-expression in the area of interest can be detected through the intact skin and skull with a fluorescent flash light (Nightsea, MA, USA) or a standard fluorescence microscope until the age P2 (Fig. 1Bii, Cii). To confirm area-, layer-, and cell type-specific transfection, pups of *in utero* electroporated dams were anesthetized with 10% ketamine (aniMedica, Germany) /

2% xylazine (WDT, Germany) in 0.9% NaCl solution (10 µg/g body weight, i.p.) and transcardially perfused with Histofix (Carl Roth, Germany) containing 4% paraformaldehyde. Brains were removed, postfixed in 4% paraformaldehyde for 24 h, sectioned coronally at 50 µm, and stored at 4°C in the dark in sterile PBS containing 0.05% sodium azide. The resulting slices were transferred to glass slides and covered with Fluoromount (Sigma-Aldrich, MO, USA). Wide field fluorescence images were acquired to localize tDimer2 expression after IUE.

Immunohistochemical stainings were performed to confirm cell type-specific expression. Free-floating slices were permeabilized and blocked in PBS containing 0.8% Triton X 100 (Sigma-Aldrich, MO, USA), 5% normal bovine serum (Jackson Immuno Research, PA, USA) and 0.05% sodium azide. Slices were washed and incubated on a shaker at 4°C for 24 h with mouse monoclonal Alexa Fluor-488 conjugated antibody against NeuN (1:200, MAB377X, Merck Millipore, MA, USA), rabbit polyclonal primary antibody against Ca^{2+}/calmodulin-dependent protein kinase II (CaMKII) (1:200, PA5-38239, Thermo Fisher Scientific, MA, USA), or rabbit polyclonal primary antibody against GABA (1:1000, #A2052, Sigma-Aldrich, MO, USA). For CaMKII and GABA, after washing, slices were incubated at room temperature for 2 h with Alexa Fluor-488 goat anti-rabbit IgG secondary antibody (1:500, A11008, Merck Millipore, MA, USA). Slices were transferred to glass slides and covered with Fluoromount (Sigma-Aldrich, MO, USA). Images were acquired with a confocal microscope (DM IRBE, Leica, Germany) to quantify tDimer2 expression and to analyze immunohistochemical stainings.

For the PFC, layer-specific targeting of neurons was obtained by conducting the IUE at distinct embryonic stages. IUE at E15.5 leads to expression in superficial layers of the medial PFC (Fig. 1Biii), whereas the same protocol at E12.5 results in expression in layers V/VI (Fig. 1Biv), due to the subsequent formation of cortical layers in an inside-out sequence. Prefrontal expression was achieved in about 80% of pups electroporated at E15.5 and in about 40% of pups electroporated at E12.5. The lower success rate for IUE at E12.5 is most likely due to the smaller size of the embryos. Co-transfection of nearby cortical regions was present in about 10% of animals when targeting PFC. The size of the expression area can be modified by the size of the electroporation paddles. Paddles with a diameter of 5 mm at E15.5 or 3 mm at E12.5 led to transfection 400-600 µm along the anterior-posterior axis in the PFC. The distinct origin of glutamatergic and GABAergic neurons allows for cell-type-specific transfections. The protocols described above led to targeting of glutamatergic neurons with the fraction of transfected cells varying between 20 and 40%. While IUE at E15.5 resulted in almost exclusive labeling of

neurons in superficial cortical layers (99.3 ± 0.2% in layer II/III), IUE at E12.5 had poorer layer specificity (87.7 ± 0.9 in layer V/VI), due to an overlap in the generation of cortical neurons in different layers from the same progenitor cells (Martínez-Garay et al., 2016). The strong intensity of the RFP tDimer2 and its distribution throughout the entire neuron enabled to detect dendritic morphology and axonal projections of expressing neurons (Fig. Biii,iv). Furthermore, expression was stable during the entire developmental period. IUE with tripolar electroporation paddles at E15.5 yielded expression in the pyramidal layer of the HP in about 60% of newborn pups (Fig. 1Ci). Weak co-transfection of neurons in the retrosplenial cortex was detected in all investigated pups. The fluorophore was detectable in the HP through the skin and skull until P2 (Fig. 1Cii). The IUE configuration yielded expression in the dorsal (Fig. 1Ciii) and intermediate HP (Fig. 1Civ). Similar to the PFC, transfection in the HP was restricted to glutamatergic neurons.

Several other brain areas and cell types can be targeted by IUE at different embryonic ages and with different paddle orientations (Baumgart and Grebe, 2015;Szczurkowska et al., 2016). Augmented specificity in targeting can be achieved by using (i) intracranial needles instead of extracranial electroporation paddles, (ii) Cre-expressing driver lines and clonal labeling techniques, such as CLoNe (Garcia-Moreno et al., 2014;Vasistha et al., 2015). Further aspects about IUE were recently described in detail (Martínez-Garay et al., 2016).

Combined electrophysiology and light stimulation *in vitro*

To decide whether transfection of neurons of interest by IUE yields sufficient expression of opsins to trigger action potentials already during the neonatal period, we performed whole-cell patch-clamp recordings from transfected neurons in brain slices from P8-10 mice *in vitro* (Fig. 2A). Pyramidal neurons in the PFC were transfected with the highly-efficient ChR2(ET/TC) under control of the CAG promoter. ChR2(ET/TC) has been reported to have high conductance upon stimulation with blue light, as well as fast kinetics allowing for fast rhythmic stimulation (Berndt et al., 2011). The RFP tDimer2 was co-expressed to identify the transfected neurons.

For whole-cell patch-clamp recordings pups were decapitated, brains were removed carefully within less than a minute, and immediately transferred into ice-cold oxygenated high sucrose artificial cerebrospinal fluid (ACSF) containing (in mM: 228 Sucrose, 2.5 KCl, 1 NaH_2PO_4, 26.2 $NaHCO_3$, 11 Glucose, 7 $MgSO_4$; 320 mOsm, pH 7.2). Coronal sections (300 µm thickness) including the area of interest were sectioned in ice-cold oxygenated high sucrose ACSF and incubated in oxygenated ACSF (in mM: 119 NaCl, 2.5 KCl, 1 NaH_2PO_4, 26.2

$NaHCO_3$, 11 Glucose, 1.3 $MgSO_4$; 320 mOsm, pH 7.2) at 37°C for 45 minutes before cooling to room temperature for recordings. Fluorescently-labeled neurons were patched under optical control using pulled borosilicate glass capillaries (tip resistance of 4-7 MΩ) filled with potassium-based pipette solution (in mM: 130 K-Gluconate, 10 HEPES, 0.5 EGTA, 4 Mg ATP, 0.3 Na GTP, 8 NaCl; 285 mOsm, pH 7.4). Recordings were controlled with Ephus software in Matlab environment (MathWorks, MA, USA). Capacitance artifacts were minimized using the built-in circuitry of the patch-clamp amplifier (Axopatch 200B, Molecular devices, CA, USA). Responses of neurons to hyper- and depolarizing current injections (Fig. 2B), as well as to single and repetitive blue light pulses (473 nm, 5.2 mW/mm²) of different duration were recorded and digitized at 5 kHz in current-clamp mode.

Data were analyzed offline using custom-written tools in Matlab software. All potentials were corrected for liquid junction potentials with -10 mV for the potassium based electrode solution (Kilb and Luhmann, 2000). The resting membrane potential was measured immediately after obtaining the whole-cell configuration. Active membrane properties and current voltage relationships were assessed by unsupervised analysis of responses to a series of 600 ms long hyper- and depolarizing current pulses. Single and repetitive light pulses of different duration and frequency were used to test for light responsiveness.

Blue light (473 nm, 5.2 mW mm^{-2}) pulses of 1 ms durations were sufficient to depolarize the opsin-expressing neurons, whereas longer light pulses reliably evoked single action potentials (Fig. 2C). Upon light stimulation for >50 ms, neurons entered a depolarizing plateau potential, similar to the responses to high positive current injections. In contrast, driving opsin expression with synapsin or human elongation factor 1 α promoters was not sufficient to drive action potentials in transfected neurons with similar light power. Thus, expression strength of the highly efficient ChR2(ET/TC) under control of the CAG promoter achieved by IUE is sufficient to optically drive action potentials during neonatal development *in vitro*. Rhythmic stimulation with 3 ms long blue light pulses triggered repetitive firing in opsin expressing neurons (Fig. 2D). The fast off-kinetics of ChR2(ET/TC) allows to trigger neuronal firing at frequencies up to 60 Hz in adult neurons (Berndt et al., 2011). Intrinsic neuronal features may explain why pyramidal neurons in the neonatal PFC did not follow rhythmic stimulation at frequencies >16 Hz.

Combined electrophysiology with light stimulation *in vivo*

To determine if neuronal spiking can be equally controlled in the intact brain, we combined optogenetic stimulations with recordings of local field potentials (LFP) and multi-unit activity (MUA) from P8-10 mice after IUE *in vivo*.

The surgery for *in vivo* electrophysiology was done as previously described (Hanganu et al., 2006;Brockmann et al., 2011). Newborn mice have a very fragile skull and their ear channels are closed. This prevents head fixation as typically used for acute extracellular recordings in juvenile or adult rodents. Neonatal mice were injected i.p. with urethane (1 mg/g body weight; Sigma-Aldrich, MO, USA) prior to surgery to achieve stable, long-lasting anesthesia during the recording. Under isoflurane anesthesia (induction: 5%, maintenance: 2.5%) the head of the pup was fixed into a stereotaxic apparatus using two plastic bars mounted on the nasal and occipital bones with dental cement (Fig. 3Ai). Interestingly, it is possible to observe the RFP expression through the bone after removal of the skin using a portable fluorescent flashlight for all ages tested (P8-25). The bone above the medial PFC (0.5 mm anterior to bregma, 0.1 mm right to the midline for layer II/III, 0.5 mm for layer V/VI) or the HP (2.0 mm posterior to bregma, 0.75 mm right to the midline for dorsal HP; 3.5 mm posterior to bregma, 3.5 mm right to the midline for intermediate HP) was carefully removed by drilling a hole of <0.5 mm in diameter. After a 10-20 min recovery period on a heating blanket, multi-site optoelectrodes (NeuroNexus, MI, USA) were inserted 2-2.4 mm deep into the PFC perpendicular to the skull surface or 1.5-1.8 mm deep into the HP with manual micromanipulators (Fig. 3Aii). One-shank multi-site optoelectrodes contained 1x16 recordings sites (0.4-0.8 MΩ impedance, 50 or 100 µm spacing) aligned with an optical fiber (105 µm diameter) ending 200 µm above the top recording site. A silver wire was inserted into the cerebellum and served as reference electrode. Extracellular signals were band-pass filtered (0.1-9000 Hz) and digitized (32 kHz) with a multi-channel extracellular amplifier (Digital Lynx SX, Neuralynx, Bozeman, MO) and the Cheetah acquisition software (Neuralynx, Bozeman, MO). Pulsed (light on-off), sinusoidal, and ramp (linearly increasing light power) light stimulations were performed with an arduino uno (Arduino, Italy) controlled diode laser (473 nm, Omicron, Austria). After recordings, animals were transcardially perfused, brains were sectioned coronally, and wide field fluorescence images were acquired to reconstruct the recording electrode position in relation to the neurons transfected by IUE. Data were analyzed offline using custom-written tools in Matlab software. Data were band-pass filtered (500-5000 Hz) to analyze MUA and low-pass (<1500 Hz) filtered using a third order Butterworth filter before downsampling to 3.2 kHz to analyze LFP, before further band-pass filtering (1-100 or 1-400 Hz).

All filtering procedures were performed in a manner preserving phase information. MUA was detected as the peak of negative deflections greater than five times the standard deviation of filtered signals. Time-frequency plots were calculated by transforming the data using Morlet continuous wavelet.

Multi-site optoelectrodes allowed simultaneous stimulation by light and recording of the neuronal activity. To validate that neuronal spiking can be reliable triggered in neonatal mice targeted by IUE, light pulses of 3 ms duration were delivered at different light intensities. To control for possible heating and photoelectric artifacts, stimulation was performed in mice transfected with opsin-containing (Fig. 3Bi) and opsin-free constructs (Fig. 3Bii). Recordings in opsin-free mice did not show any change in MUA upon light stimulation, indicating the absence of induced or suppressed neuronal activity due to potential tissue heating. Modeling of heat propagation in neuronal tissue confirmed low levels of tissue heating for our stimulation parameters (Stujenske et al., 2015;Bitzenhofer et al., 2017). In opsin-expressing mice, light stimulation caused augmented MUA, both shortly after the stimulus, as result of firing of opsin-expressing neurons and at delayed time windows after the stimulus, as result of the activation of neurons downstream to the opsin-expressing neurons.

To ensure that the detected spikes represent neuronal firing and not photoelectrical artifacts that can be evoked by photons hitting the recording sites (Cardin et al., 2010), we assessed the response to single light pulses in more detail. Photoelectric artifacts typically occur immediately after abrupt changes in light intensity (Cardin et al., 2010). No fast transitions were observed at the start and the end of the light pulse in the band-pass filtered (500-5000 Hz) signal used for spike detection (Fig. 3B), indicating that MUA was not contaminated by photoelectric artifacts. This conclusion was confirmed by the typical delay of spiking (4-8 ms) after the start of the light pulse. Thus, transfection of opsins by IUE yields sufficient expression to trigger neuronal firing in neonatal mice *in vivo*.

In contrast to MUA, LFP recordings were artifactually altered by light. Two types of artifacts were detected. First, the photoelectric artifacts were identified as short small-amplitude deflections in opsin-free animals (Fig. 3Bii). Second, large amplitude long-lasting negative deflections were present only in opsin-expressing animals (Fig. 3Bi). They presumably represent physiological extracellular current sinks that are created by the flow of sodium ions into neurons due to the simultaneous opening of the light-gated channelrhodopsins expressed in the membranes of neurons surrounding the recording sites upon light stimulation. This is

corroborated by the similarity of their timing (start 2 ms after stimulation onset and last for 8-12 ms) to the kinetics of ChR2(ET/TC). These slow negative deflections of large amplitude disappeared after a lethal injection of ketamine-xylazine, whereas photoelectric artifacts persisted (Fig. 3Ci). The photoelectric artifacts were recorded post-mortem, filtered (1-400 Hz), averaged, scaled to the immediate downstroke (0-1.5 ms after light onset) of the alive recordings and subtracted from the alive recordings (Fig. 3Ci,Cii). Thereby, photoelectric artifacts can be removed from the recordings.

Results

Different light stimulation patterns are instrumental for the characterization of neonatal firing

The protocols described above were used to manipulate the firing and network activity of different brain areas during neonatal development (Bitzenhofer et al., 2017). For this, we tested three light stimulation patterns and recorded the neuronal and network responses in the PFC and HP of neonatal mice *in vivo*: (i) trains of repetitive short square pulses, (ii) sinusoidal, and (iii) ramp stimulations (Adesnik and Scanziani, 2010;Cardin et al., 2010;Stark et al., 2013).

The most commonly used stimulation pattern is a train of short square pulses repeated at a specific frequency. This stimulation pattern drives opsin-expressing neurons to synchronously fire at the stimulated frequency. When applied to glutamatergic layer II/III neurons of the neonatal PFC transfected with ChR2(ET/TC) the stimulation (30 sweeps of rhythmic 3 ms long light pulses at 8 Hz) led to reliable and rhythmic firing (Fig 4A). No MUA response to rhythmic light pulses was observed in control mice after IUE with opsin-free plasmids, encoding only for the RFP tDimer2 (Fig. 4B).

Similar to repetitive light pulses, stimulation with sinusoidally modulated light power at 8 Hz triggered firing in opsin-expressing, but not in opsin-free animals (Fig. 4C,D). In contrast to stimulation by trains of light pulses, spiking was less precisely timed for sinusoidal stimulations and did not follow the stimulation reliably. Still, a distinct, but broader peak was observed in the inter-spike interval (ISI) histogram at the stimulation frequency of 8 Hz (Fig. 4Cii). In contrast to pulsed stimulation, the precision of light-induced firing decreased towards the end of the stimulation.

Similar to the pulsed and sinusoidal stimulations, ramp stimulation induced spiking in mice electroporated with opsins, but not in opsin-free controls (Fig. 4E,F). In contrast to the

repetitive stimulations at precisely defined frequency, ramp stimulation, with linearly increasing light power, does not time the neuronal firing to a set rhythm. It rather enables a more physiological activation and neurons spike at their preferred frequency, if any, when a certain level of depolarization has been reached. The preferred frequency can reflect intrinsic neuronal mechanisms, but also features of local networks. For example, ramp stimulation of pyramidal neurons in layer II/III of neonatal PFC led to a broad peak between 30 and 80 ms, corresponding to the beta frequency band of 12-30 Hz, in the spiking histograms (Fig. 4Eii), whereas a preferred firing frequency upon light stimulation cannot be detected in layer V/VI pyramidal neurons (Bitzenhofer et al., 2017).

Thus, different light stimulations can be applied to induce firing of neonatal neurons transfected with opsins by IUE. They allow not only timing of the activity within developing neuronal networks, but also the dissection of intrinsic rhythms of activation.

Different light stimulation patterns are instrumental for the interrogation of developing circuits

To assess the effects of distinct patterns of light stimulation on the oscillatory activity of developing neuronal networks, we simultaneously stimulated with light and recorded the LFP in layer II/III of the medial PFC of opsin-expressing and opsin-free P8-10 mice after IUE at E15.5.

In contrast to the light-induced spiking, the band-pass (4-100 Hz) filtered LFP was profoundly affected by photoelectric artifacts when trains of light pulses were used (Fig. 3B,C). The repetitive stimulation induced large negative deflections detectable in the LFP of opsin-expressing mice (Fig. 5A). While opsin-free animals showed only the photoelectric artifact (Fig. 5B), three distinct effects were detected in opsin-expressing pups: (i) immediate photoelectric artifacts when light was switched on and off, (ii) large magnitude negative deflections with slower kinetics due to the simultaneous opening of the light-gated channelrhodopsins and the resulting flow of positively charged ions into neurons, (iii) and coordinated activity within local networks resulting from light-induced spiking, which has been described above. The large deflections (ii) contaminated the time resolved frequency spectra and the power spectra not only at the frequency of stimulation, but also at the corresponding higher frequency harmonics due to their rhythmic, non-sinusoidal shape (Fig. 5A). The mixed effects of the deflections precluded a quantitative analysis of light-induced network activity during the stimulation, despite the fact that the pure photoelectric artifacts can be removed (see Methods).

Similarly, sinusoidal light stimulations resulted in a mixture of photoelectric artifacts, large light-induced deflections, and light-induced coordinated activity in the local networks of opsin-expressing animals (Fig. 5C). Photoelectric artifacts are detectable as peaks of oscillatory power at the set stimulation frequency in both opsin-expressing and opsin-free pups (Fig. 5Cii, Dii). The small broader power peak around the stimulation frequency was detected only in opsin-expressing animals and most likely reflects induced coordinated activity. The sinusoidal shape of the stimulation artifact restricts the contamination of the power spectrum to the stimulation frequency, without the induction of higher frequency harmonics. Similar to pulsed stimulation, the quantification of light-induced coordinated network activity cannot be achieved during stimulation, but only by comparison of time windows shortly before and after stimulation.

In contrast to pulsed and sinusoidal stimulations, ramp stimulation did not cause rhythmic artifacts, due to the slow change in light power (Fig. 5E,F). Only the abrupt switch from light on to off at the end of the ramp stimulation led to a small photoelectric artifact detectable in the LFP. Therefore, quantification of induced oscillatory activity during the stimulation was possible. For example, investigation of LFP effects after ramp stimulation of layer II/III pyramidal neurons of the medial PFC in P8-10 opsin-expressing mice showed that prominent beta band network oscillations can be induced by light (Fig. 5E) (Bitzenhofer et al., 2017). They correspond to the preferred firing of neurons within similar frequency range upon ramp stimulation (Fig. 4E). In opsin-free animals, light stimulation did not induce oscillatory activity and the power spectrum remained unchanged (Fig. 5F).

Thus, coordinated patterns of oscillatory activity in neonatal mice can be induced by light, yet depending on the stimulation patterns, they might be contaminated by photoelectric and physiological artifacts. These artifacts are negligible for ramp stimulation, making this pattern the method of choice for the investigation of light-induced effects on oscillatory network activity.

Discussion

Controlling the activity of specific neurons at fast time scales by optogenetics has proven successful to elucidate the contribution of identified neuronal populations to synchronous network activity in the adult brain (Cardin et al., 2009;Adesnik and Scanziani, 2010;Tye and Deisseroth, 2012). Similar investigations in developing neuronal networks have been hampered by difficulties to reliably and specifically express opsins during neonatal development. Here, we

describe a protocol that allows the application of optogenetics for the interrogation of neuronal networks during first postnatal weeks in mice, as shown for the neonatal PFC and HP.

The effective and selective expression of opsins in a subset of neurons during early life is the prerequisite for the optogenetic interrogation of the cellular interactions and their contribution to coordinated activity patterns within developing neuronal networks. Similar early targeting of neurons was required for the study of the migration of cortical neurons during embryonic and early postnatal development (Tabata and Nakajima, 2001;Borrell et al., 2005). For this, fluorescent markers were expressed early in cellular populations of interest by IUE. In the protocol described above, we used the advantages of the early expression onset achieved with this technique, as exemplified by the reliable and stable expression of opsins in specific populations of pyramidal cells in the medial PFC and the HP during early postnatal development.

Neuronal precursors, generating different neuronal populations that are intermixed in neuronal networks after migration, are spatially and temporally separated during embryonic development (Wonders and Anderson, 2006;Hoerder-Suabedissen and Molnar, 2015). The spatially separated generation of glutamatergic and GABAergic neurons prevents the need of cell type specific promoters to achieve cell-type specific expression with IUE (Wonders and Anderson, 2006;Hoerder-Suabedissen and Molnar, 2015). Furthermore, the targeting confined to specific embryonic stages and to specific groups of precursor cells in the ventricular zone enables to achieve expression that is restricted to distinct brain regions, such as different areas of the neocortex, HP, cerebellum, striatum, thalamus or hypothalamus (Baumgart and Grebe, 2015;Szczurkowska et al., 2016). The age-dependent formation of cortical layers in an inside-out sequence allows targeting of principal neurons in a layer-confined pattern, when IUE is performed at the corresponding embryonic day (Taniguchi et al., 2012). We exemplified this by separately addressing the upper (layer II/III) and deeper layers (layer V/VI) of the PFC. Therefore, expression in specific neuronal populations, that is restricted to specific brain areas, and even to specific cortical layers, can be achieved by IUE, without the need of population specific promoters. Ubiquitous promoters can be used to yield stable expression during development and comparable expression in different types of neurons. This is one of the major advantages of IUE when compared to targeting by viral injections and genetic mouse lines. Promoters specific for certain types of neurons are often unspecific during early development, or do not drive constant expression over time (Sanchez et al., 1992;Kwakowsky et al., 2007;Wang et al., 2013). IUE is suitable to investigate neuronal networks over long time periods, since it

ensures stable expression of opsins throughout the development and at adulthood (Adesnik and Scanziani, 2010). Moreover, opsin transfection using IUE did not affect the patterns of neuronal activity when compared to those from non-electroporated and opsin-free neonatal mice (Bitzenhofer et al., 2017).

The highly efficient channelrhodopsin 2 mutant ET/TC causes large photocurrents and has fast off kinetics. Transfection by IUE under the control of the ubiquitous CAG promoter yielded sufficient expression to precisely control the generation of action potentials in neonatal mice by light, both under *in vitro* and *in vivo* conditions. We compared the effects of different stimulation patterns (repetitive light pulses, sinusoidally and ramp modulated light intensity) on extracellularly recorded spiking and oscillatory activity in neonatal mice after area-, layer-, and cell-type-specific transfection with opsins by IUE. All stimulation patterns induced reliable spiking that was largely unaffected by photoelectric artifacts, indicating the general feasibility of integrated local stimulation and recording within the same volume. Pulsed stimulations induced a highly synchronous spiking reliably following the stimulation frequency. Similarly, sinusoidal stimulation also induced synchronous spiking activity although with higher variability over the stimulation period. The entrainment following pulsed stimulation is possibly excessive with spiking activity tightly following the stimulation frequency. In contrast to spiking in a defined stimulation frequency, ramp stimulation does not impose a specific frequency on neuronal firing, but drives neuronal networks to spike at an intrinsic or preferred rhythm (Adesnik and Scanziani, 2010;Bitzenhofer et al., 2017). Thus, each stimulation type induces a different type of spiking activity and synchrony in the network and can be adjusted to the experimental needs.

Photoelectric artifacts and large voltage deflections induced by repetitive pulsed and sinusoidal stimulations precluded a quantitative analysis of light-induced oscillatory activity in developing circuits. Solely the network entrainment before and after the stimulation time window can be compared. The size of the photoelectric artifact is highly dependent on the amount of light hitting the metallic recording site. It can be reduced by angling the light fiber in such that the light cone does not emit directly to the recording site, or by recording outside of the illuminated area. Alternatively, recordings with glass electrodes are not affected by photoelectric artifacts (Cardin et al., 2010). Sinusoidal stimulation is advantageous when investigating frequencies of the LFP outside the frequency used to stimulate, due to minimal induction of harmonics in the power spectrum (Akam et al., 2012). The slow change in light intensity during ramp light stimulation did not induce a photoelectric artifact or rhythmic physiological current sinks due to

the simultaneous opening of channelrhodopsins, enabling to quantify induced oscillatory activity in the local network during optical stimulation. We recently used this stimulation pattern to provide direct evidence for the contribution of layer II/III, but not layer V/VI, pyramidal cells to beta-gamma oscillatory activity in the medial PFC in neonatal mice (Bitzenhofer et al., 2017).

The protocol described here opens new perspectives for the interrogation of neuronal networks and the elucidation of cellular interactions during brain development. The method can be combined with designer receptor exclusively activated by designer drugs (DREADDs) (Ishii et al., 2015), calcium-indicators (Gee et al., 2015), or region specific gene manipulation (Niwa et al., 2010;Page et al., 2017) to get deeper insights into the mechanisms of circuit wiring. Furthermore, chronic optogenetic manipulation of defined neuronal populations and oscillatory rhythms during specific developmental periods will help to elucidate the role of early network activity for behavioral performance at adulthood under physiological and pathological conditions.

Abbreviations

ACSF - artificial cerebrospinal fluid

CAG - cytomegalovirus enhancer fused to chicken beta-actin

CaMKII - Ca^{2+}/calmodulin-dependent protein kinase II

ChR2(ET/TC) - channelrhodopsin 2 double mutant E123T T159C

DREADDs - designer receptor exclusively activated by designer drugs

E - embryonic day

GABA - gamma-aminobutyric acid

HP - hippocampus

ISI - inter-spike interval

IUE - *in utero* electroporation

LFP - local field potential

MUA - multi unit activity

P - postnatal day

PBS - phosphate buffered saline

PFC - prefrontal cortex

RFP - red fluorescent protein

Conflict of interest statement

The authors declare that the research was conducted in the absence of any commercial or financial relationships that could be construed as a potential conflict of interest.

Author and contributors

I.L.H.-O. designed the experiments. S.H.B and J.A. developed the protocol and carried out the experiments, S.H.B. and J.A. analyzed the data. I.L.H.-O., S.H.B., J.A. interpreted the data and wrote the manuscript.

Funding

This work was funded by grants from the European Research Council (ERC-2015-CoG 681577 to I.L.H.-O.) and the German Research Foundation (SPP 1665 to I.L.H.-O., SFB 936 B5 to I.L.H.-O).

Acknowledgments

We thank Annette Marquardt, Iris Ohmert and Achim Dahlmann for excellent technical assistance. I.L. H.-O is member of the FENS Kavli Network of Excellence.

Figure legends

Figure 1. Area-, layer-, and cell-type-specificity of neuronal targeting by *in utero* electroporation. (A) Diagrams and photographs illustrating the procedure for IUE. **(B) (i)** Schematic representation of the position of electroporation paddles to yield expression in pyramidal neurons in the medial PFC. **(ii)** Photograph showing the expression of RFP (red) transfected in the PFC by IUE detectable through skull and skin at P2. **(iii)** Targeting of pyramidal neurons in layer II/III of the neonatal PFC. Left, RFP expressing cells (red) in 50 µm-thick coronal slices of a P10 mouse at the level of the PFC after IUE at E15.5. Middle, RFP-expressing neurons in prefrontal layer II/III displayed at higher magnification. Right, confocal images of RFP-expressing neurons after staining for CaMKII or GABA. **(iv)** Targeting of pyramidal neurons in layer V/VI of the neonatal PFC. Same as (iii) for IUE at E12.5. **(C) (i)** Schematic representation of the position of the electroporation paddles to yield expression in pyramidal neurons of hippocampal CA1 area. **(ii)** Photograph showing the expression of RFP (red) transfected in the HP by IUE detectable through skull and skin at P2. **(iii)** Targeting of pyramidal neurons in dorsal HP. Left, RFP expressing cells (red) in 50 µm-thick coronal slices of a P10 mouse at the level of the dorsal HP after IUE at E15.5. Middle, RFP-expressing neurons in dorsal HP displayed at higher magnification after staining for NeuN. Right, confocal images of RFP-expressing neurons after staining for GABA. **(iv)** Same as (iii) for the intermediate HP.

Figure 2. Optogenetic control of action potential firing in neonatal brain slices *in vitro*. (A) Diagram illustrating combined light stimulation and whole-cell patch-clamp recordings from layer II/III pyramidal neurons in coronal slices of P8-10 mice transfected with ChR2(ET/TC) by IUE at E15.5. **(B)** Voltage responses of a ChR2(ET/TC)-transfected neuron to hyper- and depolarizing current pulses. **(C)** Voltage responses of a ChR2(ET/TC)-transfected neuron to blue light pulses (473 nm, 5.2 mW/mm²) of 2 to 500 ms duration. **(D)** Voltage responses of a ChR2(ET/TC)-transfected neuron to repetitive trains of 3 ms-long light pulses at different frequencies.

Figure 3. Combined light stimulation and multi-site extracellular recordings from the PFC of neonatal mice *in vivo*. (A) (i) Diagrams illustrating the surgery for electrophysiology *in vivo* in neonatal mice. The skin is removed from the top of the head and dental cement is applied to strengthen the fragile skull and serve as "glue" for two plastic tubes that enable head fixation. **(ii)**

Photograph showing a head-fixed P10 mouse during combined light stimulation and extracellular recordings *in vivo*. **(B) (i)** Extracellular recordings (unfiltered LFP, band-pass filtered LFP and MUA) from the PFC of a P10 mouse transfected with ChR2(ET/TC) by IUE at E15.5 in response to light pulses (473 nm, 3 ms) of different intensities. **(ii)** Same as (i) for a mouse transfected with an opsin-free construct. **(C) (i)** Representative band-pass filtered (1-400 Hz) LFP signals recorded in response to 30 trains of pulsed stimuli (473 nm, 3 ms, 14 mW/mm^2) before (Alive) and after a lethal injection of ketamine-xylazine (Dead, Dead scaled) from a neonatal mouse transfected by IUE with ChR2(ET/TC). The LFP trace after removal of photoelectric artifacts was obtained by subtraction of the scaled artifact (Alive-Dead scaled). **(ii)** Same as (i) for an opsin-free mouse. For (B) and (C) individual traces are shown in black, averages are shown in gray.

Figure 4. Optogenetic activation of pyramidal neurons in the neonatal PFC by different patterns of light stimulation *in vivo*. (A) (i) Representative raster plot and spike probability histogram displaying the firing of ChR2(ET/TC) transfected layer II/III pyramidal neurons in response to 30 sweeps of repetitive light pulses (473 nm, 3 ms, 14 mW/mm^2) at 8 Hz recorded from a neonatal mouse after IUE at E15.5. **(ii)** Corresponding ISI histogram averaged for 3 s before light stimulation (pre, black), 3 s during ramp stimulation (stimulation, blue), and 3 s after light stimulation (post, gray). **(B)** Same as (Ai) for an opsin-free control animal. **(C-D)** Same as (A-B) for sinusoidal light stimulation. **(E-F)** Same as (A-B) for ramp light stimulation.

Figure 5. Generation of coordinated network activity in the neonatal PFC as result of different patterns of light stimulation *in vivo*. (A) (i) Discontinuous oscillatory activity displayed together with the corresponding color-coded wavelet spectrum at identical time scale recorded in response to repetitive light pulses (473 nm, 3 ms, 14 mW/mm^2) at 8 Hz from a P10 mouse with layer II/III pyramidal neurons transfected by IUE at E15.5 with ChR2(ET/TC). **(ii)** Plots displaying the corresponding power spectrum for 3 s before light stimulation (pre, black), 3 s during ramp stimulation (stimulation, blue), and 3 s after light stimulation (post, gray). **(B)** Same as (A) for a P10 mouse transfected by the same procedure with an opsin-free construct. **(C-D)** Same as (A-B) for sinusoidal light stimulation. **(E-F)** Same as (A-B) for ramp light stimulation.

References

Adesnik, H., and Scanziani, M. (2010). Lateral competition for cortical space by layer-specific horizontal circuits. *Nature* 464**,** 1155-1160.

Akam, T., Oren, I., Mantoan, L., Ferenczi, E., and Kullmann, D.M. (2012). Oscillatory dynamics in the hippocampus support dentate gyrus-CA3 coupling. *Nat Neurosci* 15**,** 763-768.

Baumgart, J., and Grebe, N. (2015). C57BL/6-specific conditions for efficient in utero electroporation of the central nervous system. *J Neurosci Methods* 240**,** 116-124.

Berndt, A., Schoenenberger, P., Mattis, J., Tye, K.M., Deisseroth, K., Hegemann, P., and Oertner, T.G. (2011). High-efficiency channelrhodopsins for fast neuronal stimulation at low light levels. *Proc Natl Acad Sci U S A* 108**,** 7595-7600.

Bitzenhofer, S.H., Ahlbeck, J., Wolff, A., Wiegert, J.S., Gee, C.E., Oertner, T.G., and Hanganu-Opatz, I.L. (2017). Layer-specific optogenetic activation of pyramidal neurons causes beta-gamma entrainment of neonatal networks. *Nat Commun* 8**,** 14563.

Borrell, V., Yoshimura, Y., and Callaway, E.M. (2005). Targeted gene delivery to telencephalic inhibitory neurons by directional in utero electroporation. *J Neurosci Methods* 143**,** 151-158.

Brockmann, M.D., Poschel, B., Cichon, N., and Hanganu-Opatz, I.L. (2011). Coupled oscillations mediate directed interactions between prefrontal cortex and hippocampus of the neonatal rat. *Neuron* 71**,** 332-347.

Cardin, J.A., Carlen, M., Meletis, K., Knoblich, U., Zhang, F., Deisseroth, K., Tsai, L.H., and Moore, C.I. (2009). Driving fast-spiking cells induces gamma rhythm and controls sensory responses. *Nature* 459**,** 663-667.

Cardin, J.A., Carlen, M., Meletis, K., Knoblich, U., Zhang, F., Deisseroth, K., Tsai, L.H., and Moore, C.I. (2010). Targeted optogenetic stimulation and recording of neurons in vivo using cell-type-specific expression of Channelrhodopsin-2. *Nat Protoc* 5**,** 247-254.

Dal Maschio, M., Ghezzi, D., Bony, G., Alabastri, A., Deidda, G., Brondi, M., Sato, S.S., Zaccaria, R.P., Di Fabrizio, E., Ratto, G.M., and Cancedda, L. (2012). High-performance and site-directed in utero electroporation by a triple-electrode probe. *Nat Commun* 3**,** 960.

De Marco Garcia, N.V., Karayannis, T., and Fishell, G. (2011). Neuronal activity is required for the development of specific cortical interneuron subtypes. *Nature* 472**,** 351-355.

Fenno, L., Yizhar, O., and Deisseroth, K. (2011). The development and application of optogenetics. *Annu Rev Neurosci* 34**,** 389-412.

Garcia-Moreno, F., Vasistha, N.A., Begbie, J., and Molnar, Z. (2014). CLoNe is a new method to target single progenitors and study their progeny in mouse and chick. *Development* 141**,** 1589-1598.

Gee, J.M., Gibbons, M.B., Taheri, M., Palumbos, S., Morris, S.C., Smeal, R.M., Flynn, K.F., Economo, M.N., Cizek, C.G., Capecchi, M.R., Tvrdik, P., Wilcox, K.S., and White, J.A. (2015). Imaging activity in astrocytes and neurons with genetically encoded calcium indicators following in utero electroporation. *Front Mol Neurosci* 8**,** 10.

Hanganu-Opatz, I.L. (2010). Between molecules and experience: role of early patterns of coordinated activity for the development of cortical maps and sensory abilities. *Brain Res Rev* 64**,** 160-176.

Hanganu, I.L., Ben-Ari, Y., and Khazipov, R. (2006). Retinal waves trigger spindle bursts in the neonatal rat visual cortex. *J Neurosci* 26**,** 6728-6736.

Heck, N., Golbs, A., Riedemann, T., Sun, J.J., Lessmann, V., and Luhmann, H.J. (2008). Activity-dependent regulation of neuronal apoptosis in neonatal mouse cerebral cortex. *Cereb Cortex* 18**,** 1335-1349.

Hoerder-Suabedissen, A., and Molnar, Z. (2015). Development, evolution and pathology of neocortical subplate neurons. *Nat Rev Neurosci* 16**,** 133-146.

Ishii, K., Kubo, K., Endo, T., Yoshida, K., Benner, S., Ito, Y., Aizawa, H., Aramaki, M., Yamanaka, A., Tanaka, K., Takata, N., Tanaka, K.F., Mimura, M., Tohyama, C., Kakeyama, M., and Nakajima, K. (2015). Neuronal Heterotopias Affect the Activities of Distant Brain Areas and Lead to Behavioral Deficits. *J Neurosci* 35**,** 12432-12445.

Johansen, J.P., Diaz-Mataix, L., Hamanaka, H., Ozawa, T., Ycu, E., Koivumaa, J., Kumar, A., Hou, M., Deisseroth, K., Boyden, E.S., and Ledoux, J.E. (2014). Hebbian and neuromodulatory mechanisms interact to trigger associative memory formation. *Proc Natl Acad Sci U S A* 111**,** E5584-5592.

Khazipov, R., and Luhmann, H.J. (2006). Early patterns of electrical activity in the developing cerebral cortex of humans and rodents. *Trends Neurosci* 29**,** 414-418.

Kilb, W., and Luhmann, H.J. (2000). Characterization of a hyperpolarization-activated inward current in Cajal-Retzius cells in rat neonatal neocortex. *J Neurophysiol* 84**,** 1681-1691.

Kirkby, L.A., Sack, G.S., Firl, A., and Feller, M.B. (2013). A role for correlated spontaneous activity in the assembly of neural circuits. *Neuron* 80**,** 1129-1144.

Klein, R.L., Dayton, R.D., Leidenheimer, N.J., Jansen, K., Golde, T.E., and Zweig, R.M. (2006). Efficient neuronal gene transfer with AAV8 leads to neurotoxic levels of tau or green fluorescent proteins. *Mol Ther* 13**,** 517-527.

Kwakowsky, A., Schwirtlich, M., Zhang, Q., Eisenstat, D.D., Erdelyi, F., Baranyi, M., Katarova, Z.D., and Szabo, G. (2007). GAD isoforms exhibit distinct spatiotemporal expression patterns in the developing mouse lens: correlation with Dlx2 and Dlx5. *Dev Dyn* 236**,** 3532-3544.

Lepousez, G., and Lledo, P.M. (2013). Odor discrimination requires proper olfactory fast oscillations in awake mice. *Neuron* 80**,** 1010-1024.

Liu, X., Ramirez, S., and Tonegawa, S. (2014). Inception of a false memory by optogenetic manipulation of a hippocampal memory engram. *Philos Trans R Soc Lond B Biol Sci* 369**,** 20130142.

Martínez-Garay, I., García-Moreno, F., Vasistha, N., Marques-Smith, A., and Molnár, Z. (2016). "In Utero Electroporation Methods in the Study of Cerebral Cortical Development," in *Prenatal and Postnatal Determinants of Development,* ed. D.W. Walker. (New York, NY: Springer New York), 21-39.

Mitew, S., Xing, Y.L., and Merson, T.D. (2016). Axonal activity-dependent myelination in development: Insights for myelin repair. *J Chem Neuroanat* 76**,** 2-8.

Molnar, Z., Lopez-Bendito, G., Small, J., Partridge, L.D., Blakemore, C., and Wilson, M.C. (2002). Normal development of embryonic thalamocortical connectivity in the absence of evoked synaptic activity. *J Neurosci* 22**,** 10313-10323.

Murata, Y., and Colonnese, M.T. (2016). An excitatory cortical feedback loop gates retinal wave transmission in rodent thalamus. *Elife* 5.

Niwa, M., Kamiya, A., Murai, R., Kubo, K., Gruber, A.J., Tomita, K., Lu, L., Tomisato, S., Jaaro-Peled, H., Seshadri, S., Hiyama, H., Huang, B., Kohda, K., Noda, Y., O'donnell, P., Nakajima, K., Sawa, A., and Nabeshima, T. (2010). Knockdown of DISC1 by in utero gene transfer disturbs postnatal dopaminergic maturation in the frontal cortex and leads to adult behavioral deficits. *Neuron* 65**,** 480-489.

Olcese, U., Iurilli, G., and Medini, P. (2013). Cellular and synaptic architecture of multisensory integration in the mouse neocortex. *Neuron* 79**,** 579-593.

Page, S.C., Hamersky, G.R., Gallo, R.A., Rannals, M.D., Calcaterra, N.E., Campbell, M.N., Mayfield, B., Briley, A., Phan, B.N., Jaffe, A.E., and Maher, B.J. (2017). The schizophrenia- and autism-associated gene, transcription factor 4 regulates the columnar distribution of layer 2/3 prefrontal pyramidal neurons in an activity-dependent manner. *Mol Psychiatry*.

Sanchez, M.P., Frassoni, C., Alvarez-Bolado, G., Spreafico, R., and Fairen, A. (1992). Distribution of calbindin and parvalbumin in the developing somatosensory cortex and its primordium in the rat: an immunocytochemical study. *J Neurocytol* 21**,** 717-736.

Spellman, T., Rigotti, M., Ahmari, S.E., Fusi, S., Gogos, J.A., and Gordon, J.A. (2015). Hippocampal-prefrontal input supports spatial encoding in working memory. *Nature* 522**,** 309-314.

Spitzer, N.C. (2002). Activity-dependent neuronal differentiation prior to synapse formation: the functions of calcium transients. *Journal of Physiology-Paris* 96**,** 73-80.

Stark, E., Eichler, R., Roux, L., Fujisawa, S., Rotstein, H.G., and Buzsaki, G. (2013). Inhibition-induced theta resonance in cortical circuits. *Neuron* 80**,** 1263-1276.

Steinberg, E.E., Christoffel, D.J., Deisseroth, K., and Malenka, R.C. (2015). Illuminating circuitry relevant to psychiatric disorders with optogenetics. *Curr Opin Neurobiol* 30**,** 9-16.

Stujenske, J.M., Spellman, T., and Gordon, J.A. (2015). Modeling the Spatiotemporal Dynamics of Light and Heat Propagation for In Vivo Optogenetics. *Cell Rep* 12**,** 525-534.

Szczurkowska, J., Cwetsch, A.W., Dal Maschio, M., Ghezzi, D., Ratto, G.M., and Cancedda, L. (2016). Targeted in vivo genetic manipulation of the mouse or rat brain by in utero electroporation with a triple-electrode probe. *Nat Protoc* 11**,** 399-412.

Tabata, H., and Nakajima, K. (2001). Efficient in utero gene transfer system to the developing mouse brain using electroporation: Visualization of neuronal migration in the developing cortex. *Neuroscience* 103**,** 865-872.

Taniguchi, Y., Young-Pearse, T., Sawa, A., and Kamiya, A. (2012). In utero electroporation as a tool for genetic manipulation in vivo to study psychiatric disorders: from genes to circuits and behaviors. *Neuroscientist* 18**,** 169-179.

Tye, K.M., and Deisseroth, K. (2012). Optogenetic investigation of neural circuits underlying brain disease in animal models. *Nat Rev Neurosci* 13**,** 251-266.

Valeeva, G., Tressard, T., Mukhtarov, M., Baude, A., and Khazipov, R. (2016). An Optogenetic Approach for Investigation of Excitatory and Inhibitory Network GABA Actions in Mice Expressing Channelrhodopsin-2 in GABAergic Neurons. *J Neurosci* 36**,** 5961-5973.

Vasistha, N.A., Garcia-Moreno, F., Arora, S., Cheung, A.F., Arnold, S.J., Robertson, E.J., and Molnar, Z. (2015). Cortical and Clonal Contribution of Tbr2 Expressing Progenitors in the Developing Mouse Brain. *Cereb Cortex* 25**,** 3290-3302.

Wang, X., Zhang, C., Szabo, G., and Sun, Q.Q. (2013). Distribution of CaMKIIalpha expression in the brain in vivo, studied by CaMKIIalpha-GFP mice. *Brain Res* 1518**,** 9-25.

Washbourne, P., Thompson, P.M., Carta, M., Costa, E.T., Mathews, J.R., Lopez-Bendito, G., Molnar, Z., Becher, M.W., Valenzuela, C.F., Partridge, L.D., and Wilson, M.C. (2002). Genetic ablation of the t-SNARE SNAP-25 distinguishes mechanisms of neuroexocytosis. *Nat Neurosci* 5**,** 19-26.

Wonders, C.P., and Anderson, S.A. (2006). The origin and specification of cortical interneurons. *Nat Rev Neurosci* 7**,** 687-696.

Yizhar, O., Fenno, L.E., Davidson, T.J., Mogri, M., and Deisseroth, K. (2011). Optogenetics in neural systems. *Neuron* 71**,** 9-34.

Zhang, F., Gradinaru, V., Adamantidis, A.R., Durand, R., Airan, R.D., De Lecea, L., and Deisseroth, K. (2010). Optogenetic interrogation of neural circuits: technology for probing mammalian brain structures. *Nat Protoc* 5**,** 439-456.

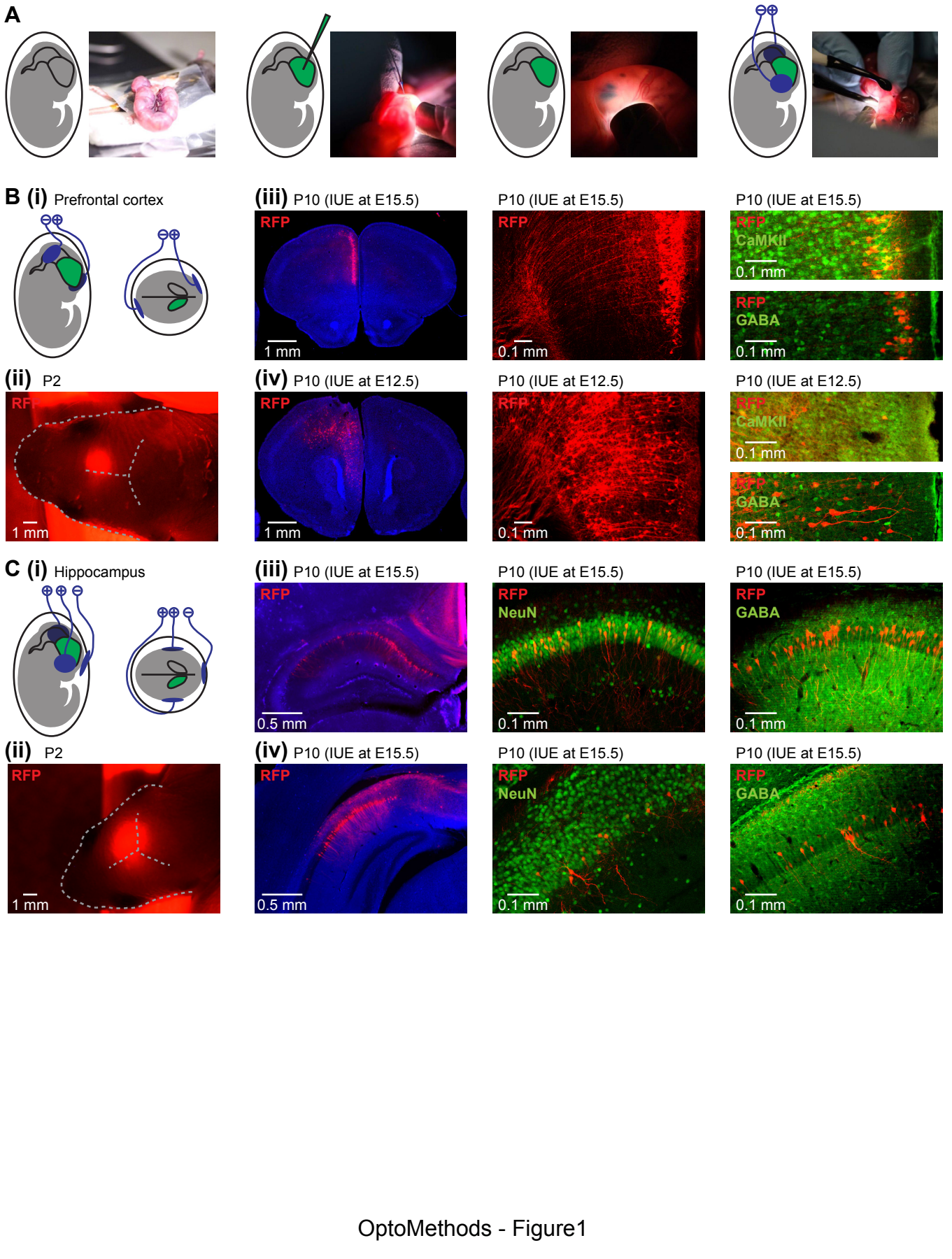

OptoMethods - Figure1

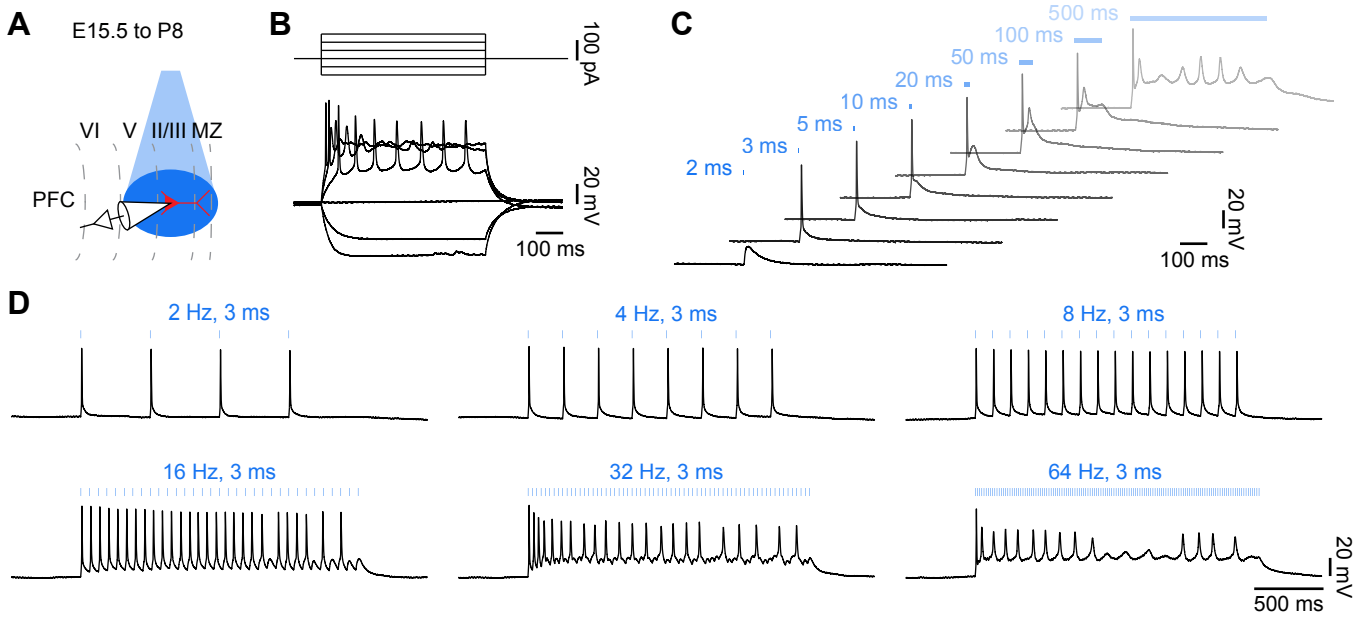
A
E15.5 to P8
VI
V
II/III
MZ
PFC
B
100 pA
20 mV
100 ms
C
500 ms
100 ms
50 ms
20 ms
10 ms
5 ms
3 ms
2 ms
20 mV
100 ms
D
2 Hz, 3 ms
4 Hz, 3 ms
8 Hz, 3 ms
16 Hz, 3 ms
32 Hz, 3 ms
64 Hz, 3 ms
20 mV
500 ms

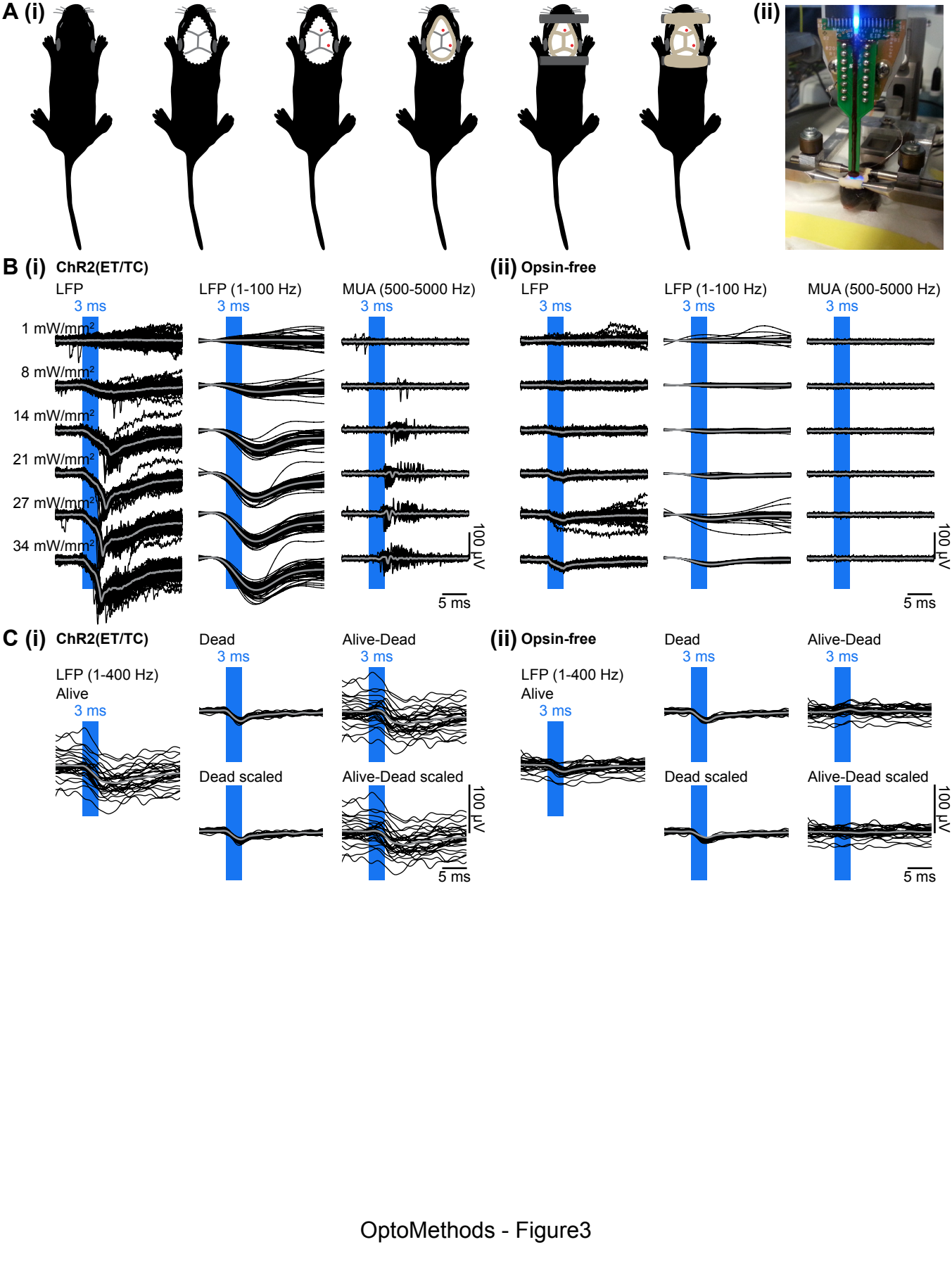

OptoMethods - Figure3

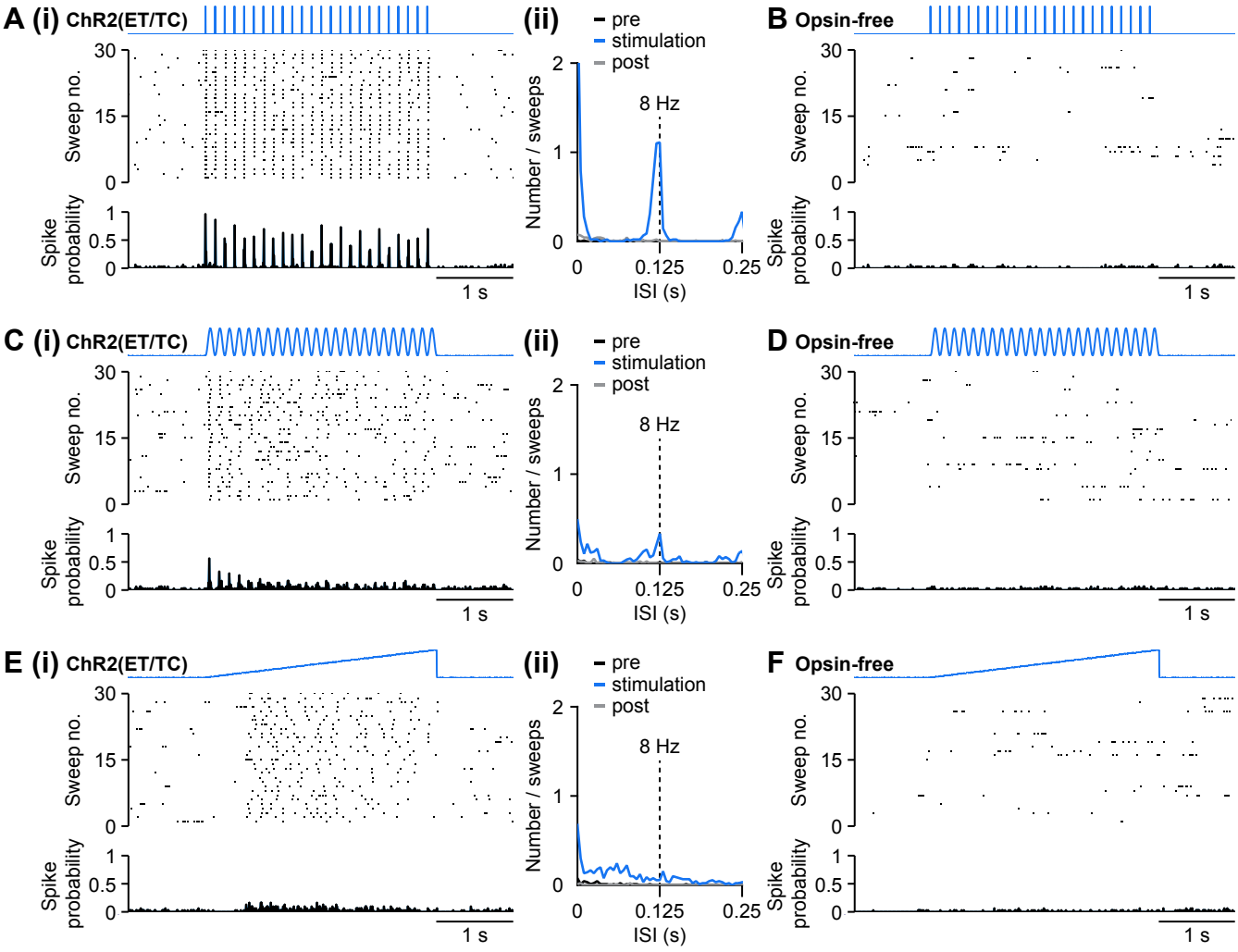
A (i) ChR2(ET/TC)
(ii)
pre
stimulation
post
8 Hz
B Opsin-free
C (i) ChR2(ET/TC)
D Opsin-free
E (i) ChR2(ET/TC)
F Opsin-free
Sweep no.
Spike probability
Number / sweeps
ISI (s)
1 s

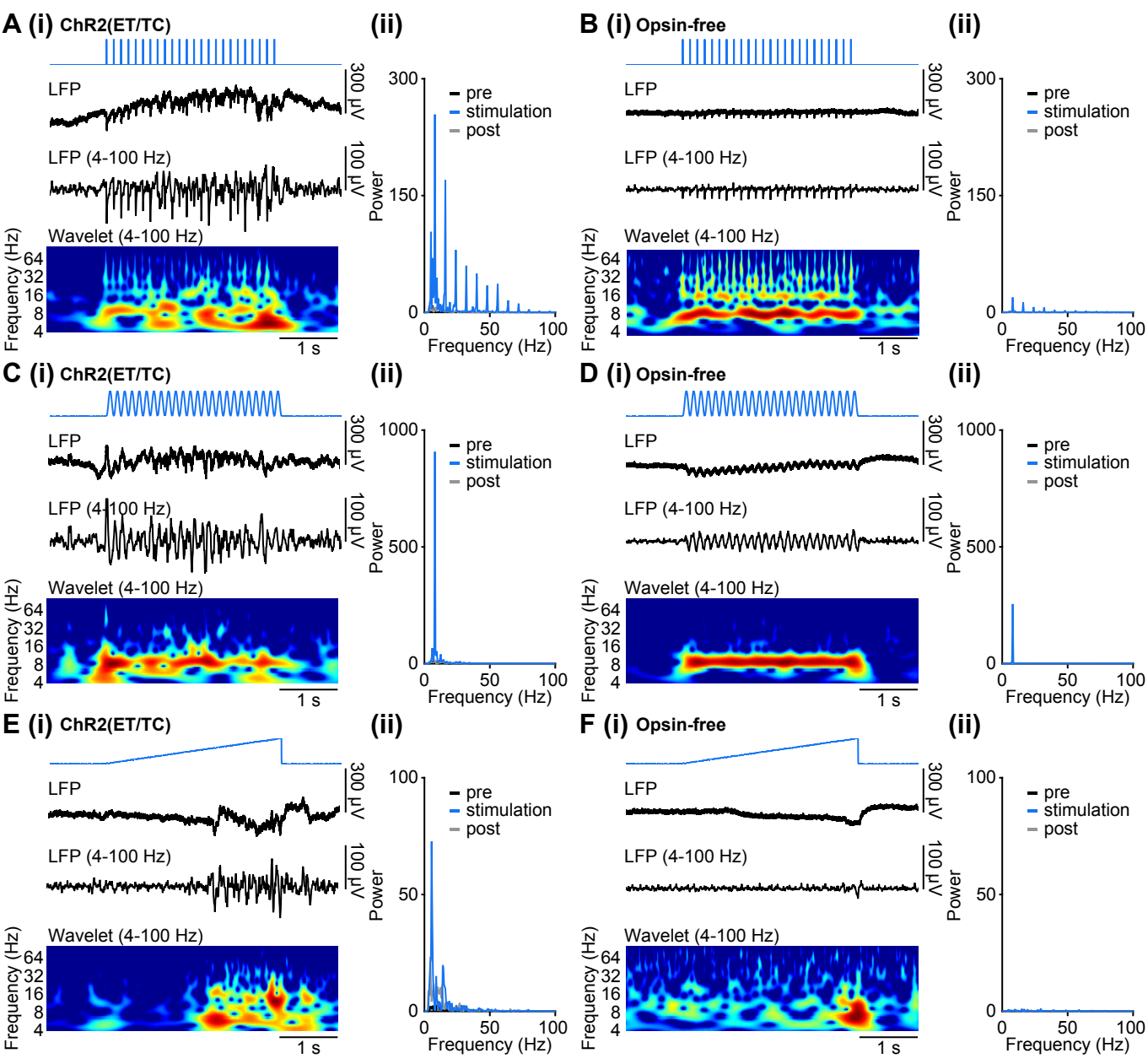
A (i) ChR2(ET/TC)
(ii)
LFP
LFP (4-100 Hz)
Wavelet (4-100 Hz)
300 µV
100 µV
Frequency (Hz)
64
32
16
8
4
1 s
Power
pre
stimulation
post
0
50
100
150
300
B (i) Opsin-free
C (i) ChR2(ET/TC)
500
1000
D (i) Opsin-free
E (i) ChR2(ET/TC)
F (i) Opsin-free

13 Declaration on oath

Ich versichere ausdrücklich, dass ich die Arbeit selbständig und ohne fremde Hilfe verfasst, andere als die von mir angegebenen Quellen und Hilfsmittel nicht benutzt und die aus den benutzten Werken wörtlich oder inhaltlich entnommenen Stellen einzeln nach Ausgabe (Auflage und Jahr des Erscheinens), Band und Seite des benutzten Werkes kenntlich gemacht habe.

Ferner versichere ich, dass ich die Dissertation bisher nicht einem Fachvertreter an einer anderen Hochschule zur Überprüfung vorgelegt oder mich anderweitig um Zulassung zur Promotion beworben habe.

Ich erkläre mich einverstanden, dass meine Dissertation vom Dekanat der Medizinischen Fakultät mit einer gängigen Software zur Erkennung von Plagiaten überprüft werden kann.

Sincerely,

Joachim Ahlbeck

_____ _____

City and date Signature